(TITLE)

SINGLE POINT DIAMOND DRESSING OF ALUMINIUM OXIDE GRINDING
WHEELS AND ITS INFLUENCE IN CYLINDRICAL GRINDING.

by

NORMAN PHILIP FLETCHER, B.Tech. C.Eng. M.I.Prod.E.

A Doctoral Thesis

Submitted in partial fulfilment of the requirements
for the award of

The Degree of Doctor of Philosophy of the Loughborough
University of Technology.
June 1976.

Supervisor: H. MADEN, M.Sc. C.Eng. M.I.Mech.E. M.I.Prod.E.
Department of Engineering Production.

Acknowledgements.

I would like to thank the following people for making this thesis possible.

Science Research Council.

Professor R.J.Sury, Head of the Department of Engineering Production.

Professor K.J.Hume my Director of Research.

Mr. H.Maden my supervisor, who has given me much encouragement and sound advice.

Mr. D.Bates for his helpfulness to me in the Machine Tool Laboratory.

My Aunt, Laura Roberts, who has shown her expertise in typing my script,

and all the other people who have helped me in many ways.

N. P. Fletcher.

-2-

SYNOPSIS

The parameter defined as "rake angle", combining the shape of the wheel-dressing diamond with its orientation, has been introduced in conjunction with other associated dressing variables, such as the depth of cut and traverse rate, into an evaluation of the dressing process, and its subsequent influence on both rough and finish cylindrical traverse grinding.

With the object of minimising diamond wear, due to the high cost of dressing diamonds, the nature and magnitude of the components of the dressing force have been recorded by means of a three-component strain-gauge type dynamometer and Ultra Violet recorder. A linear relationship was established between the radial component of force on the diamond, and the amount of diamond wear.

The "rake angle" has been shown to have a significant effect on diamond life, and a critical range of values, corresponding to stable dressing conditions, and resulting in minimum diamond wear, has been established.

The dressing parameter having the greatest influence on wheel performance was the traverse rate, with the depth of cut being of secondary importance. These variables affected grinding wheel breakdown to a wear depth greater than the dressing depth of cut, but influenced the workpiece surface finish only, during the initial stage of wheel wear. The initial rate of wheel breakdown when grinding was shown to be directly influenced by all dressing conditions.

Grinding forces measured by a dynamometer incorporating a three-component quartz force transducer, have been shown to be significantly influenced by high traverse rates and low depths of cut in wheel dressing. This is important from the point of view of grinding deflection, which is adversely affected by high values of the radial component of the grinding force, resulting from this particular combination of wheel dressing variables. Sudden increases in the ratio of radial to tangential grinding

force components, coinciding with each stage of wheel wear, gave a clear indication of the occurrence of these events.

A novel theoretical method for assessing the influence of both the dressing and grinding variables on the workpiece surface finish when fine grinding, has been established. This method was also used to predict the workpiece surface finish for known values of these variables. Close agreement was found between the values predicted by the method, and those obtained from measurements of the ground surfaces.

Nomenclature.

Dressing parameters.

h	=	dressing lead of the diamond (cross-feed).	mm/rev.
a	=	diamond depth of cut (in-feed applied).	μm
a'	=	theoretical depth of dressed profile.	μm
a^*	=	measured depth of dressed profile.	μm
x	=	diamond width at a depth of cut, a.	mm
w	=	width of the diamond wear flat.	mm
β	=	included angle of the diamond (plan view).	degrees
α	=	rake angle of the diamond.	degrees
θ	=	drag angle of the dressing tool.	degrees
F_a	=	axial component of dressing force.	N
F_r	=	radial component of dressing force.	N
F_t	=	tangential component of dressing force.	N

Grinding parameters.

N	=	rotational speed of the grinding wheel.	rev./sec.
n	=	rotational speed of the workpiece.	rev./sec.
D	=	diameter of the grinding wheel.	mm
d	=	diameter of the workpiece.	mm
W	=	width of the grinding wheel.	mm
l	=	length of the workpiece.	mm
v_t	=	traverse rate of the workpiece.	mm/sec.
a_g	=	depth of cut (in-feed).	μm
ϕ_l	=	lead angle of the grinding wheel path.	degrees
ϕ_h	=	lead angle of ground surface scratches.	degrees
F_R	=	radial component of grinding force.	N
F_T	=	tangential component of grinding force.	N

Boundary coefficients. (Chapter 3).

z_l to z_r, b_l to b_r, u_l to u_r and e_l to e_r.	dimension-
X_l to X_r, A_l to A_r, T_l to T_r and I_l to I_r.	less
K_l to K_r and z_l to z_r.	mm
p, q, m and y'	mm

Surface finish coefficients and parameters.

E_l to E_r and Δ_l to Δ_r (Chapter 3).			mm
Rp	=	smoothing depth	μm
Ra	=	average arithmetic roughness (CLA, AA).	μm

CONTENTS

CONTENTS

CONTENTS

CONTENTS

CONTENTS

CONTENTS

List of figures.

List of figures.

List of figures.

List of figures.

List of figures

List of figures

-20-

CHAPTER 1

INTRODUCTION AND STATEMENT OF PROBLEM

1.1   INTRODUCTION

In the early 1970's, Science Research Council
sponsored a co-ordinated programme of research into all
aspects in the field of grinding, from the basic mechanisms
of grinding, to the design and manufacture of grinding
machines.

This research project was the result of a contract
from Science Research Council to investigate the dressing
of grinding wheels, and its influence on the grinding
process. Single point diamond tools have been used as
the dressing medium in this work, for several reasons,
these being that they are used extensively throughout
the metal working industry as dressing tools, [1] and
have also been the subject of several notable previous
investigations. [2,3,4,5] Since the single point diamond
is the most basic dressing tool available, it was felt
that the results would be of a more fundamental nature
than those obtained using multi-point tools or crushing
rollers. Cylindrical traverse grinding was used as the
process on which to test the various dressing techniques
employed, because of its universal application in industry.

The present research comprises two basic parts.
The first part investigates the influence of the combined
effects of diamond geometry, and angular presentation of
the diamond tool to the grinding wheel, on diamond wear,
and the resulting surface condition of the grinding wheel.
This is to establish some general rules for deciding
optimum dressing conditions with respect to minimum
diamond wear, in view of the high cost, and relatively
short life of the wheel-dressing diamonds.

Grinding wheel surface topography has been examined
after dressing with both sharp and worn diamonds, to
compare and evaluate the degree of similarity between the
wheel condition and the theoretical surface geometry,

resulting from the diamond profile, diamond depth of cut, and traverse rate.

The second part investigates the effects of the variables connected with the wheel dressing operation on the grinding ratio, (i.e. the ratio of the volume of metal removed during grinding, to the corresponding volume of wheel worn away), on the radial and tangential components of grinding force generated, and on the surface finish of the workpiece etc. It is hoped that a better understanding of the influence of dressing variables on cylindrical grinding performance will be forthcoming from the results of this work.

1.2 THE NEED FOR TRUING AND DRESSING

In contrast to cutting tools having a finite number of equi-spaced and geometrically definable cutting edges, the grinding wheel is composed of a large number of randomly orientated abrasive grits supported in a bonding material; those at the periphery of the wheel providing a series of geometrically indeterminate cutting edges. This shows the grinding wheel to be an extremely complex form of cutting tool. During a grinding operation, these cutting edges are subjected to mechanical and thermal stressing caused by wheel-workpiece interaction. This results in wheel wear taking place relatively quickly. It has been suggested that the rate of wear of such abrasive grits, compared with that of other forms of cutting tool, is in the order of 1,000,000 times.[6] Since most grinding processes are regarded as finishing operations, imparting to the workpiece conditions of size and finish of the order of $\pm$ 5 μm and .5 μm C.L.A. respectively, rapid wheel breakdown must be avoided to maintain grinding efficiency. This necessitates the introduction of a cutting edge regenerative process well before wheel breakdown becomes detrimental to the workpiece size and finish. This is the objective of truing and dressing.

The optimum performance of a correctly selected grinding wheel has been shown to be markedly influenced by the wheel dressing techniques employed, since the

dressing cycle used can significantly affect the cutting action of the wheel, the wheel life between dressing, and the condition and finish of the ground work surface.[2,3,4]

In addition to the non-productive time occasioned by the frequency of the dressing operation itself, the material removed from the wheel during dressing may amount to between 3 and 9 times the wear occuring during grinding, depending upon the grade of wheel, and type of material being machined. [2] These factors directly affect productivity, and in addition may lead to the selection of lower metal removal rates in an attempt to extend wheel life between dressings. [7]

A further consideration of importance is the expenditure on diamond dressing tools, which on a world basis, is estimated to be close to $ 30 million annually. This includes an estimated $ 6 million for the actual diamonds. [1]

CHAPTER 2

INTRODUCTION TO THE TRUING AND DRESSING OF VITREOUS BONDED GRINDING WHEELS, WITH A REVIEW OF PAST WORK IN GRINDING

2.1 THE TRUING AND DRESSING FUNCTION

The ability of a grinding wheel to remove material efficiently during an abrasive machining operation is dependent, to a large extent, upon the manner in which the truing and dressing procedures, which precede the grinding operation, are applied to the grinding wheel. These procedures, which are used in the preparation of a grinding wheel, may be defined as follows:-

Truing is the machining away of a grinding wheel surface to produce any specified profile whose axis is concentric with the axis of rotation of the grinding wheel. This process, which preceeds dressing, eliminates any errors of form brought about by inconsistencies in wheel manufacture, or resulting from wheel degeneration caused by the action of a previous grinding operation.

Dressing, on the other hand, is the "fine machining" of a grinding wheel profile to impart to it a specific cutting action during a subsequent grinding operation.

It can be concluded from the above definitions that the process of wheel dressing is the one responsible for giving the grinding wheel its cutting characteristics, (particularly at the start of grinding.[8]) In practice, the functions of truing and dressing often overlap. The act of truing a grinding wheel may not satisfactorily dress it, but the act of dressing will accomplish a certain amount of truing.

Several methods of truing and dressing vitreous bonded grinding wheels are employed in industry,[9] the most common ones making use of single or multi-point diamond tools. Over the past few decades, the diamond dressing tool has become virtually indispensible for the maintenance of grinding tolerances which are better

than $\pm$ 2.5 μm, even on high volume, fully automated production lines.

In this chapter the diamond will be discussed in the light of its wheel dressing applications, along with the performance of grinding wheels dressed with diamond tools, as found by previous researchers.

2.2   THE DIAMOND AS A DRESSING TOOL

Diamond is the hardest material known to man, and as such, is employed in many machining processes as a cutting tool, either in crystal form or as a powder. It has an ideal application in wheel dressing where it is required to shear through, or pluck out the particles of abrasive grit which form part of a grinding wheel. These abrasive grits, the most common type being aluminium oxide, are relatively hard themselves, and so require a cutting tool harder than themselves for efficient machining. In terms of relative hardness, using the Knoop scale[10], diamond is approximately 4 times harder than aluminium oxide, having a hardness value of 9,000 kg/mm^2 as compared with that of 2,000 kg/mm^2 for aluminium oxide. (Diamond (111) surface $\langle 110 \rangle$ direction, 500g load. Al_2O_3 surface, direction and load not known.)

Diamond is a crystalline form of carbon where the atoms are densely packed together giving an extremely hard structure. It has several advantages as a cutting tool, these being that its coefficient of friction is very low when rubbing against other materials, ensuring that attritious wear will be low, and that being a good conductor of heat, much of the heat generated during a cutting operation will be dissipated rapidly through the diamond. It has, however, several drawbacks. At temperatures above 700° C graphitization can occur in air causing rapid degeneration. This effect can be minimised either by using coolant, or allowing the diamond to cool between dressing cycles. A second problem is that because of its crystalline structure, the diamond

relies on the orientation of its crystallographic axes
for its hardness, and will cleave readily along certain
planes. Should it be presented to a grinding wheel at a
non-preferred orientation, rapid disintegration would ensue.
Much work has been conducted over the past few years into
the effects of the changes of diamond hardness with
crystallographic orientation when machining diamonds for
the jewellery industry, and when using them for the dressing
of grinding wheels.

Denning[11] has obtained grinding hardness values for
diamond, expressed in arbitrary units, for the cube,
dodecahedron and several intermediate planes as a function
of the azimuth which were taken at some convenient
crystallographic direction in each case. Fig. 2.1 gives his
observations on the cube plane. A cube axis was chosen
as zero azimuth, and it has been shown that in a direction
inclined at an angle of 45° to the cube axis, and still
in the cube plane, the relative grinding hardness is some
800 times greater. Fig. 2.2 shows the information in
fig. 2.1 replotted in what is called a diamond grinding
hardness vector diagram. This shows in a simple form the
relative hard and soft directions in the cube plane.
Fig. 2.3 shows the relative wear of the dodecahedral,
octahedral and cube planes of diamond as a function of
the azimuth.

Wilks and Wilks[12] also found from their experiments
that the highest hardness value exists in the cube plane
at an angle of 45° to the a-a and b-b axes of the diamond
octahedron as depicted in fig. 2.4. Their findings are
related as follows:-

The soft directions in the cube face are parallel
to the a-a and b-b axes, and the hard directions are at
45° to the a-a and b-b axes. In the octahedron face it
is soft in the direction of the dodecahedron face and hard
in the direction of the cube face. In the dodecahedron
face it is soft parallel to the c-c axis and hard at 90°.
to the c-c axis.

Pahlitzsch[5] conducted a series of wheel dressing

experiments using specially prepared diamonds having the shape of a quadrangular pyramid with a square base, and the angle between the sides at the top measuring 130°. Three diamonds were held in individual steel holders such that one was held parallel to an imaginary cube face, the crystallographic axis (100) running in the direction of the tool mount, another held such that the axis (111) of a three-point face, (octahedron face, looking vertically on the face) lay in the direction of the tool mount, and the third held such that the axis (110) of a two-point face (rhombic dodecahedron, looking vertically towards one edge) lay also in the direction of the tool mount. Results from the dressing tests showed that the two-point face diamond (110) had the most amount of wear, and the three-point face diamond (111) had the least amount of wear. He concluded that in order to obtain the maximum tool life from a truing diamond, it should be gripped so that the crystallographic axis lies in a line with the tool shaft, or so that whilst truing is in progress, wear takes place on the diamond parallel to an octahedral plane.

More recent investigations, cited by Busch[13], also indicate that octahedron diamond dressing tools should be set in a preferred direction relative to the grinding wheel for minimum diamond wear to occur, although the settings specified by the investigators are at variance. Fig. 2.5 shows the diamond orientation according to Frank and Busch, whilst fig. 2.6 shows that according to Grodzinski. Busch states that for Grodzinski's recommended diamond setting, both the velocity vector of the grinding wheel and the cutting forces run parallel to the octahedron faces, which is the most favourable gap direction for octahedrally crystallised diamonds; and that the result of such a setting is chipping of the octahedron diamond such that wear occuring through chipping is greater than the diamond wear resulting from abrasion. It must be pointed out, however, that Grodzinski's recommendations fall into line with those stated by Pahlitzch.[5]

It can be concluded that for wheel dressing, the use of regular, well formed diamonds would make setting of the diamond for preferred crystallographic orientation relatively simple. In practice, however, many dressing tools make use of irregular shaped diamonds and diamond chips. To determine the crystallographic axes in these cases, inspection using x-ray techniques would be necessary, which may be neither practical nor economical in an industrial situation.

2.3   TYPES OF DIAMOND DRESSING TOOL

The main factor which influences the choice of diamond dressing tool is the nature of the grinding operation to be performed, this operation falling into one of two categories, namely, plain or form grinding. In plain grinding, the wheel is "straight" dressed. This entails the use of a straight-line dressing movement without change of direction, and gives either a parallel or tapered cylindrical surface to the grinding wheel. This is the simplest form of wheel dressing, and makes use of single or multi-point diamond tools, see fig. 2.7. In form grinding , the type of diamond dressing tool used depends upon the complexity and size of the profile required. For profiles having simple shapes made up from curves and straight lines, single point and multi-point diamond tools are used in conjunction with a tracing system, most probably of the pantograph type. Since the form dressed onto the grinding wheel is transferred directly to the workpiece, the dressing medium must be extremely accurate, which calls for the use of well formed diamonds of known geometry. In this case, natural diamonds have to be specially ground and very accurately set to meet the particular requirements of the dressing system. For more complex shapes, roller truers, or block truers are employed. These consist of a metal roller or block, which has a coating of diamond dust or chips impregnated into the roller or block profile, see figs. 2.8 and 2.9. When using a roller truer, the roller, which can be driven in either direction relative

to the wheel or allowed to rotate freely, is brought into contact with the grinding wheel, and the form of the truer is impressed onto the wheel periphery. In the case of the block truer, wheel dressing is achieved by traversing the block in a reciprocating motion past the grinding wheel face at right angles to the wheel axis whilst infeed is applied. Grinding wheels dressed in this manner are used mainly for plunge cut grinding, although plain cylindrical rollers are sometimes used to prepare wheels for plain traverse grinding.

2.4 A GENERAL VIEW OF DRESSING FOR PLAIN GRINDING

Since plain cylindrical traverse grinding is the subject of this research, only single point diamond tools will be discussed henceforth. Information regarding other dressing techniques using diamonds can be obtained from several sources.[14,15,16]

2.4.1 Requirements of diamonds used in single point dressing tools.

Single point diamond tools utilise all forms of natural diamond, e.g. octahedrons, rhombic dodecahedrons, triangular shapes and diamond points, although the latter two forms are not so well suited, because they embody fewer usable cutting points.

The principal qualities required when assessing rough diamonds are:-

1). The stone must be a self-contained crystal.
2). An undamaged crystal surface must be present.
3). There must be the required number of perfect, natural points and angles.
4). There must be no internal flaws.

2.4.2 Diamond size related to grinding wheel diameter and face width.

Diamonds are selected for dressing applications according to their weight, the standard of weight being the carat, (designated K). This standard of weight originated in the Far East where certain fruit trees grew, whose seeds or "carats," which were remarkably uniform in weight

and size, were used as the basis of small weight for trading purposes. Fig. 2.10 shows the recommended diamond weight according to grinding wheel diameter and face width. In practice, the maximum size of diamond used for dressing is around 4 carats, and the majority no larger than 2 carats.

2.4.3 Shank sizes for diamond dressing tools.

In 1953 a British standard was drawn up covering shank sizes for diamond dressing tools, the shanks being manufactured from mild steel. Fig. 2.11 describes BS 2002:1953.

2.4.4 Orientation of the diamond tool during dressing.

To minimise diamond wear during a dressing operation, the dressing tool is presented to the grinding wheel at preferred settings, measured relative to the vertical and horizontal planes. It is recommended that the dressing tool be inclined towards the grinding wheel face in the vertical plane, such that the diamond points in the direction of rotation of the grinding wheel, as shown in fig. 2.12. The angle then measured between the axis of the dressing tool and a radial line passing through the wheel centre is called the "drag" angle, and has been given values of between 5° and 15°, [14,15,16,17]. This setting reduces the possibility of cleavage or fracture due to shock or induced vibrations, and helps to maintain a good point at the tip of the diamond. The tool is sometimes set over at a similar angle to the wheel face in the horizontal plane, as indicated in fig. 2.13. When this is done, the diamond trails behind the direction of the crossfeed. This, however, implies that dressing should always be conducted in one direction only across the wheel face, resulting in an increase in dressing time which may be intolerable under modern production conditions. In conjunction with the above two settings, it is common practice to rotate the dressing tool frequently through 20° to 40° in its holder, to ensure that the wear flat produced at the diamond tip remains as small as possible, since dressing efficiency is impaired if the

wear area exceeds 1 mm^2. (17)

2.4.5 Diamond depth of cut and traverse rate.

Diamond depth of cut and traverse rate are a major
consideration when dressing grinding wheels, particularly
when using single point diamond tools. These two para-
meters, which influence both the cutting ability of the
dressed grinding wheel and the wear rate of the diamond
tool itself, have been the subject of much investigation.
18,19,20. This work will be dealt with in detail later.
The latest British Standard covering diamond dressing
tools, BS 2 002: 1973, recommends that for maximum
diamond life when dressing, the depth of cut should not
exceed 50 μm. Several other sources give general values
of diamond depth of cut and traverse rate, which cover a
range of "plain" grinding conditions to be met in industry.

Selby[17], suggests that when dressing grinding
wheels, it is preferable to take several small depths of cut
between 12.5 μm to 25 μm, rather than fewer large cuts.
These depths of cut used in conjunction with a fast traverse
rate of the diamond across the grinding wheel face will give
an open structured wheel suitable for large stock removal,
but poor workpiece surface finish. A slower diamond traverse
rate will give a more superior workpiece surface finish at
the expense of high stock removal. For very good surface
finishes, a slow diamond traverse rate should be combined with
a depth of cut of between 5 μm to 10 μm. To ensure optimum
conditions whilst dressing, the diamond traverse rate should
be such that the diamond cuts each abrasive grain twice,
since unnecessary wear occurs when the traverse rate is too
slow, and a poor workpiece surface finish occurs when it
is too fast, see fig. 2.14.

Jones and Shipman[21], one of the leading grinding
machine manufacturers in Great Britain, make recommendations
relating to dressing depth of cut and traverse rate for
rough and finish grinding similar to those stated by Selby.
They are less explicit regarding diamond traverse rate,
and leave a lot to the judgement of the machine operator.

On the question of wheel dressing for fine grinding, they suggest that the diamond traverse rate should be in the region of 76 mm/min to 125 mm/min approximately, whilst taking several passes across the wheel face with an initial depth of cut of 10 µm, and gradually reducing this in steps to 2.5 µm.

Busch,[13] gives more comprehensive data on the depths of cut and traverse rates in wheel dressing, and relates the dressing tool traverse rate to the grinding wheel speed. He states that the diamond depth of cut should not exceed 10 µm to 40 µm, because of the possibility of unnecessarily high diamond consumption. The lower depths of cut apply to ground profile diamonds, small single dressing diamonds and fine-grained multi-grain dressing tools, and the upper value to large single dressing diamonds and coarse-grained multi-grain dressing tools. The traverse rate of the diamond tool should be in the region of .1 mm to .2 mm for each grinding wheel revolution. This means that for a grinding wheel rotating at 2,000 rev/min, the dressing tool traverse rate would be between 100 mm/min to 200 mm/min. He recommends that for finish grinding, the lower traverse rate of .1 mm/rev should be adopted, and that the higher rate of .2 mm/rev should not be exceeded.

The above three views are representative of the general concensus of opinion concerning diamond depths of cut and traverse rate in wheel dressing.

2.4.6 The use of coolant in dressing.

From the point of view of diamond economy, dressing without the use of a coolant is avoided wherever possible because of the high temperature experienced, remembering that graphitization of diamond starts around 700°c. In cases where dry dressing is encountered, e.g. when grinding machines are not supplied with coolant, or when small grinding wheels are used for very accurate form grinding, small wear resistant diamonds with well defined cutting points are recommended. In such cases, time is

allowed between each successive cut to allow the diamond
to cool naturally. Where coolant is used for dressing,
it is normal to use the same coolant as for grinding, and
to play it onto the diamond tip before dressing commences.
This reduces the possibility of diamond disintegration
through subjection to high temperature gradients.

2.5 A REVIEW OF PAST RESEARCH INTO ABRASIVE MACHINING AND THE INFLUENCE OF WHEEL DRESSING ON THE GRINDING PROCESS

Grinding, which is the best known and most common
abrasive machining process, has been a topic for research
for some considerable time, with such aspects as mechanisms
of metal removal, abrasive wheel wear and forces in
grinding being the subject of such research. In more
recent years, the influence of wheel dressing on the
grinding process has been studied in depth. The following
is a review of work conducted by some research workers in
the field of grinding, and their findings.

2.5.1 The grinding action of abrasive grains.

Alden,[22] (1914), and Guest[23] (1915), were pioneers
in formulating basic expressions for chip-forming geometry
during grinding based purely on the geometrical relation-
ships between the grinding wheel and workpiece, their
dimensions and speed, and the depth of cut. In terms of
application, Guest's approach was more practical since it
contained terms which were more easily measured. Work of
a similar nature was carried out by several other investig-
ators up to 1952, when for the first time, Backer, Marshall
and Shaw established by means of a formula, a relationship
between chip thickness and the macrogeometrical form of
the ground suface.

Backer, Marshall and Shaw[24] in studying the size
effect in metal cutting, investigated the cutting process
involving the formation of very small chips at high cutting
speeds, (Micromilling), and applied the results to the
grinding operation. They compared the shear energy
involved in grinding to that in turning, micromilling

and tensile testing, and observed a significant increase
in shear energy with decrease in chip size. The shear
strength involved in grinding metals under mild conditions
was found to correspond to the theoretical strength which
is about 12.41 GPa for steel. They also showed that the
grit depth of cut is a more important variable in inter-
preting grinding data than the more conventional wheel
depth of cut.

Reichenbach et al.,[25] classified grinding chips
into five types depending upon their relative thickness-
to-length ratio, (this being a function of work speed
relative to wheel speed). and derived equations for
computing the length or thickness of chips of all types
for external, surface, internal, and plunge-grinding
operations. From this work, they predicted that under
fine grinding conditions, Guest's assumption that the
maximum force per grit would vary with the square of chip
thickness, would hold true, whilst for somewhat coarser
grinding, Alden's assumption that the maximum force per
grit would vary directly with chip thickness, was
correct. They concluded from their experimental work
that chip thickness has an important role to play as a
grinding parameter, and can be used as a criterion for
evaluating the power required to remove metal in
grinding.

Hahn[26,27], has studied the mechanisms of the
grinding process under plunge-cut conditions, and found
two distinct mechanisms, namely a ploughing and rubbing
process where the abrasive grain plastically ploughs a
groove and throws up alongside small particles of highly
distorted metal, and secondly, a cutting process where a
chip is formed ahead of the grain. The effects of wheel
speed, work speed, and conformity, i.e. external, internal
or surface grinding, are found to differ depending upon
which category the grinding action falls into. He found
that for wheel-work combinations where little or no
rubbing and ploughing takes place, the relationship between
the plunge velocity and force intensity is a linear one,

and that from this a well defined metal removal parameter exists. However, for wheel-work combinations where ploughing and rubbing predominate, the relationship between plunge velocity and force intensity is non-linear, and high force intensities are required before cutting is possible. From this work, Hahn presents a theory relating the metal removal parameter to the force intensity, which holds good when grinding with negligible rubbing and ploughing present.

Grisbrook[28] investigated the cutting points on the surface of a grinding wheel, using a projection microscope, and measured the number of active cutting points per unit area, and the cutting-point spacing. He observed that the active cutting points wear, and form readily distinguishable striated flats on the grits, and that the number of active cutting edges decrease, and the area of the flats or wear lands increase as the wheels wear. Grisbrook has thus concluded that a grit may have a number of active cutting edges which merge into one as the grit wears. He quotes the number of active points per square inch for a newly dressed wheel, and a worn wheel, as 15,000 and 2,000 respectively.

Takeno and Nagaoka[29] have observed the cutting action of abrasive grains in the precision grinding operation by the use of electron-microscopic techniques. They found by observation of the shape of the abrasive grit cutting edge, that the angle of negative rake was very large, and that the majority of the chips formed in grinding tended to be removed from the workpiece in the lateral direction relative to the motion of the grit, rather than in the direction of cutting, the chips escaping ahead of the grit.

Tanaka, Tsuwa and Kawamura[30] have studied the rubbing of abrasive grits in the grinding process, and have observed by use of a microscope, a transition from rubbing to cutting as well as what is considered to be a scratch made by the bonding material. They conclude that when the depth of cut is smaller than the critical value

which is dependent on speeds, work materials and cutting edge condition,the cutting edges can only rub without chip formation. The critical grit depth of cut (independent of type of abrasive), becomes deeper for larger grit size, harder wheels, slower grinding speeds and wider wear lands.

Shonozaki and Shigematu[31] have also studied mechanisms of rubbing and biting of the cutting edge of abrasive grits. On microscopic examination of grooves made on a work surface when grinding with a single grit, they observed a transition from ploughing to cutting, and noticed a swelling in front of the cutting edge, and on both sides of the trace left by the tool. It is suggested that the frontal swelling may facilitate the bite of the cutting edge. Further observations showed that as the front swelling becomes larger, the shear stress along the cutting edge increases until it exceeds the ultimate strength of the work surface layer, and micro-cracks grow as the grit cutting edge bites into the work surface. They concluded that if a work metal loses the ultimate strength of its surface layer due to the very high temperature of the grinding action, chips will be formed even if the rake angle of the cutting edge is greater than -40 degrees, but by a mechanism peculiar to that case.

Takenaka[32] studied the grinding action using a single grit attached to the periphery of a steel disc. His results showed that metal is removed mainly by the cutting action of the grit, but that the rate of the process decreases with decreasing depth of cut. From his observations he concluded that in the case of small depths of cut of about .5 μm or less, all three processes of grinding action, namely cutting, ploughing, and rubbing exist. For extremely small depths of cut of .2 μm. rubbing predominates with the metal being torn in the form of 'leaves' from the workpiece, or comming from the flattened flank of the grains to which they had once adhered.

Sato[33] has reviewed the work of several researchers

on grinding in Japan. Okoshi et al., examined the effect of cutting speed on piling up when cutting various metals with a triangular pyramidal diamond tool having a rake angle of -45 degrees. The results suggested that a sufficiently high grinding speed may improve the efficiency of the grinding wheel. Sasaki and Okamura studied the effect of rake angle on piling up using ceramic tools to cut chromium steel. They found that the piling up increased linearly with the increase in rake angle. Sasaki et al., extended their research to speeds in the order of 3,000 m/min and found that both side piling up and normal piling up were linearly related to cutting speed. For all rake angles considered, an increase in cutting speed resulted in a decrease in piling up, and the greater the negative value of the rake angle became, the more an increase in cutting speed reduced the value of the piling up indices. Two piling up indices were used which may be defined as follows:-

The normal piling up index is the sum of the heights of the peaks on either side of a groove above the surface datum line, divided by twice the depth of the groove below the datum line. The side piling up index is the difference between the width of the groove and the length between the two outer bases of the peaks, both measured along the surface datum line, divided by the width of the groove. From their tests of oblique and triangular section cutting, they confirmed that flow type chips were obtained when the cutting edge angle (side rake), reached 40 to 50 degrees, even if the rake angle was -60 degrees.

2.5.2 Abrasive wheel wear.

Guest[23] was interested in determining which variables in grinding had to be altered to prevent the wheel from glazing , or wearing too rapidly. He considered that glazing occurs when the worn grits are not fractured or dislodged from the grinding wheel, and that by increasing the forces acting on each grit, the worn grits can be fractured or pulled out of the bond, thus exposing new

and sharp cutting points. Similarly, rapid wheel wear
was thought to occur when high forces act on the grits.

Guest concluded that to prevent the grinding wheel
from glazing, in the case of external cylindrical grinding,
there should be an increase in force per grit, i.e. an
increase in work speed and work diameter, or a decrease
in wheel speed. The reverse applies to prevent the wheel
from wearing too rapidly.

Krabacher[34] has shown that the grinding wheel wear
curve is similar to that for a single point tool, see
fig. 2.15, and explains the curve as follows:-

The initial wheel wear (1) is rapid, since the grits
are very sharp and likely to fracture when subjected to
the cutting forces. The second stage (11) shows a gradual
increase in wear caused by the dulling of the cutting
edges forming flats or wear lands (i.e., attritious wear),
as well as some grit fracture and pull out. The third
stage (111) is caused by excessive grit fracture and pull
out, when a large proportion of the grits are dulled, and
the cutting forces are increased. He states that the wear
of grinding wheels is both physical and chemical in
nature.

Hahn[26] studying the mechanisms of abrasive wheel
wear under plunge-cut grinding conditions, puts forward
the theory that wheel wear is caused by thermal stresses
set up in the surface layers of the grit, which cause a
gradual flaking out of the developing wear flats. He
disputes the conventional idea of wheel wear, where grains
become dull and are splintered or broken away from the
wheel bond due to increased force on them. Hahn argues
that mechanical failure of structures, on which the
conventional theory of wheel wear is based, is in general,
rapid and catastrophic, and this does not hold true under
the conditions he found of slow and controlled wheel wear.

Tarasov[35] states that there are three kinds of
interaction between grinding grits and work surfaces which
result in wheel wear, the generation of heat in the work
surface, and the formation of chips and abrasive particles.

Unlike cutting tool operations, the wear is an integral part of the process. Several different types of wear may occur, i.e. grain fracture, chemical reaction between abrasive and workpiece, bond-post fracture and attritious wear. He suggests that grain fracture occurs as a result of mechanical forces associated with chip formation, or due to thermal shock induced by instantaneous high temperatures. Attritious wear is also grit fracture, but on such a minute scale that grit surfaces appear smooth and glazed. The bond post may fracture as a result of the forces acting on it. Abrasion between the workpiece surface and the bond post may promote premature failure. When grinding some materials, e.g. titanium, the high temperatures occurring at grinding contact promote chemical reactions between chip and grit, resulting in rapid wear.

Yoshikowa and Sata[36] investigated the fracture of bond posts or bridges through brittle fracture. They have shown that the wear rate of grinding wheels can be expressed as an exponential function of the grinding force. Experimental results confirm their theoretical interpretation.

Tsuwa[37] conducted an investigation into grinding wheel cutting edges involving photography of the wheel face under a microscope. He concluded that the changing behaviour of cutting edges can be classified into several causes, i.e., wear, breakage, dig-out, newly appeared and partial breakage. The mechanisms of change of the cutting edge start with the dressed grits, where the cutting edge area has a rugged surface formed by grit breakage or cleavage. When these grits make contact with the workpiece the cutting edge starts to wear. At this time, some portion may be broken off, and if the amount of breakage is much larger than that of wear the breakage part no longer forms the cutting edge. In other words, the part which forms a cutting edge is always the worn surface of the grit.

Sato[33] describes the investigations of several researchers on abrasive wheel wear. Shiozaki, using a device in which the fragment of a grinding wheel was cemented to the periphery of a rotating disc, noticed that different

types of abrasives fractured into relatively small or large fragments depending on the material being ground. Takazawa and Yokoyama also studied the wear of different types of abrasive, and confirmed the results obtained by Shiozaki. Takenaka and Sasuya, by photographing the cutting edge of a grit from three different directions at intervals during grinding, found that grit wear occured in the form of flat areas on the grit flank side, and also as a result of the fracture of small portions of the grit adjacent to the cutting edges. They also observed that many small cracks and steps existed after grit cleavage.

Eiss Jr.[38] measured the fracture strength of a single grit of alumina abrasive when cutting mild steel, and expressed it as a function of depth of cut, the tangential force, and the number of cuts made before fracture. He concluded that the failure mechanism during the first few cuts is different from the mechanisms which cause long term failure, the definition of which must include progressive fracture and wear.

King,[39] investigating ceramic tool wear, has identified three separate wear processes when cutting steel, i,e,, plastic deformation, chemical reaction and micro-spalling. Wear of ceramic is dependent upon its deformational, chemical and fatigue properties, and to a degree can be varied by utilising work hardened ceramics. Although aluminium oxide is inert, it will react slightly with metal oxides, and these reactions do contribute materially to the wear process. When aluminium oxide and iron are heated in contact in an oxidising environment, the iron oxide film can and does react with alumina to form a thin layer of spinel ($FeO\ Al_2O_3$).

Duwell et al.,[40] have observed the role of chemical reactions in the preparation of metallic surfaces by abrasion, and the effects of lubricants on the process. They state that chemical reactions are promoted by the high temperatures produced by the dissipation of mechanical energy in the chip making process, causing dulling of grits

by chemical attrition. Freshly-formed metal surfaces may form strong adhesive bonds to the abrasive grits, leading to mechanical rupturing of the bond between the grit and the surrounding matrix. The introduction of sulphur and chlorine-containing hydrocarbon lubricants to the grinding process improved the wear resistance of the abrasive grits by reducing atmospheric oxidation.

Buttery and Archard[41] conducted a series of wear experiments using a wide range of abrasive grits, which were rubbed against metals (usually steels), the results being observed through optical and scanning electron microscopes. They found that under certain conditions, the rate of wear decreased with time, and at the same time, the worn debris changed from metallic particles to finely divided oxides, with the surface of the abrasive becomming glazed.

2.5.3 Forces in grinding.

Guest[23] realised that when grinding, the forces on the grits are related to the size of cut taken by each grit, and derived three equations for maximum undeformed chip thickness for external, internal and surface grinding. He assumed that the grit profile is approximately triangular , so that the maximum area of cut is proportional to the square of the maximum undeformed chip thickness, and that the force on the grit is directly proportional to the area of cut. Combining these ideas, he derived formulae for calculating the force per grit.

Alden[22] on the other hand, assumed that the maximum force per grit would vary directly with the chip thickness, and derived his equations on this assumption.

Marshall and Shaw[42] were perhaps the first researchers to produce a grinding force dynamometer which they used in their work on dry surface grinding. With this dynamometer, they measured the radial and tangential components of force seperately, and related them to wheel speed, table speed, depth of cut, table direction, grit

material and size, specimen hardness and dressing technique. Because the grinding was conducted without the use of coolant, work speed was limited to a maximum of 5 m/min, which imposed limitations on their work. From this work they established the co-efficient of grinding, i.e. Tangential force/Normal force = $\frac{1}{2}$, and found that the specific energy in grinding (calculated from force measurements and the volume of metal removed), is higher than that for single-point tool cutting processes by a factor of about ten.

Backer et al.,[24] have shown that specific energy decreases as the size of cut increases. They suggested that the high specific energy values are associated with a size effect in metals, based on the dislocation theory. They explained that due to the very small undeformed chip thicknesses involved in grinding, the deformation occurs on specimens containing few or no imperfections or dislocations, and the shear stress and specific energy are high.

Backer and Merchant[43] applied Merchant's solution of the mechanics of metal cutting, and the hypothesis that grinding is anologous to milling, and presented new geometrical concepts of grinding. From values of force ratio, interpreted in light of tool-face friction when turning with cemented-oxide tools, they suggested that the effective mean rake angle of the abrasive grits is roughly -30 degrees. They found from their experiments that higher cutting speeds can reduce the unit force (specific energy) on the grit by decreasing the grit-chip friction.

Grisbrook[44] and Grisbrook et al.,[45] also investigated the forces developed in surface grinding, and substantiated the values of specific energy and the co-efficient of grinding as found by Marshall and Shaw[42]. From his investigation, Grisbrook assumed an effective mean rake angle for the abrasive grits of -50 degrees.

Ono[46] has put forward theoretical expressions for the values of radial, tangential and axial components of . force in grinding. He considered the grinding force to be the product of mean force acting on one grit, and the

number of grits cutting at that moment in time, and assumed that the force on one grit is proportional to the grit cutting area. Ono concluded from the equations he derived, that the force in grinding increases as the depth of cut and wheel speed increase, and the wheel diameter decreases. He also finds that the grinding force increases with decrease in grit size, increase in wheel hardness, and decrease in wheel structure number.

Kobayashi[47] has derived formulae for the radial and tangential component of grinding force for five types of grit shape, i.e., cone, pyramid, sphere, worn cone and worn pyramid. Using these expressions, he suggests that wheel clogging and glazing give an increase in grinding force, and that wheel wear by grit fall-out reduces the grinding force.

Sato[33] conducted experiments into constant load grinding, and attempted to separate the friction term from the shearing term of the tangential component of grinding force. He found that the friction term in dry grinding of annealed steel can account for 70 - 80% of the tangential force component, whereas the shearing term accounts for only 20 - 30%. Sato cites the work of Kobayashi et al., who also separated the friction and shear terms of the tangential component of grinding force. They found that in surface grinding, as the width of specimen was increased in size, the shearing force term increased from zero to approximately 1.25 times the friction term. For a narrow specimen, the friction force term was higher than the shearing force term until the specimen reached a width of eight millimetres. From this point on, the shearing force term became dominant.

Yang[48] devised a surface grinding dynamometer using elongated octagonal rings with strain gauges fixed to them. This form of force transducer has advantages over the circular ring type since clamping of the dynamometer is made easy as well as the fixing of the strain gauges. He discusses the various design considerations, calculations and working principles, and also illustrates the method

of calibration and circuitry involved.

Landberg[49] describes a cylindrical grinding dynamometer for recording the tangential and radial components of grinding force whilst traverse or plunge grinding. Two cone centres are used which have flats ground on them to accept strain gauges. The strain gauges are so arranged to record the two components of grinding force through the use of two independent Wheatstone bridge circuits.

2.5.4 Influence of wheel dressing on the grinding process.

Pahlitzsch and Appun[2] are regarded as the first research workers to undertake a study in depth on the effects of truing conditions on circular grinding. Their paper, presented in 1954, gives a detailed account of the influence of the dressing tool shape (diamond profile), dressing depth of cut and traverse rate on grinding wheel surface roughness, called effective roughness, and designated R_s. The method they used to study the effective roughness of the wheel face was to rotate a steel test piece against the rotating grinding wheel such that the wheel and test piece both made one revolution in the same time. The surface of the test piece therefore became a "replica" of the surface of the rotating grinding wheel, and effective roughness could then be evaluated. Preliminary tests were conducted using a dressing diamond with a large clearance face, and altering the dressing traverse rate. They found that in all cases, the screw thread effect dressed onto the grinding wheel was apparent, and the uniform shape of the grooves showed that the diamond cuts through the individual grain as well as the binder, more or less according to the truing conditions. Further tests were conducted where the depth of cut in dressing was altered for progressively coarse traverse rates, their conclusion being that the screw thread effect became more pronounced as the traverse rate coarsened. Pahlitzsch and Appun concluded from their tests that the truing feed has a greater effect on the surface structure of the grinding wheel and its effective roughness than the infeed.

Using diamonds with different clearance faces, varying from .02 mm^2 to 1.1 mm^2, they found that changes in wheel effective roughness were considerable. For diamonds with clearance faces less than .3 mm^2, large values of effective roughness were observed, whilst those with clearance faces larger than .3 mm^2 gave little improvement on the effective roughness beyond a point. From grinding tests conducted after the dressing experiments, they reached the conclusion that the grinding wheel with the greatest original roughness shows the greatest wear for a minimum removal of stock.

Pahlitzsch and Thoeing[3] conducted new research into the truing process in grinding, in 1959. The dressing tools chosen by them were single point diamond tools using natural stones, Igel diamond truers, (which consist of several small natural diamonds bonded in a hard matrix) and diamond truing tools with well defined shapes, (diamonds cut in the shape of an equilateral pyramid with a square base, and a point angle between the sloping sides of 130°). By recording effective surface roughness, using the method described by Pahlitzsch and Appun,[2] they observed the wheel roughness before and after grinding. Immediately after truing, the grinding wheel possesses a sharpened profile which becomes more and more flattened during the grinding process as a result of wear. During the first subsequent grinding strokes, only the points of the surface irregularities come into contact, and they are therefore highly stressed, and wear away very quickly with a reduction in abrasive surface roughness. After further use, the area of the grinding wheel surface comming into contact with the workpiece is increased, so that the individual abrasive grain is under less pressure, the wear is less, and the abrasive surface roughness drops more slowly. Pahlitzsch and Thoeing conducted several experiments with single and multi-point diamond tools to examine their influence on the abrasive surface roughness with different infeeds and traverse rates. They found that for all Igel diamonds, the abrasive surface roughness at small traverse rates and infeeds, appeared to be

greater than with single diamonds, and explained the
reason for this as being that the single diamond was
comparatively blunt and had a large surface, whereas the
Igel diamond, which had been used for the first time, had
sharper diamond grits. Their overall conclusion was that
the more diamond particles used in an Igel dresser, the
smaller they are, giving a greater reduction in effective
height of roughness within the range of higher feeds and
depths of cut, in comparison with single point diamond
tools.

Thoeing derived an equation for abrasive surface
roughness in terms of dressing depth of cut and traverse
rate, and diamond-point geometry, from which he showed that
traverse rate had a more marked influence on surface roughness
than depth of cut, which he also proved experimentally.
This confirmed the opinions of Pahlitzsch and Appun.

Further work was conducted by Pahlitzsch and Thoeing
in which they derived a formula for wheel surface roughness
in terms of diamond inclination (drag angle), and point
geometry, and showed that as the value of drag angle increased,
the wheel surface roughness decreased. This was confirmed
using the specially prepared diamond tools.

Grisbrook et al.[45] noticed whilst conducting research
into the effects of wheel wear, forces and surface finish
in surface grinding, that wheel dressing had a marked
influence on the forces in grinding, particularly at the
commencement of grinding when the wheel breakdown was rapid.
For wheels dressed with sharp diamonds, the forces were
lower than for those dressed with blunt diamonds. They
also found that wheels having similar surface characteristics
obtained with either a blunt diamond or a sharp diamond,
traversed slowly across the wheel face, behaved differently
when grinding. To obtain repeatable results when grinding,
they had to adopt a standardised dressing technique.

Tsuwa[37] has looked at grinding wheels through an
electron microscope after dressing. He found that dressed
grits formed sharp cutting edges as a result of small
grit breakages. Heavy cuts using a diamond tool resulted

in poor cutting edges, and progressively worse results were
found using a crushing roller and a grinding stone respect-
ively. He concluded that when using diamond dressing tools,
an optimum dressing condition is obtained when the traverse
rate is equal to the width of the point on the diamond,
resulting in the most favourable distribution of cutting
edges. If the traverse rate is higher than this condition,
cutting edges become less than those necessary, and if
lower than this condition, the cutting edges become more
than is necessary to maintain good grinding conditions.

Pattinson and Chisholm[4] conducted work into the effect
of dressing techniques on grinding wheel wear using a sharp
diamond dressing tool, and varying the depth of cut and
traverse rate. They noticed that the coarser the dressing
feed, the greater was the initial wheel wear. After fine
dressing, the wheel had a high dimensional accuracy but
poor cutting efficiency. High metal removal rates were
not possible because of premature wheel loading. By
increasing the severity of dressing, the wheel structure
was made more open, providing more chip clearance for
higher metal removal rates. However, owing to the more
severe dressing, the grits and bond experienced greater
damage, and their loss or fracture during the initial
stages of grinding resulted in a high wheel wear rate.

Lindsey and Hahn[20,50,51] examined the effects of
wheel dressing on internal plunge grinding and set up
equations for abrasive wheel wear involving terms of
dressing lead, L and dressing depth of cut, $C/2$. They
found that the initial workpiece surface finish is
closely related to the lead dressed on the grinding wheel,
and that in dressing, the abrasive grits are cut and not
simply dislodged. Comparisons of surface records with
profiles of the wheel, showed close correlation. They
state that surface finish is dependent on dressing,
conformity, and normal force intensity only. Dressing the
wheel to act 'soft', i.e. $C/L = 1$, causes fast initial
wear, low force, and lower temperatures (heat carried
away with chip). Dressing the wheel to act 'hard', i.e.,

C/L = .05, causes glazing, high temperatures, and increased forces. (N.B. L remaining constant.)

Busch[13] cites several research workers who have studied the effect of wheel dressing on grinding. Ganger and Schwartz comment on the effects of wheel dressing on the way in which grits are cut, chipped or dislodged from the grinding wheel. For low depths of penetration, the abrasive grits are cut or chipped by the dressing tool, whilst at large depths of penetration the grits are dislodged from the bonding material. Both Schwartz and Stade have noticed that large dressing forces arise when fine-grained wheels are dressed. A very rapid increase in this force takes place when the diamond of the dressing tool begins to be even slightly worn. Busch has commented on the depths of cut and traverse rate in dressing as put forward by Ganger, Schwartz, Stade, Krekeler and Hornung. These have been reported on earlier, see statement 2.4.5.

Vickerstaff[19] conducted experiments into the effects of diamond dressing on work surface roughness in surface grinding, and used statistical methods to evaluate the influence of the dressing variables. He chose seven variables and allocated a high and low value to each. Dressing was then conducted using specially prepared single point diamond tools. From his significance test results he found that diamond shape, traverse rate, and combinations of the two with spark-out, were highly significant in affecting work surface roughness; number of diamond passes, spark-out passes and combinations of the two with traverse rate and diamond shape were less significant, and diamond depth of cut and wheel speed were least significant.

Kornberger and Koziarski[52] carried out a research programme to evaluate the cutting characteristics of grinding wheels dressed by different methods. The dressing tools chosen were a single point diamond tool, a helically grooved crushing roll and a rotating diamond-coated roll. Evaluation was conducted· on circular steel specimens using the cylindrical plunge grinding process. They concluded that grinding wheels dressed by means of rotating diamond-

impregnated rolls produced work surfaces of the highest
standards of surface finish, and those dressed with single
point diamond tools produced work surfaces which were only
slightly inferior to the diamond rolls. Crush-dressed
wheels could not ensure the standards of surface finish
which were achieved easily by the other two methods.
Grinding wheels which were dressed by diamond coated rolls
had the longest working life, and wheels dressed with single
point tools were only slightly less durable. Those which
were crush-dressed required dressing more frequently. On
the question of power consumption, when grinding was
performed with crush-dressed wheels, less power was required
in comparison with those dressed by other techniques, and
wheels dressed by means of diamond-coated rolls had the
worst performance of all. They found overall, that dressing
with rotating, diamond-coated rolls has much the same effect
as dressing with single-point diamond tools, and that the
helical-grooved crushing roll was inferior to both.

Bhateja et al.,[18,53] studied the effects of a care-
fully controlled dressing treatment on the wheel surface
characteristics, together with an assessment of the resulting
wheel performance during the grinding of a steel workpiece
when surface grinding. Two approaches to the study were made.
In one, the radial wheel wear, the active grit density, and
two components of the grinding force, were measured as the
wheel was used to grind material at a uniform rate. They
supplemented the result with a computer assisted investiga-
tion of a number of the characteristics of the wheel and
workpiece surfaces, in an attempt to predict the corres-
ponding characteristic properties of the ground workpiece
surface. For this they set up differential equations relat-
ing the number of peaks and valleys, relative to an arbitary
height level on the workpiece profile, after the passage
of a number of wheel cutting profiles. From this research
they concluded that fine dressing feed may give low wheel
wear, but result in a high grinding force, whilst a coarse
dressing feed can result in metal removal with a low force
but with a much larger loss of wheel material. From the

computer assisted approach they obtained theoretical workpiece asperity distributions which were compared with experimental results, and found discrepencies in the shapes of some of their predicted curves. The discrepencies were thought to be due to a neglect in the mathematical model of side displacement and back transfer of work material.

Baul et al.,[54] have looked at abrasive wheel surface topography after dressing with single point diamond tools, using a fibre optic transducer and an electro-mechanical (inductive) transducer. These transducers, when passed over a rotating grinding wheel, pick up surface irregularities i.e., in the case of the inductive pick-up, surface irregularities are monitored at slow-speed scanning of the surface, due to the low frequency response of the instrumentation; in the case of the fibre optic transducer, high speed scanning is possible. The transducer, which consists of a bundle of small diameter randomly distributed optic fibres, transmits light through some of the fibres on to the wheel surface. The other fibres receive the reflected light and transmit it to a photocell receiver which generates a current output dependent on the intensity of light received. The signals received from the two transducers (used independently) were fed through a correlator which computed values of the probability density function, the cumulative distribution function, and the autocorrelation function. Using these statistical parameters, Baul et al., analysed wheel surface topography and attempted to translate the results into meaningful terms. They found, using the probability density function, that the concentration of asperities (peaks) at the outermost level of the wheel surface is greater for finely dressed wheels i.e., wheels having a smooth surface. Coarse dressing conditions result in the concentration of asperities at the outermost level of the wheel surface to be fewer and perhaps less flat. They conclude that in-process measurement of grinding wheel surfaces is a possibility using the above mentioned statistical techniques, and that the optical transducer used for the few high-speed

tests carried out, is capable of resolving wheel out-of-roundness, wheel glazing and wheel loading.

Tsuwa and Yasui[55] conducted a micro-structure analysis of the dressed abrasive cutting edges using an elecron microscope after dressing with single point diamond tools. They found that the surface layer of the dressed abrasive cutting edges is formed of a fragile layer which can be classified into two kinds, depending on their mechanical properties. The first kind is composed of loosely bonded micro-fragments which are removed from the cutting edge under an extremely light load. The other possesses considerable mechanical strength in comparison with that of the former, though a lot of microcracks were observed on the surface. From grinding tests conducted, they gave the following analysis. The cutting edge surface, after a stock removal of 50 mm^3, was observed to be similar to that as just after dressing. After a stock removal of 300 mm^3 a micro-unevenness was noted, and a worn surface appeared on the cutting edge. As the stock removal increased beyond this point, the worn surface increased on the cutting edge, and finally the micro-unevenness disappeared from the abrasive surface altogether. They concluded that the fragile layer of the abrasive cutting edge only affected the grinding operation during the initial stage of grinding.

Malkin and Anderson[56] conducted an investigation into the relationship between the size distribution of abrasive particles removed from grinding wheels by dressing, and the number of active grains per unit area on the wheel for different grain sizes and wheel grades. They found that the number of active grains which are obtained during initial grinding is directly related to the size distribution of the particles removed by dressing. With finer grains and softer wheels, the active grain ratio is smaller, and relatively less fragmentation of the abrasive grains occurs during dressing. The smaller active grain ratio is attributed to relatively larger dressing particles with finer grain sizes and softer wheels, thereby generating a relatively rougher grinding wheel surface. For all

grain sizes and wheel grades, a single relationship was found between the active grain ratio and the percentage bond fracture during dressing. They concluded that the larger percent bond fracture with softer wheels was due to weaker bonding, thereby enabling fewer internal grain fractures to occur prior to dislodgement of the grain at the bond. Two explanations given for the smaller percent bond fracture with finer grain sizes, were increased toughness and a relatively larger dressing depth of cut and traverse rate with finer grains.

Pacitti and Rubenstein[57] have examined the influence of the dressing depth of cut on the performance of a single point diamond dressed alumina grinding wheel during surface grinding. They state that the useful working life of a grinding wheel cannot be determined with precision from either the force or wheel wear characteristics, but that it can be determined accurately from a plot of the normal force component against the tangential force component in grinding, when considering the slope Fn/Ft. This conclusion is based on the propostion that, provided the wheel is in a "stabilized" condition, then the normal component of the grinding force, Fn, is linearly related to the tangential component of the grinding force, Ft. They have shown, that for different dressing conditions, the point where efficient grinding becomes impared by rapid wheel wear, is heralded by an increase in the slope of the plot Fn/Ft.

2.6   A SUMMARY OF THE ABOVE WORK.

The following narrative is a summary of the above work, highlighting those aspects of the dressing and grinding processes that have been shown to be important. parameters in their study, and have consequently been used by the author as a guide when planning this research work.

It has been shown by several researchers[5,11,12,13] that when dressing, the orientation of the diamond tool . relative to the grinding wheel is an important parameter which can influence the degree of diamond wear considerably,

and must therefore be regarded as a powerful variable. The implications here are that diamond orientation must be maintained constant to ensure a constant wear rate, other things being equal, and that wherever possible, the selection of a "preferred" orientation is advantageous if diamond wear is to be minimised.

Another parameter which is considered by the author to be equally important, but has not received the same degree of consideration as diamond orientation is that of drag angle. Many researchers [14,15,16,17] quote a preferred range of drag angle values of between 5° to 15° but do not discuss its influence on dressing performance. It is hoped to show in this research that this parameter is inadequately specified since it does not take into consideration the geometry of the dressing diamond itself, this being thought to be important, particularly where shaped diamonds are used.

Early work in dressing[2] has stressed the importance of the cross-feed of the dressing tool as a dressing variable, and this opinion has been supported by later work. [3,4,18,19,53.] Several researchers have linked cross-feed and in-feed together in their analyses of the dressing process,[2,3,4,18,19,20] and have shown that in-feed is of secondary importance when compared with the influence of cross-feed in dressing. Equations have been derived[3,19,20] relating in-feed, cross-feed and diamond tool geometry to wheel surface roughness after dressing, which show that theoretical values of surface roughness can be predicted which compare reasonably well with those obtained in practice. Following on from this initial work it will be shown by the author that the cross-feed and in-feed (modified) in dressing can be combined with the in-feed, traverse rate, wheel and work speeds when cylindrical grinding, to predict the workpiece surface roughness, this being verified experimentally.

It has been observed from the study of the cutting action of the dressing tool,[8,45] that grinding wheels having similar surface characteristics obtained with

either a blunt or sharp diamond behave differently when grinding, making it necessary to adopt a standardised dressing technique to obtain repeatable results when grinding. This fact raises the point that it may also be necessary to adopt a standardised pre-dressing technique to ensure a consistent wheel surface prior to dressing.

The forces in dressing have been measured by several researchers in the past,[13,62] and comments about the outcome have been made which are somewhat general in nature and of little practical value. In the author's opinion, a knowledge of such forces can be used as a means of assessing the importance of the variables in dressing, and has been made use of in this research.

Much work has been done which shows the importance of grinding force measurement as a means of analysing the influence of the dressing variables on the grinding process.[20,42,45,50,51,57] In particular it was noted by several researchers[45] that wheel dressing had a marked influence on grinding forces at the commencement of grinding when the wheel breakdown was rapid.

The final parameter to be mentioned here is that of the grinding ratio. It was used initially two decades ago to show the rate of grinding wheel wear with volume of metal removed in grinding,[34] and has since been used by many researchers[18,44] to assess the influence of dressing and grinding variables on the grinding process. The author found it of particular use as a means of assessing the influence of dressing variables on cylindrical grinding at the commencement of grinding.
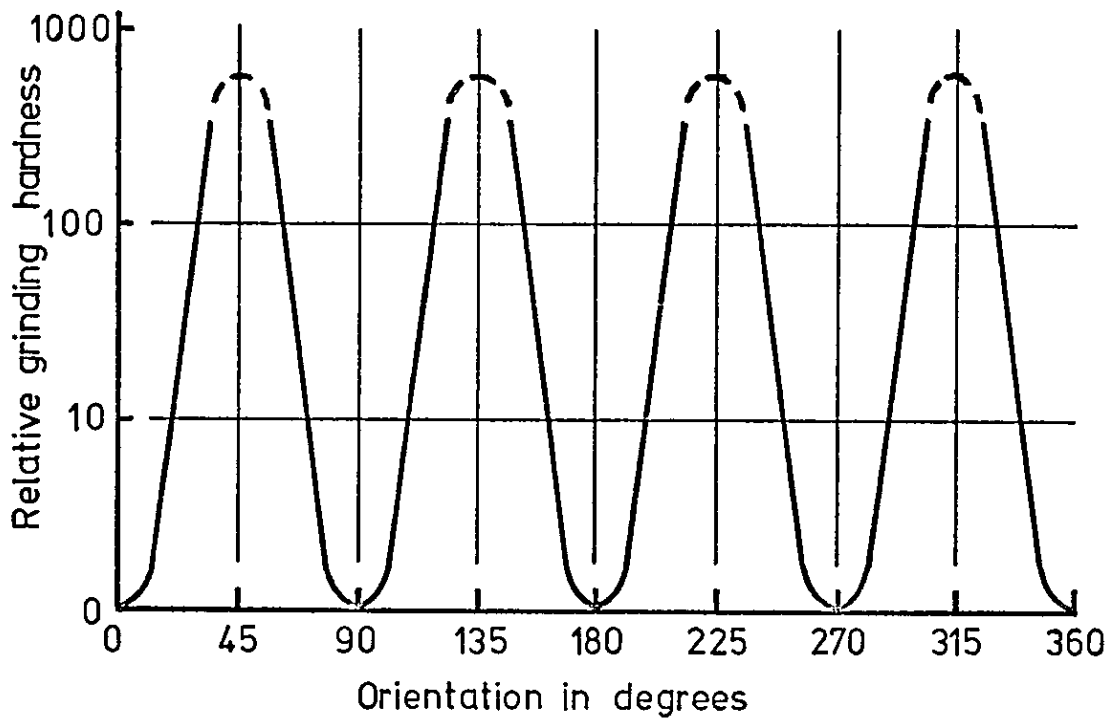
Fig. 2.1   The relative grinding hardness of the cube
plane of diamond. A cube axis of the diamond
is taken as zero azimuth.
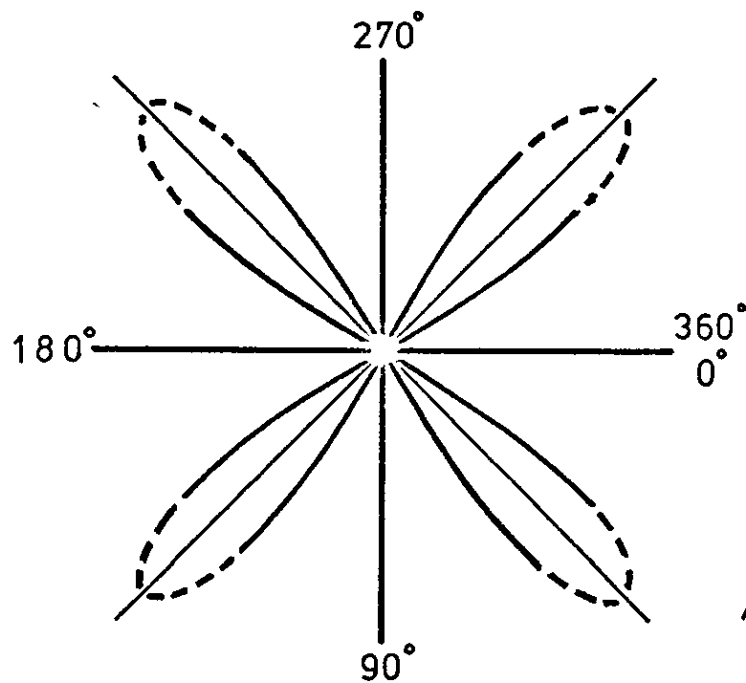
Fig. 2.2   The vector grinding hardness of the cube
plane of diamond derived from figure 2.1
and plotted as a function of the azimuth.
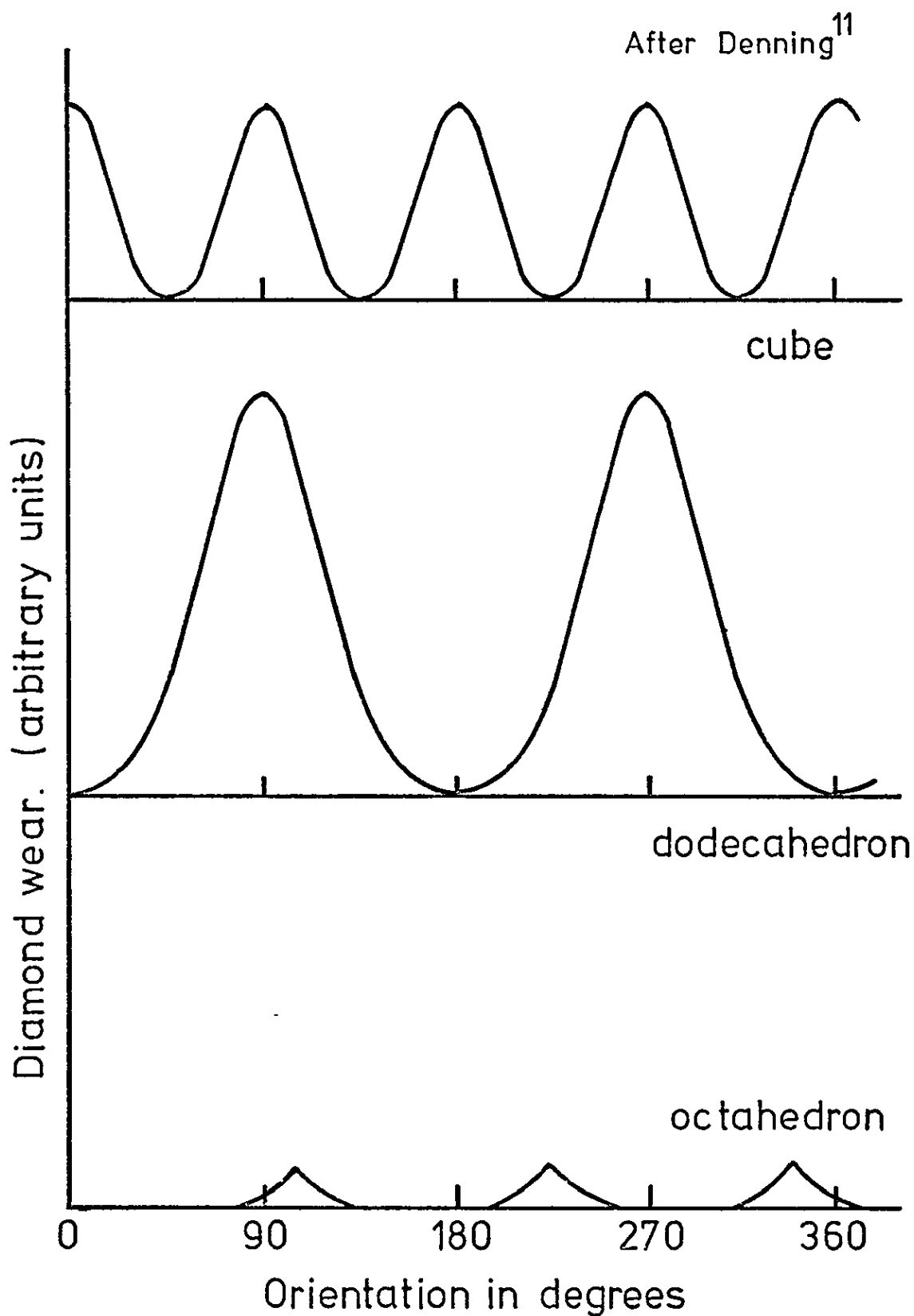
Fig. 2:3   The relative wear of the dodecahedral, octahedral and cube planes of diamond as a function of the azimuth.

cube face (001)

a

octahedron
face (111)

dodecahedron face (110)
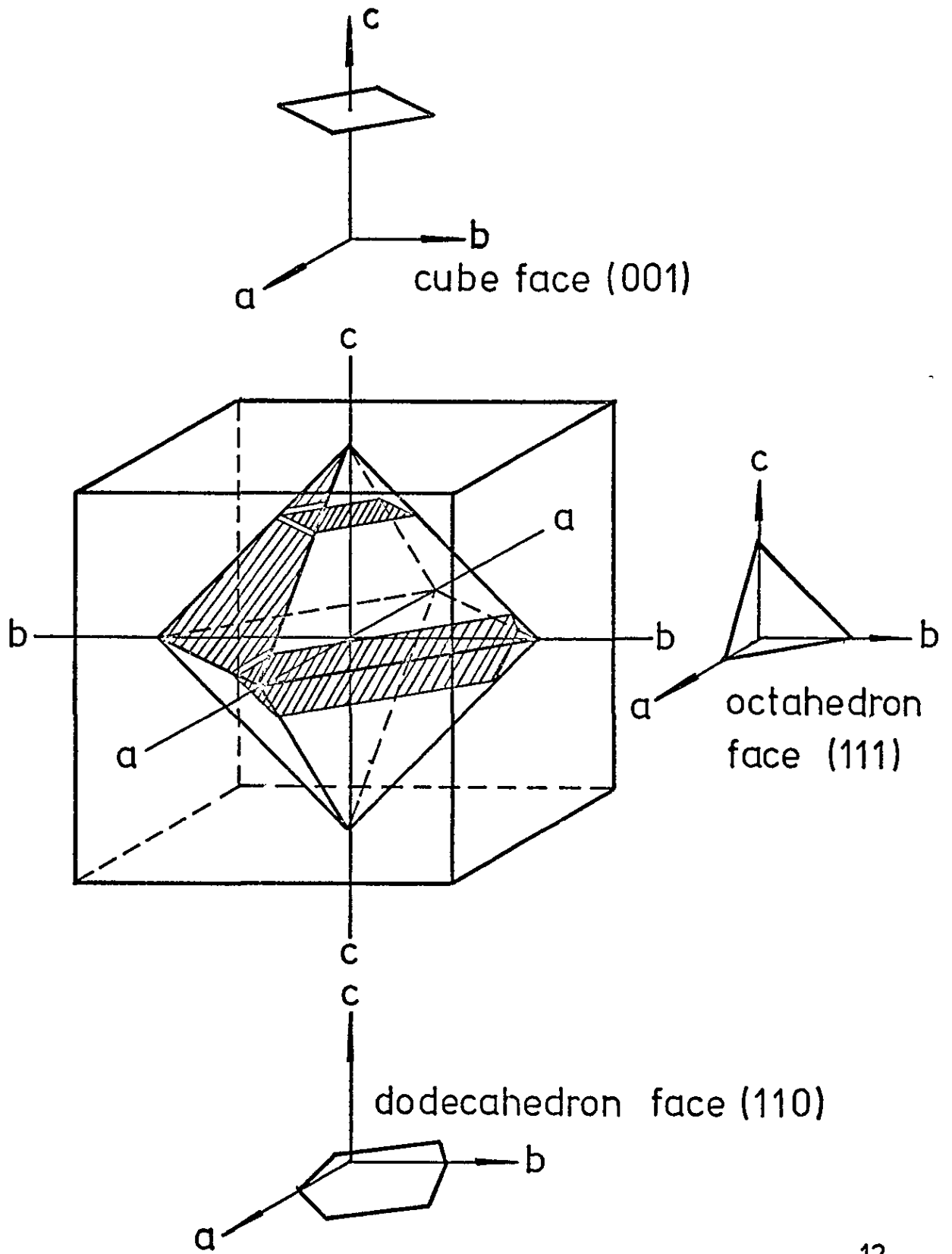
After Wilks & Wilks[12]

Fig. 2.4   Representation of the diamond
octahedron in the diamond cube.

grinding wheel

diamond

velocity and cutting force vectors

Fig. 2.5

grinding wheel
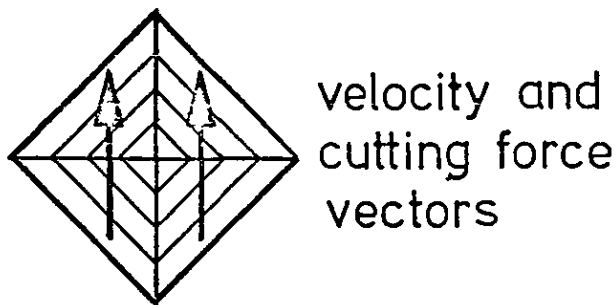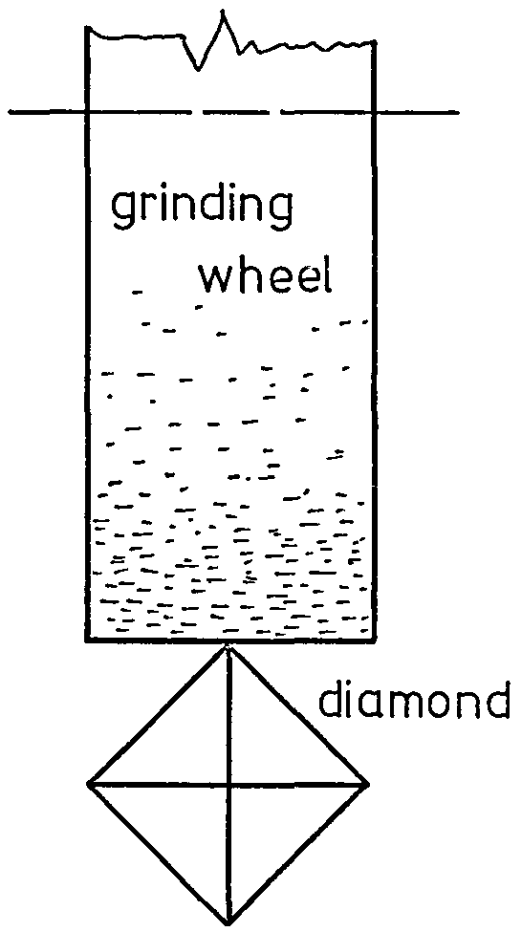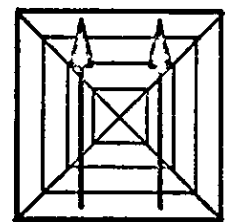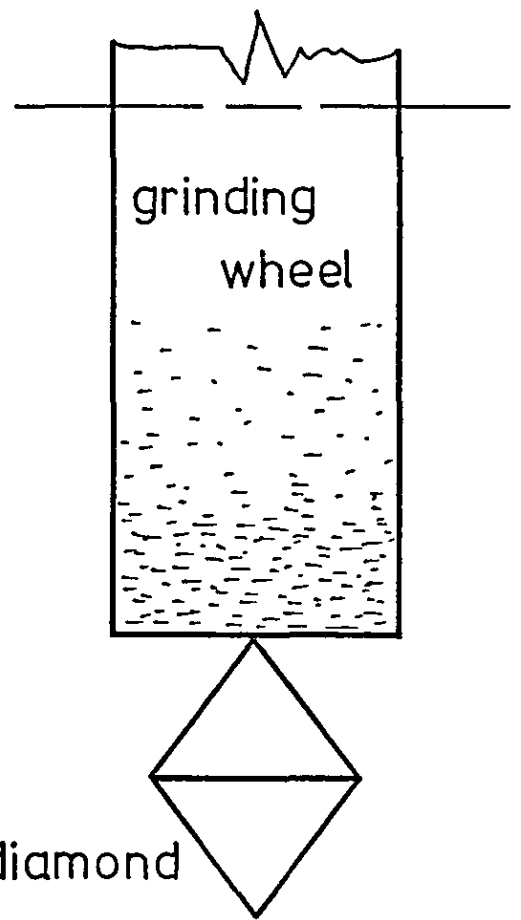
diamond

Fig. 2.6

Fig. 2.5   Orientation for preferred dressing direction according to Frank and Busch.[13]

Fig. 2.6   Orientation for preferred dressing direction according to Grodzinski.[13]
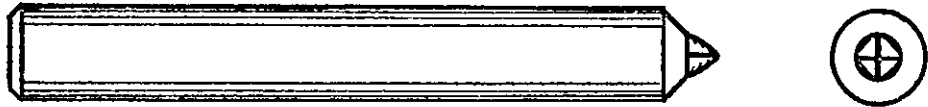
single point diamond tools
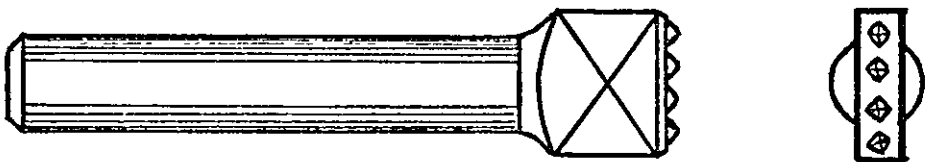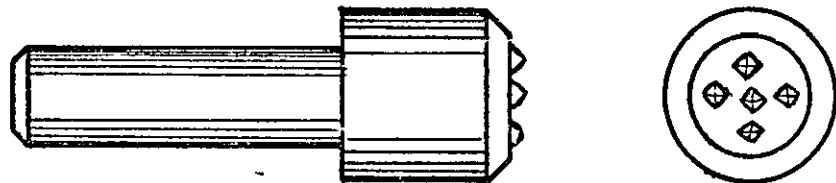
multi-point diamond tools

Fig. 2.7   Single and multi-point
            diamond dressing tools
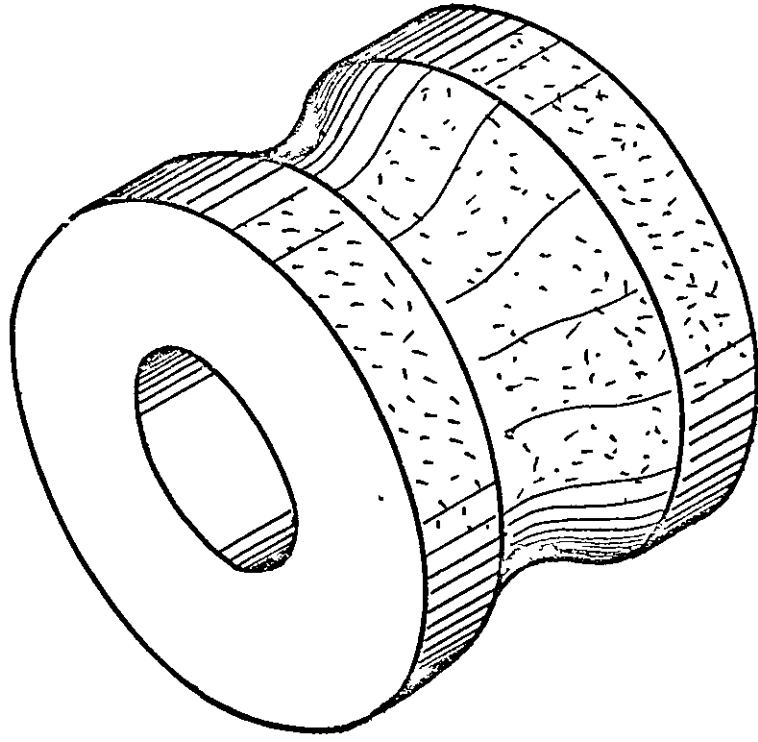
Fig. 2.8   Diamond impregnated
dressing roller
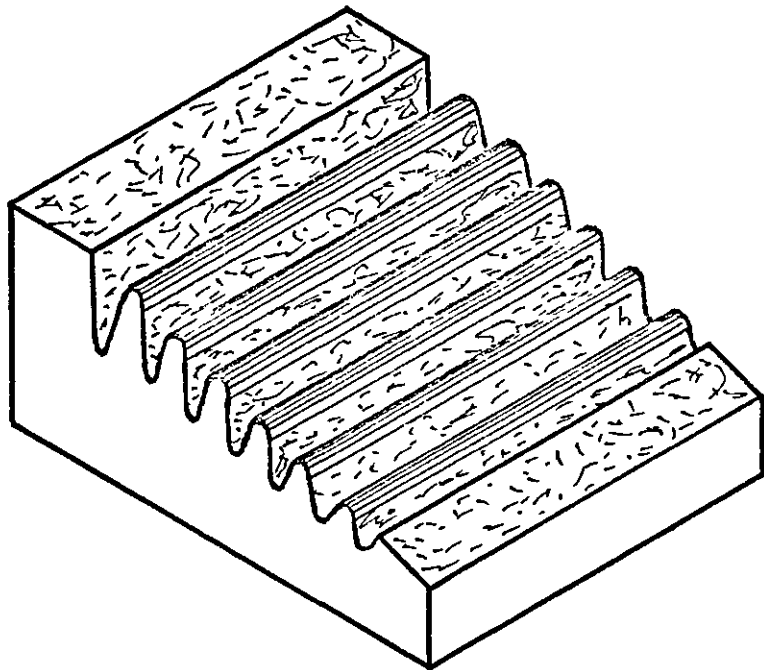
Fig. 2.9   Diamond impregnated
dressing block

| Wheel Diameter & Face Width | | Diamond Wt. |
inches	mm	Ave. Carats
6 x ·5	152 x 13	·25 to ·3 K
8 x 1	203 x 25	·5 to ·75 K
10 x 1	254 x 25	
12 x 1·25	305 x 31	1 to 1·5 K
14 x 1·5	356 x 38	
18 x 1·5	457 x 38	
18 x 2	457 x 51	1·5 to 2 K
20 x 2	508 x 51	
24 x 2	610 x 51	
24 x 3	610 x 76	2K and over
and over		

After Smith[14]

Fig. 2.10 Recommended diamond weights
for different grinding wheel diameters
and face widths.

DIMENSIONS OF DIAMOND DRESSING TOOLS (To BS 2002:1953)										
Straight and Headed Shank Types								Taper Shank Type		
SHANKS				SHANK HEADS				SHANK	HEAD	
Diameter D		Length L		Dia. HD		Length HL			Dia. HD	
in.	mm	in.	mm	in.	mm	in.	mm		in.	mm
1/4	6	2	50							
5/16	8	2	50	1/2	12.5	1/2	12.5	No. 1 Morse Taper * as BS 1660	1/2	12.5
3/8	9.5	2	50							
7/16	11	2	50	5/8	16	5/8	16		Length HL	
1/2	12.5	6	150	3/4	19	3/4	19		in.	mm
5/8	16	6	150						1/2	12.5
3/4	19	6	150							

Straight Shank Type Tool

L

D

90°
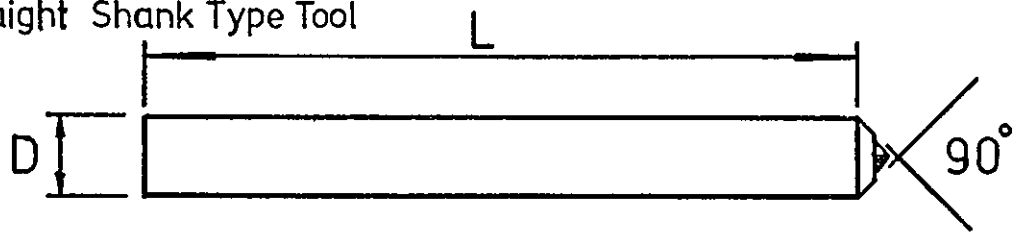
Headed Shank Type Tool

L   HL

D   HD   90°
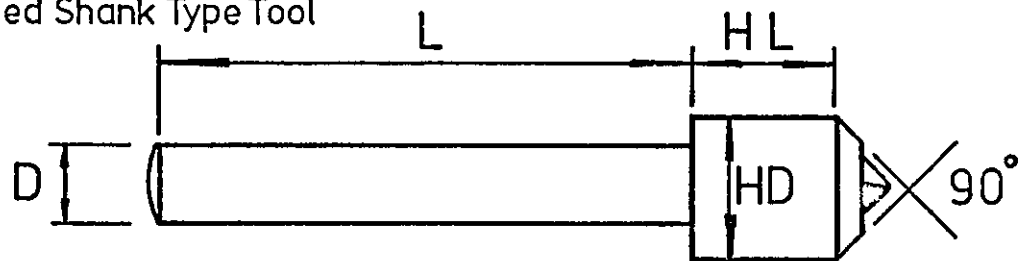
Taper Shank Type Tool

2.25″   .5″

.369″*   *D   .5″   90°

L*
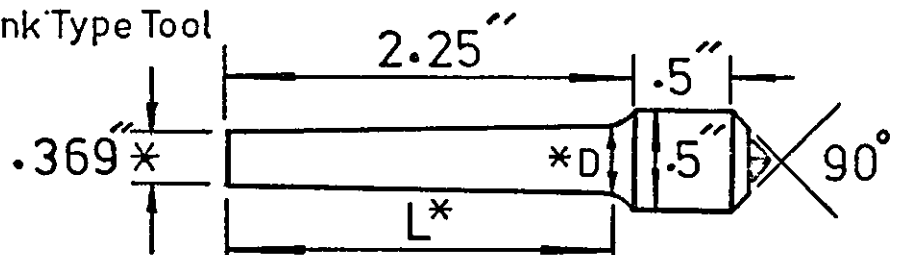
Fig. 2.11   Dressing tool shank dimensions covered by BS 2002 : 1953
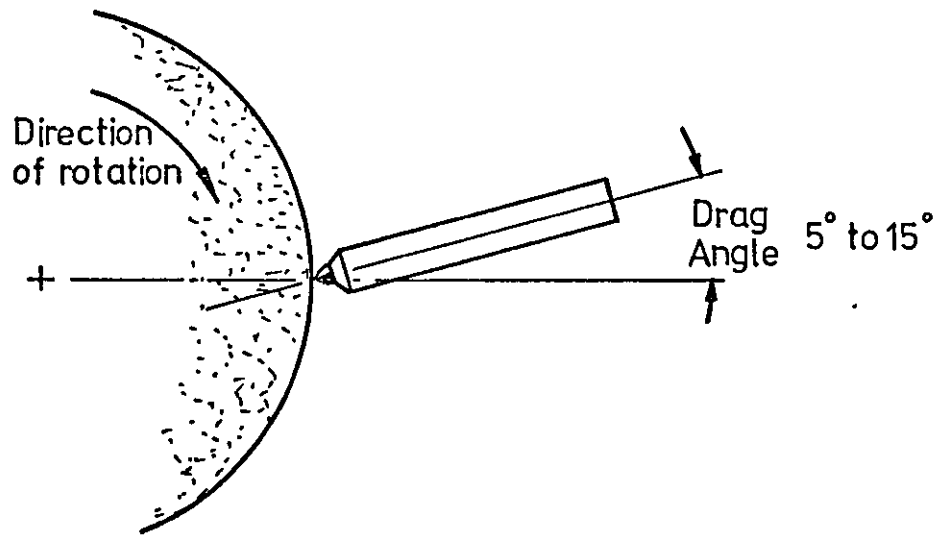
Fig. 2.12   Inclination of the diamond dressing tool to the grinding wheel in the vertical plane
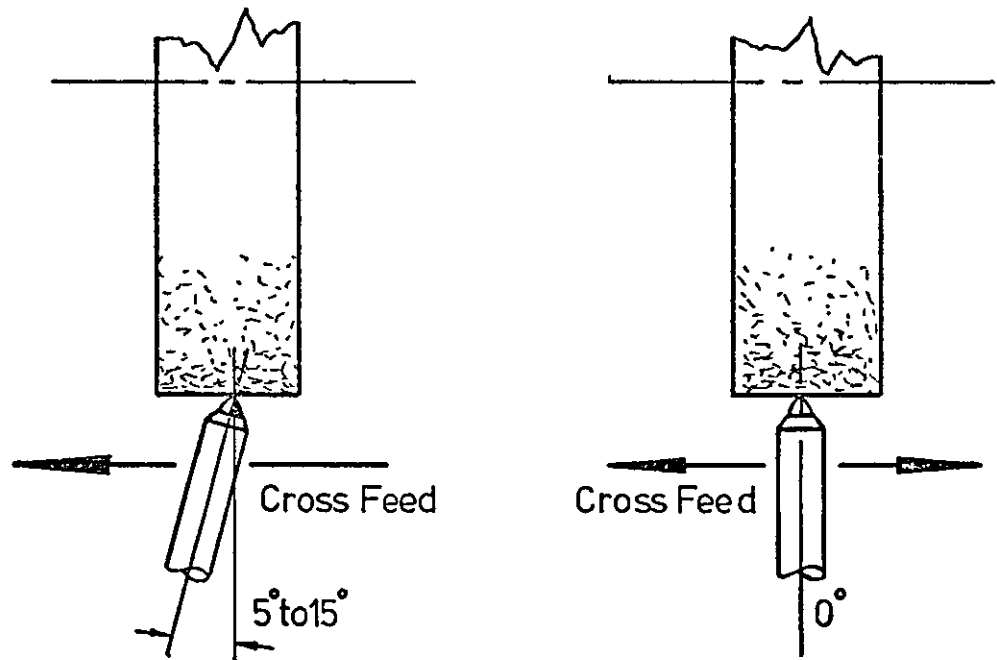
Fig. 2.13   Two views showing the effect of diamond dressing tool inclination in the horizontal plane on cross feed direction.
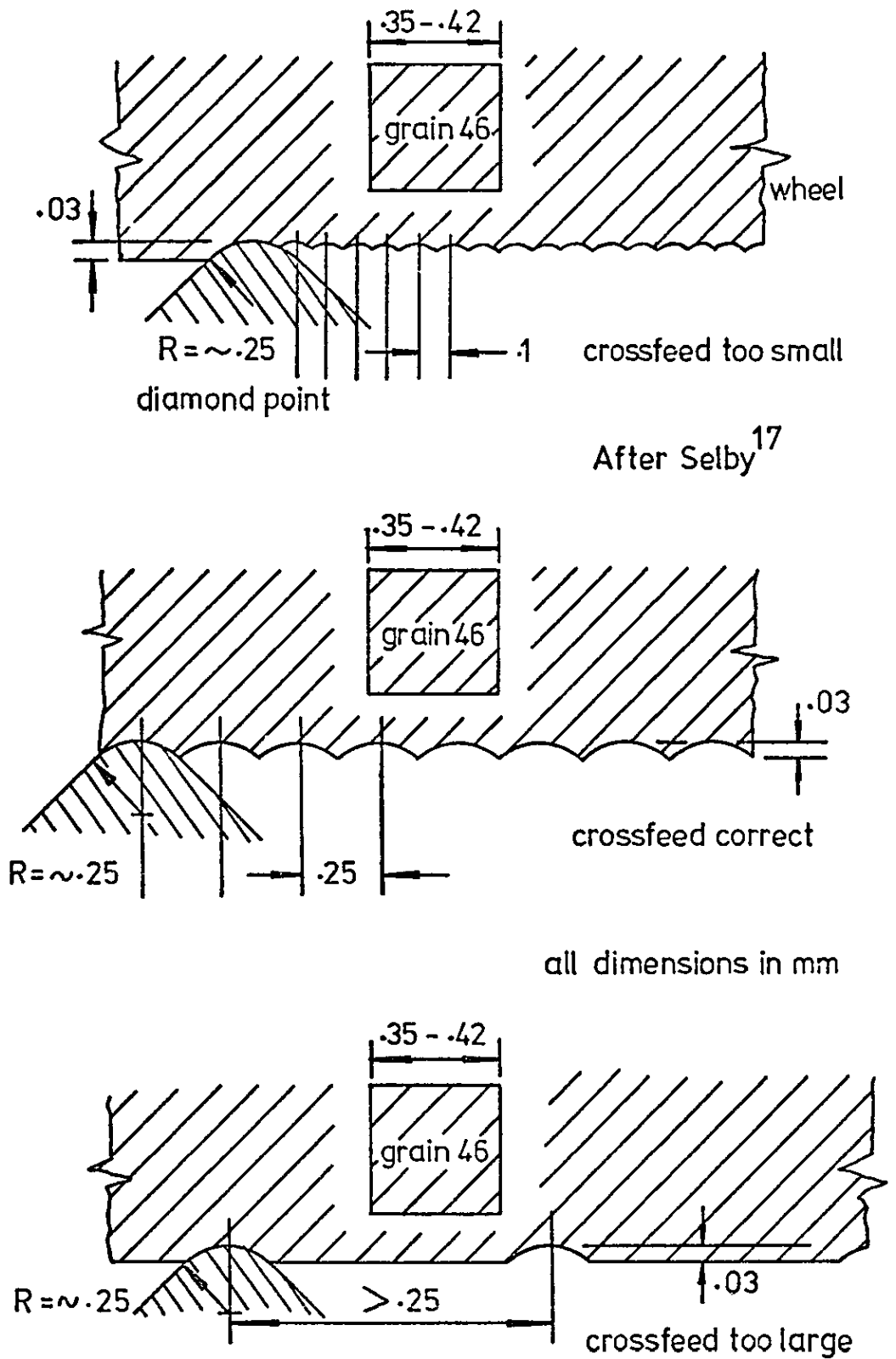
Fig. 2.14　Influence of crossfeed in dressing on grinding wheel surface roughness

$$\text{Grinding ratio} = \frac{x}{y} = \frac{\text{volume of metal removed}}{\text{volume of wheel worn away}}$$

Fig. 2.15   Grinding wheel wear curve
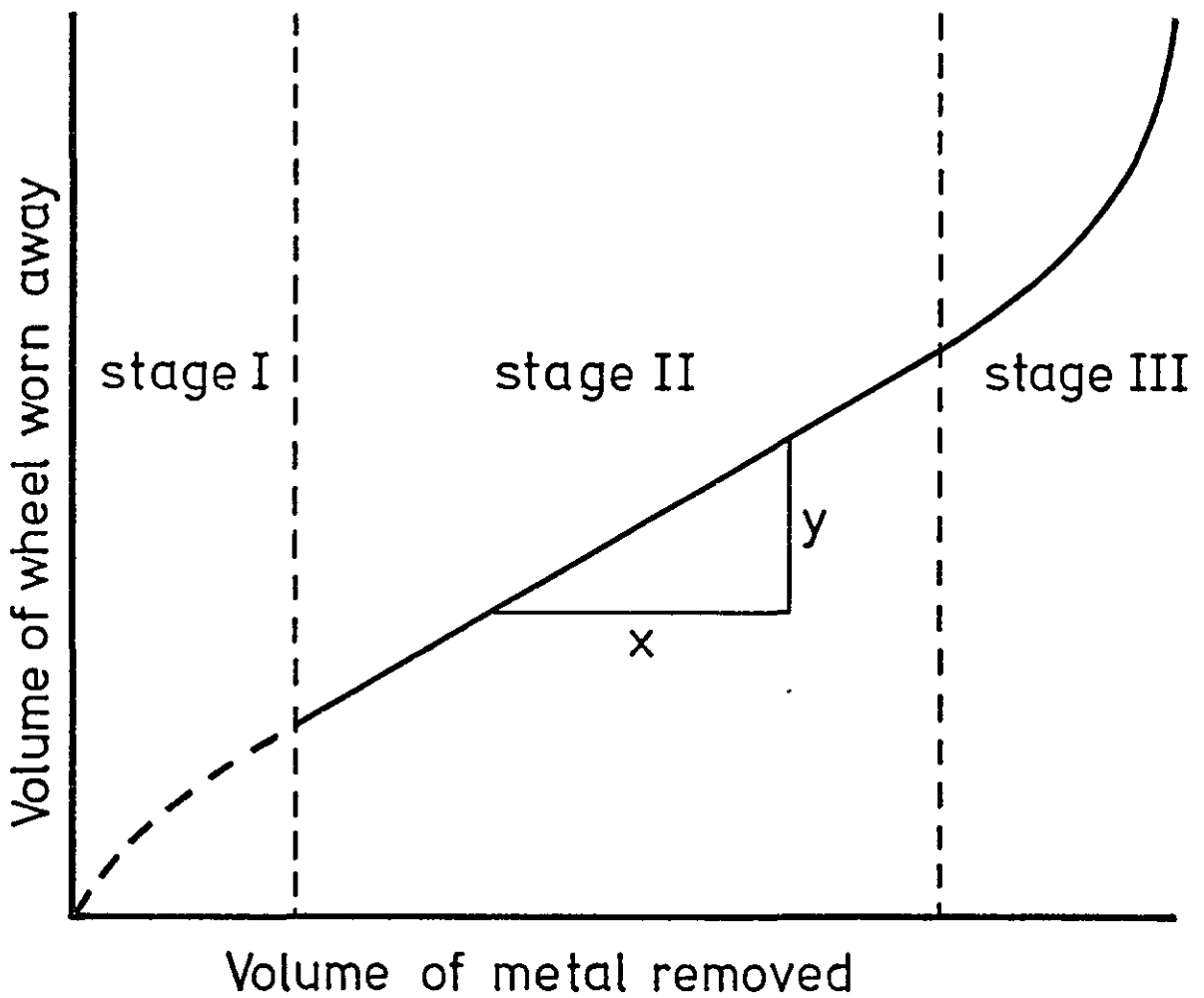
after Krabacher[34]

Stage I	rapid wheel wear
Stage II	uniform wheel wear
Stage III	catastrophic wheel wear

CHAPTER 3

THE INFLUENCE OF DRESSING AND GRINDING VARIABLES
ON THE SURFACE CONDITION OF THE GRINDING WHEEL
AND WORKPIECE, FROM A THEORETICAL POINT OF VIEW

3.1 INTRODUCTION

Grinding is considered primarily, as a finishing
process, and is used to produce components to fine limits
of size. Where fine limits are concerned, the surface
finish produced by grinding becomes an important parameter,
and can affect the components function in service, and
its working life considerably, particularly if the
component is to be used wholly or in part as a bearing
surface.

Several researchers in the past have shown that
the surface finish produced on a component by grinding
bears a close resemblance to the grinding wheel surface
condition, and that this in turn is dependent on the way
in which the grinding wheel has been dressed.[2,3,19,20,50,51]
In particular, Thoeing[3] derived an expression for the
theoretical abrasive surface roughness Rm, for a grinding
wheel dressed with a sharp, single-point diamond tool, and
explained the relative importance of diamond apex angle,
depth of cut and traverse rate, and how they affect surface
roughness.

In this chapter, Thoeing's approach has been adopted
by the author, and alternative expressions for abrasive
surface roughness have been derived which take into account
diamond wear. Extending this approach to cylindrical
grinding, an expression for workpiece surface roughness has
been derived in terms of dressing and grinding variables,
from which values of workpiece surface roughness can be
predicted for any given set of conditions.

The validity of these expressions is discussed in
Chapter 7, where calculated values of wheel and workpiece
surface roughness are compared with those obtained
experimentally.

3.2   CHOICE OF SURFACE MEASUREMENT PARAMETER

The surface measurement parameter which has been chosen to analyse the theoretical surface roughness of both grinding wheel and ground workpiece is Ra. Whilst this parameter is not an ideal means of assessing surface quality, since it gives only an arithmetical average value of surface roughness, it is used extensively in industry. (Definitions of surface finish terms are found in Appendix I)

3.3   THE INFLUENCE OF DRESSING VARIABLES ON THE GRINDING WHEEL SURFACE CONDITION

3.3.1   Assumptions made:-

1. The grinding wheel is considered as a homogenous structure.
2. The diamond dressing tool is considered to have a geometrically uniform profile.
3. The dressed wheel takes on the same shape as the diamond tool producing it.
4. There is negligible waviness in the dressed profile.

3.3.2   Dressing parameters:-

h =	dressing lead of the diamond	mm/rev
a =	diamond depth of cut	μm
β =	included angle of the diamond	degrees
w =	width of the diamond wear flat	mm
x =	diamond width at a depth of cut a	mm

3.3.3   Dependency of the parameters.

Parameters selected by the operator	a and h
Natural parameters	β and w
Dependent parameter	x (fn of a, β and w)

3.3.4   Calculation of Ra (and Rp)

The derivation of the following expressions for Rp and Ra (Mean Line and Centre Line Average values of surface roughness respectively) are found in Appendix II.

Case 1. (hypothetical)   (w = 0 , h = x)
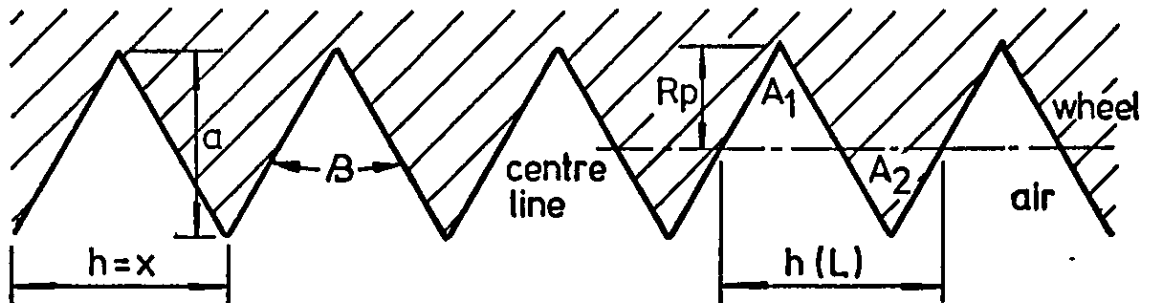
Fig. 3.1

From fig. 3.1 it can be shown that

$$Rp = \frac{a}{2} \qquad\qquad \dots (3.1)$$

and $\quad Ra = \frac{a^2}{2h} \tan \frac{\beta}{2} \qquad\qquad \dots (3.2)$

Simplifying Ra in terms of a

Now $\quad h = 2a \tan \frac{\beta}{2}$

Substituting for h in eqn. (3.2)

$$\therefore \quad Ra = \frac{a}{4} \qquad\qquad \dots (3.3)$$

Equation (3.3) gives the basic form of Ra in terms of a. This is a hypothetical case, where the diamond dressing tool is considered to be "sharp" (w=0), and the dressing lead h, is equal to the diamond width x, at a depth of cut, a.

The following cases can be checked against equation (3.3) for their truth.
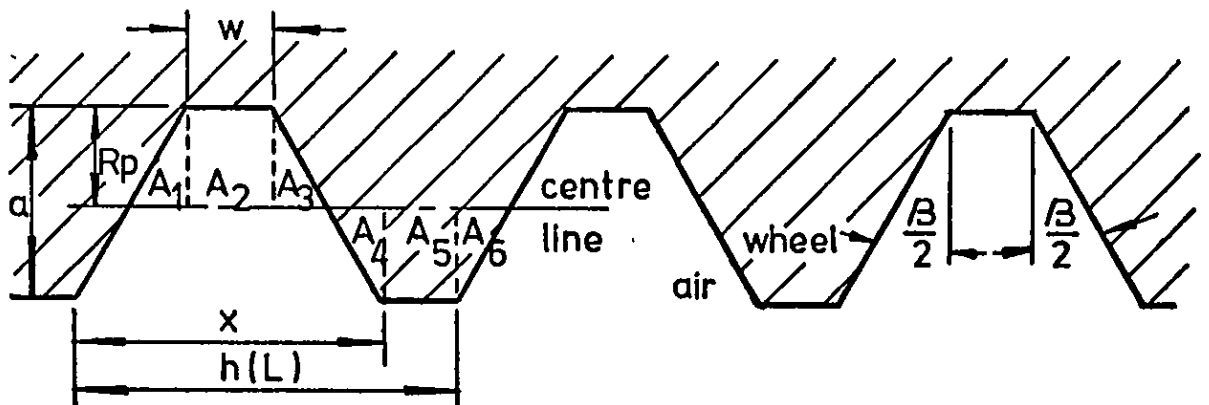
Fig. 3.2

From fig. 3.2 it can be shown that

$$Rp = \frac{a}{h}(h - w - a \tan\frac{\beta}{2}) \qquad \ldots (3.4)$$

$$\text{and } Ra = \frac{2a}{h^2}\left(\frac{a}{h} \tan\frac{\beta}{2} (h - w - a \tan\frac{\beta}{2})^2 \right.$$
$$\left. + w(h - w - a \tan\frac{\beta}{2}) \right) \qquad \ldots (3.5)$$

Case 3. $(x = h)$
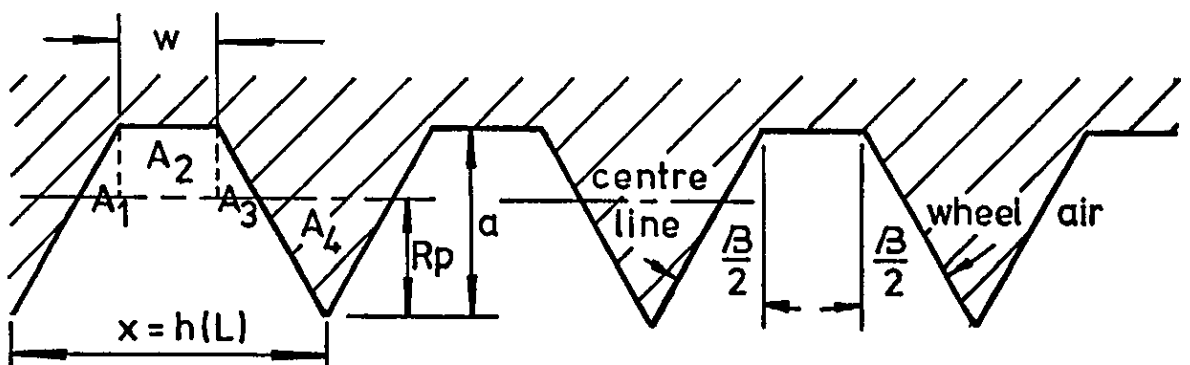
Fig. 3.3

From fig. 3.3 it can be shown that

$$Rp = \frac{a^2 \tan \frac{\beta}{2} + wa}{w + 2a \tan \frac{\beta}{2}} \qquad \ldots (3.6)$$

$$\text{and} \quad Ra = \frac{2}{h^3} \left(a^2 \tan \frac{\beta}{2} + wa \right)^2 \tan \frac{\beta}{2} \qquad \ldots (3.7)$$

Case 4. <u></u>   (x > h)

Fig. 3.4

a = apparent depth of cut
a´ = actual depth of cut
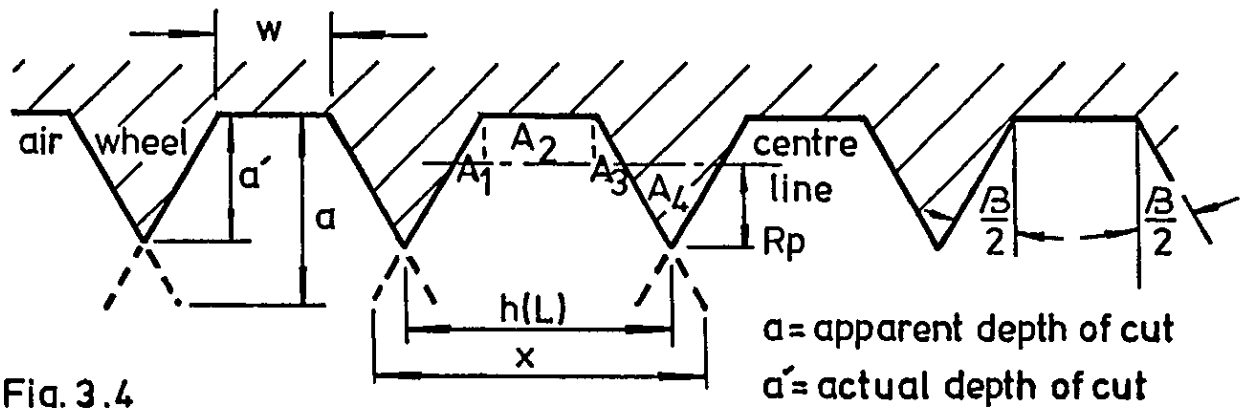
From fig. 3.4 it can be shown that

$$Rp = \frac{(a´)^2 \tan \frac{\beta}{2} + wa´}{w + 2a´ \tan \frac{\beta}{2}} \qquad \ldots (3.8)$$

$$\text{and} \quad Ra = \frac{1}{8h^3} \cot \frac{\beta}{2} \left(h^4 - 2h^2 w^2 + w^4 \right) \qquad \ldots (3.9)$$

Equations (3.5), (3.7) and (3.9) are used for obtaining mean values of surface roughness, Ra, for a grinding wheel when dressing with a single point diamond tool. In the limiting case of equation (3.9), when $h = w$, the value of Ra is zero, and the grinding wheel surface is considered to be perfectly flat.

The effects of the dressing variables on the grinding wheel surface roughness, Ra, will be discussed later in the chapter, after the following section.

3.4 THE INFLUENCE OF DRESSING AND GRINDING VARIABLES ON THE WORKPIECE SURFACE CONDITION

3.4.1 Introduction

In circular traverse grinding, only a portion of the wheel width is involved in grinding the workpiece, leaving the remainder to trail behind the cutting portion. This causes the wheel to overlap the previously ground surface, and results in the reduction of the effective surface roughness. The grinding variables causing this effect, i.e, wheel width and workpiece traverse rate, and rotational speed, will be considered in conjunction with workpiece diameter, wheel diameter and rotational speed, dressing conditions, and depth of cut in grinding, to establish a relationship between these variables and the average arithmetic roughness, Ra, of the ground workpiece surface.

3.4.2 Assumptions made:-

1. The assumptions for the dressing conditions are the same as those in statement 3.3.1.
2. The dressed surface condition of the grinding wheel is transferred to the workpiece when grinding, with no sideways displacement.
3. The depth of cut in grinding is greater than, or equal to the depth of cut in dressing.
4. There are no spark-out passes.

3.4.3 Parameters considered:-

Dressing

The same as those stated in statement 3.3.2.

Grinding

N	=	rotational speed of grinding wheel.	rev/sec
n	=	rotational speed of workpiece	rev/sec
D	=	diameter of grinding wheel	mm
W	=	width of grinding wheel	mm
d	=	diameter of workpiece	mm
l	=	length of workpiece	mm
V_t	=	traverse rate of workpiece	mm/sec

ϕ_L = Lead angle of the grinding wheel path
over the workpiece surface.   degrees

ϕ_h = Lead angle of the ground surface
scratches on the workpiece   degrees

Boundary coefficients

z_1, z_2, z_3 ....z_r ; b_1, b_2, b_3 ....b_r dimensionless

u_1, u_2, u_3 ....u_r ; e_1, e_2, e_3 ....e_r dimensionless

X_1, X_2, X_3 ....X_r ; A_1, A_2, A_3 ....A_r dimensionless

T_1, T_2, T_3 ....T_r ; I_1, I_2, I_3 ....I_r dimensionless

K_1, K_2, K_3 ....K_r mm

$\bar{z}_1$, $\bar{z}_2$, $\bar{z}_3$ ....$\bar{z}_r$ mm

p and q   mm

m and y'   mm

Surface finish coefficients

E_1, E_2, E_3 ....E_r mm

Δ_1, Δ_2, Δ_3 ....Δ_r mm

3.4.4 Factors affecting workpiece surface finish in circular traverse grinding.

Before values of average arithmetic roughness, R_a, can be calculated for a ground surface, a relationship has to be established between the surface patterns produced on the workpiece and the variables producing them.

Fig. 3.5 shows the set up for cylindrical traverse grinding.
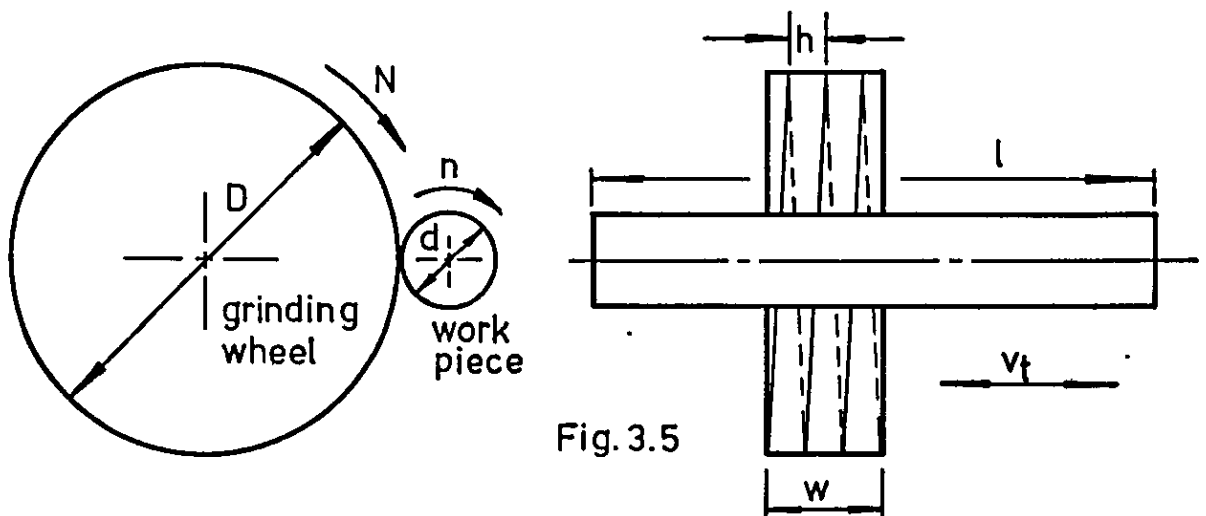
Fig. 3.5

Consider a grinding wheel of diameter D mm, which has been dressed with a single point diamond tool, at a traverse rate of h mm/rev. This will produce on the wheel surface a screw thread of pitch h mm. Let the wheel rotate through one revolution in the time $1/N$ seconds. If, during this rotation, the wheel is brought into contact with the workpiece, which is rotating at n rev/sec, grooves will be ground in the workpiece surface, corresponding to the dressing lead on the wheel surface. See fig. 3.6.

Consider now one revolution of the workpiece in the time $1/n$ seconds. During this time, the grinding wheel will make N/n revolutions, and the surface pattern produced will extend a distance of hN/n mm along the workpiece axis. For further revolutions of the workpiece, interference may occur between the surface pattern previously ground, and that being ground. See fig. 3.7.

Fig. 3.6
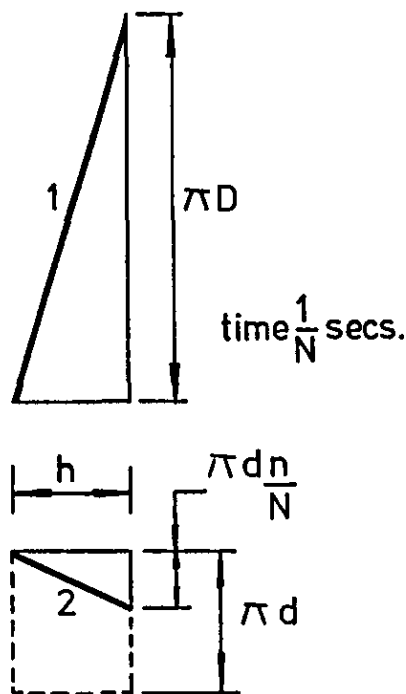
Fig. 3.7

1. screw thread effect on grd. wheel.
2. .. .. wk.piece.
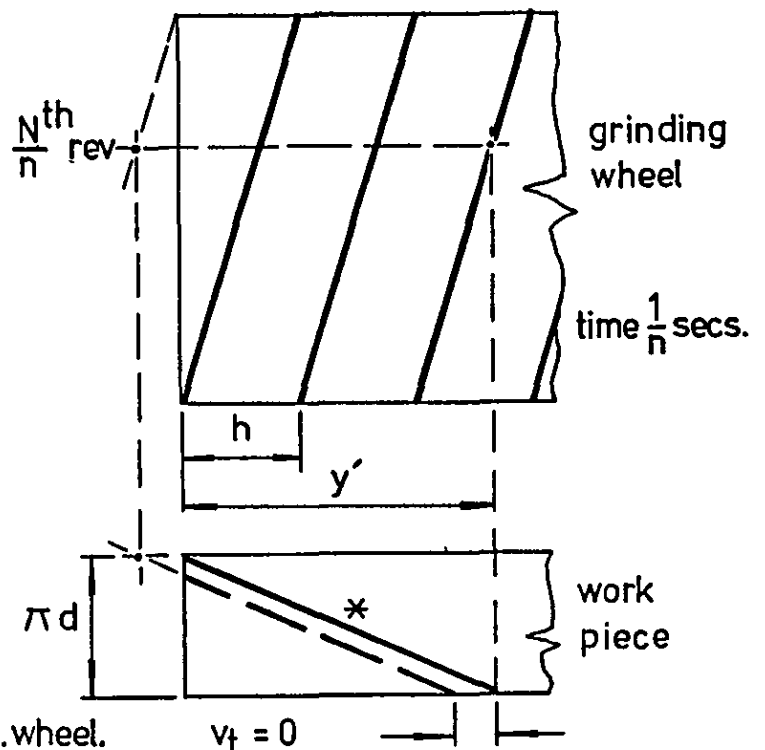
Interference on the second workpiece revolution.

✳ For simplicity, only one ground groove on the workpiece is considered.

By symmetry:-

$$\frac{h}{\pi d \frac{n}{N}} = \frac{y'}{\pi d}$$

$$\therefore \quad y' = \frac{\pi d h}{\pi d \frac{n}{N}} = \frac{Nh}{n} \qquad \ldots (3.10)$$

The value of y' obtained from equation (3.10) gives the length of the ground surface pattern, measured along the axis of the workpiece, for one workpiece revolution with no axial traverse being applied. This is the case for plunge cut grinding.

Equation (3.10) infers that the interference produced between the ground surface patterns for each subsequent revolution of the workpiece, is a function of wheel and workpiece rotational speed, (coupled with dressing traverse rate), and is independent of wheel and workpiece diameters.

If the value of N/n is a whole number, no interference will occur, and the value of workpiece surface roughness will remain constant.

Consider now the case where the workpiece is traversed past the grinding wheel at a rate of v_t mm/sec, all other conditions remaining the same as before. Fig. 3.8 shows the relationship between the dressed grinding wheel and the ground workpiece.

From fig. 3.8

By symmetry:-

$$\frac{h + \frac{v_t}{N}}{\pi d \frac{n}{N}} = \frac{y'}{\pi d}$$

$$\therefore \quad y' = \frac{\pi d (h + \frac{v_t}{N})}{\pi d \frac{n}{N}} = \frac{N}{n}(h + \frac{v_t}{N}) \qquad \ldots (3.11)$$
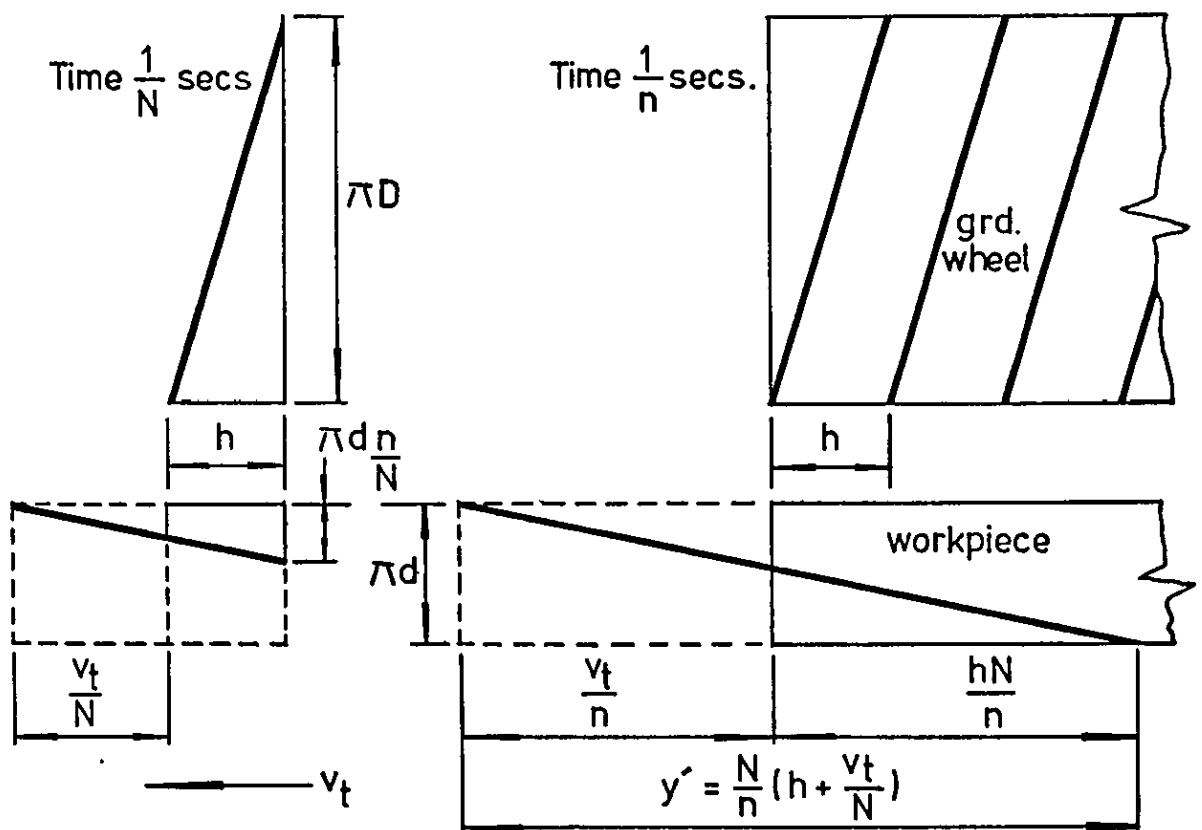
Fig. 3. 8

The value of y' obtained from equation (3.11) gives the length of the ground surface pattern, measured along the axis of the workpiece for one workpiece revolution, when an axial traverse rate of v_t mm/sec is applied. This is the case for plain cylindrical traverse grinding.

If the traverse is applied in the same direction when grinding as that when dressing, then equation (3.11) becomes

$$y' = \frac{N}{n}\left(h - \frac{v_t}{N}\right) \qquad \qquad \dots \dots (3.12)$$

Equations (3.10), (3.11), and (3.12) establish the relationship between the path of the dressed form on the grinding wheel, and the corresponding form on the workpiece, for one workpiece revolution and different conditions of traverse. The value of N/n, which is the factor that determines whether interference will occur between subsequent surface patterns ground on the workpiece, or not, will be used as a basis for obtaining equations relating to values of interference per workpiece revolution.

-64-

Consider now, the complete surface pattern produced
by the grinding wheel on the workpiece, after the completion
of one workpiece revolution. Let the grinding wheel be
dressed at a rate of h mm/rev, and the workpiece be traversed
past the grinding wheel at v_t mm/sec. Fig. 3.9 shows a
section of the ground cylindrical workpiece laid out flat.

Fig. 3. 9

1. path of grinding wheel

2. path of ground surface scratches

n rev/sec

time period $\frac{1}{n}$ secs.

direction vectors

$*$ enlarged view

-65-
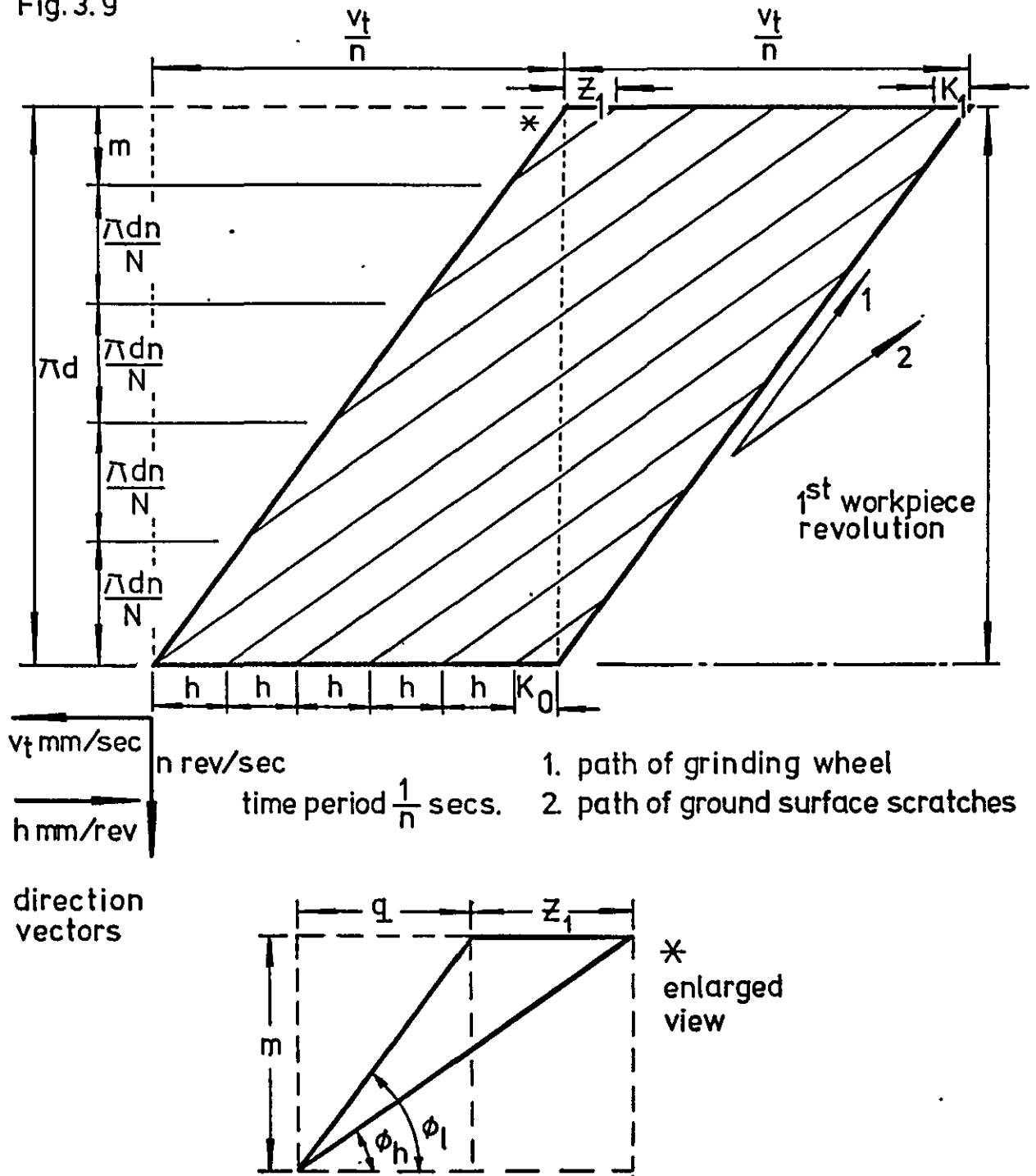
As the grinding wheel and workpiece rotate against each other, a band of width v_f/n is ground on the workpiece during each revolution. (For plain cylindrical traverse grinding, the value of v_f/n is generally of the order of $1/2$ to $2/3$ times the wheel width, W.) The dressing marks on the grinding wheel, which form the surface patterns on the workpiece, are shown for simplicity as starting at the bottom left hand corner of the diagram in fig. 3.9 .

From this diagram, certain relationships can be established.

As the workpiece makes one revolution in the time $1/n$ seconds, the grinding wheel makes N/n revolutions.

Let $\dfrac{\dfrac{\pi d}{\pi d n}}{N}$ $=$ $(X + z)$

$\therefore$ $\dfrac{N}{n}$ $=$ $(X + z)$ $\qquad$ .... (3.13)

where X is an integer
and z is a fraction

For interference to occur between subsequent surface patterns ground on the workpiece, the following conditions must be true:-

. $z \neq 0;$ and $W > \dfrac{v_f}{n}$

The value(s) of interference are calculated from the boundary coefficients K and $\cancel{Z}$, which occur at the leading and trailing edges of the feed band, v_f/n .

3.4.5 Calculation of the boundary coefficients K and $\cancel{Z}$.

Calculation of $\cancel{Z}$
From fig. 3.9

$m = \dfrac{\pi d n}{N} \times z$ $\qquad$ ....(3.14)

and $\tan \phi_l = \dfrac{\pi dn}{v_t} = \dfrac{m}{q}$

$\therefore \qquad q = \dfrac{mv_t}{\pi dn}$ . . . . . (3.15)

substituting for m in equn. (3.15)

$\therefore \qquad q = \dfrac{\pi dnz}{N} \times \dfrac{v_t}{\pi dn} = \dfrac{z\,v_t}{N}$ . . . . . (3.16)

Now $\tan \phi_h = \dfrac{\pi d}{y'}$ . . . . . (3.17)

taking y' from equn. (3.10) and substituting in equn. (3.17)

$\therefore \qquad \tan \phi_h = \dfrac{\pi dn}{Nh} \quad (v_t = 0)$ . . . . . (3.18)

taking y' from equn. (3.11) and substituting in equn. (3.17)

$\therefore \qquad \tan \phi_h = \dfrac{\pi dn}{(Nh + v_t)}$ . . . . . (3.19)

$\left(\begin{array}{l} v_t \longrightarrow \\ h \longleftarrow \end{array} \right) \begin{array}{l} \text{direction} \\ \text{vectors} \end{array}$

taking y' from equn. (3 12) and substituting in equn. (3.17)

$\therefore \qquad \tan \phi_h = \dfrac{\pi dn}{(Nh - v_t)}$ . . . . . (3.20)

$\left(\begin{array}{l} v_t \longrightarrow \\ h \longrightarrow \end{array} \right) \begin{array}{l} \text{direction} \\ \text{vectors} \end{array}$

Also $\tan \phi_h = \dfrac{m}{q + z_1}$

$\therefore \qquad z_1 = m \cot \phi_h - q$ . . . . . (3.21)

substituting for m and q in equn. (3.21)

$$z_1 = \dfrac{\pi dnz}{N} \cot \phi_h - \dfrac{z\,v_t}{N}$$

$\therefore \qquad z_1 = \dfrac{z}{N}(\pi dn \cot \phi_h - v_t)$ . . . . . (3.22)

For fig. 3.9, the value of $\tan \phi_h$ is found from eq023. (3.19)

hence
$$Z_1 = \frac{Z}{N} \left(\pi dn \times \frac{(Nh + v_t)}{\pi dn} - v_t \right)$$

$$= \frac{Z}{N} (Nh + v_t - v_t)$$

$\therefore \qquad \underline{\underline{Z_1 = zh}} \qquad\qquad \dots (3.23)$

Calculation of K

Consider fig. 3.10, which is an enlarged view of the upper part of fig. 3.9.
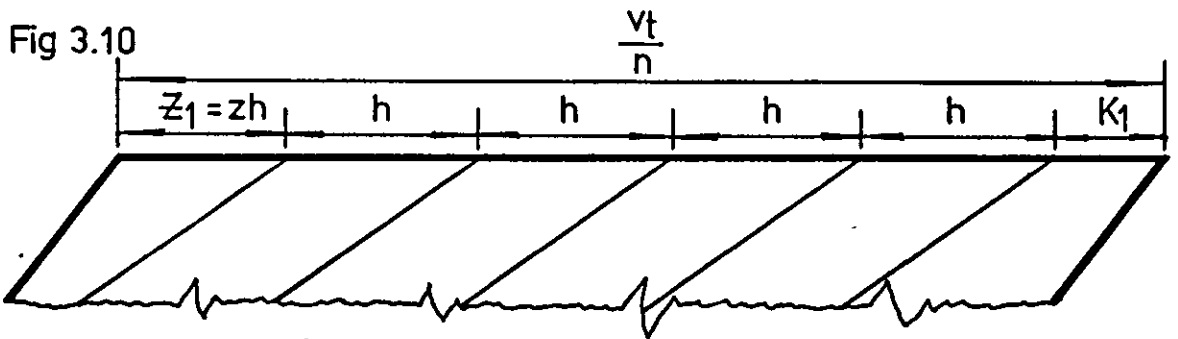
Fig 3.10

From fig. 3.10

$$K_1 = \frac{v_t}{n} - zh - \sum h \qquad \dots (3.24)$$

Let
$$\frac{\frac{v_t}{n} - zh}{h} = (T + u)$$

where $\quad T$ is an integer
and $\quad u$ is a fraction

$\therefore \qquad \underline{\underline{K_1 = uh}} \qquad\qquad \dots (3.25)$

The boundary coefficients K and Z, can be found in a similar manner for the cases of plunge-cut grinding, where $v_t = 0$, and traverse grinding, where the traverse is applied in the same direction when grinding as that when dressing.

Considering plunge-cut grinding. ($v_t = 0$)

By substituting $\tan \phi_h$ from equation 3.18, into equn. 3.22, and putting $v_t = 0$, a value for $Z_{1_{(v_t=0)}}$ is found.

Hence $\quad Z_{1_{(v_t=0)}} = \dfrac{Z}{N}(\,\pi dn \times \dfrac{Nh}{\pi dn} \, - 0)$

$\therefore \quad \underline{\underline{Z_{1_{(v_t=0)}} = z\,h}} \qquad\qquad \ldots\ldots \text{(3.26)}$

It can also be shown that

$\underline{\underline{K_{1_{(v_t=0)}} = u\,h}} \qquad\qquad \ldots\ldots \text{(3.27)}$

Considering traverse grinding , where $\begin{smallmatrix}v_t \longrightarrow \\ h \longrightarrow\end{smallmatrix}$
Fig. 3.11 shows the boundary coefficients, K and Z, on completion of the first workpiece revolution.

Fig. 3.11

✻ enlarged view

direction vectors

-69-
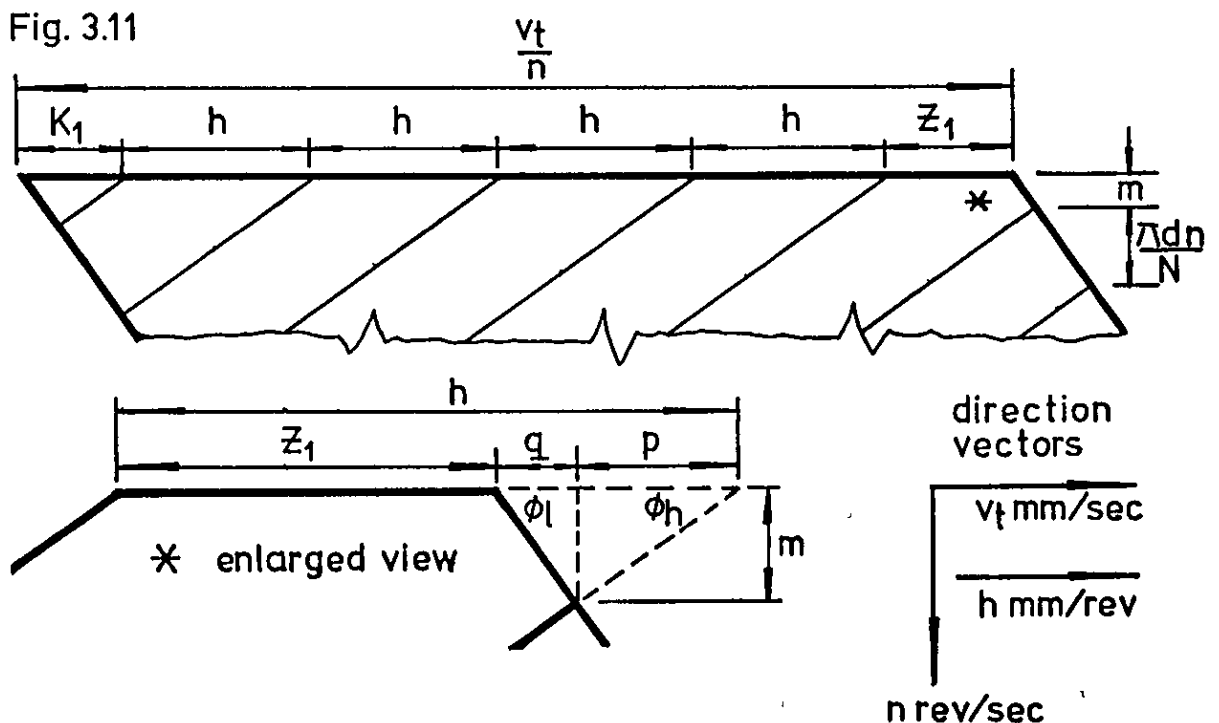
From fig. 3.11

$$Z_1 = h - (q + p) \qquad \ldots (3.28)$$

also $\quad \dfrac{m}{q} = \tan \phi_l$

$\therefore \qquad q = m \cot \phi_l \qquad \ldots (3.29)$

and $\quad \dfrac{m}{p} = \tan \phi_h$

$\therefore \qquad p = m \cot \phi_h \qquad \ldots (3.30)$

now $\quad \tan \phi_l = \dfrac{\pi dn}{v_t}$

$\therefore \qquad q = \dfrac{m\, v_t}{\pi dn} \qquad \ldots (3.31)$

substituting $\tan \phi_h$ from equn. (3.20) into equn. (3.30).

$\therefore \qquad p = \dfrac{m(Nh - v_t)}{\pi dn} \qquad \ldots (3.32)$

substituting for p and q in equn. (3.28)

$$Z_1 = h - \dfrac{m}{\pi dn}(v_t + Nh - v_t)$$

$\therefore \qquad Z_1 = h - \dfrac{mNh}{\pi dn} \qquad \ldots (3.33)$

substituting m from equn. (3.14) into equn. (3.33).

$$Z_1 = h - \left(\dfrac{\pi dnz}{N} \times \dfrac{Nh}{\pi dn} \right) = h - zh$$

$\therefore \qquad \underline{\underline{Z_1 = h(1 - z)}} \qquad \ldots (3.34)$

Calculation of K

From fig. 3.11

$$K_1 = \frac{Vt}{n} - h(1-z) - \sum h \qquad \dots \dots (3.35)$$

Let $\dfrac{\frac{Vt}{n} - h(1-z)}{h} = (T + u)$

where   T is an integer
and   u is a fraction

$$\therefore \qquad K_1 = uh \qquad \qquad \dots \dots (3.36)$$

Equations are now established for calculating initial values of the boundary coefficients, K and Z, for circular plunge-cut grinding and plain cylindrical traverse grinding.

For subsequent revolutions of the workpiece, the values of K and Z will change, causing changes in interference between the ground surface patterns.

Let the total number of workpiece revolutions be r . The values of K and Z for each rotation are found as follows.

Values of Z.   (For all cases.)

Values of z are calculated first from equn. (3.13) for each workpiece rotation.

Hence

$$(X_1 + z_1) = (\frac{N}{n}) \; ; \qquad \qquad (X_2 + z_2) = 2(\frac{N}{n})$$

$$(X_3 + z_3) = 3(\frac{N}{n}) \; ; \qquad \qquad (X_4 + z_4) = 4(\frac{N}{n})$$

$$(X_5 + z_5) = 5(\frac{N}{n}) \; ; \qquad \qquad (X_r + z_r) = r(\frac{N}{n})$$

From which

$$z_i = i\left(\frac{N}{n}\right) - x_i \qquad \text{(for the } i^{th}\text{ revolution)}$$

substituting for z_i in equn.s (3.23), (3.26) and (3.34)

$$\therefore \qquad Z_i = z_i h \qquad \left(\text{for } \begin{array}{c} v_t \longrightarrow \\ h \longleftarrow \end{array}\right)$$

and
$$Z_i = z_i h \qquad \text{(for } v_t = 0\text{)}$$

and
$$Z_i = h(1 - z_i) \qquad \left(\text{for } \begin{array}{c} v_t \longrightarrow \\ h \longrightarrow \end{array}\right)$$

Values of K (For $v_t = 0$, and $\begin{array}{c} v_t \longrightarrow \\ h \longleftarrow \end{array}$)
values of u are calculated first, as follows:-

$$(T_1 + u_1) = \frac{v_t}{nh} - z_1 ; \qquad\qquad (T_2 + u_2) = \frac{v_t}{nh} - z_2$$

$$(T_3 + u_3) = \frac{v_t}{nh} - z_3 ; \qquad\qquad (T_4 + u_4) = \frac{v_t}{nh} - z_4$$

$$(T_5 + u_5) = \frac{v_t}{nh} - z_5 ; \qquad\qquad (T_r + u_r) = \frac{v_t}{nh} - z_r$$

From which

$$u_i = \left(\frac{v_t}{nh} - z_i\right) - T_i \qquad \text{(for the } i^{th}\text{ revolution)}$$

substituting for u_i in equn. (3.25)

$$\therefore \qquad K_i = u_i h$$

Values of K   (For $\frac{vt}{h} \Longrightarrow$)
values of u are calculated first, as follows :-

$$(T_1 + u_1) = \frac{vt}{nh} - 1 + z_1 \; ; \qquad (T_2 + u_2) = \frac{vt}{nh} - 1 + z_2$$

$$(T_3 + u_3) = \frac{vt}{nh} - 1 + z_3 \; , \qquad (T_4 + u_4) = \frac{vt}{nh} - 1 + z_4$$

$$(T_5 + u_5) = \frac{vt}{nh} - 1 + z_5 \; ; \qquad (T_r + u_r) = \frac{vt}{nh} - 1 + z_r$$

From which

$$u_i = (\frac{vt}{nh} - 1 + z_i) - T_i \qquad (\text{for the } i^{th} \text{revolution.})$$

substituting for u_i in equn. (3.36)

$$\therefore \qquad K_i = u_i h$$

Equations are now established for obtaining values of the boundary coefficients, K and Z , for all workpiece revolutions. Before values of interference can be calculated using these coefficients, the effect of wheel width, W , on interference, must be considered.

3.4.6 Effect of wheel width, W , on workpiece surface-pattern interference.

The degree of interference that will occur between ground surface patterns in the same band, of width vt/n, is dependent upon the relationship between the band width, and the grinding wheel width, W . This relationship determines the amount of overlap that will occur between the grinding wheel, and the previously ground workpiece surface.

1.   If the width of the feed band, v_t/n , is equal to the width of the grinding wheel, W , no overlapping will occur. The value of the workpiece surface roughness, R_a , will remain constant over the workpiece length, l , and be equal to the as-dressed condition of the grinding wheel. (Slight aberration will occur at the boundaries of the feed bands.) See fig. 3.12 .

Fig. 3.12
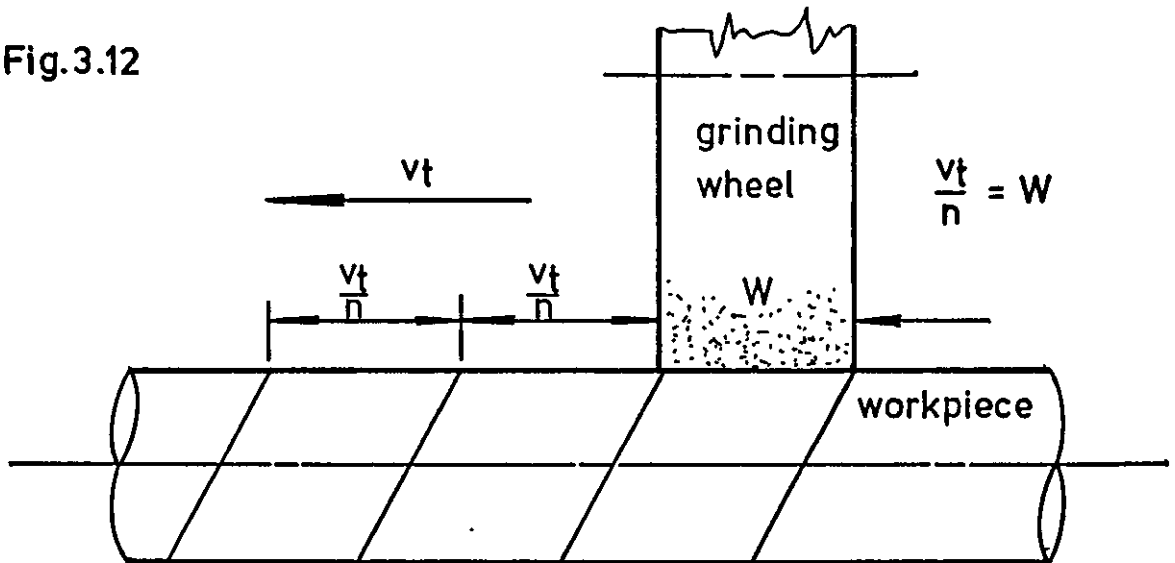
2.   If the width of the feed band, v_t/n , is exactly divisible into the width of the grinding wheel, W , the degree of overlap for each feed band will be equal to :-

$$\frac{W}{\frac{v_t}{n}} - 1 \qquad \text{(See fig. 3.13)}$$

Hence   The degree of wheel overlap $= \frac{Wn}{v_t} - 1 = 1, 2, 3$ etc $\dots$ (3.37)

N.B.   The degree of wheel overlap will be taken to mean the number of times the grinding wheel cuts the previously ground surface of the workpiece, in any feed band, as the workpiece traverses past the grinding wheel.

Fig. 3.13

$$\frac{Wn}{v_t} = 2,3,4 \dots \text{etc.}$$
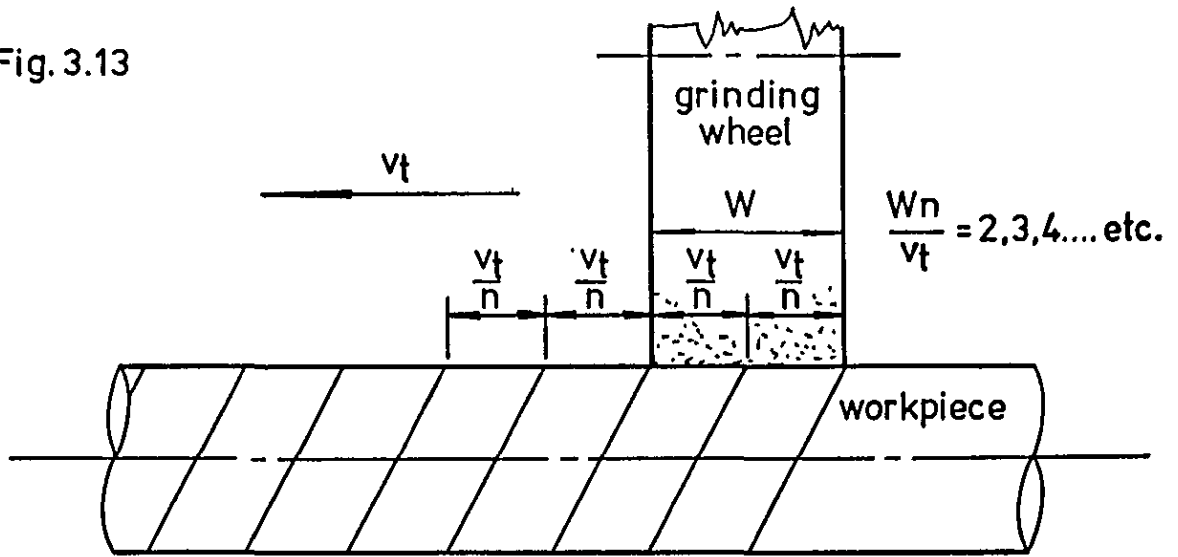
3.   If the width of the feed band, v_t/n , is not exactly divisible into the width of the grinding wheel, W , the degree of overlap for each feed band will consist of two parts. Consider the following:-

Let $\dfrac{Wn}{v_t}$ = $(A + b)$ .... (3.38)

where A is an integer $(A \geqslant 2)$
and b is a fraction

.Each feed width covered by the trailing edge of the grinding wheel will have two distinct parts, namely:-

1. A part towards the leading edge of the feed band, of width $b.v_t/n$.

2. A part towards the trailing edge of the feed band, of width $(1-b)v_t/n$.

For each part, the degree of overlap is as follows:-

For the part $b v_t/n$. The degree of wheel overlap $=$ $(A-1)$ ....(3.39)

For the part $(1-b)v_t/n$. The degree of wheel overlap $=$ $(A-2)$ ....(3.40)

(See fig. 3.14)

The two parts of each feed band will have, in general, different average values of workpiece surface roughness, Ra .

Fig.3.14

grinding wheel

v_t

W

$b\frac{v_t}{n}$ $\frac{v_t}{n}$ $\frac{v_t}{n}$

$\frac{Wn}{v_t} = (A+b)$

where $A \geqslant 2$

workpiece

$(1-b)\frac{v_t}{n}$
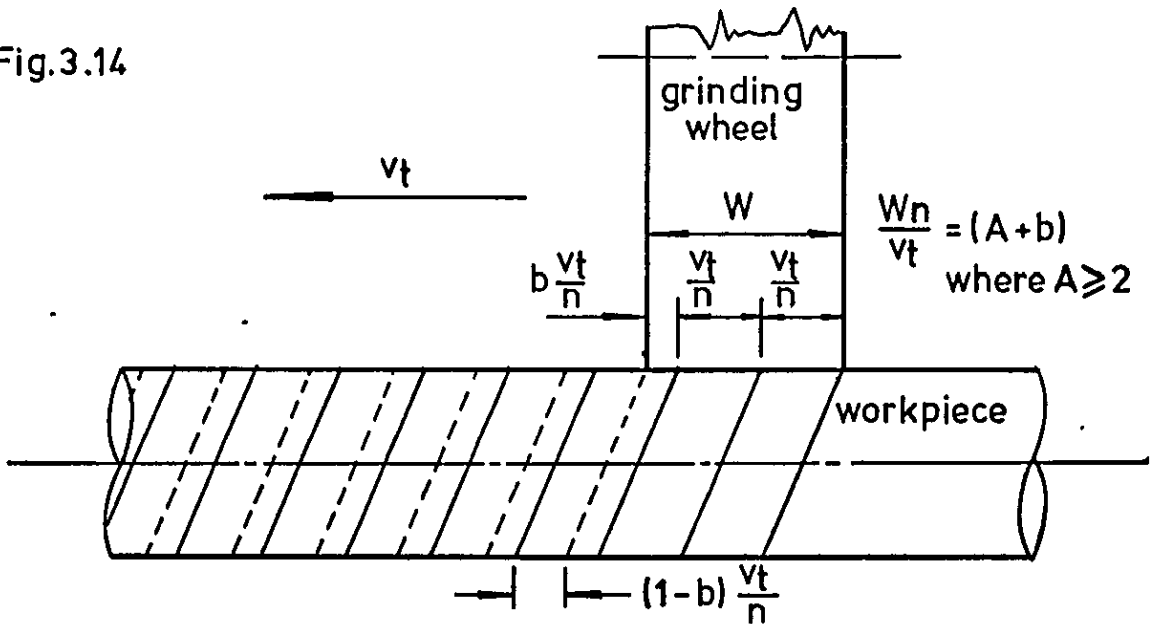
3.4.7 Calculation of the values of workpiece surface-pattern interference, for any set of circular grinding conditions.

Consider fig. 3.15. This shows feed bands of width v_t/n side by side, with values of zh and uh, for each workpiece revolution.

Fig.3.15

$\frac{v_t}{n}$ $\frac{v_t}{n}$ $\frac{v_t}{n}$

$u_1 h$ $u_2 h$ $u_3 h$

$z_1 h$ $z_2 h$ $z_3 h$

h

workpiece

r^{th} rev.

v_t
h

interference 1st rev. interference 2nd rev. 3rd rev.
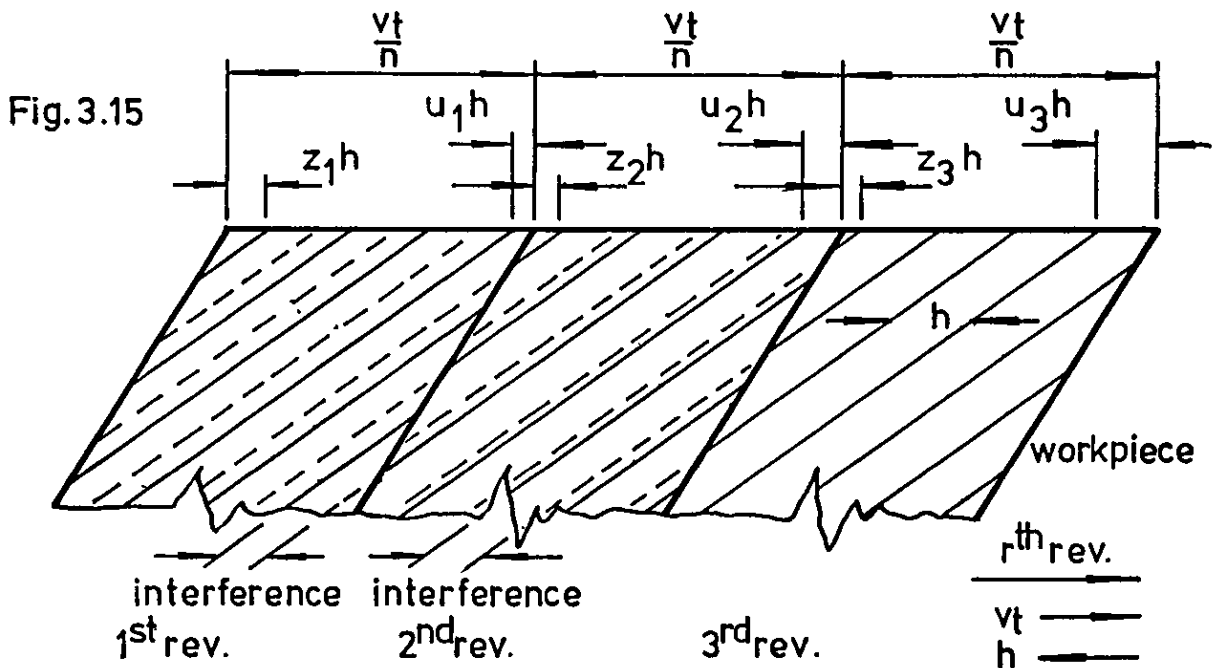
From this diagram, a series of "potential" values of workpiece surface-pattern interference can be established, as follows:-

The values of interference will always be numerically less than the value of dressing traverse rate, h.

Consider the first workpiece revolution.

Let $h(I_{1;1} + e_{1;1}) = (u_1 h + z_2 h)$

where I is an integer $\begin{bmatrix} \text{NB. notation}_{1;1} \text{ means} \\ \text{first rev. on first feed band} \end{bmatrix}$
and e is a fraction

The value of interference is $h.e_{1;1}$

Hence the value of interference for the first feed band, subject to overlapping of the grinding wheel on the second workpiece revolution, is:-

$$h.e_{1;1} = h(u_1 + z_2) - I_{1;1} \qquad \dots \dots (3.41)$$

Equation (3.41) can be used as a basis for establishing further values of interference, for example:-

Value of interference
for second feed band $= h.e_{2;1} = h\left[(u_2 + z_3) - I_{2;1}\right]$

Value of interference
for third feed band $= h.e_{3;1} = h\left[(u_3 + z_4) - I_{3;1}\right]$

Value of interference
for r^{th} feed band $= h.e_{r;1} = h\left[(u_r + z_{r+1}) - I_{r;1}\right]$

Using these initial equations as a basis, others can be developed for calculating values of workpiece surface-pattern interference, which occur in any feed band along the length of a cylindrical workpiece, due to the action of prevailing dressing and grinding conditions.

Such equations will now be established.

<u>Case 1</u>

$$\frac{Wn}{vt} = A, \quad \text{where } A = 2,3,4....\infty$$

Degree of grinding wheel
overlap for each feed width $\quad = \quad (A-1)$

Consider the condition $\dfrac{vt}{h} \overset{\longrightarrow}{\underset{\longleftarrow}{}}$ (direction vectors)

Values of interference are as follows :-

1st feed band

Value of $(A-1)^{th}$ degree
of interference $\quad = h.e_{1;(A-1)} = h \left\{ \sum\limits_{u_1}^{u_{A-1}}(u) + \sum\limits_{z_2}^{z_A}(z) \right\} - h.I_{1;(A-1)}$

Value of $(A-2)^{th}$ degree
of interference $\quad = h.e_{1;(A-2)} = h \left\{ \sum\limits_{u_1}^{u_{A-2}}(u) + \sum\limits_{z_2}^{z_{A-1}}(z) \right\} - h.I_{1;(A-2)}$

down to

Value of 1st degree
of interference $\quad = h.e_{1;1} \quad = h(u_1 + z_2) - h.I_{1;1}$

r^{th} feed band

Value of $(A-1)^{th}$ degree
of interference $\quad = h.e_{r;(A-1)} = h \left\{ \sum\limits_{u_r}^{u_{r+A-2}}(u) + \sum\limits_{z_{r+1}}^{z_{r+A-1}}(z) \right\} - h.I_{r;(A-1)}$

Value of $(A-2)^{th}$ degree
of interference $\quad = h.e_{r;(A-2)} = h \left\{ \sum\limits_{u_r}^{u_{r+A-3}}(u) + \sum\limits_{z_{r+1}}^{z_{r+A-2}}(z) \right\} - h.I_{r;(A-2)}$

down to

Value of 1st degree
of interference $\quad = h.e_{r;1} \quad = h(u_r + z_{r+1}) - h.I_{r;1}$

Case 1 continued

Consider the condition $\dfrac{Vt}{h} \Longrightarrow$ (direction vectors)

Values of interference are as follows :-

1st feed band

Value of $(A-1)^{th}$ degree of interference $= h.e_{1;(A-1)} = h\left\{ \displaystyle\sum_{u_1}^{u_{A-1}} (u) + \sum_{(1-z)_2}^{(1-z)_A} (1-z) \right\} - h.I_{1;(A-1)}$

Value of $(A-2)^{th}$ degree of interference $= h.e_{1;(A-2)} = h\left\{ \displaystyle\sum_{u_1}^{u_{A-2}} (u) + \sum_{(1-z)_2}^{(1-z)_{A-1}} (1-z) \right\} - h.I_{1;(A-2)}$

down to

Value of 1st degree of interference $= h.e_{1;1} = h\left(u_1 + (1-z)_2 \right) - h.I_{1;1}$

r^{th} feed band

Value of $(A-1)^{th}$ degree of interference $= h.e_{r;(A-1)} = h\left\{ \displaystyle\sum_{u_r}^{u_{r+A-2}} (u) + \sum_{(1-z)_{r+1}}^{(1-z)_{r+A-1}} (1-z) \right\} - h.I_{r;(A-1)}$

Value of $(A-2)^{th}$ degree of interference $= h.e_{r;(A-2)} = h\left\{ \displaystyle\sum_{u_r}^{u_{r+A-3}} (u) + \sum_{(1-z)_{r+1}}^{(1-z)_{r+A-2}} (1-z) \right\} - h.I_{r;(A-2)}$

down to

Value of 1st degree of interference $= h.e_{r;1} = h\left(u_r + (1-z)_{r+1} \right) - h.I_{r;1}$

<u>Case 2</u> . $\dfrac{Wn}{v_t} = (A+b)$, where $A \geqslant 3$

Degree of grinding wheel overlap
for the $b.v_t/n$ part of the feed width $= (A-1)$
.(Values of interference are the same as Case 1.)

Degree of grinding wheel overlap for
the $(1-b)v_t/n$ part of the feed width $= (A-2)$

Consider the condition $\quad \dfrac{v_t \longrightarrow}{h \longleftarrow}$ (direction vectors)

Values of interference are as follows:-

<u>1st feed band</u>

Value of $(A-2)^{th}$ degree
of interference $= h.e_{1;(A-2)} = h\left\{\displaystyle\sum_{u_1}^{u_{A-2}} (u) + \sum_{z_2}^{z_{A-1}} (z)\right\} - h.I_{1;(A-2)}$

Value of $(A-3)^{th}$ degree
of interference $= h.e_{1;(A-3)} = h\left\{\displaystyle\sum_{u_1}^{u_{A-3}} (u) + \sum_{z_2}^{z_{A-2}} (z)\right\} - h.I_{1;(A-3)}$.

down to

Value of 1st degree
of interference $\quad = h.e_{1;1} \quad = h(u_1 + z_2) - h.I_{1;1}$

<u>r^{th} feed band</u>

Value of $(A-2)^{th}$ degree
of interference $= h.e_{r;(A-2)} = h\left\{\displaystyle\sum_{u_r}^{u_{r+A-3}} (u) + \sum_{z_{r+1}}^{z_{r+A-2}} (z)\right\} - h I_{r;(A-2)}$

Value of $(A-3)^{th}$ degree
of interference $= h.e_{r;(A-3)} = h\left\{\displaystyle\sum_{u_r}^{u_{r+A-4}} (u) + \sum_{z_{r+1}}^{z_{r+A-3}} (z)\right\} - h.I_{r;(A-3)}$

down to

Value of 1st degree
of interference $\quad = h.e_{r;1} \quad = h(u_r + z_{r+1}) - h.I_{r;1}$

Case 2 continued

Consider the condition $\begin{matrix} \vec{v}t \\ \vec{h} \end{matrix} \rightrightarrows$ (direction vectors)

Values of interference are as follows:-

1st feed band

Value of $(A-2)^{th}$ degree of interference $= h.e_{1;(A-2)} = h\left\{\displaystyle\sum_{u_1}^{u_{A-2}}(u) + \sum_{(1-z)_2}^{(1-z)_{A-1}}(1-z)\right\} - h.I_{1;(A-2)}$

Value of $(A-3)^{th}$ degree of interference $= h.e_{1;(A-3)} = h\left\{\displaystyle\sum_{u_1}^{u_{A-3}}(u) + \sum_{(1-z)_2}^{(1-z)_{A-2}}(1-z)\right\} - h.I_{1;(A-3)}$

down to

Value of 1st degree of interference $= h.e_{1;1} = h\left(u_1 + (1-z)_2\right) - h.I_{1;1}$

r^{th} feed band

Value of $(A-2)^{th}$ degree of interference $= h.e_{r;(A-2)} = h\left\{\displaystyle\sum_{u_r}^{u_{r+A-3}}(u) + \sum_{(1-z)_{r+1}}^{(1-z)_{r+A-2}}(1-z)\right\} - h.I_{r;(A-2)}$

Value of $(A-3)^{th}$ degree of interference $= h.e_{r;(A-3)} = h\left\{\displaystyle\sum_{u_r}^{u_{r+A-4}}(u) + \sum_{(1-z)_{r+1}}^{(1-z)_{r+A-3}}(1-z)\right\} - h.I_{r;(A-3)}$

down to

Value of 1st degree of interference $= h.e_{r;1} = h\left(u_r + (1-z)_{r+1}\right) - h.I_{r;1}$

<u>Case 3</u> $\dfrac{Wn}{v_t} = (A + b)$; where $A = 2$

Degree of grinding wheel overlap for the $b.v_t/n$ part of the feed width = 1. The single value of interference for each feed band is calculated as shown previously.

For the $(1-b)v_t/n$ part of the feed width there is no overlap, and the value of workpiece surface roughness, Ra, is the same as that for the "as dressed" condition of the grinding wheel.

Having established means for evaluating values of workpiece surface-pattern interference, for any set of cylindrical grinding conditions, equations for average workpiece surface roughness, Ra , can be derived.

3.4.8 Calculation of Ra , for any set of circular grinding conditions.

When interference occurs in any feed band, the degree of interference repeats itself every h mm across the feed band width. This is due to the "as dressed" condition of the grinding wheel, which produces the ground workpiece surface pattern. For simplicity when calculating values of Ra , only one width of value h mm will be considered.

It can be shown that when dressing a grinding wheel for fine grinding, with a relatively blunt diamond, w = 1.09 mm at a low traverse rate, h = .1 mm/rev , and a small depth of cut, a = .025 mm, dressing marks on the grinding wheel surface are still discernible, and the dressed wheel profile can be approximated to a series of small triangles. (See Chapter 7, fig. 7.147 for confirmation.) This results in a similar form being ground on the workpiece.

Fig. 3.16 depicts a portion of the ground workpiece surface profile, with interference occuring. Let the term "value of interference," be denoted by the symbol E , and the peak to valley height of each triangular form be denoted by the symbol Δ .
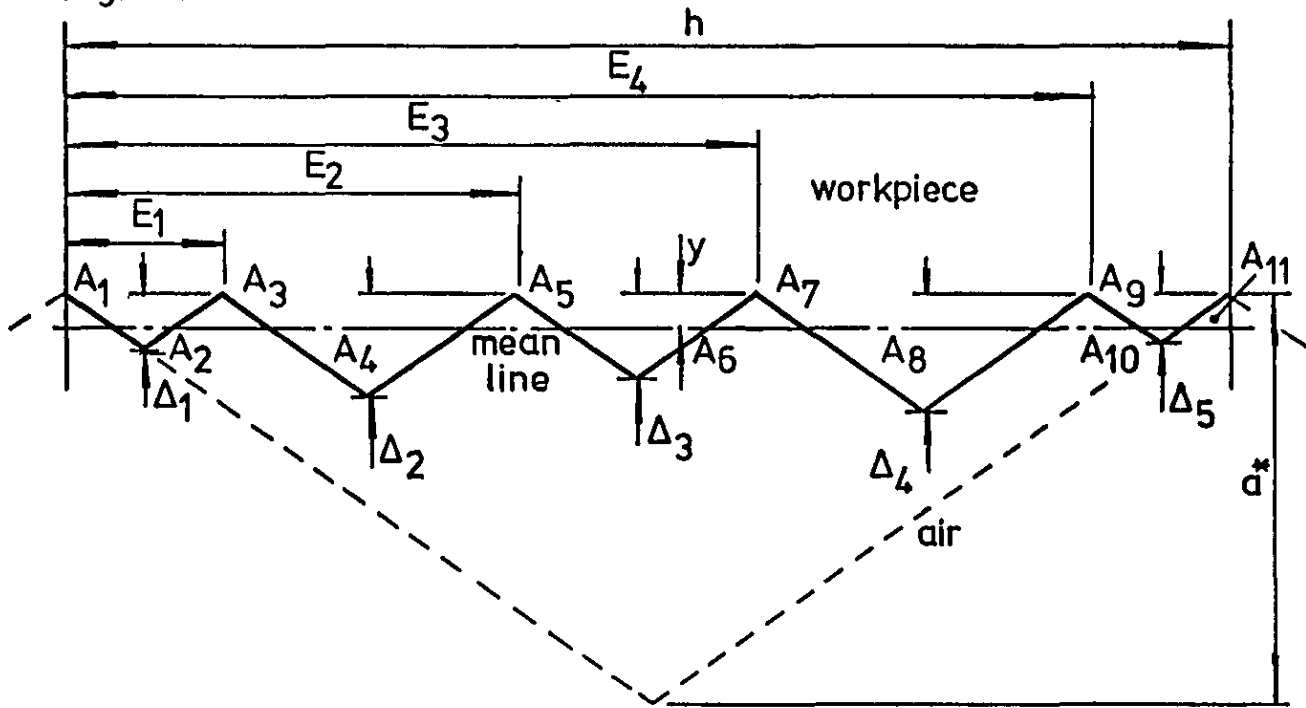
Fig. 3.16

From fig. 3.16 it can be shown that the workpiece surface roughness Ra is given by $\begin{bmatrix} \text{See Appendix II} \\ \text{for the derivation} \end{bmatrix}$

$$Ra = \frac{5a^*}{h^4}\left[\left(E_1^2+E_2^2+E_3^2+E_4^2\right)-\left(E_2E_1+E_3E_2+E_4E_3\right)-hE_4+\frac{h^2}{2}\right]^2$$

From which the following general form of Ra can be written

$$Ra = \frac{(M+1)a^*}{h^4}\left[\sum_{j=1}^{j=M}(E_j)^2-\sum_{j=2}^{j=M}(E_jE_{j-1})-hE_M+\frac{h^2}{2}\right]^2 \quad \ldots(3.44)$$

where M is the number of non-repeated values of E.

From equation (3.44), values of workpiece surface roughness, Ra, can be evaluated for a cylindrical workpiece, subjected to any set of cylindrical grinding conditions. (The equation assumes the grinding wheel to have a shallow "saw-tooth" profile dressed on it.) NB. The parameter a^* in equation (3.44), represents the peak to valley height of the saw-tooth profile on the grinding wheel.

3.5 DISCUSSION OF THE EFFECTS OF DRESSING VARIABLES
ON GRINDING WHEEL SURFACE ROUGHNESS, R_a.

Equations (3.5), (3.7) and (3.9) describe the surface finish that would be obtained on a grinding wheel under ideal(theoretical)dressing conditions, that is to say, using a diamond tool having straight sides, the included angle at its tip being equally displaced about the tool axis, and any wear flat on the diamond tip being flat in a direction perpendicular to the traverse motion of the tool. In practice, these conditions vary, (unless specially prepared dressing tools are used), causing discrepencies between actual and theoretical values of surface roughness, R_a. This being so, the values obtained from the above mentioned equations are used to show trends only. To ensure that the values of surface finish obtained from the equations are representative of the true situation, values of h , a , β , and w have been chosen that are met in practice.

Equation (3.3) is a hypothetical case from which R_a is found in terms of depth of cut, a only. In the limit, ($w=0$ and $h=x$), equations (3.5), (3.7) and (3.9) revert to equation (3.3), showing the abrasive surface roughness, R_a , to be equal to a quarter of the depth of cut, a .

To establish the effects of h , a , β and w , on abrasive surface roughness, a computer programme has been written embracing equations (3.5), (3.7) and(3.9). This is found in Appendix III. Values of R_a have been plotted in figures 3.17 to 3.21 inclusive, for changing values of h , a , and w ; β remaining constant at 120°. The value of 120° was considered to be the average value for β when using natural diamonds, the upper and lower limits being 150° and 90° respectively. Values of R_a for β constant at 90° and 150°(h , a and w changing) , have been evaluated, but not plotted. See Appendix III.

Consider initially fig. 3.17. This shows the effects of changes in dressing rate, h and depth of cut, a on R_a , for a sharp diamond ($w=0$). At low traverse

rates ($h > .1$ mm/rev), the value of Ra increases sharply, and linearly, for small increases in h (a constant), to attain a maximum value at a point where $h = x = 2a\tan\beta/2$. Beyond this point, as h is increased, the value of Ra decreases quickly at first, then more slowly, tending towards a "plateau" value, this depending to some extent upon the condition of the grinding wheel before dressing. For values of $h < 2a\tan\beta/2$, the influence of a on Ra is less than that of h . As a is increased in value (h constant), Ra increases to a maximum value when $h = x$. Beyond this point Ra remains constant for any further increase in a . For values of $h > 2a\tan\beta/2$, the influence of a on Ra is greater than that of h . The practical implications of the above are that increasing the depth of cut a beyond the point where $h = x$ would mean a loss of grinding wheel diameter for no change in wheel surface roughness, and that increasing the traverse rate, h , beyond this point , would result in part of the grinding wheel surface not being dressed.

In practice, a diamond tool would not be perfectly sharp, but would have a flat on the tip due to either wear or natural cleavage. Figs. 3.18 to 3.21 inclusive, show the effect on the grinding wheel surface roughness, when the flat on the tip of the diamond (w) is increased. As W increases in size, several changes are brought about. The value of h (a constant) at which Ra is a maximum , is increased, and is governed by the equation $h = x = w + 2a\tan\beta/2$, also Ra max. takes on a higher value. In the region $0 < h < w + 2a\tan\beta/2$, the increase in Ra due to an increase in h is rapid, and non-linear. For values of $h < w$, the value of grinding wheel surface roughness is zero (theoretically). The influence of a and h on Ra , are the same as for the case of the sharp diamond ($w = 0$).

The angle of the diamond tip, β , also affects the value of grinding wheel surface roughness as it is changed. Values of Ra , calculated for $\beta = 90°$; $120°$ and $150°$ are shown in Appendix III. As β is decreased from $120°$ towards $90°$, the value of Ra increases for any

set of values of a and h , and the value of a at which Ra attains a maximum value (h constant) is raised. For a further increase in a beyond this point ($h=w$), the value of Ra remains constant as before. As β is increased from 120° towards 150°, the opposite of the above statements is true.

Since the abrasive surface roughness of a grinding wheel affects the surface finish of a component being ground, there are limits of Ra for a grinding wheel surface, beyond which it is impractical to go. Figs. **3.17** to **3.21** inclusive, show some values of Ra in excess of those recommended for rough and finish grinding, e.g.,

Rough ground .38 to 1..27 μm
Finish ground .25 to .64 μm (Steeds.W.[59])

In practice, values of h , a , w and β that give values of Ra above those recommended would not be used. The above analysis helps to pinpoint such values.

3.6 DISCUSSION OF THE EFFECTS OF DRESSING AND GRINDING VARIABLES ON WORKPIECE SURFACE ROUGHNESS, Ra .

The analysis shows that for circular grinding, the workpiece surface roughness is dependent for its value upon two factors, namely, the ratio of the grinding wheel and workpiece rotational speeds N/n , and the ratio of the grinding wheel and workpiece-feed widths Wn/v_f. (The parameters D , d , and l have no effect on workpiece surface roughness.) The above ratios determine the degree of interference, E , between overlapping ground profiles, and their values when related to the dressing feed h .

To establish the effects of N, n, W, v_f, h and a^* on workpiece surface roughness Ra, a computer programme has been written which embraces the equations derived in this study. This programme is found in Appendix **IV**. A range of values for a^*, v_f and h have been used to cover the conditions that would be expected in practice ; the wheel and workpiece rotational speeds (N and n) are taken directly from the grinding machine used for this research.

From values of N, n, V_t and h entered into the first computer programme, two facts are established, namely, that for any given set of cylindrical traverse grinding conditions, the values of interference, E, calculated for the first feed band on the workpiece are repeated for every other feed band along the workpiece length, and secondly, that traversing the workpiece past the grinding wheel in either the same or opposite direction to that when dressing, gives approximately the same value of workpiece surface roughness, all other things being equal. These facts greatly simplify the analysis.

From the second programme results, three diagrams have been drawn (figs. 3.22 to 3.24 inclusive) to show the effects of N, n, W, V_t, h and d^* on workpiece surface roughness. These results show that changes in h (d^* constant, V_t variable), produce little change in workpiece surface roughness, R_a, for some of the conditions, and large changes for others. To simplify matters, only minimum values of R_a have been plotted for the range of values of h used. The maximum value of R_a for any set of values of d^*, V_t and h is $d^*/4$.

Consider figs. 3.22 to 3.24. These show that the reciprocal of the ratio W_n/V_t, being the parameter which governs the amount of grinding wheel width actively engaged in grinding, has a major influence on workpiece surface roughness when it is assigned low values. This is because of the increase in the number of values of interference as the value of V_t/W_n is reduced, (i.e. V_t/n reduced.) From figures 3.22 and 3.23, it can be seen that the minimum value that R_a can attain for values of $V_t/W_n > \cdot 4$, and any value of d^*, is approximately half the value that would occur if no interference took place at all. For values of $V_t/W_n < \cdot 4$, the value of R_a is reduced considerably as V_t is reduced, particularly at the higher values of d^* (10 μm). For the lower values of d^* (2 μm), changes in V_t have only a minimal effect on R_a. In general, for values of $V_t/W_n > \cdot 4$, the influence of d^* on R_a is greater than that of V_t, and visa-versa. Increasing

the value of n , N remaining constant, reduces the value
of v_t/Wn „ and hence reduces Ra . When the ratio Wn/v_t
has a value greater than 2, and is not an integer, the
workpiece takes on two values of surface roughness per
feed width.

The theoretical values of workpiece surface roughness,
evaluated from equation (3.44), can be reduced further by
modifying the equation to consider the dressed grinding
wheel surface as having a form composed of trapezoidal
elements instead of triangular ones.

The above analysis can be used to predict the
minimum value(s) of workpiece surface roughness that can
be attained theoretically, for any values of N , n ,
v_t , W and a^*. For plain cylindrical traverse grinding,
it is generally accepted in industry that the value of
v_t/Wn is in the order of .5 to .67. Since these values
are above the value of the turning point, $v_t/Wn = .4$, a
reduction in Ra can be brought about only by reducing
the value of a^*. In practical terms, this means using a
relatively blunt diamond with a low traverse rate when
dressing.
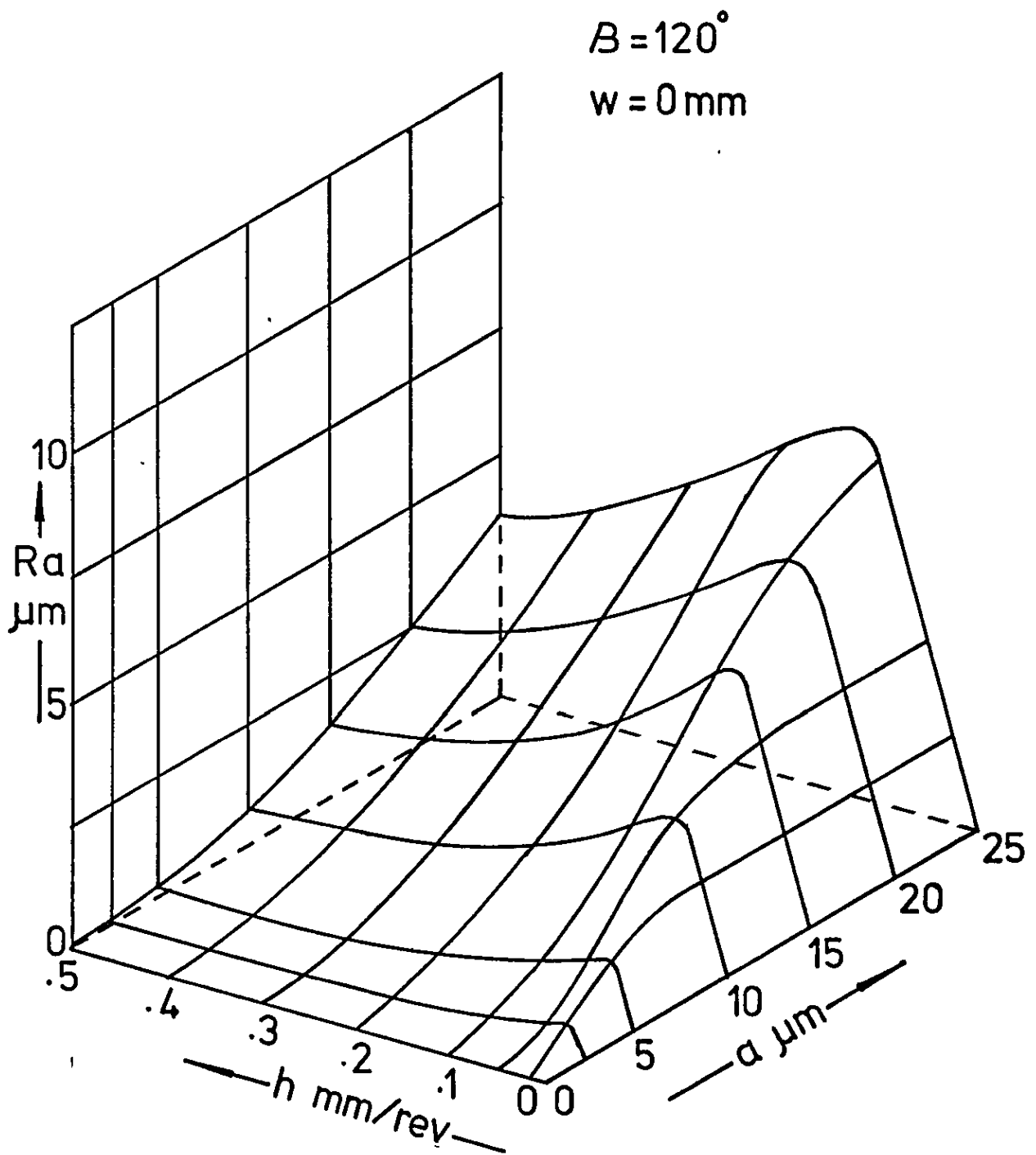
Fig. 3.17   Variation of grinding wheel surface
roughness, Ra, for changes in the dressing
parameters h and a ; β and w constant
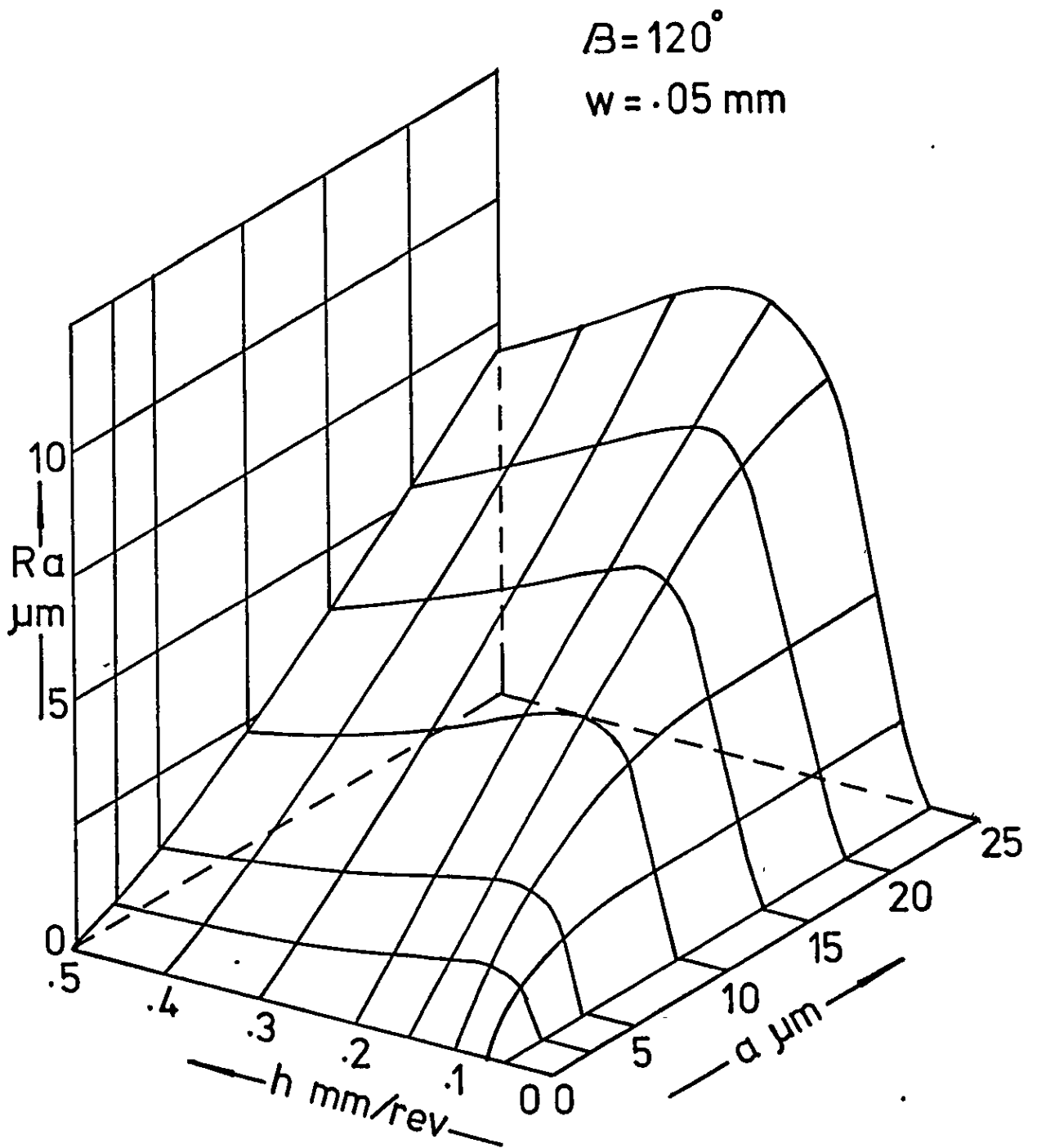
Fig. 3.18   Variation of grinding wheel surface roughness, Ra, for changes in the dressing parameters h and a; β and w constant
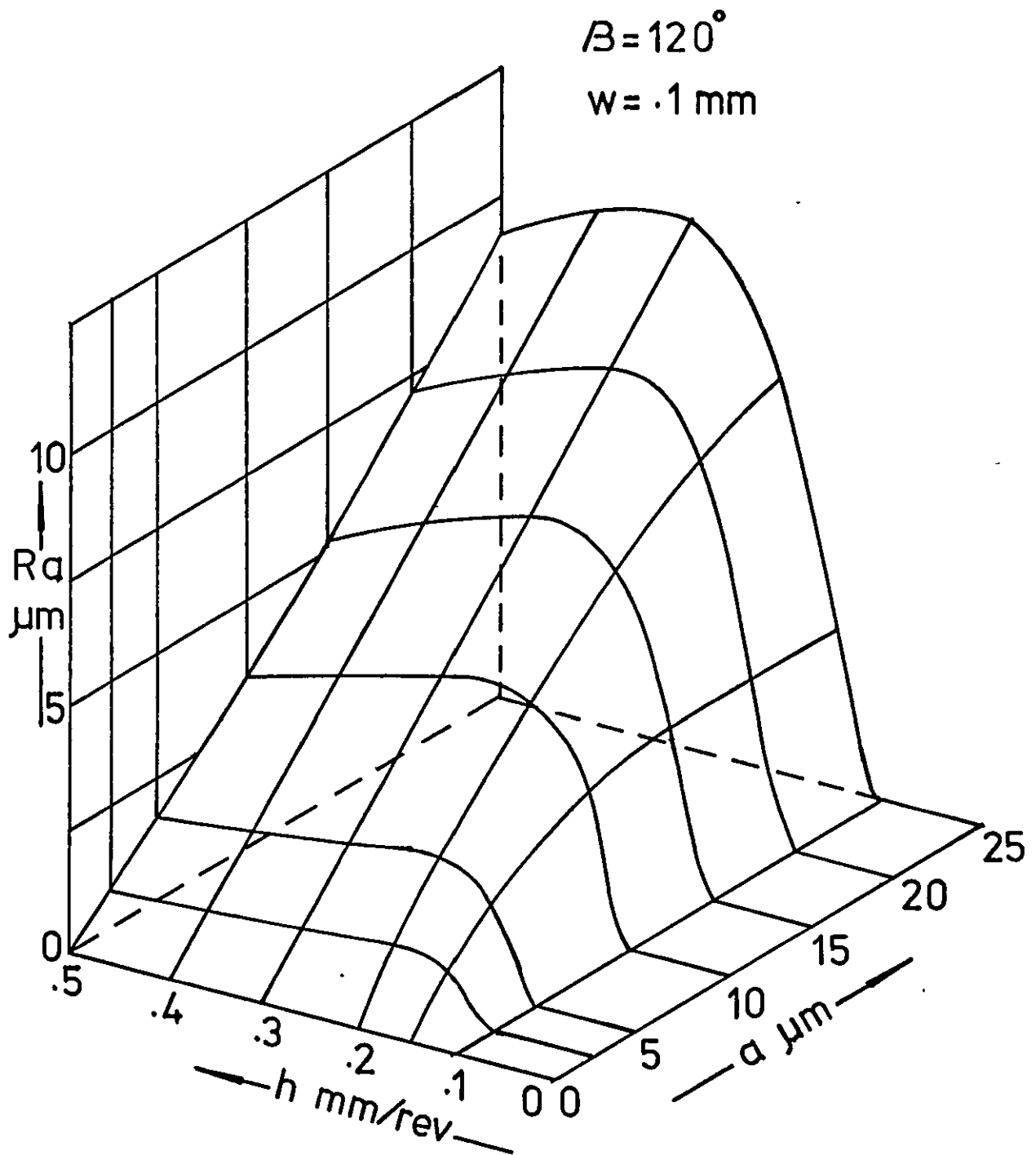
Fig. 3.19   Variation of grinding wheel surface roughness, Ra, for changes in the dressing parameters h and a ; β and w constant
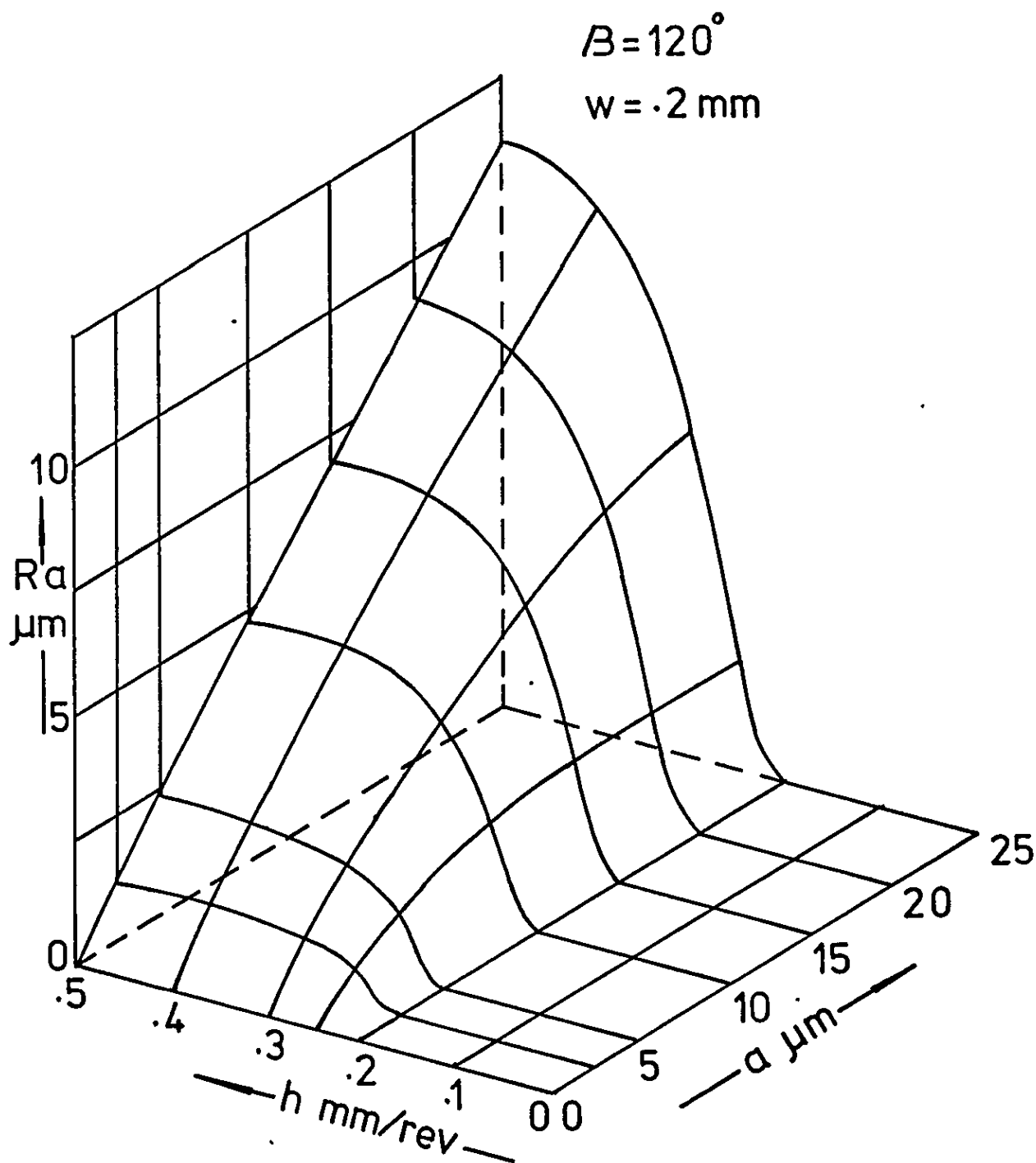
Fig. 3.20 Variation of grinding wheel surface roughness, Ra, for changes in the dressing parameters h and a ; β and w constant
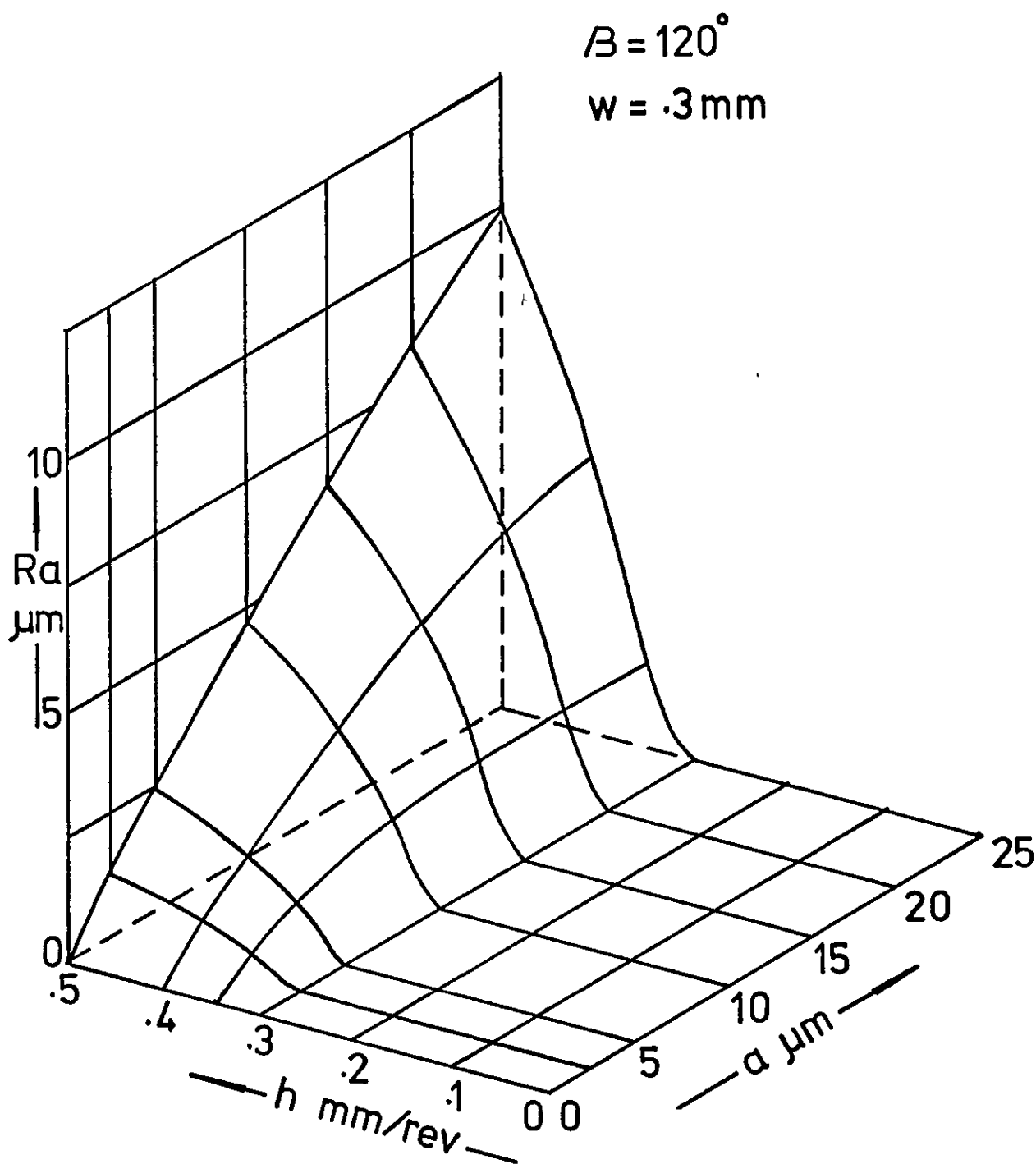
Fig. 3.21 Variation of grinding wheel surface roughness, Ra, for changes in the dressing parameters h and a ; β and w constant
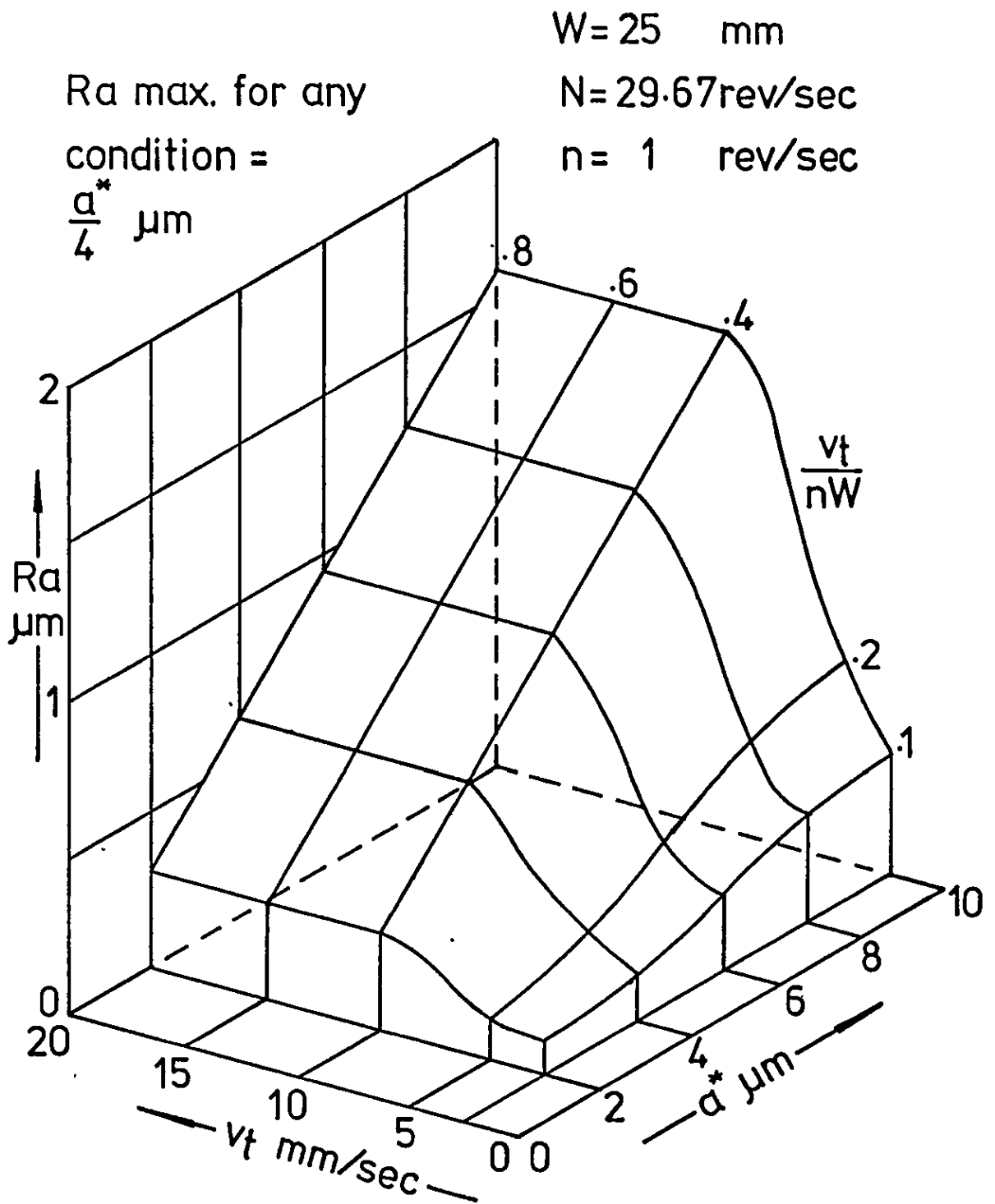
Fig. 3.22 Variation of workpiece surface roughness, Ra, for changes in the grinding parameters v_t and a^*; W, N and n constant.
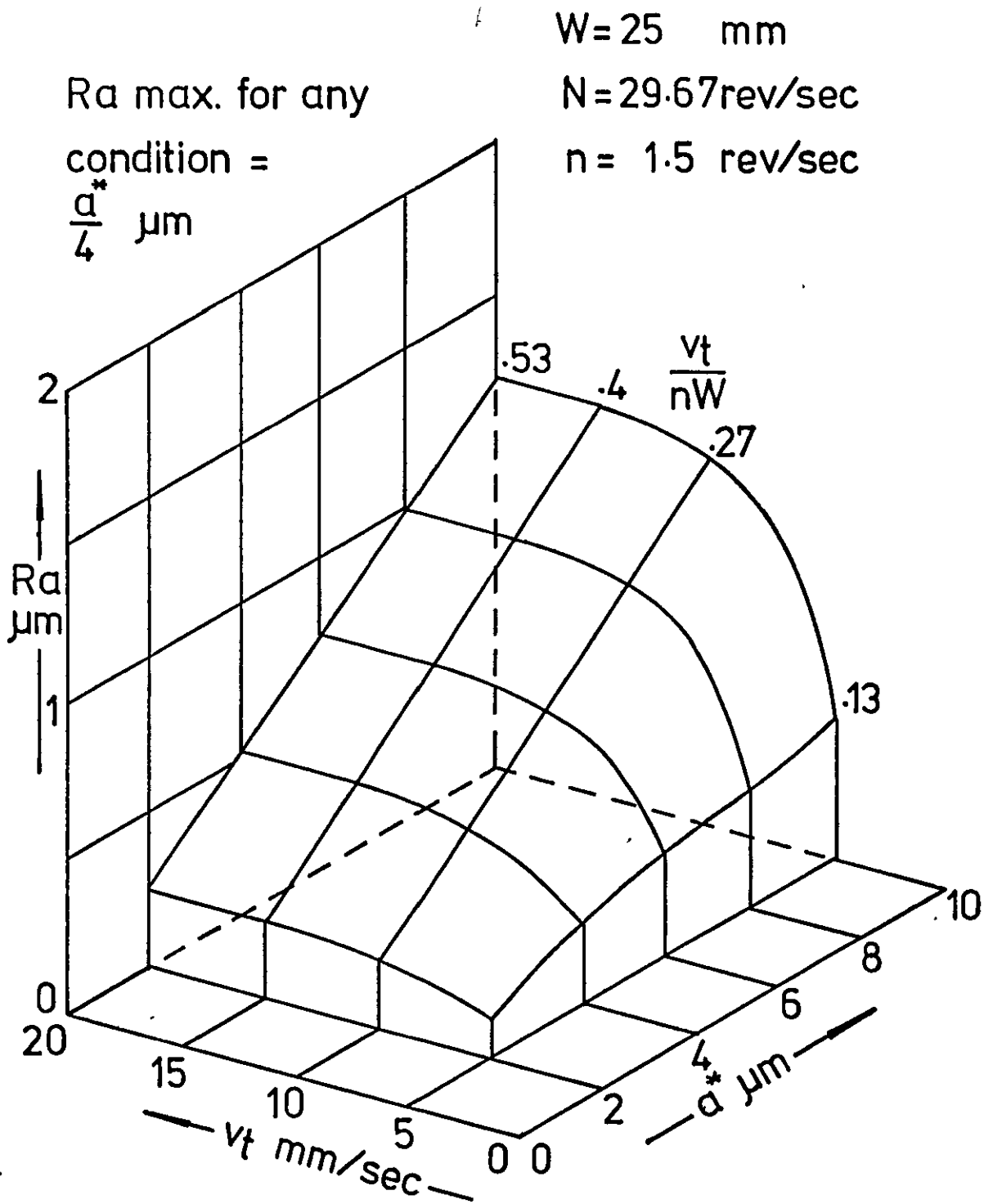
Fig. 3.23 Variation of workpiece surface roughness, Ra, for changes in the grinding parameters v_t and a^*; W, N and n constant
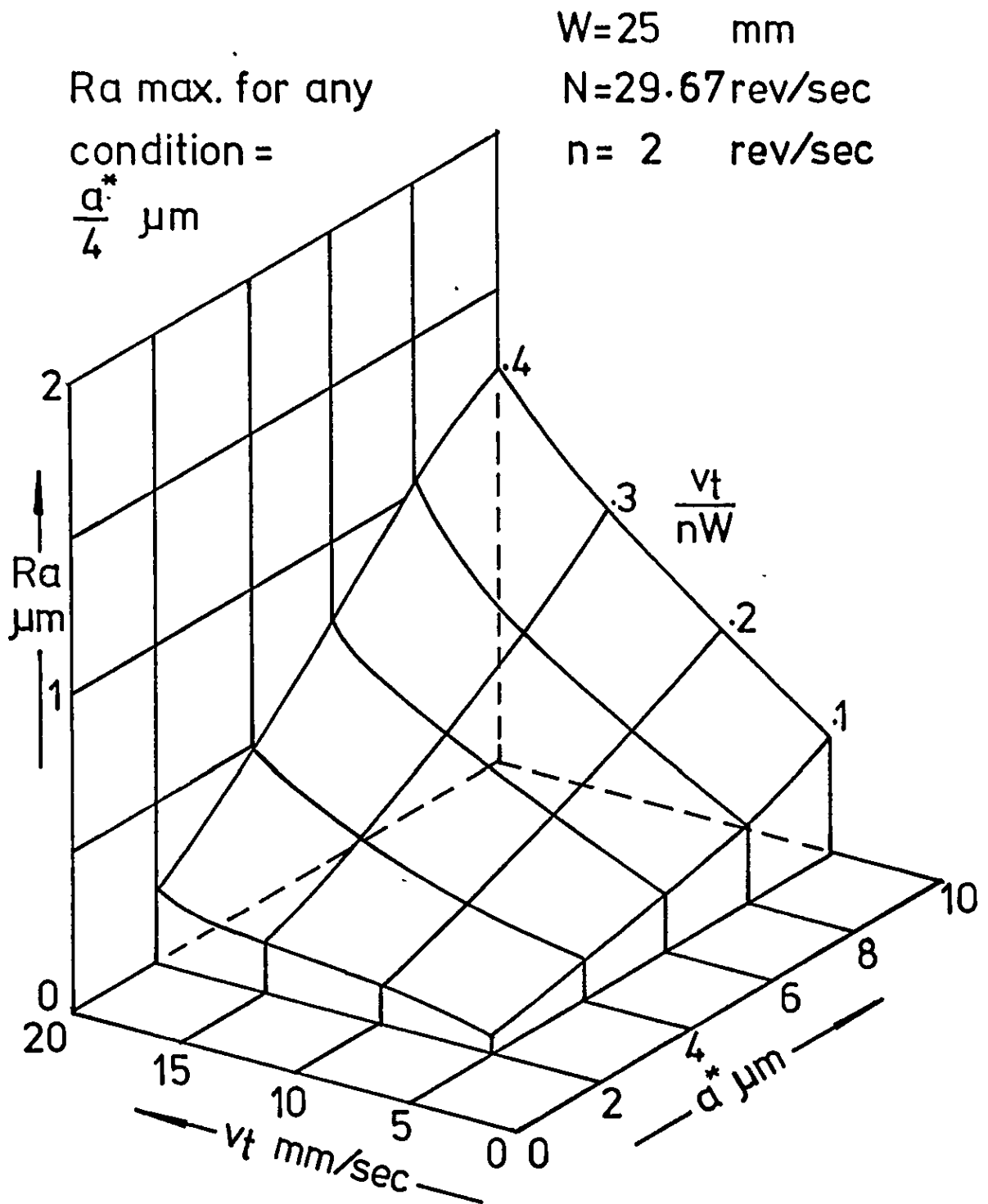
Fig. 3.24 Variation of workpiece surface roughness,
Ra, for changes in the grinding parameters
v_t and a^*; W, N and n constant

CHAPTER 4

THE CYLINDRICAL GRINDING MACHINE AND ITS ASSOCIATED
EQUIPMENT

4.1   INTRODUCTION

The research was conducted on a Jones and Shipman
Universal Grinding Machine, model 1300 E.I.U. This is a
standard production machine capable of performing both
internal and·external grinding operations. (See fig. 4.1
for a general front view of the machine.)

For external cylindrical grinding, the workpiece is
mounted between the tailstock and workhead centres on the
machine table, and grinding is performed at about 5,000
s.f.m. (25 m/sec), using a standard 305 mm diameter by
25 mm wide grinding wheel.

The table traverse, which determines the longitudinal
dressing or grinding rate, is governed by a hydraulic spool
valve which is infinitely variable over its speed range.
Infeed of the wheel head for dressing or grinding operat-
ions, can be carried out automatically by the machine at
each reversal of the table traverse, or applied manually
by the operation of two hand wheels situated at the front
of the machine.

Provision for dressing the grinding wheel is made
by mounting a diamond tool in the tailstock. This is
usual on most cylindrical grinding machines, as the tail-
stock provides a rigid means of support for the dressing
tool. The dressing operation is normally performed at
the same peripheral wheel speed as that for grinding.

Coolant is supplied to the grinding wheel via a
pump from a tank situated at the rear of the machine, and
filtration of the coolant is achieved by using a
Philips Universal Coolant Clarifier.

4.2   MACHINE SPECIFICATION FOR EXTERNAL CYLINDRICAL
GRINDING

Standard grinding wheel	12" x 1" x 5"
	(305mm x 25.4mm x 127mm)
Wheel speeds, rev/min (two)	1,750-2,300
H.P. of wheel head motor	2
Max. diameter ground with new wheel	10" (254mm)
Max. grinding length between centres	27" (686mm)
Table traverse rates, infinitely variable per minute	3" to 144" (76mm to 3,658mm)
Feed range at reversal of table, reduction in diameter	.0002" to .0012" (.005mm to .030mm)

(See fig. 4.2 for table traverse and
cross feed hydraulic circuit diagrams)

Workhead speeds, rev/min	40,60,90,140,210,320.
H.P. of workhead motor	3/4

4.3   MODIFICATION TO THE TABLE TRAVERSE

4.3.1 Problems associated with the hydraulic drive

From the results of preliminary tests conducted on
the machine to ascertain the limitations of the hydraul-
ically operated table traverse, it was thought necessary
to find an alternative mode of operation. Whilst this
method of traversing the table was adequate to fulfill
grinding requirements, it was thought unsuitable to
cover the range of dressing conditions required. The
main problems associated with the hydraulic drive were
twofold, namely, the large variations of traverse rate

observed for small incremental changes of spool valve
setting, and the effects of change of viscosity of the
hydraulic oil during the warm up period of the machine.
The first of these problems was caused by a poorly
calibrated spool valve, which could best be solved by
installing a more precise method of oil regulation. The
second problem was responsible for variations of traverse
rate at any spool valve setting during the warming up
cycle of the machine, and for stick-slip occuring between
the machine bed and table, at traverse rates around 3mm/sec.
These phenomena could be overcome partially by thermostatically
-controlled heating of the hydraulic oil, thus assisting
it to reach its stable operating temperature sooner.
Fig. 4.3 shows the variation of table traverse against
hydraulic valve position. It can be seen that the full
range of table traverse rate occurs between valve settings
of 1 and 5, this corresponding to a valve rotation of
approximately 70 degrees, with a maximum traverse rate of
76mm/sec. Since most dressing is done in the range
.1mm/rev to .5mm/rev of grinding wheel, this corresponding
to traverse rates of 3mm/sec to 15mm/sec respectively, for
a wheel revolving at 1,800 rev/min, then the possibility
of inaccurate traverse rate settings due to the above
mentioned adverse conditions, is large.

4.3.2 Alternative method of table traverse using a
      fractional h.p. d.c. motor drive.

Fractional h.p. d.c. motors have been used success-
fully at Leeds University, Dept. of Mechanical Engineering,
and Salford University, Dept. of Mechanical Engineering,
where infinitely variable speed drives to grinding machine
tables were required, which needed accurate control. It
was therefore decided to adopt a similar system. An
advantage of variable speed d.c. motor drives over other
types of drive, is that motor control gear with thyristor
actuation is simple in construction, and relatively cheap
to manufacture.

Tests conducted on the grinding machine showed that

a 1/4 h.p. motor adequately fulfilled the traverse requirements.

Fig. 4.4 shows a schematic view of the variable speed d.c. motor drive to the grinding table. The motor unit (7), is bolted to a backplate, which in turn is fastened to the grinding machine frame just below the traverse hand wheel. A toothed wheel (5), which is mounted on the motor shaft, works in conjunction with a magnetic perception head (6), to form part of an electrical feedback circuit, giving motor speed regulation. The end of the motor shaft is connected to a reduction gear box (4), where the drive is taken up by a toothed gear (3). Final drive to the traverse hand wheel is provided by a toothed belt which passes over the two, toothed gears (3) and (2).

The electrical connections from the d.c. motor field and armature windings, and magnetic perception head, are taken to the motor regulator module, and digital feedback circuit, respectively. Fig. 4.5 shows an overall view of the d.c. motor drive to the machine table.

4.3.3 Description of the Motor Regulator Module and Digital Feedback System.

To obtain accurate speed regulation for the d.c. motor from standstill, to a maximum speed of 3,000 rev/min a regulation system incorporating a feedback circuit had to be employed.

The system chosen was a type TR11-B d.c. Motor Regulator Module, and a type MH1-A Digital Feedback Circuit, both manufactured by G.E.C.-Elliot Industial Controls Lts. The feedback circuit was used in conjunction with a Magnetic Perception Head, manufactured by Smiths Industries Lts.

The TR11-B is a motor regulator module incorporating a thyristor drive, suitable for controlling the speed of a d.c. shunt wound motor by providing a constant field voltage, and a variable armature voltage. It is suitable for shunt wound motors requiring up to 1.5 amp mean armature current, i.e. about 1/4 h.p. at 180 volt d.c.,

the motor field being wound for 110 volt.

The unit incorporates a current limit, and a soft start circuit for use with any of the following modes of feedback.

1). Armature voltage feedback.

2). Tachogenerator feedback.

3). Digital feedback with MH1-A amplifier and magnetic perception head.

The feedback system chosen was of type (3). This system is more accurate than that of type (1), and much cheaper than type (2). Fig. 4.6 shows the external electrical connection diagram for the TR11-B d.c. motor regulator module with digital tacho feedback. Motor regulation from standstill to maximum speed, is set using a 10K potentiometer.

An inexpensive electronic tacho-generator system, comprising a magnetic perception head, and a digital feedback circuit of the type MH1-A was used to give a feedback signal which is directly proportional to motor speed.

The magnetic perception head consists of a coil wound on a permanent magnet, which is then fixed close to a toothed wheel mounted on the motor shaft. Fig. 4.7 gives mounting details. As the shaft rotates, the reluctance of the air gap changes, and a voltage is induced in the coil. The frequency of the voltage is the same as the number of teeth passing the magnetic poles in one second, and the magnitude of the voltage is proportional to the gap between the teeth and the magnetic poles. The induced voltage signal is passed to the MH1-A amplifier, and hence to the motor regulator module. The MH1-A unit operates at frequencies up to 1,500 Hz. This corresponds to a 30 toothed wheel on the shaft of a motor rotating at 3,000 rev/min.

4.3.4 Calibration of the variable speed d.c. motor drive.

Since the variable speed d.c. motor drive was to be
employed for wheel dressing operations, it was decided to
match the maximum wheel dressing rate required, to the
maximum motor speed. In this way, the greatest accuracy
would be obtained from the equipment over the full range
of dressing rate.

The grinding wheel could be rotated at one of two
speeds, depending upon the wheel diameter. For a new wheel,
i.e. 12 inches diameter (305 mm), the speed would be
1,750 rev/min, making the peripheral wheel speed 5,500 s.f.m.
(28 m/sec), and for a wheel reduced in diameter below
10 inches (254 mm), the speed would be 2,300 rev/min,
thus maintaining a peripheral wheel speed in the region
5,000-6,000 s.f.m. (25-31 m/sec). To simplify conditions,
the wheel speed was fixed at the lower of the two avail-
able, making replacement of the grinding wheel necessary
on reaching a diameter of 10 inches (254 mm), to main-
tain the correct grinding speed. This would require only
one calibration chart.

The feed rate is defined in terms of distance moved
by the diamond tool per revolution of the grinding wheel.
This is more meaningful than expressing it as a velocity,
since it takes into account the wheel speed.

The maximum dressing rate required was .020 inch/rev
(.5 mm/rev), of grinding wheel, this fact being used as a
basis for deciding the drive requirements from the d.c.
motor to the traverse hand wheel on the grinding machine.

The following calculation shows how the motor speed
was matched with the required dressing rate.

Gear ratios are as depicted in fig. 4.4

Starting at the wheel head:-

Actual speed of grinding wheel   = 30 rev/sec

Max. traverse rate required   = .5 mm/rev

∴ Traverse rate of table   = .5 x 30 mm/sec

                                      = $\underline{\underline{15}}$ mm/sec

Considering the d.c. motor side:-

Actual max. motor speed   = 48 rev/sec

Reduction rate of gear box used = 20:1

∴ Output from gear box   = $48 \times \frac{1}{20}$ rev/sec

                                      = 2.4 rev/sec

Speed reduction from gear
box to traverse hand wheel   =

         $\underline{\text{Number of teeth on driver gear at gear box}}$
         Number of teeth on driven gear at hand wheel

                                    = $\frac{10}{20} = \frac{1}{2}$

Speed of hand wheel   = $2.4 \times \frac{1}{2}$ rev/sec

                                      = 1.2 rev/sec

Now, one revolution of hand wheel moves table 12.7 mm

Traverse rate of table   = 1.2 x 12.7 mm/sec

                                      = $\underline{\underline{15}}$ mm/sec

Calibration of the system was achieved using a
tachometer connected to the gear box on the motor shaft.
The electrical element responsible for varying the speed
of the d.c. motor was a 10K potentiometer, giving full
speed adjustment through 180 degrees of rotation. Fig. 4.8

shows the calibration chart of table traverse, using the variable speed d.c. motor drive.

4.4   WHEEL DRESSING

The grinding machine is provided with two means for wheel dressing. One is a toolholder forming an integral part of the tailstock, and the other is a table mounted fixture.

The tailstock arrangement is shown in fig. 4.9. It can be seen from the diagram that the drag angle of the dressing tool varies according to the diameter of the grinding wheel, and as such, control of the dressing geometry is limited. Since such control is of prime importance, this method of dressing was disregarded.

The table mounted fixture is shown in fig. 4.10. The original fixture was modified to accept the special tool-holder designed for use with the wheel dressing dynamometer (see chapter 5). This arrangement presents the diamond tool to the grinding wheel so that the point of contact between the wheel and diamond always lies in a horizontal plane passing through the wheel centre. In this way, the dressing geometry remains constant, irrespective of wheel diameter. This attachment was supplementary to the dressing dynamometer.

4.5   WHEEL BALANCING

4.5.1 Reasons for dynamic wheel balancing being chosen as opposed to static balancing.

Present requirements in respect of surface finish cannot, in most cases, be fulfilled with wheels which have been statically balanced. The tolerance in the taper, as well as the run-out of the balancing arbor, limit the accuracy of this balancing method. Under operating conditions, the grinding wheel becomes saturated with coolant and because of inherent inhomogeneity in the wheel structure, the saturation is not uniform, and coolant unbalance cannot be corrected by static balancing. Often a grinding

wheel becomes unbalanced after it has been dressed a few times, and removal of the wheel to check the unbalance is usually inconvenient and time wasting. Since much of the present research work is involved with measuring the force generated during dressing, this generally being of a low order of magnitude, it can be seen that any residual out of balance force in the grinding wheel could impare the accurate recording of the dressing force. Because of tnese reasons, it was decided to introduce dynamic balancing to the machine, and balance the wheel in situ.

4.5.2 ELTRODYN balancing unit for grinding wheels.

The equipment chosen for dynamic wheel balancing was the ELTRODYN balancing unit made by REUTLINGER & Son, of Germany. The equipment consists of four basic parts, these being a stroboscopic hand lamp and out of balance indicating unit, and a vibration pick-up with an accompanying electronic device. Fig. 4.11 shows a general view of the balancing equipment mounted on the machine.

4.5.3 Mode of operation of the ELTRODYN balancing unit.

The schematic diagram, fig. 4.12, shows the basic design of the measuring apparatus for use with a single grinding machine. In it, is the headstock of the machine (A), the electronic measuring system (B), and the indicating instrumentation (C). The vibration pick-up (1), is mounted on the headstock casing, with its axis at right angles to the spindle axis, and parallel to the grinding pressure. The rest of the equipment, B and C, is positioned in front of the machine for ease of manipulation by the operator.

The unbalance of the grinding wheel forces the headstock (A), to oscillate at the same frequency as the speed of rotation of the wheel. The vibration pick-up (1) transforms this mechanical vibration into an analogous alternating voltage, which is then fed to the electronic measuring system (B), by way of a sensitivity regulator (2),

and an electrical filtering circuit (3). This circuit only admits alternating voltages with a frequency corresponding to the speed of rotation of the grinding wheel. In this way, parasitic vibrations which do not originate from the unbalance of the grinding wheel, are eliminated from the circuit. The alternating voltage, which is proportional to the magnitude of wheel unbalance, is fed to the indicating instrumentation (C), and can be read on the measuring instrument (5). As the wheel unbalance is corrected, by placing weights symmetrically at the same angle of arc to the "light spot" of the wheel, then the scale of the indicating instrument is graduated in degrees of arc. The measuring sensitivity can be increased for precision balancing by means of a switch (6). In the case of high sensitivity setting, the indication is given on a second linear scale of the measuring instrument. It shows how many mm. approximately, the weights in the wheel flange plate must be moved to achieve exact compensation for the unbalance.

The filtered measuring voltage (sinusoidal voltage) in the electronic system, is fed parallel to the indicating instrument to the impulse generator (4), which transforms its sinusoidal maxima into impulses, i.e. a short voltage impulse occurs for each revolution of the grinding wheel. This impulse causes the stroboscopic hand lamp (8) to flash in rythm with the speed of rotation of the grinding wheel. These light flashes are of so short a duration, that the grinding wheel appears to stand still when it is illuminated by the hand lamp, Before the start of the test, the grinding wheel face is divided up into a number of segments, using chalk, each segment being numbered. The numbered portion which is highlighted with the stroboscopic hand lamp, indicates the light spot about which the weights should be set, according to the reading obtained from the measuring instrument (5). When the wheel is dynamically balanced, the stroboscopic lamp will cease to flash.

4.6 TEMPERATURE AND RELATIVE DISPLACEMENT TESTS

4.6.1 Introduction to the tests.

A series of tests were conducted on the grinding machine to establish a relationship between the temperature changes induced in the machine, due to the motion of the machine elements, and the resulting relative displacement between the table and wheel head.

The reasons for these tests are as follows:-

1). To determine the "warming up" time required for the machine to achieve equilibrium conditions.

2). To ascertain the relative displacement between the wheel head and table, over the "warming up" period of the machine.

3). To provide information on the best location for a wheel dressing dynamometer on the machine table.

All the tests were commenced at the start of the working day, and continued until the times shown on the various figures. The pattern of these tests was temperature/relative displacement against time for various machine elements in operation.

All temperatures were taken using a WYMARK THERMOMETER with magnetic base, positioned on the belt drive side of the wheel head. The reason for this position being chosen, was to eliminate the possibility of errors in temperature recording, due to the effect of air currents generated by the rotating grinding wheel. The relative displacement measurements were taken using STEINMEYER DIAL TEST INDICAT-ORS, located on magnetic stands on the machine table.

4.6.2 General Conclusions From The Tests.
1). The idle-running time for the machine to reach thermal stability is about 80 minutes.
(Figs. 4.13 to 4.16)

2). The idle-running time for the machine to reach positional stability varies between 80 minutes to 160 minutes, depending upon whether the traverse hydraulics are running, or off. (Figs. 4.13 and 4.14). These show also, that the wheel head has a tendency to twist, relative to the table as it warms up from rest.

3). The traverse displacement of the table relative to the wheel head, as measured when their mid-positions coincide (Fig. 4.15), reaches a maximum during warm-up, but subsequently diminishes by approximately 50%. This tendency is also observed with the table mid-position, located 18 inches (457 mm) to the wheel head mid-position (Fig. 4.16). However, in this position, the steady state relative displacement is approximately 75 % of the maximum value.

4). That the best position for locating a wheel dressing dynamometer on the table, is as near to the table centre as possible. This position gives minimum relative displacement between wheel head and table. (Figs. 4.15 and 4.16).
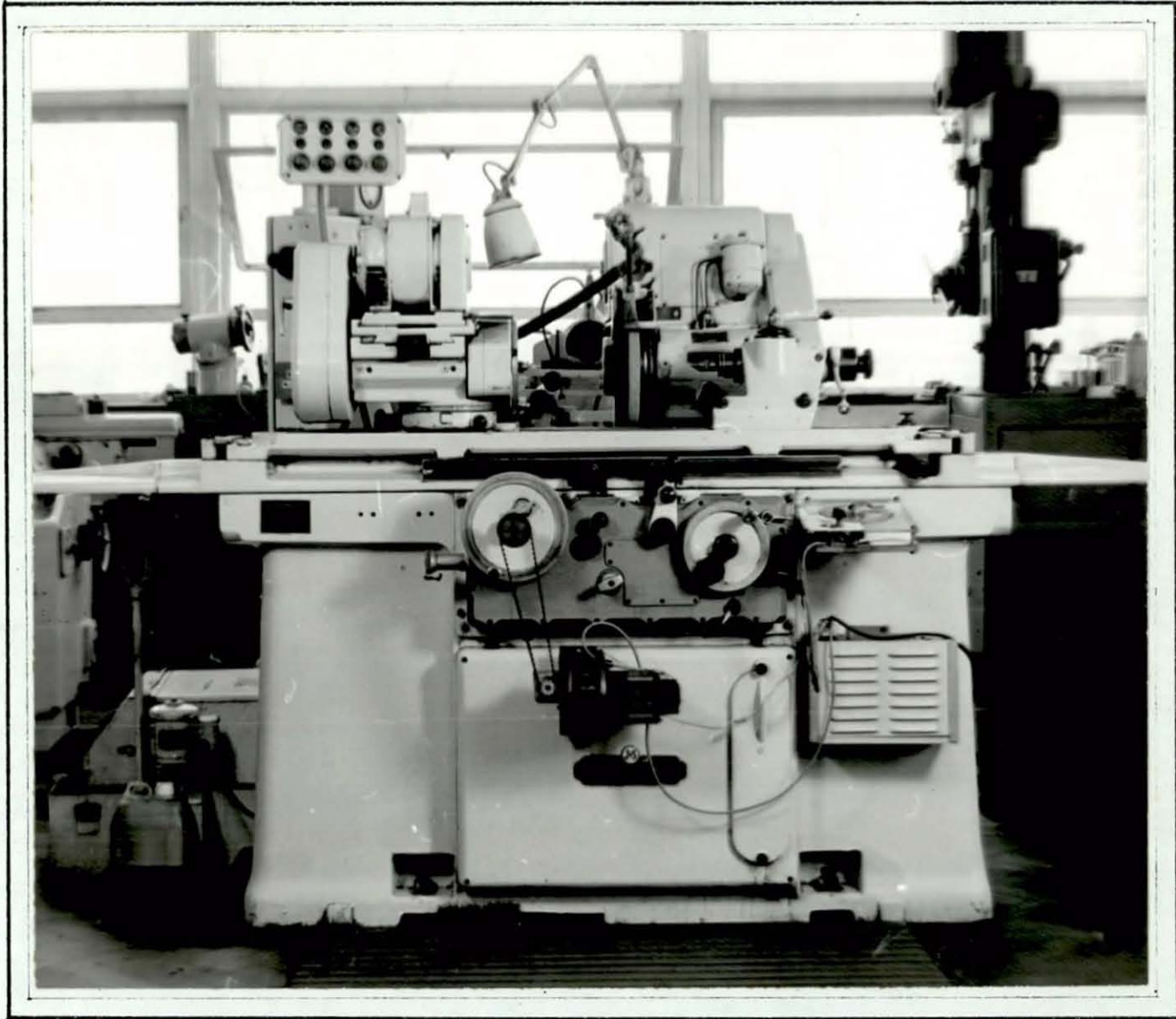
Fig. 4.1 View of the cylindrical
grinding machine.
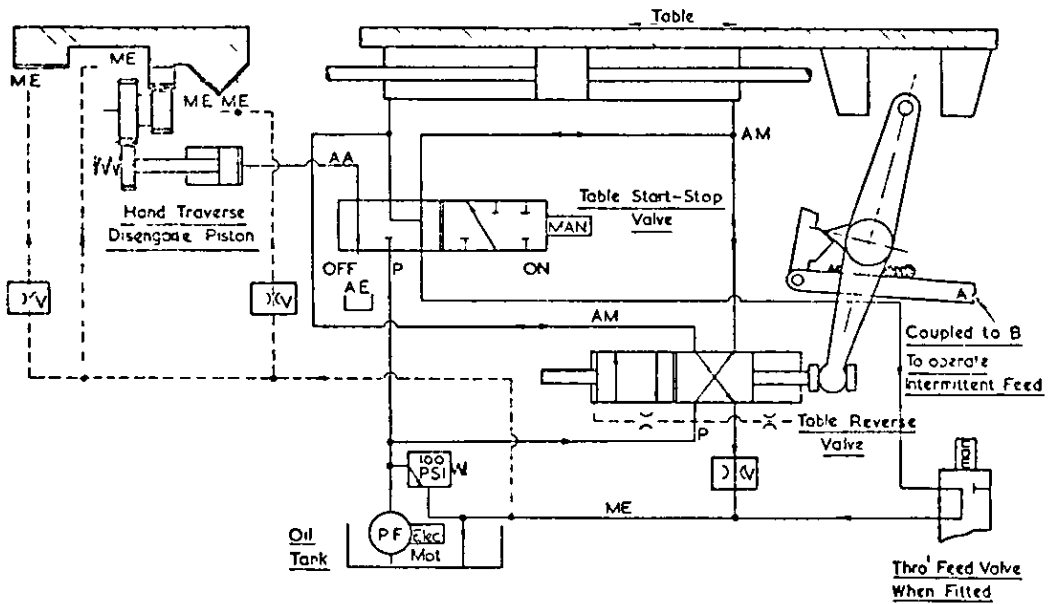
Table traverse hydraulic circuit diagram
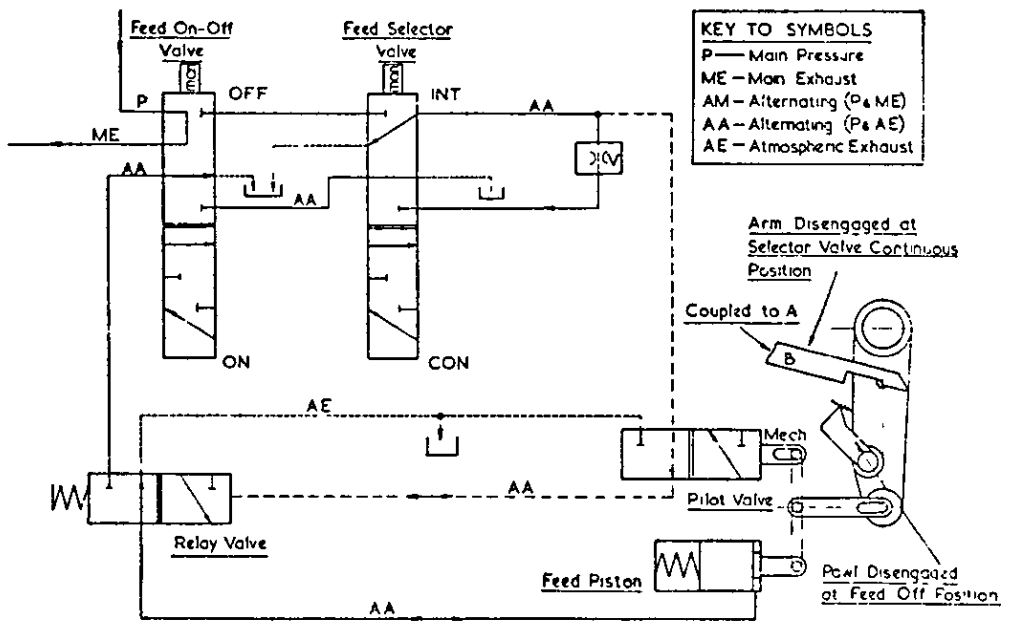
Cross feed hydraulic circuit diagram

Fig. 4.2 Hydraulic Circuit Diagram for Jones & Shipman Cylindrical Grinding Machine, Model 1300 E.I.U
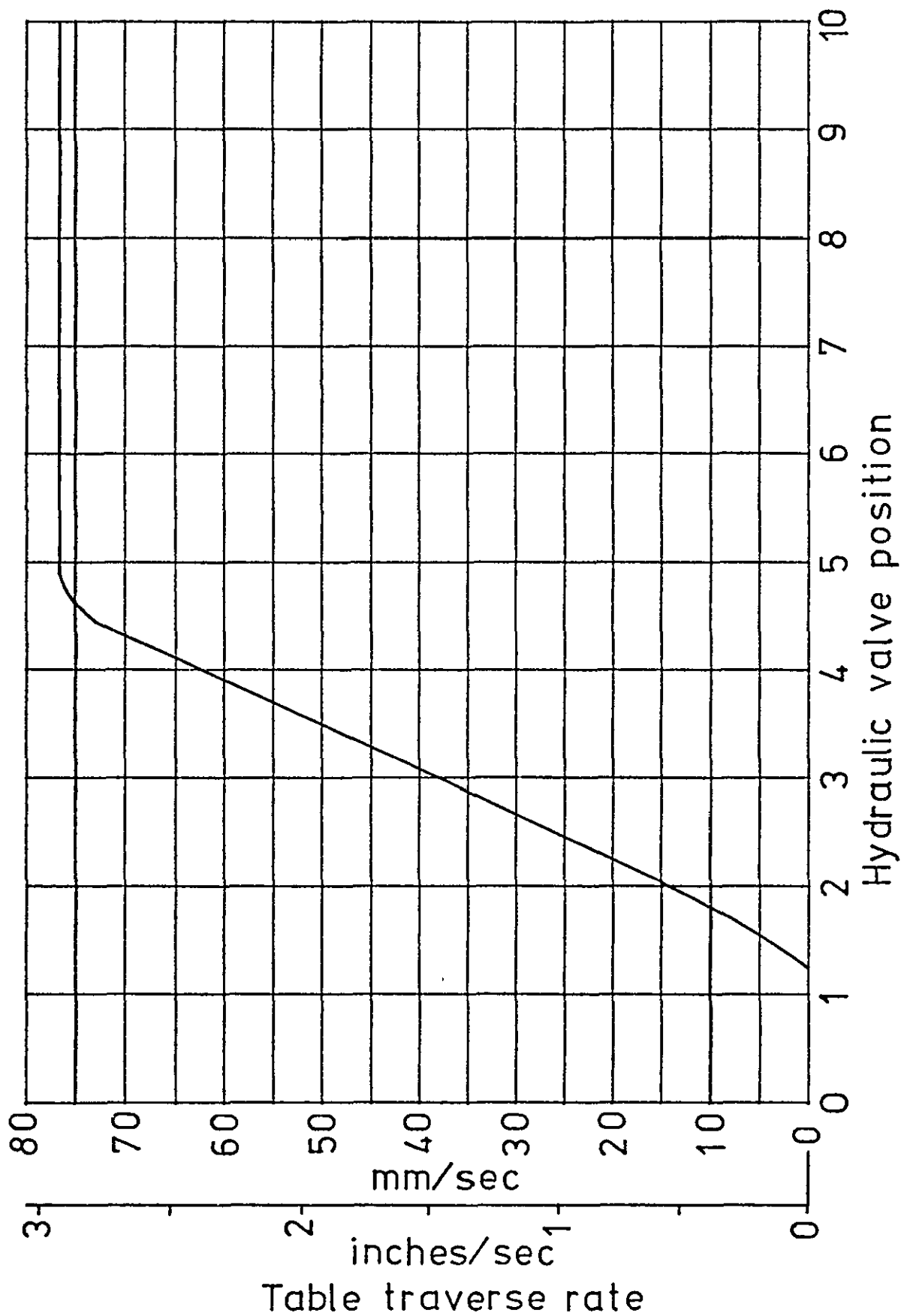
Fig. 4.3   Calibration chart of hydraulic table traverse for Jones & Shipman Precision Grinding Machine. Type E.I.U   Model 1300.

Traverse motion.

Machine Table

Handwheel motion

Traverse Handwheel

1 revolution of handwheel gives a table movement of 12·7 mm or ·5 inch.
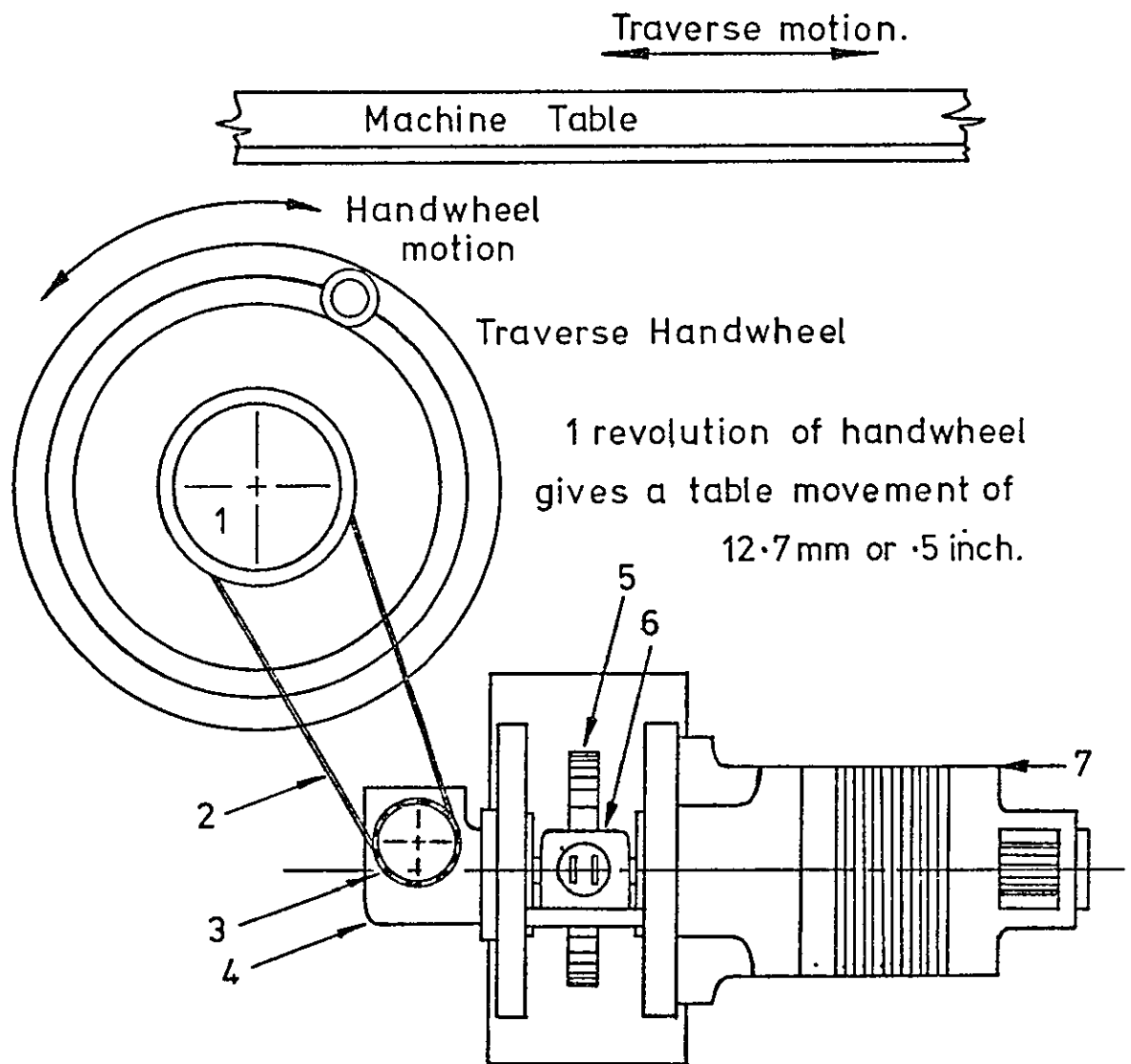
1. Toothed gear 20 teeth
2. Toothed belt
3. Toothed gear 10 teeth
4. Reduction gear 20:1
5. Toothed wheel 30 teeth
6. Magnetic Perception Head
7. 1/4 hp dc Motor 3000 rev/min

Fig. 4.4   Schematic view of Variable Speed dc Motor Drive to Grinding Machine Table.
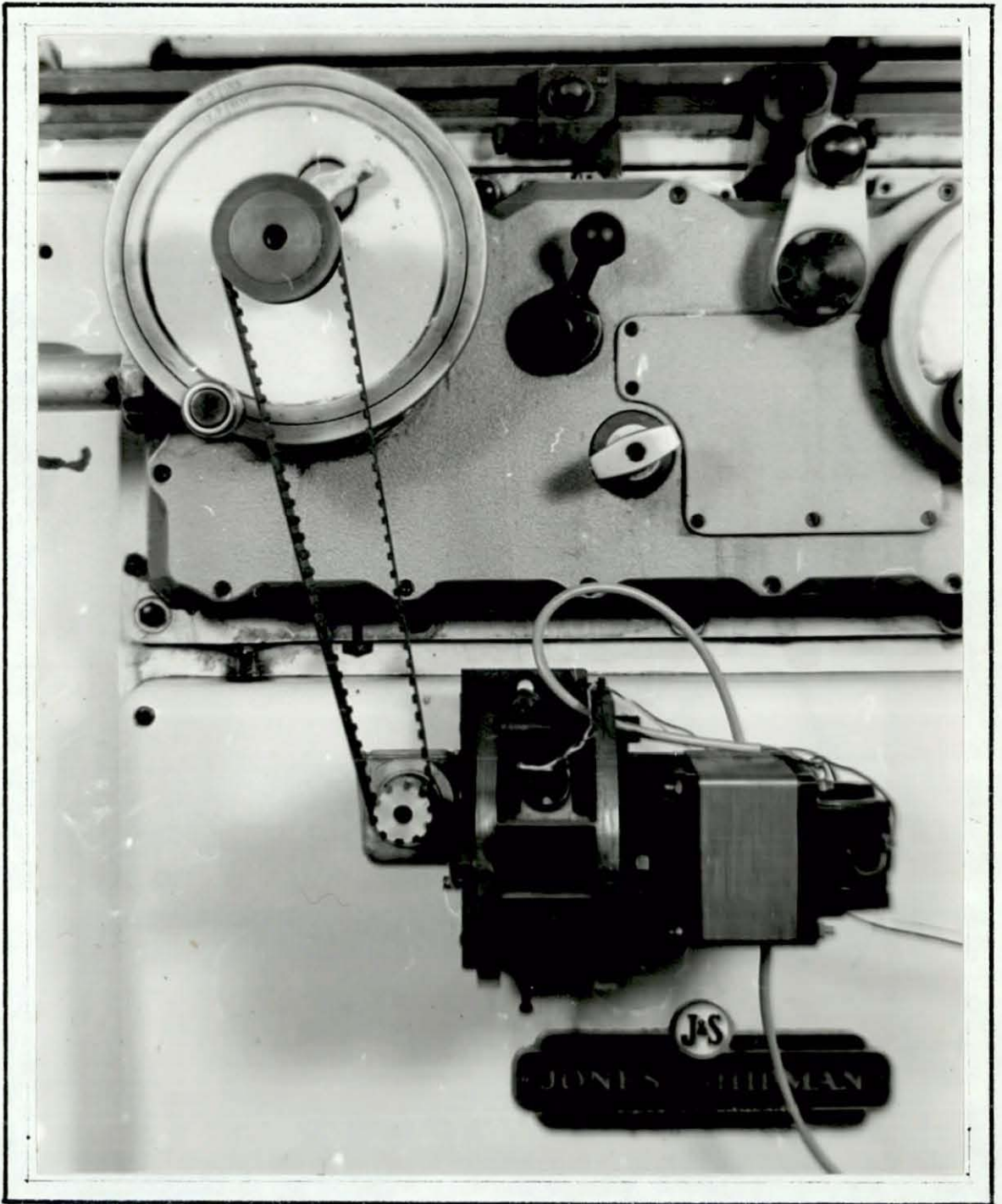
Fig. 4.5   Variable speed d.c. motor drive to
the cylindrical grinding machine table

$R_S = 100K\Omega$
.5watt

$C_S = 1\mu F$
400V dc

$R_L = 3.3\Omega$
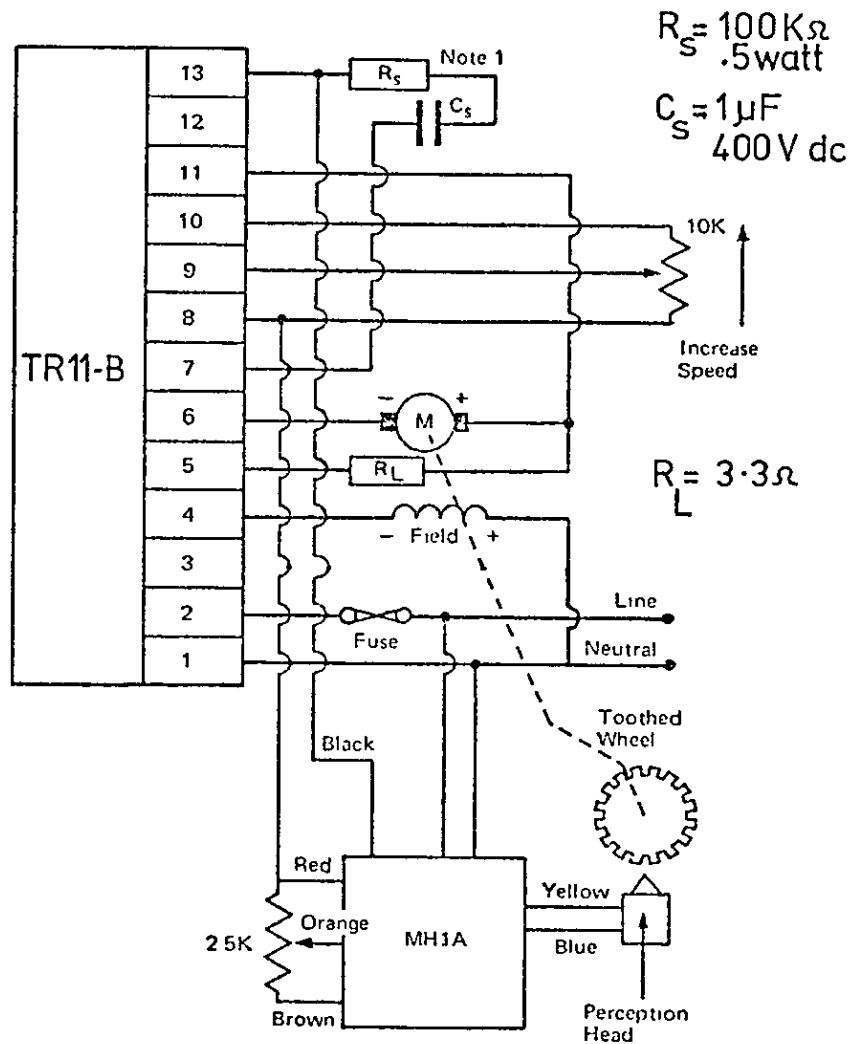
Fig. 4.6   Electrical connection diagram
for TR 11-B dc motor regulator
module with Digital Tacho Feedback.
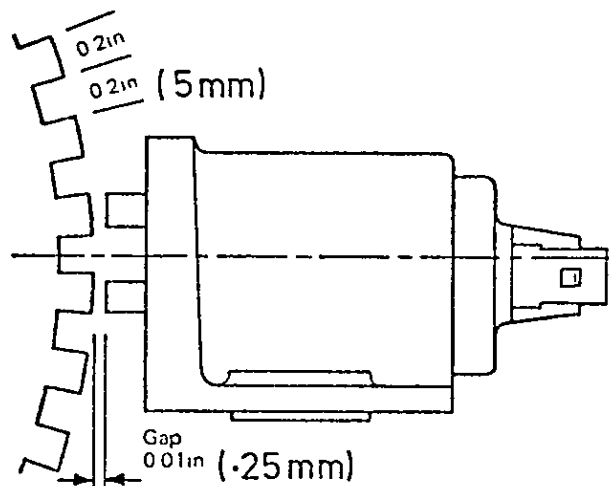
Fig. 4.7   Mounting details for Magnetic
Perception Head.
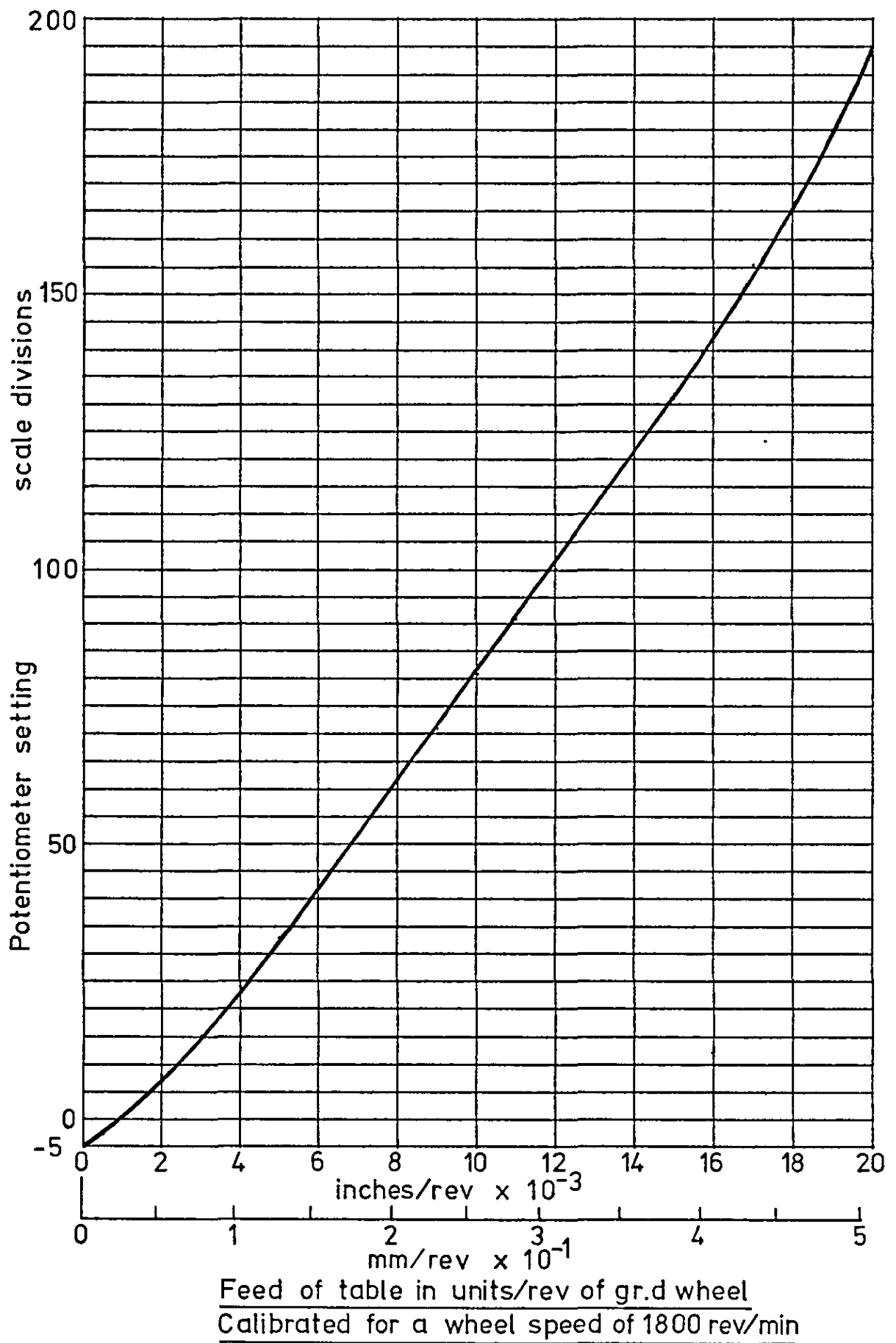
Fig. 4.8   Calibration chart of table traverse using variable speed dc motor drive.
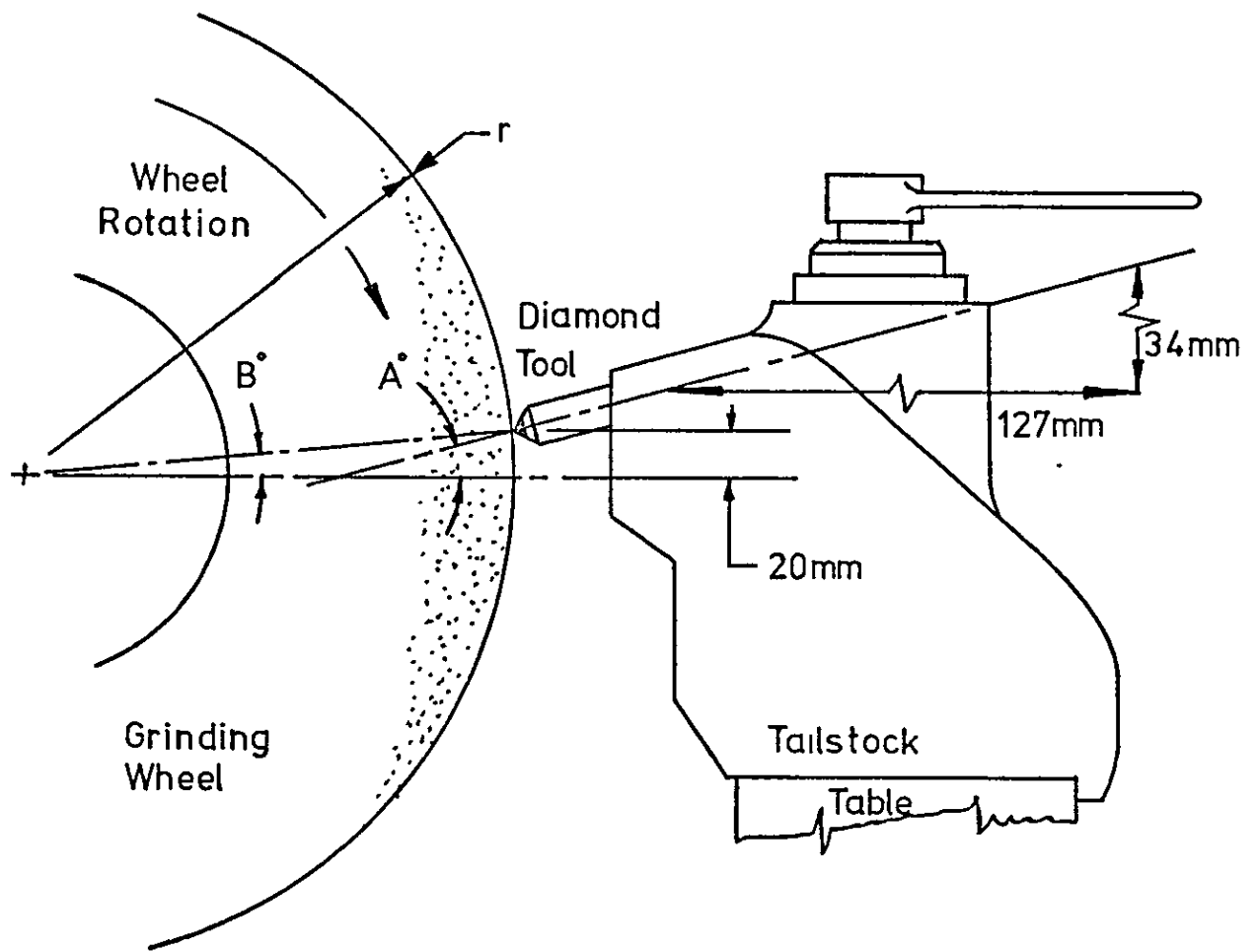
Angle A = $\tan^{-1} \dfrac{34}{127}$ = 15°

Angle B = $\tan^{-1} \dfrac{20}{r}$

When r = 152 mm, Angle B = 7° 30′

When r = 127 mm, Angle B = 9°

Max. Drag Angle of Diamond Tool = 15° - 7° 30′ = 7° 30′

Min.   „   „   „   „   „   = 15° - 9° = 6°

Fig. 4.9   Dressing tool mounted
in machine tailstock.

Wheel Rotation

Diamond Tool

Drag Angle

Grinding Wheel

Dressing Fixture
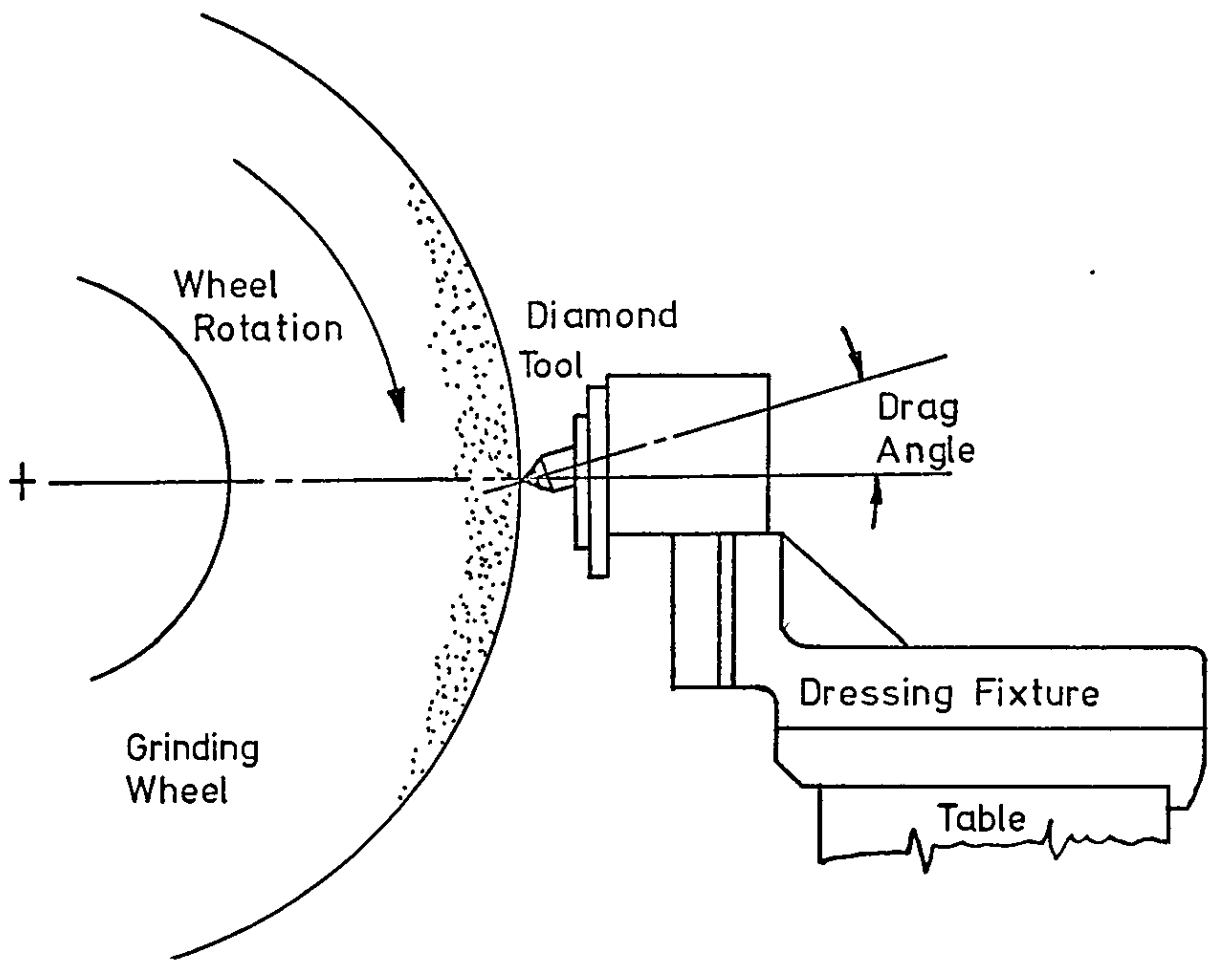
Table

Drag Angle constant at Tool Holder setting

Fig. 4.10   Dressing tool mounted in table fixture.
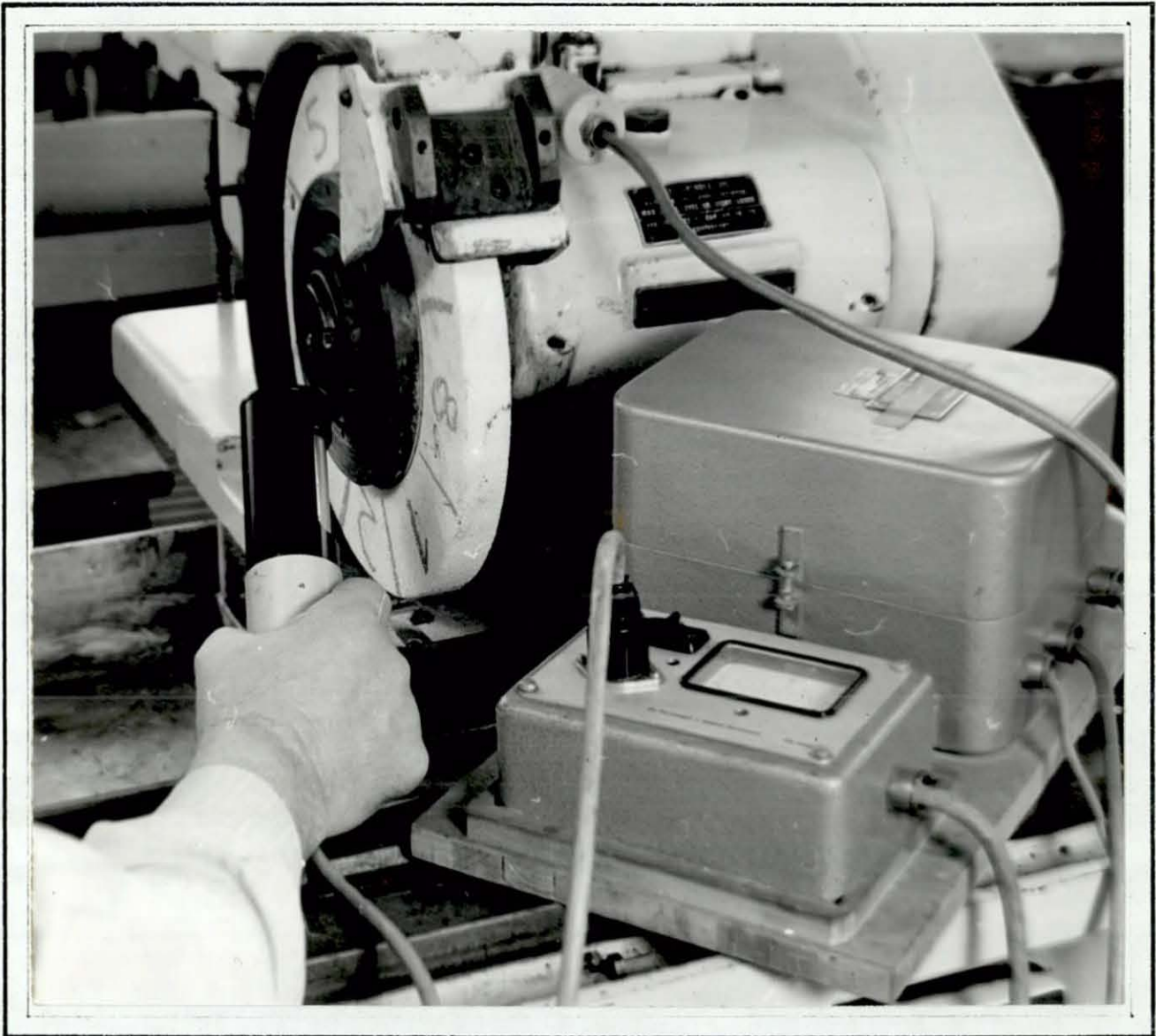
Fig. 4.11 View of the grinding wheel dynamic balancing equipment in use.
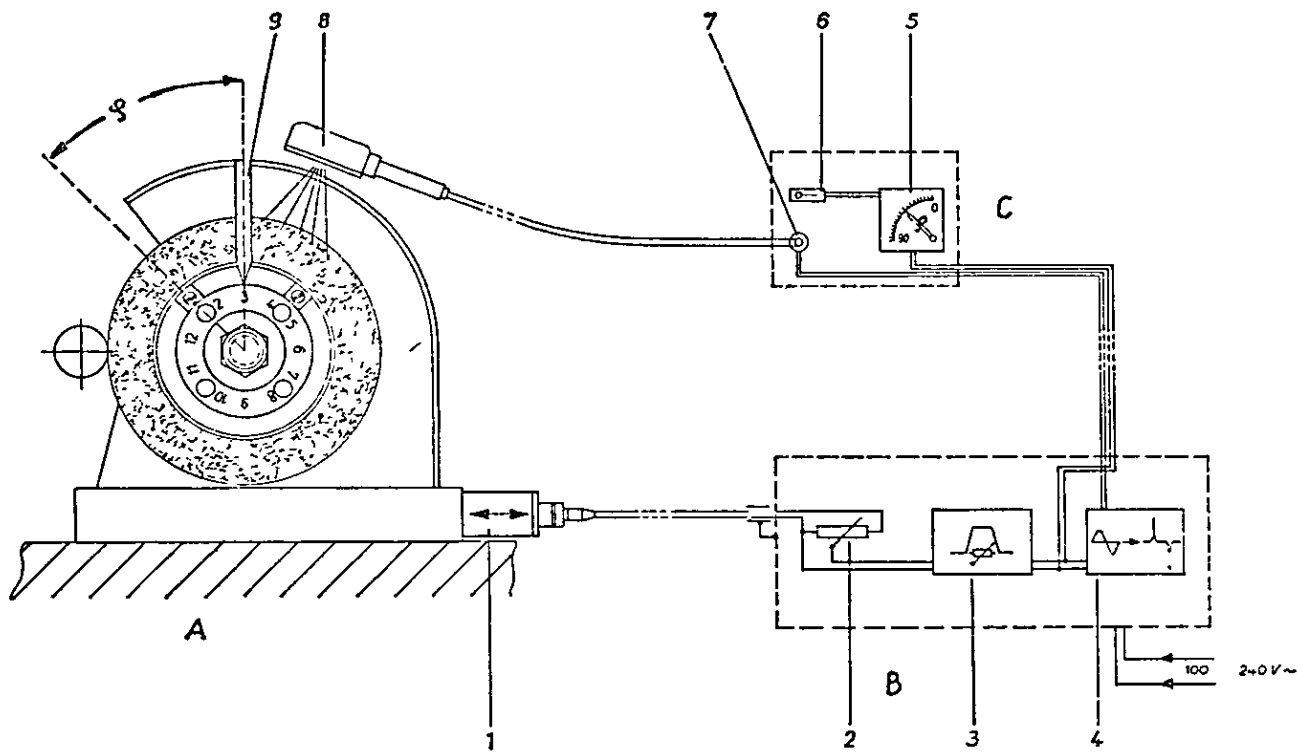
A: Grinding head
B: Measuring electronic
C: Indicating instrument
1 Vibration pick-up
2: Sensitivity control
3: Filter circuit

4: Impulse generator
5 Instrument for weight angle indication
6 Sensitivity selector switch
7. Socket for stroboscopic handlamp
8: Stroboscopic handlamp
9 Datum mark for "light place"

Fig. 4.12 Schematic diagram of
ELTRODYN-N1 device for dynamic
balancing of grinding wheels in situ.

Fig. 4.13 Temperature & Relative displacement of machine parts versus time, for Jones & Shipman Precision Grinding M/c. Type 1300 E.I.U.
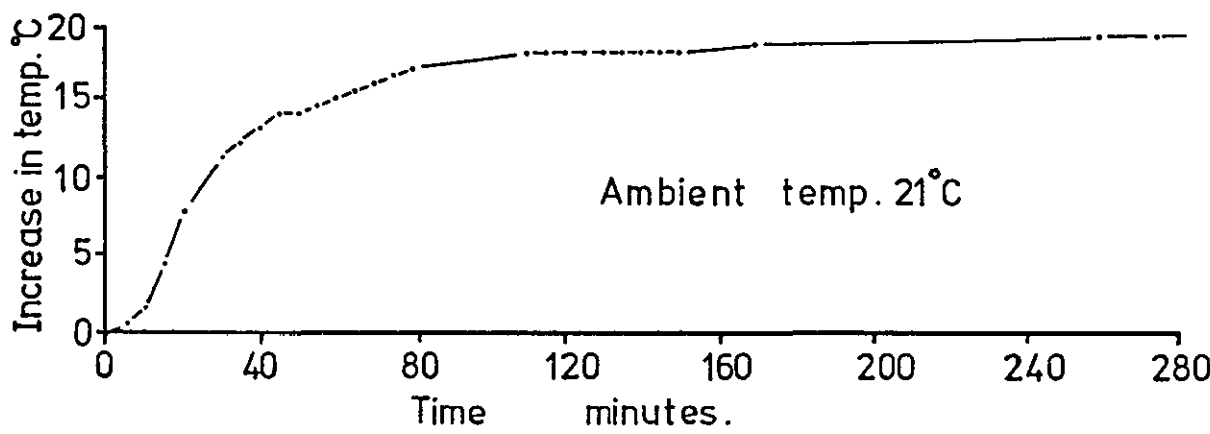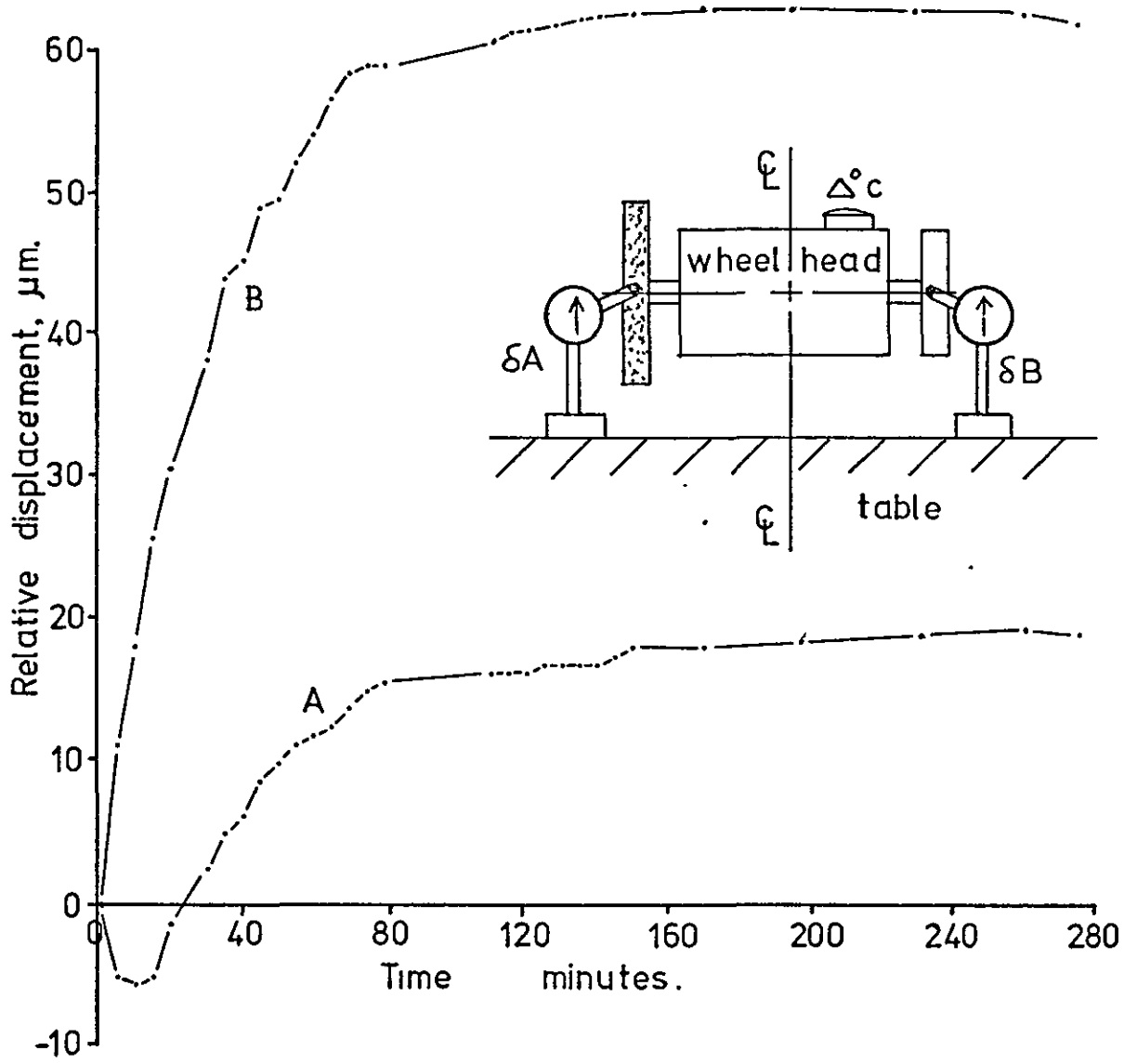
Wheelhead running and traverse hydraulics off.

Fig. 4.14 Temperature & Relative displacement of machine parts versus time, for Jones & Shipman Precision Grinding M/c. Type 1300 E.I.U.

Fig. 4.15   Temperature & Relative displacement
of machine parts versus time, for Jones &
Shipman Precision Grinding M/c .Type 1300 E.I.U .
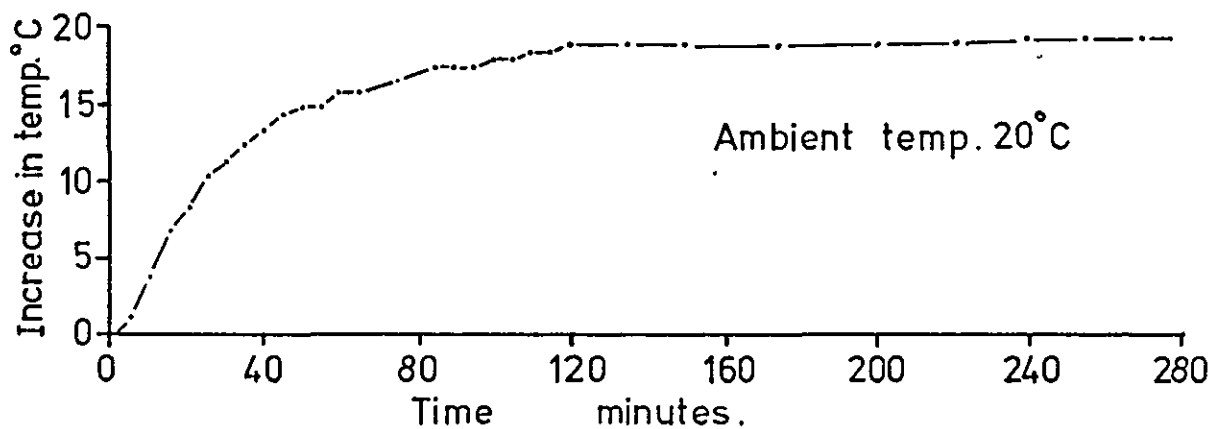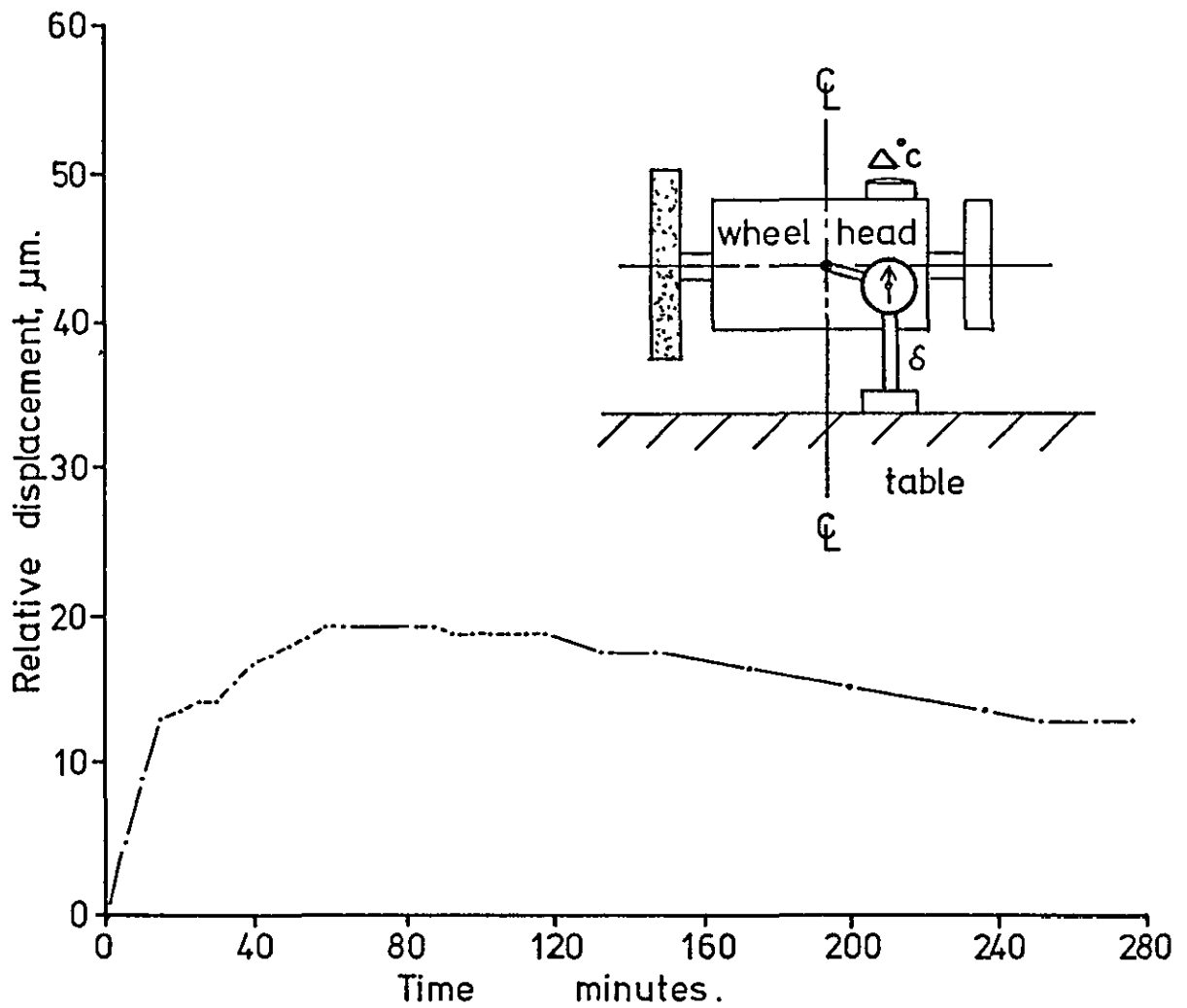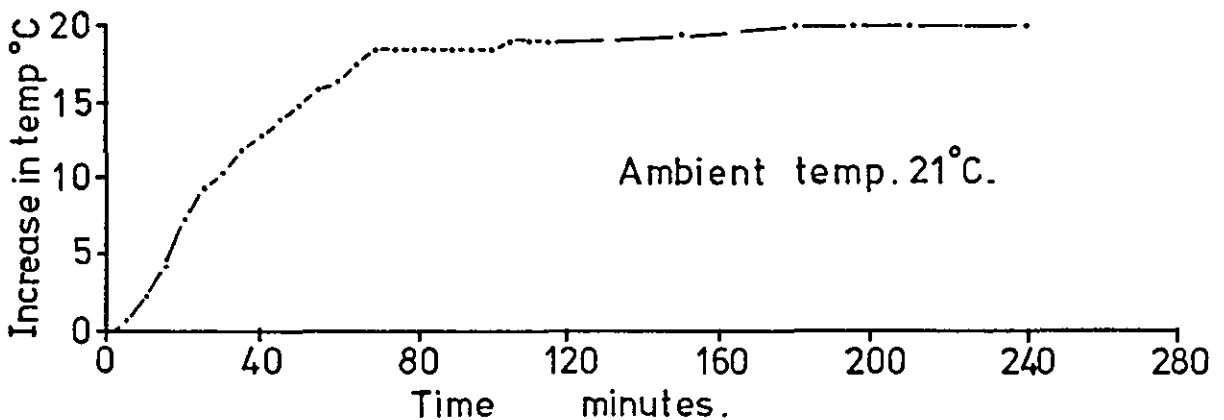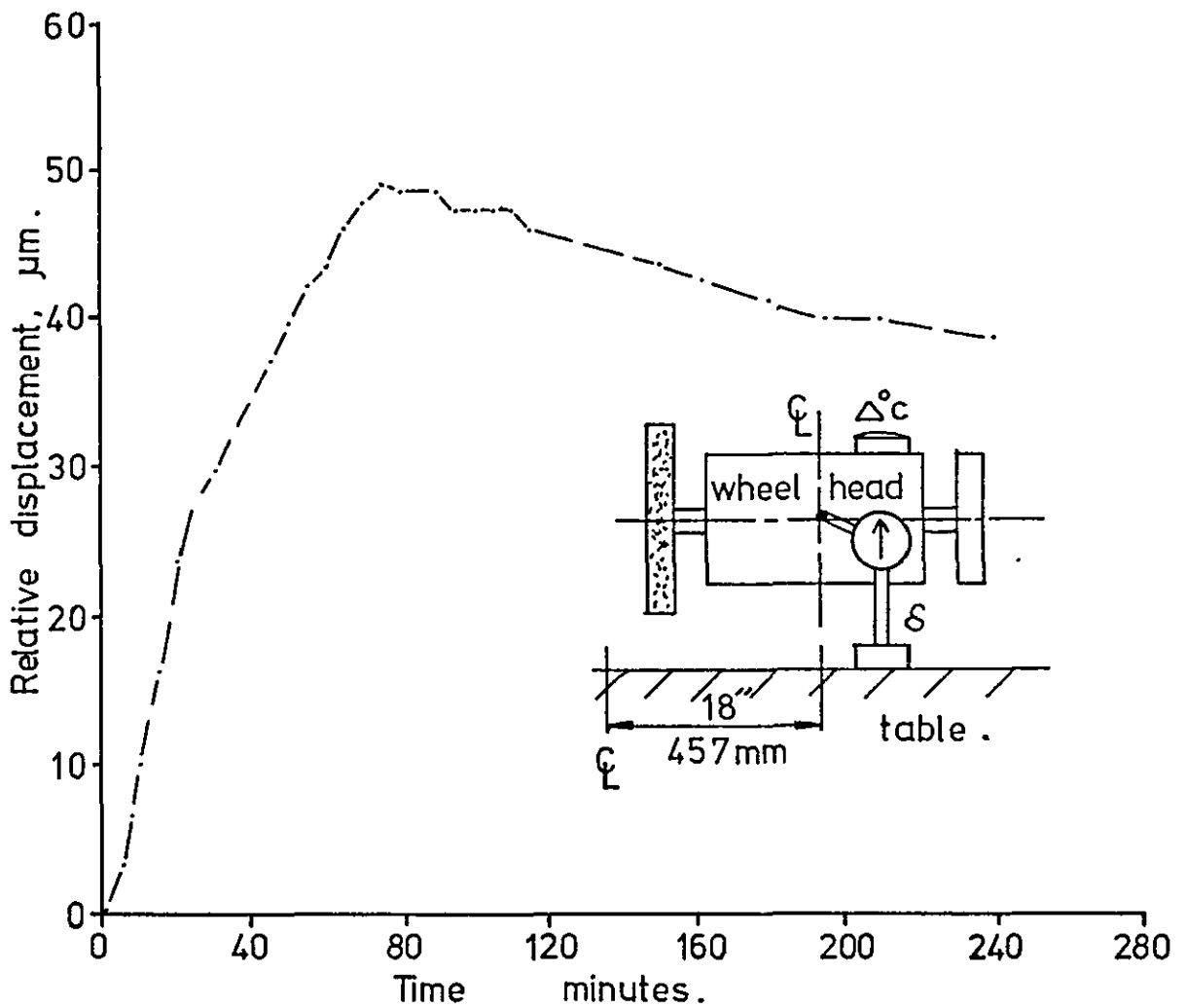
Wheelhead, workhead and traverse hydraulics running.

Fig. 4.16   Temperature & Relative displacement
of machine parts versus time, for Jones &
Shipman Precision Grinding M/c. Type 1300 EIU.

CHAPTER 5

THE DRESSING AND GRINDING DYNAMOMETERS AND THEIR ASSOCIATED EQUIPMENT

5.1 INTRODUCTION TO FORCE MEASUREMENT

It was envisaged that in the research conducted by the author, two force-measuring dynamometers should be used, these being a wheel dressing dynamometer, and a grinding dynamometer.

For the dressing of grinding wheels, the basic tool used was a single point diamond, mounted in a holder. It is known that as a diamond traverses across the face of a grinding wheel, the individual grits in the wheel surface are either fractured, or removed wholly from the wheel structure by bond post fracture. It is thought that the mechanism by which these grits are removed from the wheel face, may depend upon one, or a combination of three factors, these being dressing depth of cut, diamond traverse rate, and the geometry of the diamond tool relative to the wheel periphery, all other things being equal.

Taking force as a parameter, it was envisaged that a study of the influence of the before mentioned factors on wheel dressing, would be undertaken with a view to establishing stable dressing conditions, giving maximum dressing tool life.

In the grinding of metals, it is known that the performance of the wheel during grinding, depends upon several factors, e.g. hardness of wheel bond, grit type and size, depth of cut, workpiece traverse rate, wheel and work speeds, coolant type, dressing conditions, and many others. Again it was envisaged, using force measurement and analysis as a parameter to study several of these combined effects on grinding performance. This would require a grinding dynamometer, purpose-built to suit the particular conditions.

5.2 FUNDAMENTAL REQUIREMENTS OF DYNAMOMETERS

In a force measuring dynamometer, some form of

transducer is used to receive the force, or one of its
component parts, and convert it into an electrical signal
capable of being measured and recorded by appropriate
instruments. To ensure that true values are recorded,
several factors need to be considered at the design stage of
the dynamometer.

The ideal dynamometer should have the ability to
measure two or three orthogonal components of force without
interaction, have good repeatability, and a frequency response
which is high enough to allow the dynamometer to follow any
rapidly fluctuating force on the sensing member. Sensitivity
should be large enough to enable the output signals to be fed
into a recorder without excessive amplification, and at the
same time, the deflection of the force sensing members should
be small compared with the depth of cut into the workpiece.
Output signals should increase linearly with applied force,
and be free from any hysteresis or frictional effects.

In practice, conflict can arise between desired
characteristics, e.g., sensitivity and natural frequency.
For a force measuring element to have a high sensitivity,
and hence low stiffness, its natural frequency will be low.
This results in a reduction of the frequency range over which
dynamic measurements of force can be recorded accurately.
Also, reductions in stiffness resulting in larger values
of deflection to depth of cut ratio, may lead to inaccurate
values of force being recorded. In cases where transducers
having a low sensitivity value are used in conjunction
with extra-stiff members, then amplification equipment
which is costly, is necessary to bring the electrical signal
representing the force, up to a measurable level. It can
be seen, therefore, that the question of high sensitivity,
or high natural frequency, is a matter of compromise.

In practice, it is virtually impossible to constr-
uct a multiple-axis dynamometer that is free from inter-
action. This is because in most cases, axes are linked
mechanically at some point or other. This fact need not
be detrimental, as a note of the interactions can be made
at the calibration stage, and compensations made to the
recorded force values, assuming that the interactions

are not negligible.

In comparative tests, small differences in cutting force are often significant, and so a high degree of accuracy under all conditions is desirable. For accurate response to input signals, hysteresis effects must be guarded against. These usually occur through overloading of the force sensors, resulting in straining beyond the elastic limit, and hence, permanent deformation. Knowledge of the probable maximum force to be encountered would ensure that the load sensors could be designed to have adequate load bearing capacity.

5.3 ASSESSMENT OF THE PROBABLE FORCE DUE TO WHEEL DRESSING

An essential requirement when force measurement is to be undertaken, is a prior knowledge of the possible maximum force to be encountered, under any given set of conditions, as this will influence the choice of measuring system to be used.

Since information relating to the magnitude of forces in wheel dressing was unobtainable, a simple dynamometer was devised to fulfill this requirement.

The principle upon which this dynamometer was based, is that the deflection of a ring under diameteral loading, is directly proportional to the force causing the deflection. Fig. 5.1 depicts the instrument so devised. Its mode of operation was such that the deflection of the ring (2), caused by the force generated during dressing, was monitored on a dial indicator(1), mounted inside the ring; the scale of the dial indicator being calibrated in force units. Figs. 5.2 and 5.3 show how the dynamometer was used in conjunction with a supporting cradle for measurement of the three components of dressing force, namely, F_r (radial), F_t (tangential), and F_a (axial).

From a series of dressing tests conducted with the above mentioned apparatus, the following average values of force were derived.

Grinding wheel type :- Universal WA 46 KV 250 mm φ Wheel speed :- 1800 rev/min Dressing condition .- dry				
Dressing force N			Depth of cut μm	Traverse rate mm/rev
F_a	F_r	F_t		
—	1·2	·8	25	·25
—	2·2	1·4	25	·5
—	3·0	2·0	50	·5
—	4·0	2·5	75	·5

These values were used as a basis in design
calculations for the main dressing dynamometer.

5.4   THE THREE COMPONENT DRESSING-FORCE DYNAMOMETER.

5.4.1 Introduction to the dynamometer.

A three-component, low force dressing dynamometer
was developed from a basic design produced by F.K. Grosz-
mann and C. Rubenstein,[60] at U.M.I.S.T., for their
research into single grit appraisal in grinding. The
concept behind their dynamometer, and hence the one being
described here, is that the strain observed for a given
displacement, is a maximum when taken in the direction
of a direct stress.

Employing this principle, strain elements in the
form of thin rings, used in conjuction with foil-type
strain gauges, were arranged to monitor three components
of dressing force mutually at right angles. In this way,
the resultant force was described completely in magnitude
and direction.

5.4.2 Mechanical design.

The dynamometer consists basically of a rigid frame
which houses the strain (force sensing) elements. A schema-
tic representation of the dynamometer is depicted in
fig. 5.4 The strain elements are arranged such that
maximum strains are observed for an applied force in the

three principal directions to the plane of cutting. In this plane the axial and tangential force components are sensed by foil-type strain gauges mounted on opposing ring elements, these rings being suspended between the frame and central spindle carrying the dressing tool. This configuration is advantageous since it allows the setting up of two complete Wheatstone bridge circuits, giving full temperature compensation. To maintain a rigid system, the rings are held in tension by applying a preload. This is advantageous where strain gauges are used, since the stresses remain positive (tensile) when a load is applied, and the gauges are not subjected to compression. The stiffness of the two independent ring systems in the plane of cutting, are provided by the rings themselves.

The force component taken perpendicular to the plane of cutting is sensed by a single ring element having foil-type strain gauges mounted on its interior and exterior surfaces. In this way, a complete Wheatstone bridge circuit is again possible. This ring is fixed at its front end to the frame, and is supported at its rear end by the central spindle carrying the dressing tool. The spindle is itself attached to the frame at its rear end via a thin diaphragm, its front end being supported by the ring elements in the plane of cutting. The function of the diaphragm is to act as a fulcrum point for the axial and radial movements of the central spindle, caused by the dressing action between the diamond tool and grinding wheel. Preload is applied to the ring element by adjustment of a screw passing through the centre of the diaphragm. This causes the central spindle to be drawn towards the rear of the frame, thus tensioning the ring.

Initially, the stiffness of the axis perpendicular to the plane of cutting was to be provided by the ring element, the diaphragm being of such a thickness that its stiffness is negligible. It was found, however, from subsequent dressing tests, that the radial component of force could be considerably greater than at first thought possible, resulting in larger deflections being

observed for force measurement, than could be tolerated.
This resulted in the introduction of a thicker diaphragm
to provide additional stiffness to that of the ring element
in the plane perpendicular to the plane of cutting.

5.4.3 Constructional details.

The constructional details of the dynamometer are
shown in several views in fig. 5.5. The more important
parts will be described here.

The Main Frame.

The main frame which houses the strain sensors
consists basically of four parts, these being the main
body (14), the head (8), the front cover plate (5), and
the top cover plate (not shown). These parts are dowelled
and bolted together. The material chosen for the frame
construction is an aluminium alloy. This material had
been used with success previously, by Yang,[48] for the
construction of a grinding dynamometer, the main advantages
being its lightness and ease of machining. To ensure
maximum rigidity, the main body (14), and the head (8),
were machined from solid.

The Central Spindle.

The central Spindle is of a three-part construction.
This consists of a circular stem and head (3), which carries
the dressing tool and holder; a rectangular portion with
centre section machined away (15), in which is secured one
end of the strain sensor measuring the force component F_r ,
and a threaded tail piece (20), which is anchored to
the rear end of the frame, via a diaphragm. Parts (3)
and (15), are made from aluminium alloy, and part (2) is
made from mild steel, all parts being bolted together.
Since the central spindle forms part of the infeed measuring
unit, it was necessary to make it as light as possible
for dynamic reasons, the resulting total weight of the spindle
being .638 kg.

Dressing Tool Holder.

The dressing diamond is presented to the grinding wheel by a steel tool-holder mounted in the central spindle of the dynamometer, the diamond tool being machined such that its cutting point in contact with the grinding wheel, lies on the axis of the central spindle. The tool and holder are shown in fig. 5.6. A series of four holders are available, giving a range of "drag angles" of $0°$ to $15°$ in $5°$ increments. Inversion of the holders gives a further three values of "drag angle", these being $-15°$, $-10°$ and $-5°$. These holders can also be used in conjunction with the dressing fixture mentioned in statement 4.4.

The Force Sensing Elements.

Two types of thin ring element (11) and (18), are employed in the dynamometer for force detection, both types being manufactured from mild steel. To ensure maximum rigidity in service, the elements, which are thin rings with securing arms mounted diametrically opposite, are made of one piece construction from individual blocks of mild steel. Because of the slender nature of these elements, special fixtures were devised to hold them rigidly throughout the sequence of turning and milling operations required for their manufacture. Fig. 5.7 gives details of the ring element (18), employed in the plane perpendicular to the plane of cutting. The second type of ring element (11), which is used in the two principle axes in the plane of cutting, is shown in fig. 5.8. One arm of the ring element is extended into a threaded steel shank which is dowelled and soldered in position. This provides a means by which opposing ring elements in the same axis are preloaded, the threaded shanks passing through the dynamometer head, and being held in position by steel nuts. Using this form of force sensing element in preference to that of strip construction, elements having increased cross-sectional areas of seventy times can be employed, giving similar stiffness values, resulting

in a more robust system.

The Diaphragm.

The circular diaphragm (22), which is made from mild
steel gauge plate, provides a fulcrum point for the rear
end of the central spindle. The original diaphragm, which
was made having negligible stiffness, is shown in fig. 5.9.
Commissioning tests of the dynamometer showed that additional
stiffness was .required in the axis perpendicular to the
plane of cutting, for satisfactory results to be obtained.
A second, stiffer diaphragm was made to replace the original
one, and can be seen in fig. 5.10. To ensure that the
actual and theoretical values of stiffness were the same,
a calibration rig was devised. This consists of a rigid
steel plate, machined to represent the diaphragm housing in
the dynamometer, a load carrier, and a sensitive displace-
ment measuring instrument. The set up is shown in fig. 5.11.
The thickness of the diaphragm was reduced until a pre-
determined deflection was recorded by the measuring instru-
ment, for a known load, thus giving the required value of
stiffness.

5.4.4 Static and dynamic characteristics of the force
measuring systems.

In any dynamometer design, the conflicting require-
ments of adequate sensitivity and high natural frequency
have to be balanced against each other, to produce a
practical force measuring system designed to meet a specific
set of requirements. The stiffness of the system, which
influences both sensitivity and natural frequency, is
dependent upon the range of forces and depth of cut to be
met in practice. When determining the stiffness, a maximum
displacement of 10% of depth of cut was considered tolerable
for force measurement in any of the three axes of the
dynamometer, to give a reasonable signal output from the
foil-type strain gauges, and at the same time have
minimum interference with the cutting action of the dressing

tool. Taking a maximum infeed of 25 µm, corresponding to a force of 2.2 N in the plane perpendicular to the plane of cutting, a theoretical stiffness value of 880 kN/m was derived for a tool deflection equal to 10% of depth of cut. This value was initially adopted for all three axes. The resulting natural frequency of each axis for a moving mass of .638 Kg is 187 Hz. As stated earlier, commissioning tests showed that larger values of the radial component of force were possible under certain dressing conditions. To keep tool deflections small in comparison with the depth of cut, the stiffness of the axis perpendicular to the plane of cutting was increased by four times to approximately 3,520,000 N/m, giving a natural frequency of 374 Hz. This is low compared with 690 Hz for the dynamometer designed by Groszman and Rubenstein. According to Yang,[48] the optimum value of natural frequency for a tool dynamometer should be about 500 Hz. In practice, however, the dynamometer performed satisfactorily under all conditions tried.

5.4.5 Electrical instrumentation.

Three independent full-bridge circuits are used for monitoring the three components of dressing force mutually at right angles. This allows full temperature compensation and the maximum possible strain signal from each circuit.

The strain gauges.

Foil-type strain gauges were chosen as opposed to silicon type for several reasons, the prime one being cost. On average, silicon type strain gauges can cost 60 times more than foil-type gauges.

Potma[61] lists the main disadvantages of silicon type strain gauges as follows:-

1). Although the gauge factor is many times higher than a foil-type gauge, its actual value depends on the temperature.

2). The linearity is not so good.

3). There can be a large spread of values of the
     parameters R (gauge resistance),α_t (coefficient
     of expansion per ^{o}C) and K factor (gauge factor)
     from gauge to gauge.

Another disadvantage is that silicon-type strain
gauges are fairly brittle and can easily be broken when
being installed. On the other hand, foil-type gauges are
more robust, have good linearity and are generally more·
stable. The main disadvantage is their relatively low
gauge factor, i.e. in the order of 2 as compared with
120 for silicon-type gauges. This means that amplification
of the strain signal is necessary. The gauges chosen were
of 120 ohm nominal resistance, with a gauge factor of
approximately 2, and strain limits of 30,000 to 50,000
microstrain (3% to 5%) tension or compression. By
mounting four gauges on the strain ring in the plane
perpendicular to the plane of cutting, and two gauges
on each of the four strain rings in the plane of cutting,
the strain signals were increased by a factor of 4.
Figs. 5.12 and 5.13 show the full bridge circuits used.
Soldered connections were made to each strain gauge
using fine screen-wire, the wires being connected to
form three independent full bridge circuits by soldering
to three five-pin D.I.N. plugs mounted in the top cover
lid of the dynamometer, the central pin carrying the
screen grid.

The amplifier.

The choice of foil-type strain gauges necessitated
the use of three bridge amplifiers, one for each strain
system. The main consideration was again cost, resulting
in d.c. equipment being chosen as opposed to a.c. equipment.
With modern technology, d.c. amplifiers are manufactured
which have relatively low drift. Type FE-154-ABS, FYLDE
d.c. bridge amplifiers were chosen because of their compact
design, low drift and general suitability. Each amplifier
is supplied from 200-250V Hz supply and provides gains

from 10 to 5,000 in nine steps. The bridge voltage can
be varied from 0 to 12 volts d.c. and is zeroed by null
method, shunt balance. The input drift is 5 V/$^{\circ}$C
maximum, and accuracy and stability better than 1%.

The direct-recording oscillograph and galvonometers.

The choice of the strain-signal recording instrument
was determined by the nature of the force components
which in the case of wheel dressing is of a dynamic form.
A direct-recording ultra-violet oscillograph, type 10-350
manufactured by Shandon Southern Instruments was used in
conjunction with three fluid damped galvonometers, one
for each channel. The oscillograph is supplied by a
200-250V 50 Hz supply, and will accept up to 12 input signals
in the frequency range d.c. to 20 kHz. Each signal is fed
to a minature tubular galvonometer, which reflects a
spot of intense ultra-violet light on a moving roll of
photo-sensitive recording paper. The deflection of the
galvonometer, and hence the movement of the light spot,
is a function of the amplitude of the input-signal
current.

The choice of galvonometer was governed by the
maximum frequency and magnitude of input signal expected,
and became a compromise between galvonometer natural
frequency and sensitivity. these two factors being
inversely proportional. Three Southern Measuring Instrument
galvonometers, type SMI/M were used, having a natural
frequency of 1,000 Hz, a sensitivity of 1,75 mV/mm and
a maximum allowable current of 75 mA.

Connection between the amplifier terminals and
each of the three channels used on the oscillograph
was by twin screened-cable, with 10 kΩ variable
resistances connected between the amplifiers and
oscillograph to prevent overloading of the galvonometers.
These resistances were later found to be unnecessary
under test conditions and were removed from the
circuits.

5.4.6 Static and dynamic calibration.

Static calibration of the dynamometer was carried out using a system of dead weights suspended from a dummy tool holder mounted in the dynamometer head. The load was applied in ten increments of .2 Kg, giving a final load of approximately ten times the maximum at first thought possible. Each axis was loaded separately and readings taken of all three axes using the d.c. bridge amplifiers and ultra-violet oscillograph, the results being recorded on ultra-violet light sensitive paper. In this way, any cross interference between any two axes was directly measurable. At the same time, readings of tool deflection in the direction of the applied load were recorded using a Mitronic indicator and electrical transducer placed under the dummy tool holder. To ensure absolute rigidity of the dynamometer during calibration tests, the dynamometer was clamped to a cast iron cube, with each of its three axes to be calibrated pointing downwards in turn, the cube being bolted to a rigid cast iron marking-out table. Fig. 5.14 shows a schematic representation of the calibration set up for each axis, and fig. 5.15 shows an actual calibration set up. From the readings taken of tool deflection and paper trace width, for known increments of load, two calibration charts were plotted. Fig. 5.16 shows the chart relating to tool deflection in each of the three axes for load applied in the same axis. All three plots show a linear relationship as would be expected. The following stiffness values were deduced from the chart:-

| Stiffness in the plane of cutting. | F_a axis | 853 | kN/m |
| | F_t axis | 1.079 | MN/m |

| Stiffness in the plane perpendicular to the plane of cutting. | F_r axis | 3.336 | MN/m |

These compare favourably with the design values of stiffness:-

F_a axis

F_t axis   888   kN/m

and F_r axis 3.520   MN/m

The discrepencies between the actual and design values of stiffness are due to the machining tolerances on the various dynamometer parts.

Fig. 5.17 shows the chart relating to ultra-violet paper trace readings for each of the three axes, (F_a, F_r, and F_t) against applied force. The three traces are for various amplifier gain settings, the F_r trace being at a higher value of gain than the F_a and F_t traces due to the higher stiffness value in that axis. The following calibration values of force per unit deflection were obtained from the chart:-

F_a axis   .30 N/mm at   2,000   gain

F_t axis   .25 N/mm   at   2,000   gain

F_r axis   .40 N/mm   at   5,000   gain

Using these values, force readings could be interpreted from ultra-violet paper trace recordings for any amplifier gain setting used.

Since interaction between any two axes was within 1%, allowances were not necessary on the static calibration charts.

Dynamic calibration of the dynamometer was performed by introducing a vibrating load of known magnitude and frequency to the three axes in turn, and recording by suitable means, the ensuing amplitude and frequency of vibrations set up. Fig. 5.18 is a schematic diagram of the dynamic calibration set up. A Goodman vibration

generator, model V47, was attached to the dummy tool holder by a stiff connecting rod in each of the three principal directions to be calibrated in turn. The dynamometer was again secured to the cast iron cube, the cube being bolted to the marking-out table. The signal to the vibrator was supplied from a Bruel and Kjaer beat frequency oscillator, type 1,014, through a Heathkit 10 watt high-fidelity amplifier, model MA12. A current output from the amplifier of 1 ampere, corresponding to a dynamic force in the vibrator of $\pm$ 4N, was set using an avometer, and an oscilloscope connected between the amplifier and vibrator provided a check against any distortion of waveform over the current range used.

Output signals from the three axes of the dyanmometer were fed through the d.c. bridge amplifiers to the oscillograph, and their amplitudes recorded on ultra-violet light sensitive paper for a frequency range of 120 Hz to 3 KHz. Since the fundamental resonances of the vibrator and galvonometer in the oscillograph were 120 Hz and 1KHz respectively, true responses for the dynamometer could not be plotted at these two frequencies. The three frequency response curves plotted for the dynamometer show its fundamental resonances in the plane of cutting and perpendicular to the plane of cutting, and hence points of instability. These are represented in figs. 5.19 to 5.21 inclusive. Figs. 5.19 and 5.20 show the frequency response curves for the two axes in the plane of cutting, namely F_a and F_t respectively. Both axes have similar resonant frequencies around 260 Hz and 360 Hz. The following shows the comparison between actual and theoretical values.

Axis	f_n actual	f_n theoretical
F_a	253 Hz 370 Hz	184 Hz
F_t	273 Hz 360 Hz	207 Hz

Fig. 5.21 shows the frequency response curve for the axis perpendicular to the plane of cutting. It can be seen that in this plane the dynamometer has only one fundamental resonance at 315 Hz. The following shows the comparison between actual and theoretical values:-

Axis	f_n actual	f_n theoretical
F_r	315 Hz	364 Hz

No exact analysis of the frequency response curves obtained has been attempted because of the complex nature of the strain member supports. For practical purposes it is necessary to note the points of instability and ensure, if possible, that these regions are avoided. All three figures show interactions on each axis due to loading in adjacent axes. These are not thought to be true values since vibrator oscillation in only one plane could not be guaranteed.

5.4.7 Dynamometer slide.

The dynamometer is carried on a slide arrangement as depicted in fig. 5.22. The main parts of the slide are manufactured from an aluminium alloy to be compatible with the dynamometer, and the whole arrangement is mounted on a steel base plate. The point of contact of the diamond dressing tool with the grinding wheel lies in the same horizontal plane as the axis of rotation of the grinding wheel spindle. The dynamometer can be fed forwards in accurate steps of the order of 2 μm. This is achieved by the use of a very fine pitch screw (24), which is in turn geared down through a worm and gear drive (15 and 16). The forward movement of the dynamometer is sensed by an electrical transducer (11), and monitored on a "Mitronic" indicating instrument, the lowest setting on this instrument being $\pm$ 3 μm full scale deflection. The external micrometer spindle (8), as seen in the diagram, is used only as a means of setting a zero datum on the "mitronic"

indicating instrument prior to each infeed requirement.
After setting the infeed requirement, the top slide (3),
is locked in position by the knurled screw (12). This
causes the bottom slide (14) to expand into the dovetail
of the top slide. Because the locking action takes place
perpendicular to the feed motion, no error is experienced
in the feed direction. To compensate for backlash in the
system, the top slide (3), is held positively against the
bottom slide (14), with a tension spring (25). Fig. 5.23
shows the dynamometer and slide mounted on the grinding
machine table.

5.5   THE TWO COMPONENT DRESSING-FORCE DYNAMOMETER

5.5.1 Introduction to the dynamometer.

Wheel dressing tests conducted using a blunt diamond
tool having a wear flat of approximately 10 mm (limiting
wear conditions), gave unsatisfactory results when using
the three component dressing-force dynamometer. To assess
the probable dressing forces under the above mentioned
diamond tool condition, a further dynamometer was con-
structed. A cantilever design was chosen capable of
monitoring radial and tangential components of dressing
force separately.

5.5.2 Dynamometer design and construction.

A schematic arrangement of the dynamometer is shown
in fig. 5.24. The dynamometer body (5), was machined
from a single steel plate 100 mm x 115 mm x 16 mm thick, and
secured to the steel angle base (8) by three high tensile
steel cap-headed screws. The diamond tool holder (1)
presents the dressing tool to the grinding wheel such that
the point of contact between tool and grinding wheel lies
in the same horizontal plane as the axis of rotation of
the grinding wheel spindle. The tool holders are
interchangeable with the three component dressing-force
dynamometer. Force measurement is obtained using a
Kistler quartz force transducer (4) mounted in the slot

separating the cantilever section from the main frame.
The transducer is located positively using two ball-
bearings (3), and preloading is accomplished with a screw
(7) and locknut (6).

A high stiffness value was chosen for the canti-
lever arm, namely 10 MN/m. This value was achieved pract-
ically by extending the slot in which the transducer is
housed, up towards the top corner of the dynamometer body.
The machining of the slot was stopped at several stages
and a known value of load applied to the tool holder.
Deflection of the cantilever at the point of application
of the load was monitored using an electrical transducer
and "mitronic" indicating instrument. When a predeter-
mined value of deflection was observed, machining was
completed. The above mentioned stiffness value was taken
with the quartz force transducer in situ.

In the set up as shown, the dynamometer senses the
tangential component of dressing force. By rotating the
dynamometer body through 90° and repositioning the tool-
holder on top of the frame so that the dressing tool tip
lies on the axis of the quartz force transducer, the
radial component of dressing force is monitored.

5.5.3 Electrical instrumentation.

Signals received from the quartz force transducer
are passed into a Kistler electrostatic charge amplifier,
and readings taken visually from a galvonometer scale.

Quartz force transducer characteristics:-

Type   903 SN. 22291

Force range   +600 kp   (5,886N)

Sensitivity   42.7 pc/kp   (4.4 pc/N)

Linearity $\pm$.4%

Temperature range   -150°C to 240°C

Electrostatic charge amplifier characteristics:-

Type   Model 566

Output voltage   +10V; -5V
(to high-impedance
load)

Output current $\pm$10 mA
(to low-impedance
load)

Ranges for 10V   0.05; 0.1; 0.2; 0.5; 1.0; 2.0;
output   5.0;   10; 20;   50; and 100mV/pc

Frequency response d.c. to 150 kHz

Linearity error   .1%

Line power   115V at 60 Hz

5.5.4 Dynamometer calibration.

Calibration of the two axes of the dynamometer was
carried out statically using a dummy tool holder and a
quantity of dead weights, the set up being similar to that
for the three component dressing-force dynamometer. Fig.
5.25 shows a schematic representation of the calibration
set up for each axis. The dressing forces on the dynamom-
eter under working conditions were thought to be at the
lower end of the force range for the quartz force trans-
ducer. This being the case, a setting of 100 mV/pC,
(highest value) was set on the charge amplifier to give
a reasonable swing to the galvonometer. Deflections of
the tool holder were recorded for each load increment   .
using an electrical transducer and "Mitronic" indicating
instrument.

Calibration charts for the tangential and radial
components of dressing force can be seen in figs. 5.26 and
5.27 respectively.

The main disadvantage found with the two component
dressing-force dynamometer was the drift observed on the
galvanometer at the setting of 100 mV/pC. In practice
this phenomenon was overcome by using a "short" time-
constant for the charge amplifier and zeroing the amplifier
just before readings were to be taken.

Fig. 5.28 shows the dynamometer in position on the
grinding machine with the electrostatic charge amplifier.

5.6   TWO COMPONENT GRINDING-FORCE DYNAMOMETER.

5.6.1 Introduction to the dynamometer.

Two of the parameters to be measured during the
cylindrical traverse grinding operation were the radial
and tangential components of force generated. To accom-
plish this a two component grinding-force dynamometer
was designed and constructed.

A simple idea used by researchers in the past was to
make one or both grinding centres part of the dynamometer;
this was the basis for the design chosen. In operation,
the dynamometer acts as a cantilever and transmitts force
signals through an appropriate transducer. These signals
are then amplified and recorded. If, under a cylindrical
traverse grinding operation, two dynamometers are used,
(one in the machine tailstock and the other in the work-
head), output signals in the same axis are additive and
give a signal of constant magnitude, this being simple to
to analyse. If a single dynamometer is used, the out-
put varies inversely to the distance between the point
of application of the load and the transducer. For
plunge grinding operations only one dynamometer need be
used to obtain a signal of constant magnitude.

In the present research, only one dynamometer has ·
been used to measure grinding forces because of the high
cost of the force transducer. Fig. 5.29 shows the dyna-

mometer installed in the tailstock on the grinding machine.

5.6.2 Dynamometer design and construction.

    The dynamometer consists of a specially designed grinding centre in which is fitted a Kistler three component quartz force transducer. Only two of the transducer outputs are utilised, the third "axial" output has been ignored. Details of the dynamometer are shown in fig. 5.30. The cone centre (1) is made from a standard high-carbon steel centre, the morse taper shank portion behind the cone being reduced to form a parallel spindle which passes through the bore of the quartz force transducer (3). A taper shank body (4) fits on the spindle behind the transducer and locates the dynamometer in the grinding machine tailstock. Preloading of the transducer is achieved by a split-collet arrangement which is located at the rear end of the cone spindle in a "knecked down" portion. A retaining ring (5) holds the two halves of the threaded split-collet (6) together whilst axial loading is applied through the preload nut (7). A small key is fitted between the collet and cone spindle to prevent rotation whilst preload is applied.

5.6.3 Electrical instrumentation

    Electrical signals from the three component quartz force transducer are passed into a Kistler electrostatic charge amplifier, and galvonometer amplifier, and then to two fluid damped galvonometers housed in an ultra-violet oscillagraph where traces are recorded on ultra-violet light sensitive paper.

    Description of the quartz force transducer.

    Three quartz disc pairs are hermetically welded in a stainless steel housing. One pair is sentitive to compression (in the transducer axis which is the Z direction) the two others to shear (in two perpendicular directions of the transducer plane, which are the X and Y directions). A force acting on the transducer is measured in its three

components X, Y and Z.   In order to allow transmission of sufficient forces in the X and Y directions, the transducer must be preloaded with a force of approximately 25 kN. Details of the quartz force transducer are given in fig. 5.31.

Kistler electrostatic change amlpifier characteristics:-

Type	5,001
Measuring ranges, 12 steps, 1:2:5...,	
Continuous 1:10	pC $\pm$ 10-500,000
Range capacitors 1:2:5...	pF 10-50,000
Calibration factor setting	pC/N .1-110,000
Output voltage	V $\pm$ 10
Output current	mA 50
Frequency range (with standard filter-3dB)	kHz 0-180
Linearity	% .05
Calibration input	pF 1,000 $\pm$ .5%
Sensitivity	pC/mV 1
Maximum drift (due to leakage current)	pC/s $\pm$ .03
Temperature drift	mV/^{o}C $\pm$ .5/5

Kistler galvonometer amplifier characteristics:-

Type	5,211A

Measuring range	V $\pm$ 10	
Sensitivity: current outputs 4 ranges in decadal steps	mA/V	.01-10
Continuous adjustment range	X	0-10
Sensitivity: voltage output	V/V	0-10
Frequency range	kHz	0-10
Linearity	%	$\pm$ .4
Temperature drift referred to input	mV/^{o}C	2

Bryans-Southern ultra-violet oscillograph characteristics:

Type	10-350
Number of channels	12
Supply voltage	200-250V r.m.s.
Supply frequency	50-60 Hz
Frequency range	0-20 kHz

Fluid-damped galvonometer characteristics:-

Type Shandon Southern Instruments	SMI/M
Terminal resistance	32
D.c sensitivity: current	0.05 mA/mm
voltage	1.6 mV/mm
Maximum current	75 mA

5.6.4 Dynamometer calibration.

Before calibrating the dynamometer a preload of about
25 kN was applied to the quartz force transducer to ensure
its correct function in service.

The dynamometer was calibrated on the grinding machine
under conditions similar to those operative during grinding.
The grinding wheel was removed and a fixture mounted in its
place to receive a "Clockhouse" proving ring dynamometer
which provided the means of measuring the applied load.
A dummy test piece, identical to the test pieces to be
ground, was mounted between a standard cone centre in the
workhead and grinding dynamometer in the tailstock.
The dynamometer was positioned so that its X and Y axes
were in the correct orientation to measure the tangential
and radial components of force respectively. Known incre-
ments of load were applied at a series of positions along
the test piece, and readings taken from the grinding dyna-
mometer using the ultra-violet oscillograph. The calibration
set up can be seen in fig. 5.32. Calibration charts for
the radial and tangential components of force are reproduced
in figs. 5.33 and 5.34 respectively. Interaction between
the two axes was small and was therefore ignored.

As can be seen from the charts, the relationship
between the applied force and the distance moved away from
the quartz force transducer is a linear one. The system
can be compared to a simply supported beam with a moving
point load. The recorded force is a maximum, and equal to
the applied force at a point where the tailstock cone centre
enters the test piece, and zero at a point where the work-
head cone centre enters the test piece.

Clockhouse proving-ring dynamometer characteristics:-

Ring number		1527
Dial gauge number		74462
Mean sensitivity	.1332 lbf/div.	(.59 N/div.)
Maximum load	200 lbf	(890 N)

Plan view

Front view
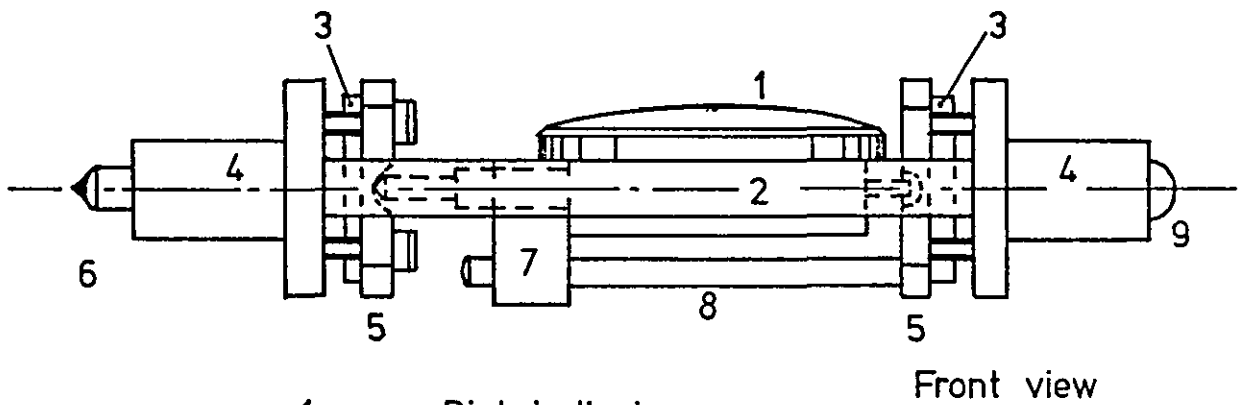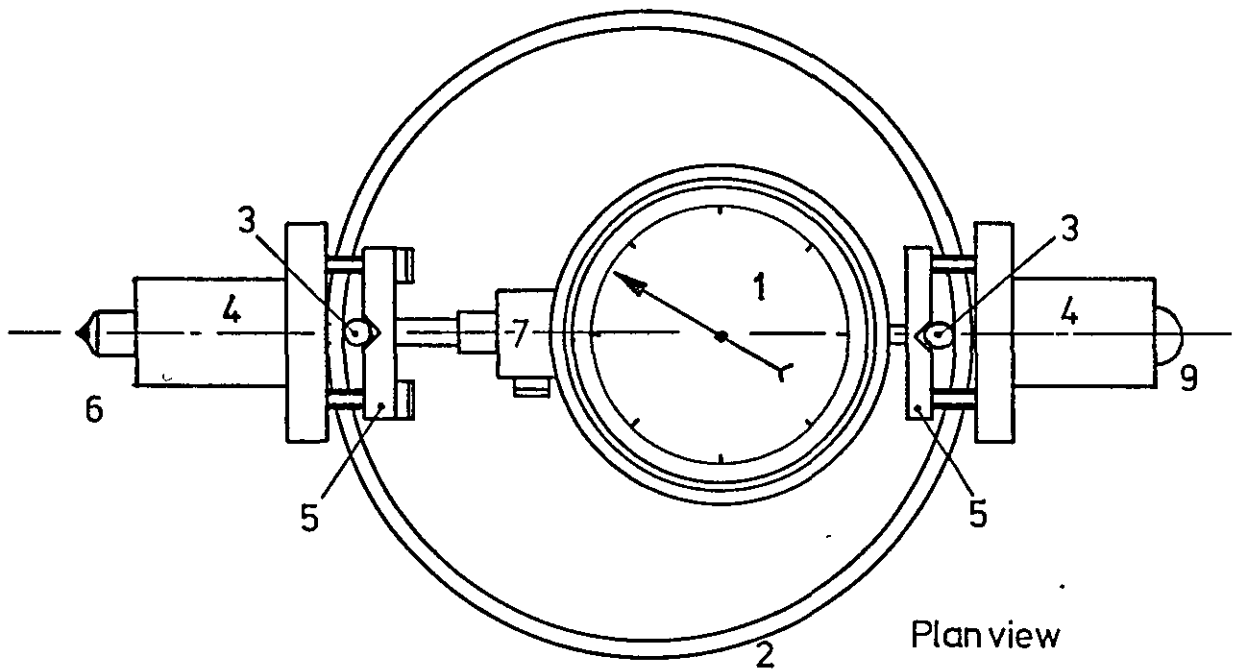
1	Dial indicator
2	Proving ring
3	Fulcrum pin
4	End support
5	Clamp plate
6	Diamond tool
7	Clamp block
8	Support pin
9	Ball pivot

Fig. 5.1   Schematic representation of the
Proving ring dressing-force dynamometer
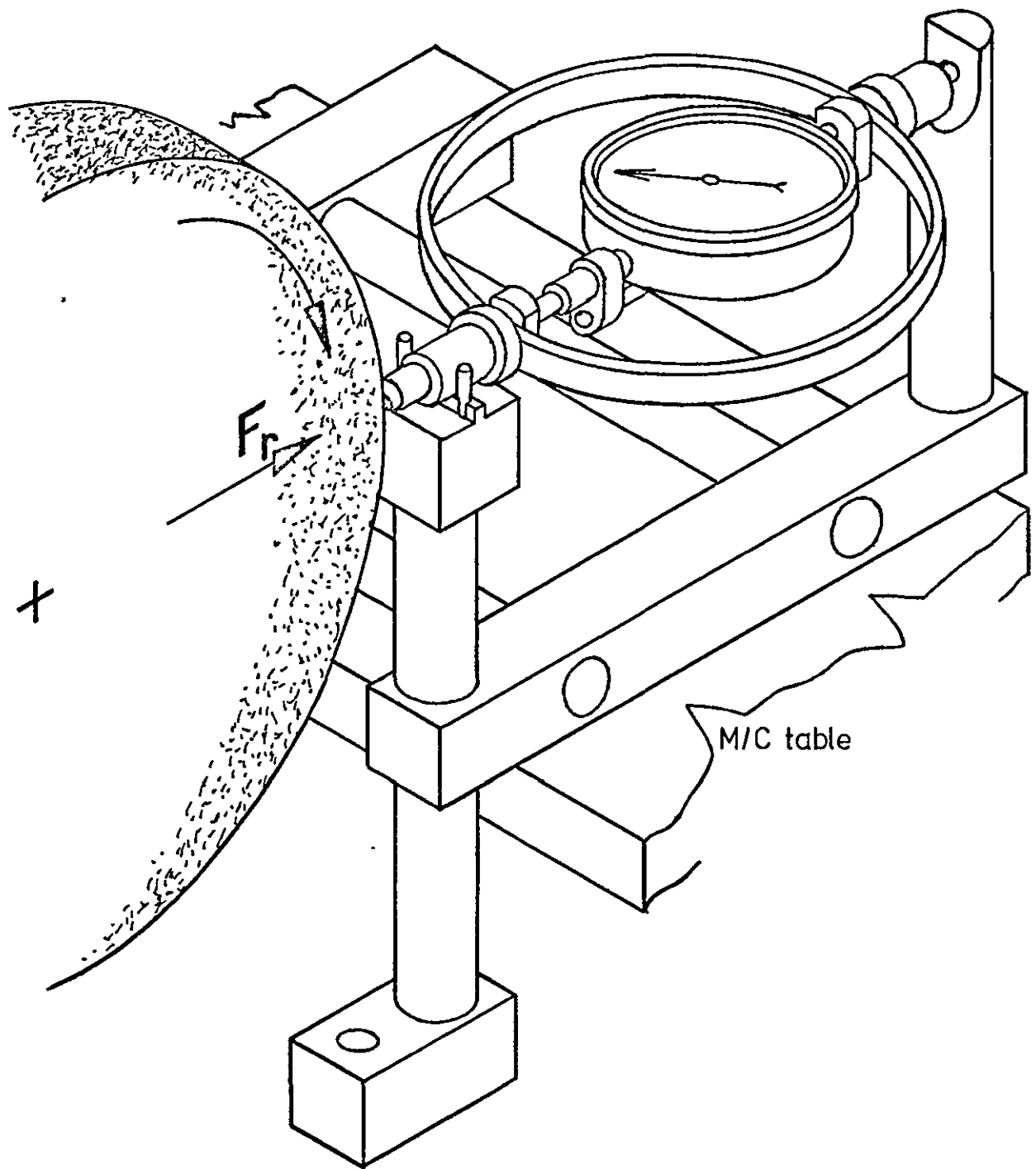
Fig.5.2   Set-up of the Proving Ring
Dynamometer with supporting cradle
for measuring the radial component
of dressing force.
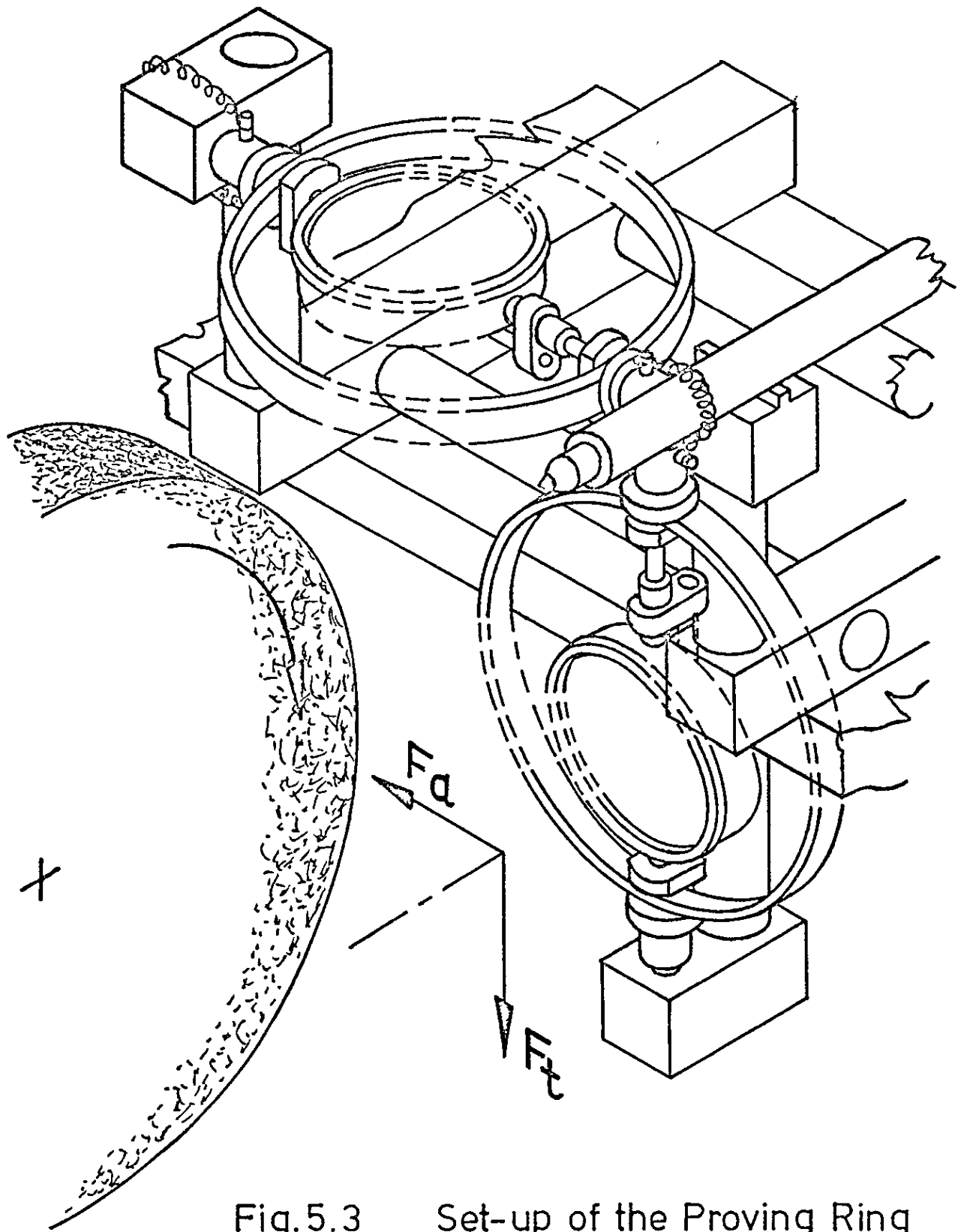
Fig. 5.3   Set-up of the Proving Ring
Dynamometer with supporting cradle for
measuring the axial, F_a, and tangential,
F_t, components of dressing force
seperately.
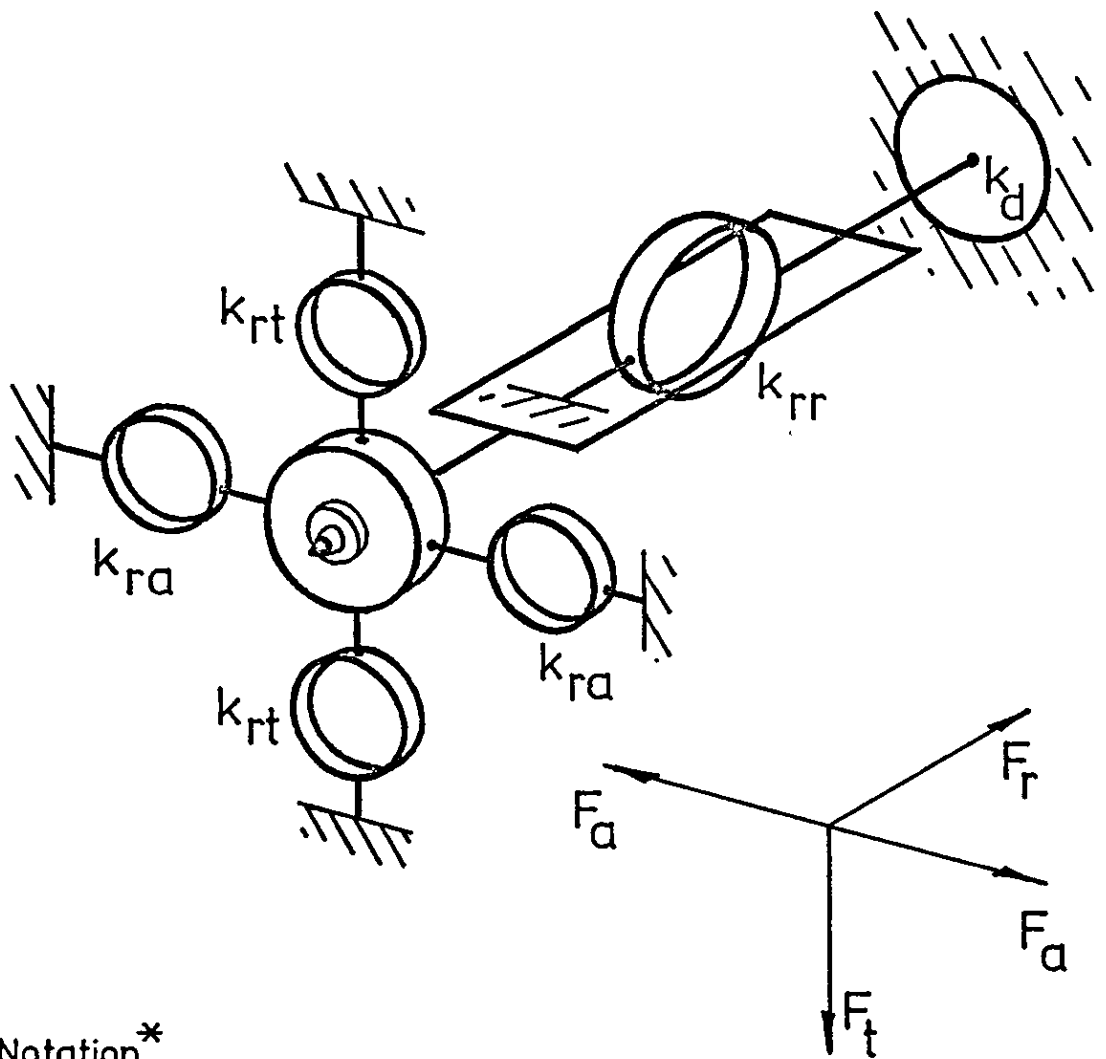
Fig.5.4   Schematic representation of the
three component dressing-force
dynamometer. ·

Part No.	Part name.
1	Diamond dressing tool.
2	Diamond tool holder.
3	Central spindle head.
4	Dust shroud.
5	Front cover plate.
6 7	Locking collar (twin rings).
8	Dynamometer head.
9	Locking nut (8 off).
10	Spacer (4 off).
11 A & B	Force sensing element (Fa & Ft components) (2 pairs).
12	Dowel pin (4 off).
13	Dowel pin (2 off).
14	Dynamometer body.
15	Central spindle body.
16	Front clamp block *.
17	Dowel pin (2 off).
18	Force sensing element. (Fr component)
19	Rear clamp block *.
20	Adjuster nut (2 parts).
21	Circular diaphragm locating ring.
22	Circular diaphragm.
23	Circular diaphragm clamping ring.
24	Dynamometer body end cap.

* for securing the Fr component
force sensing element

Parts list for the three component
dressing-force dynamometer
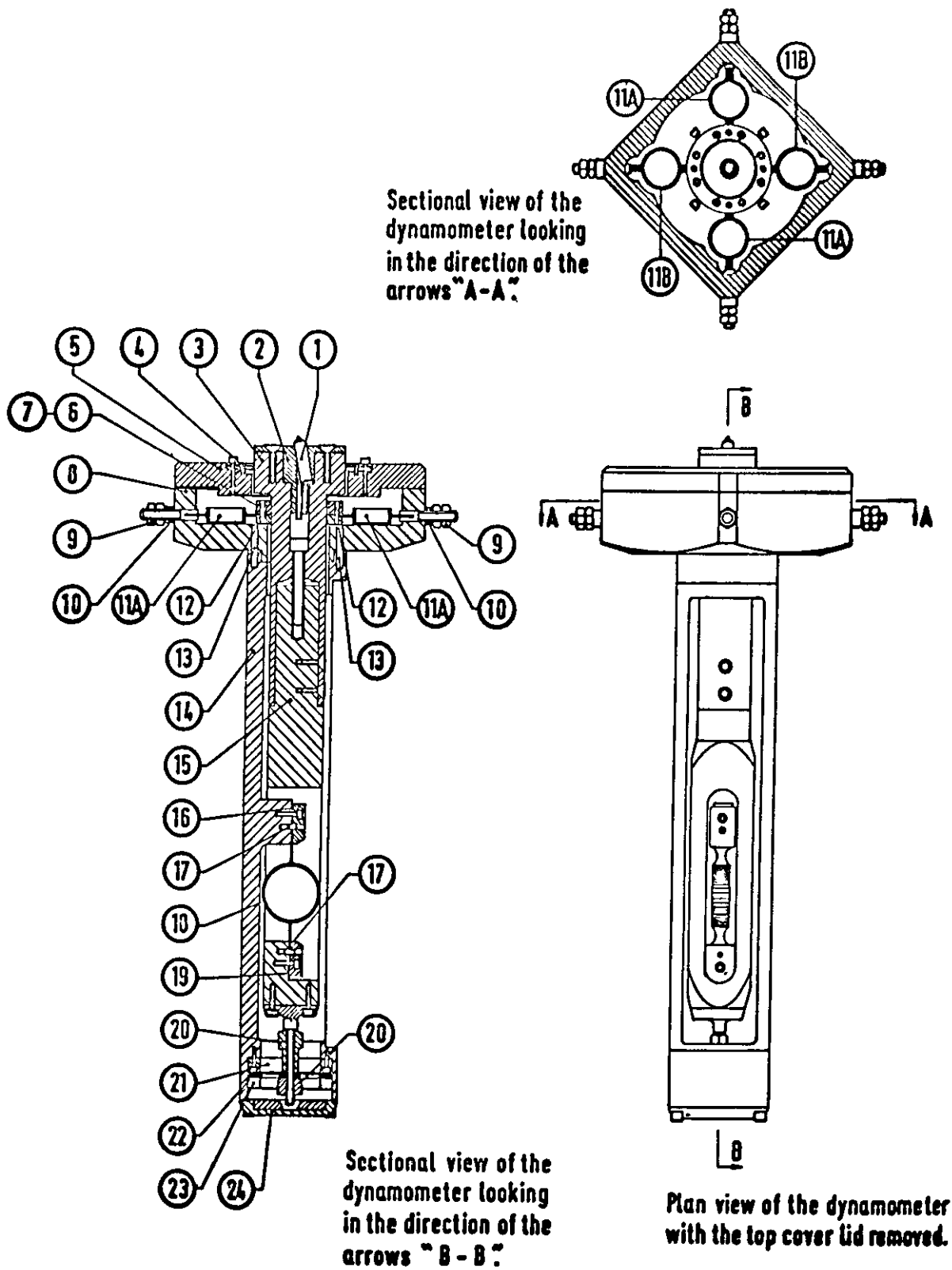
Sectional view of the dynamometer looking in the direction of the arrows "A-A".

Sectional view of the dynamometer looking in the direction of the arrows "B - B".

Plan view of the dynamometer with the top cover lid removed.

Fig. 5.5   Views of the three component dressing-force dynamometer.

19

3.2

X

20.3 φ

X

20 A/F

Plan view

All dimensions in mm

47.6 φ

28.6 φ

A

A = 4.8 φ

9.5 φ

6.4 φ

θ°

θ = 5°,10°,15°& 0°

2 BA thread

A

Sectional
view on `x-x´

6.5
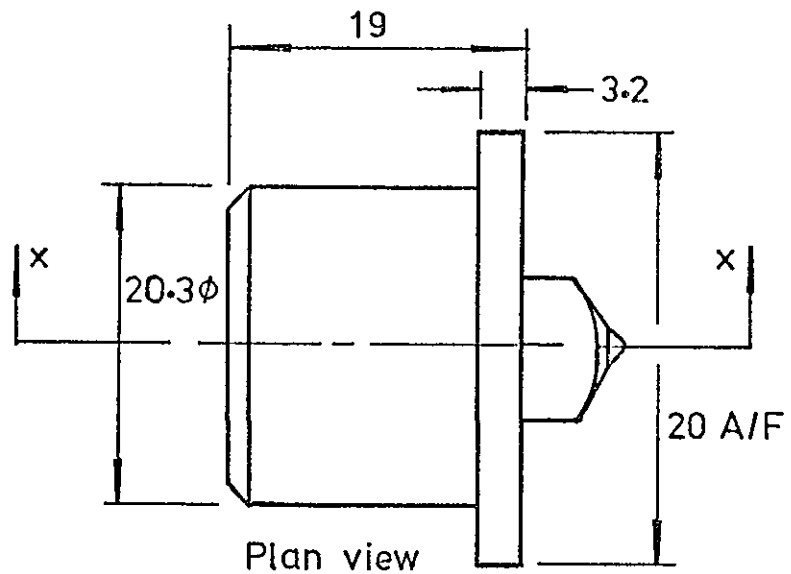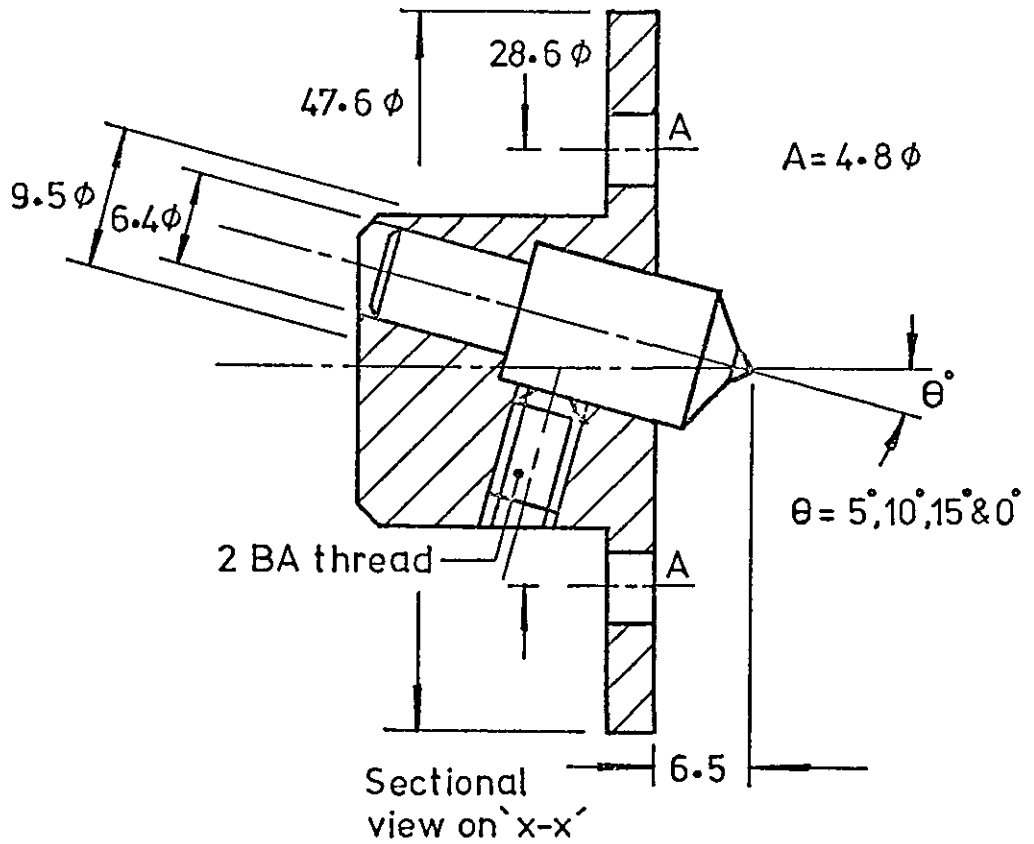
Fig. 5.6 Dressing tool and holder for use
with the two and three component
dressing-force dynamometers

Front view

Plan view
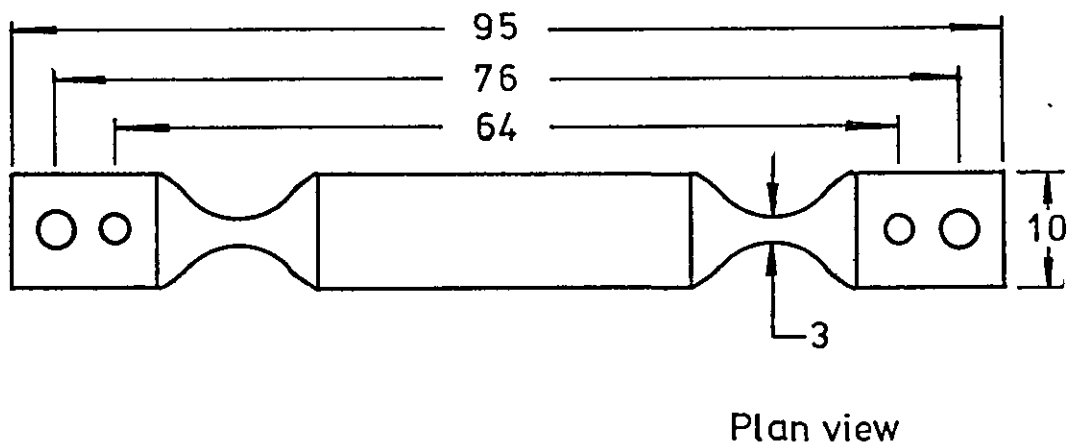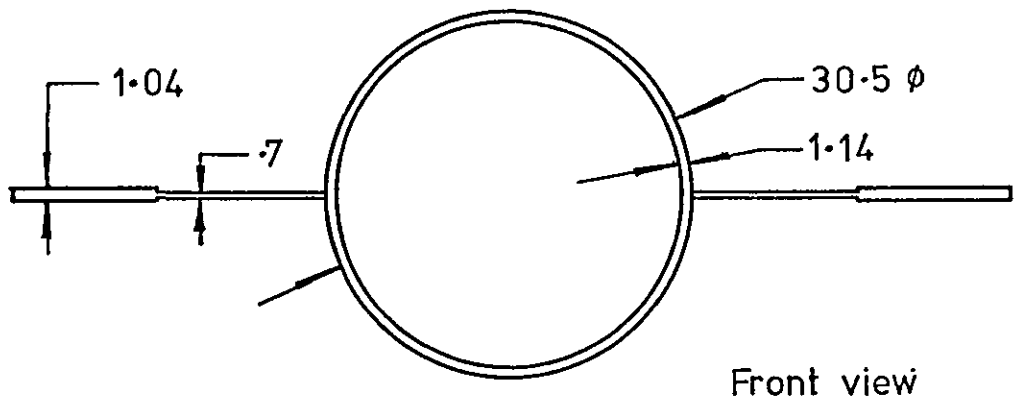
All dimensions in mm

Fig. 5.7   Force-sensing element for the
plane perpendicular to the plane of
cutting in the three component
dressing-force dynamometer

2 BA thread form

20·3 φ

·75

Front view

70

4·8 φ   ·5   8·9

Plan view
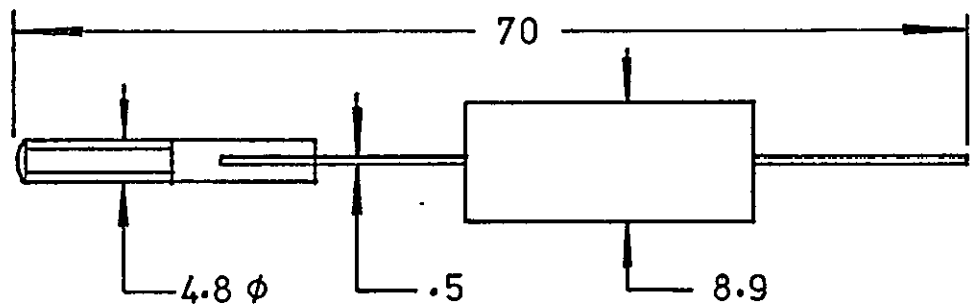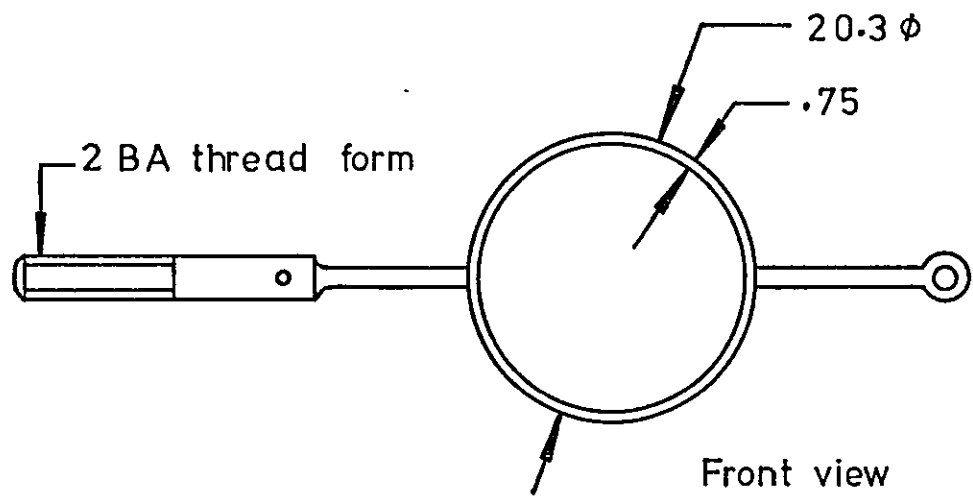
All dimensions in mm

Fig. 5.8   Force-sensing element for the two axes in the plane of cutting in the three component dressing-force dynamometer.

44.5 φ — 30 φ — 7 φ

— 5.2 φ

x   x

All dimensions in mm

six 4·8 φ holes on a 37·6 P.C.D

·64   1·5

Sectional view on 'x-x'
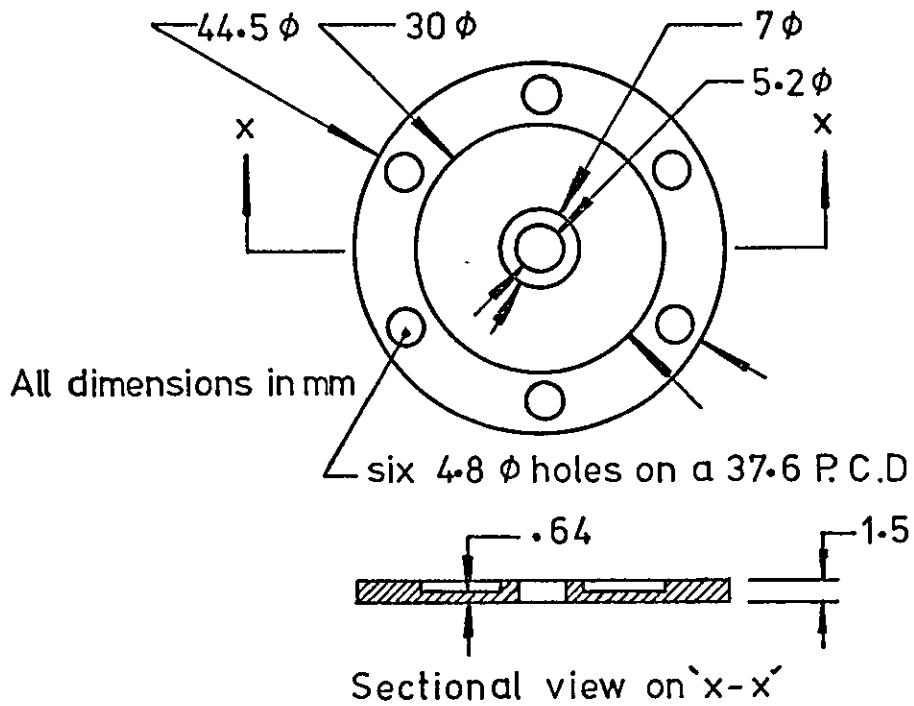
Fig.5.10   Final diaphragm for the three
component dressing-force dynamometer

six 11 φ holes on a 19 P.C.D

y   y

All dimensions in mm

six 4·8 φ holes on a 37·6 P.C.D

·25   1·5

Sectional view on 'y-y'
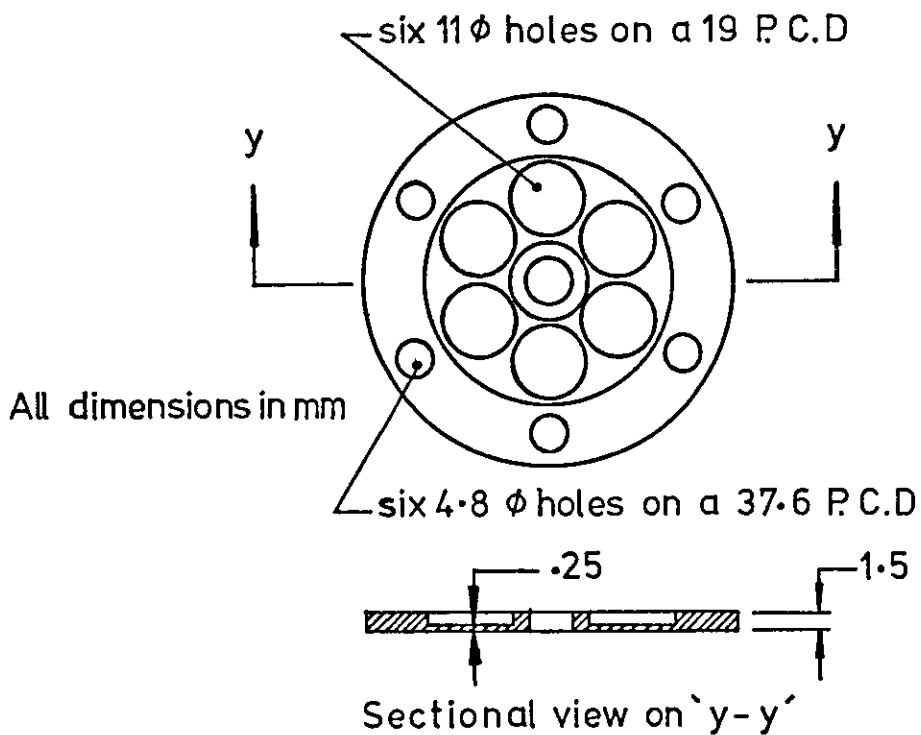
Fig.5.9   Original diaphragm for the three
component dressing-force dynamometer

to the
indicating unit
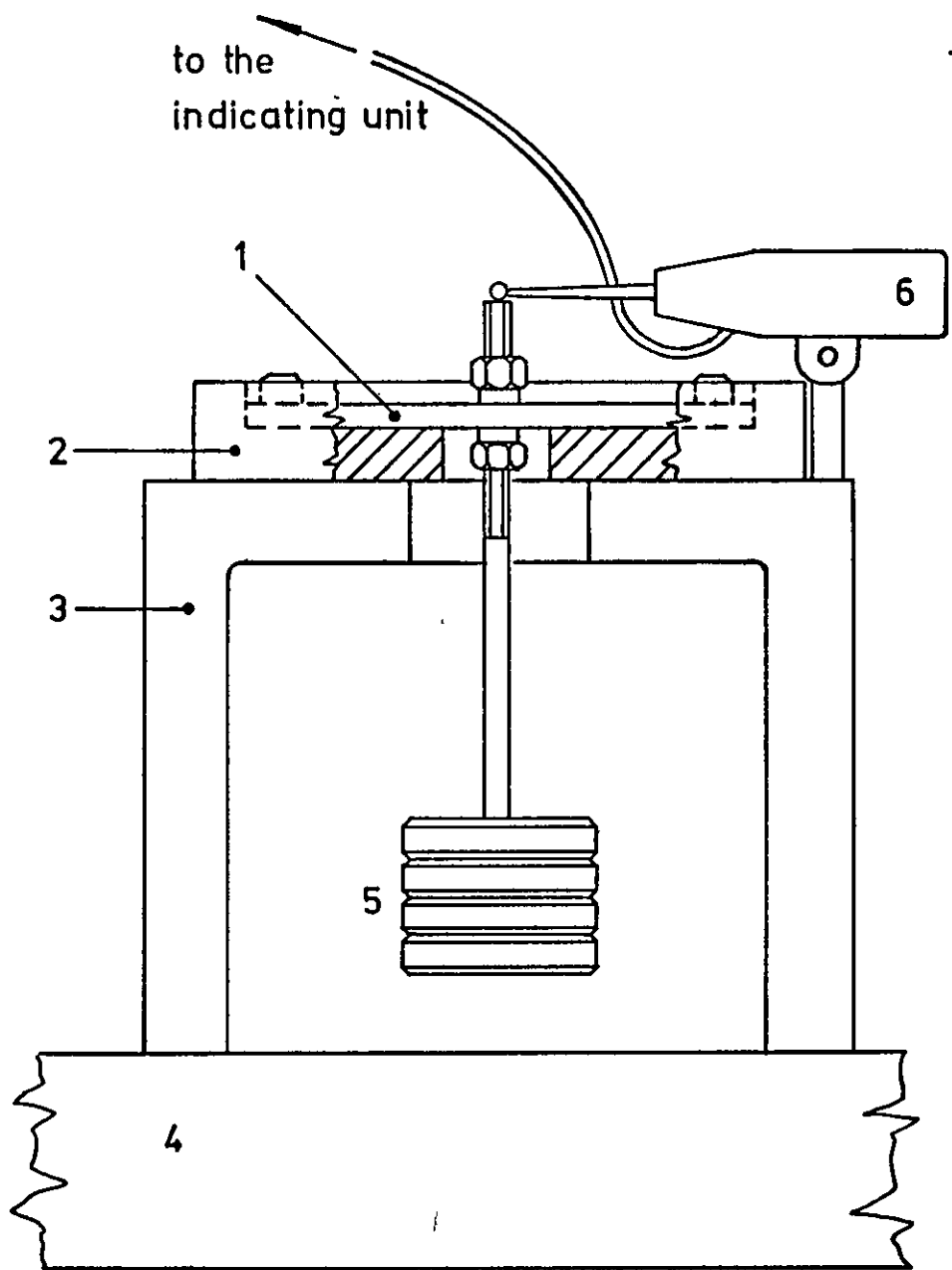
1   Steel diaphragm
2   Steel diaphragm housing
3   Cast iron cube
4   Cast iron table
5   Load hanger with deadweights
6   "Mitronic" displacement indicator

Fig.5.11   Calibration set-up for
evaluation of diaphragm stiffness

red
leads

green
leads

blue
leads

yellow
leads

R_1 R_2 R_4 R_3

F

F

Mechanical layout of
the strain gauges

red   blue

R_1 R_2

red   to
bridge
amplifier   blue

yellow   green

R_4 R_3

yellow   green
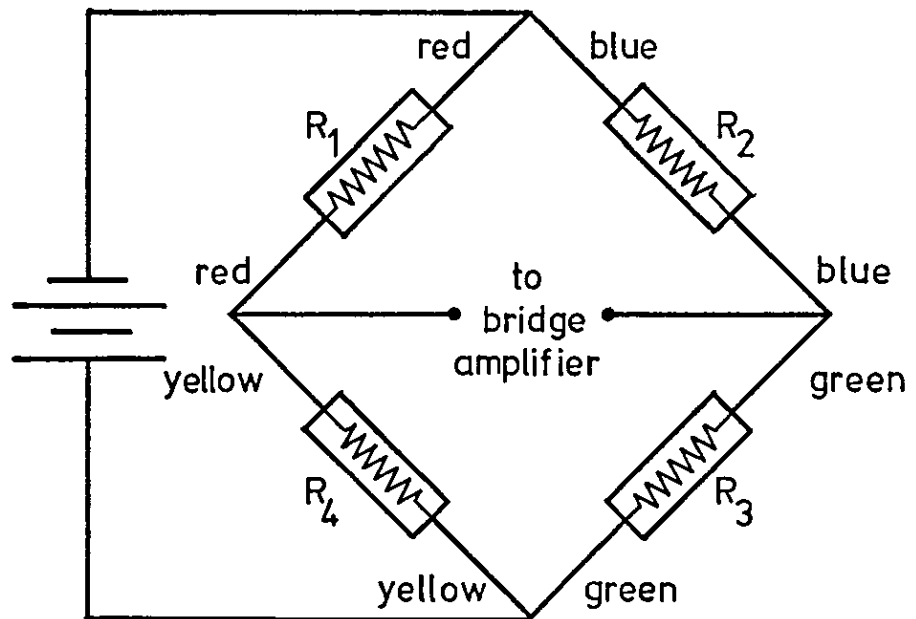
Electrical layout of
the strain gauges

Fig. 5.12   Strain gauge layout for the
measurement of the component of
dressing force, F_r.
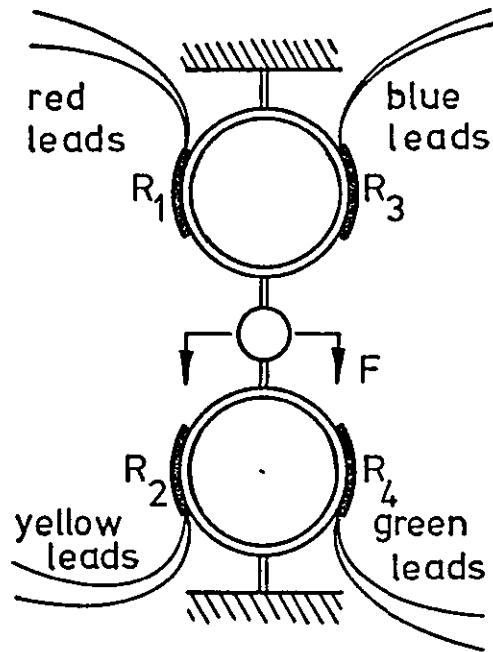
Mechanical layout of
the strain gauges
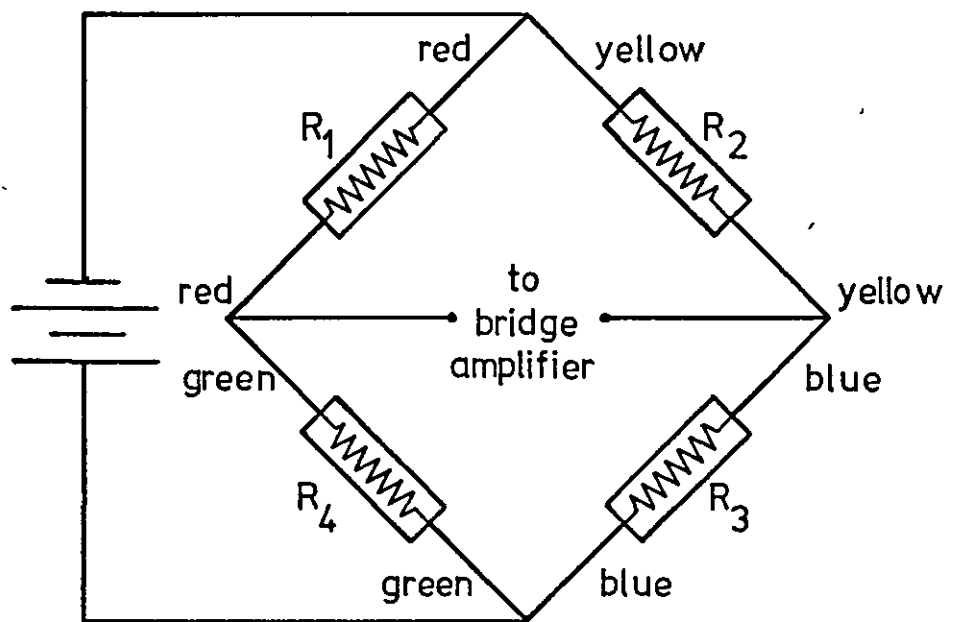
Electrical layout of
the strain gauges

Fig. 5.13 Strain gauge layout for the
measurement of the two components
of dressing force, F_a and F_t.
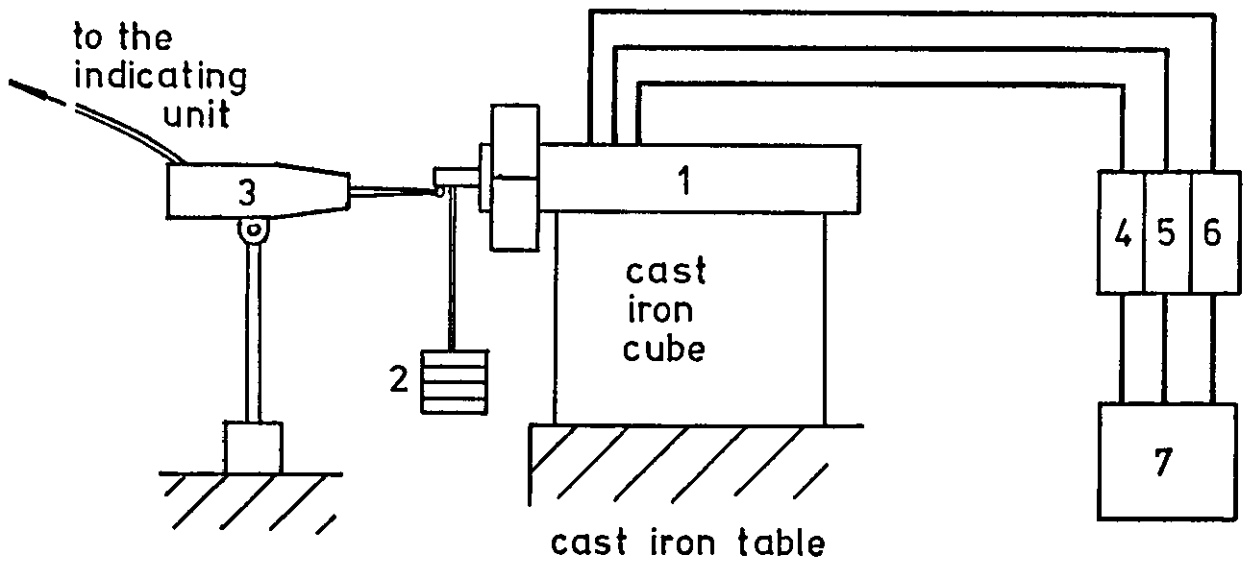
Set-up for calibration of the two axes in the
plane of cutting

1   dynamometer

2   dead weights

3   "Mitronic" displacement indicator

4,5,6   d.c. strain bridge amplifiers

7   ultra-violet oscillograph
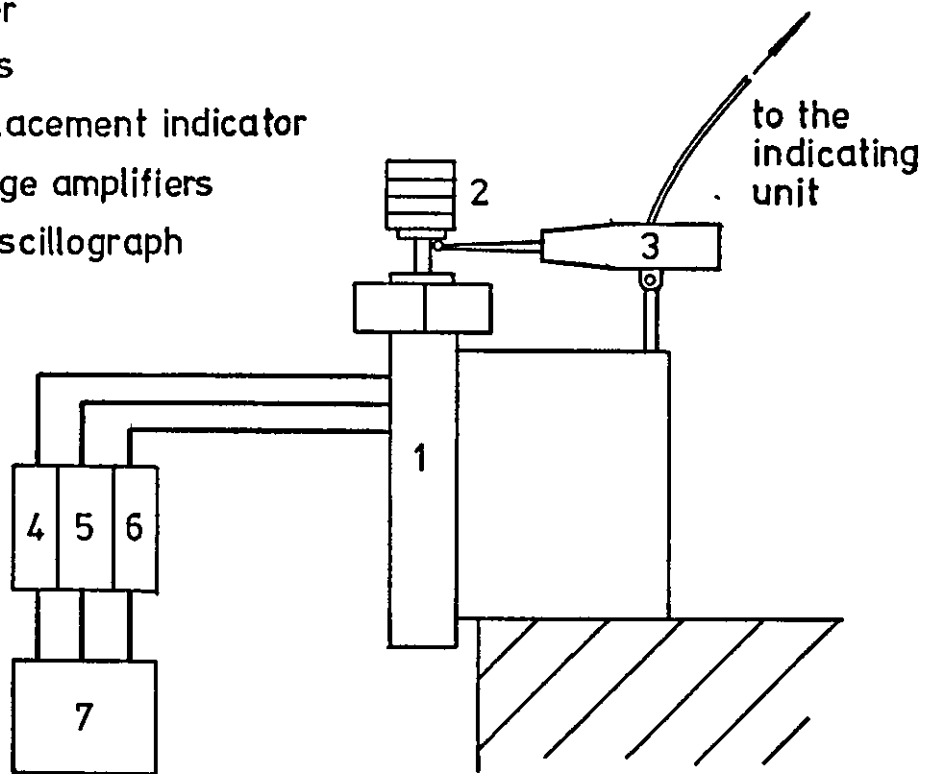
Set-up for calibration of the axis perpendicular
to the plane of cutting

Fig.5.14   Static calibration set-up for the
three component dressing-force dynamometer
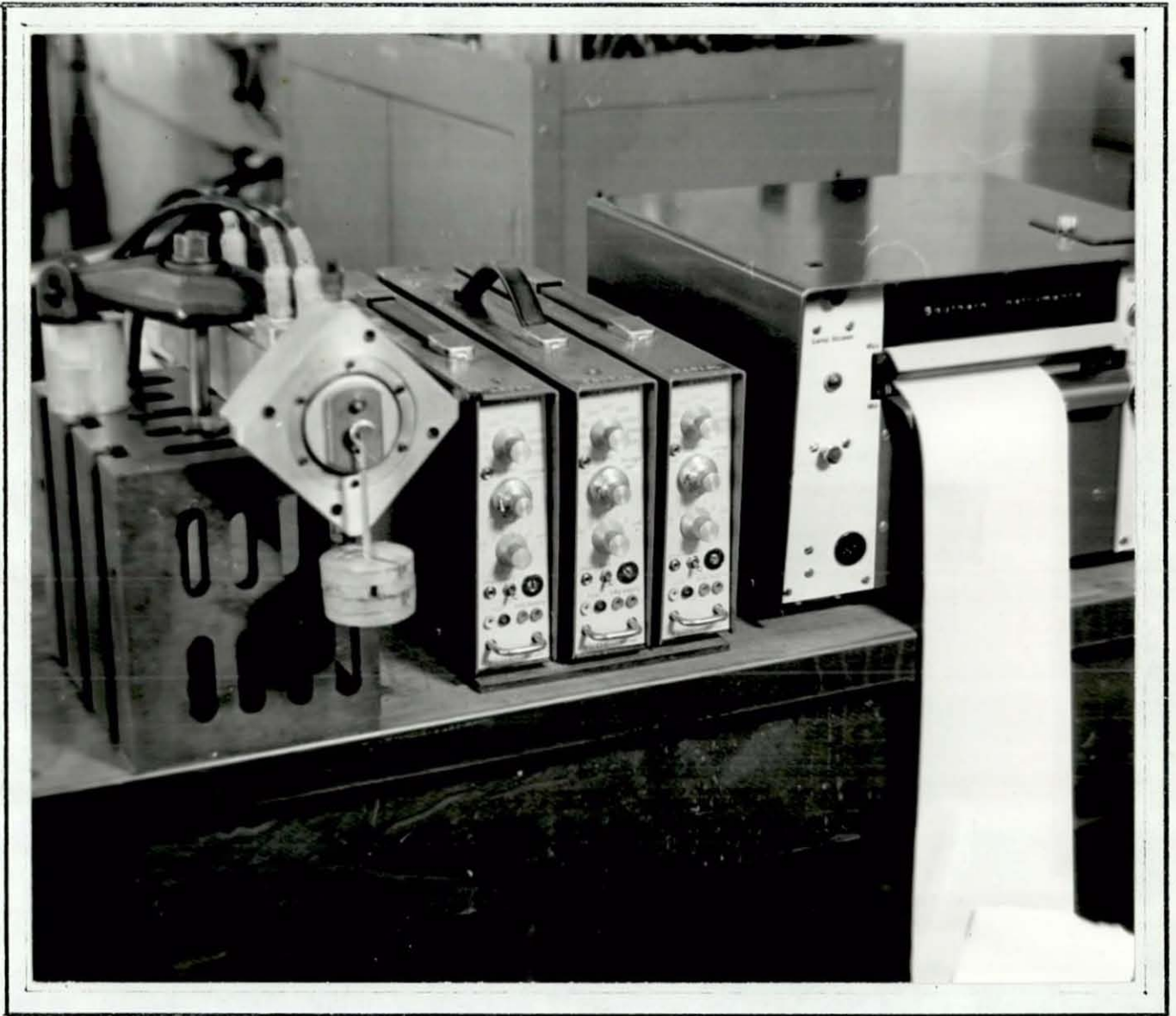
Fig. 5.15 Static calibration of the F_t axis
for the three component dressing-
force dynamometer.
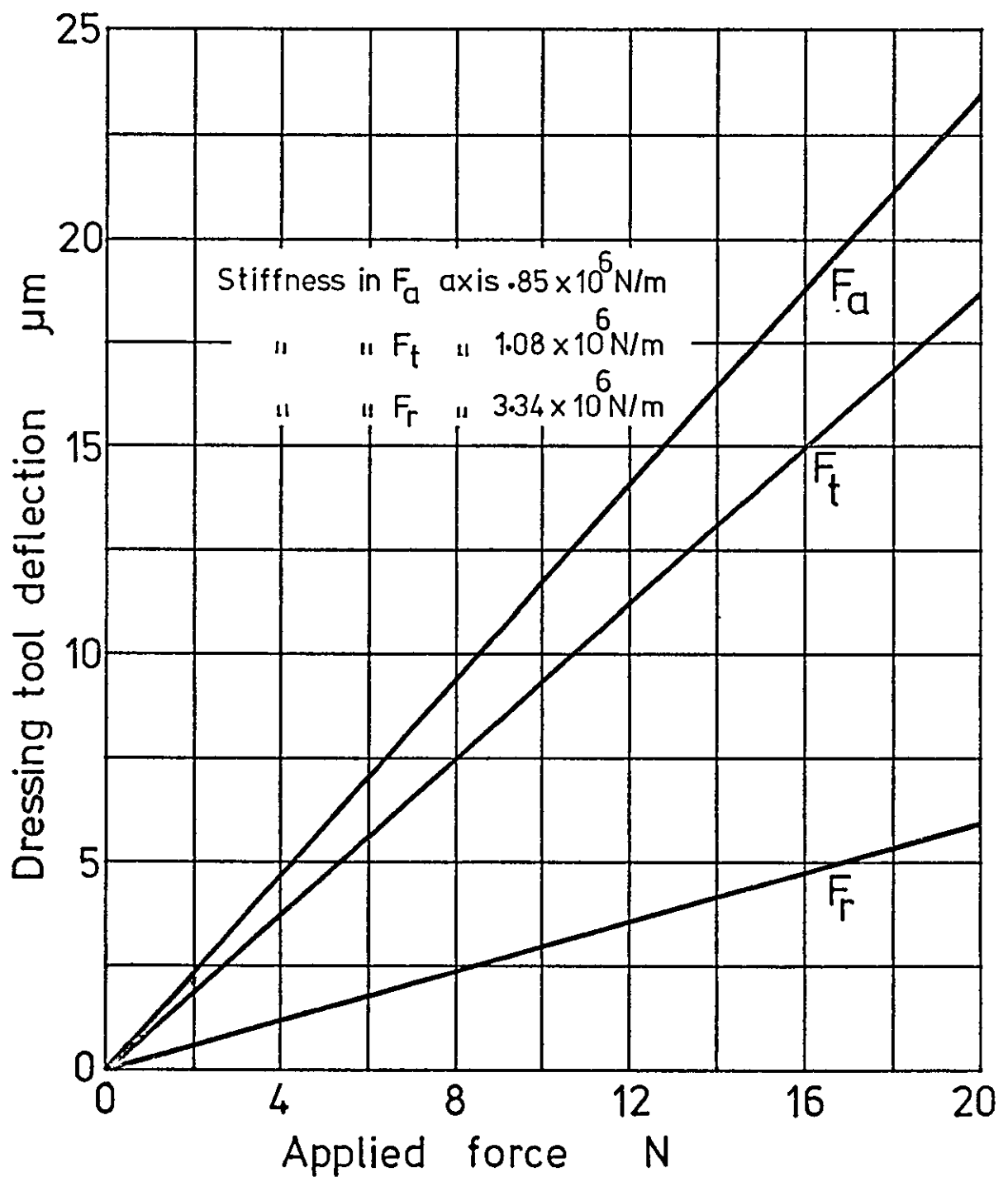
Fig. 5.16   Calibration chart of dynamometer
stiffness in each axis for the three
component dressing-force dynamometer
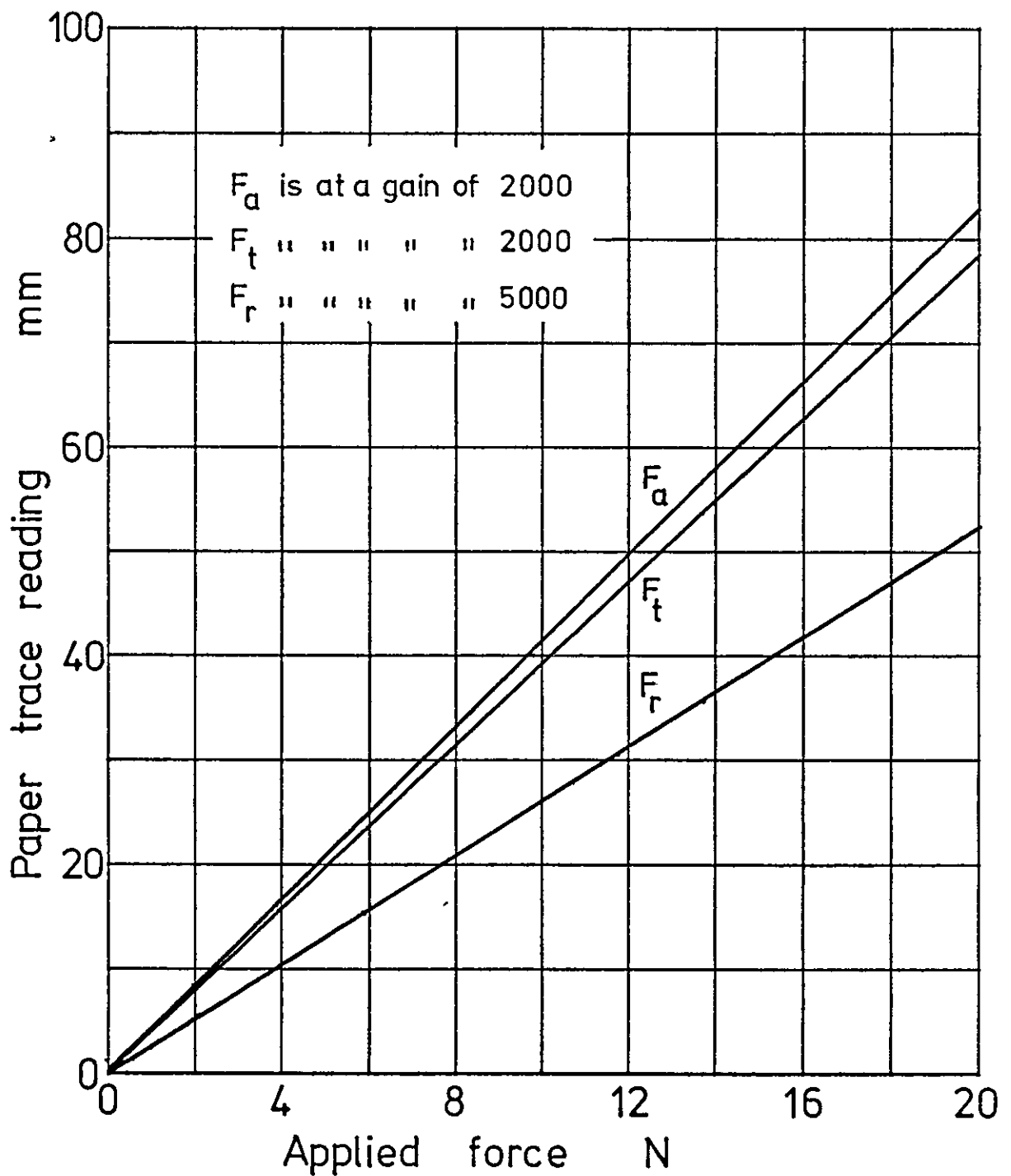
Fig. 5.17 Calibration chart of paper trace reading versus applied force for each axis of the dressing force dynamometer
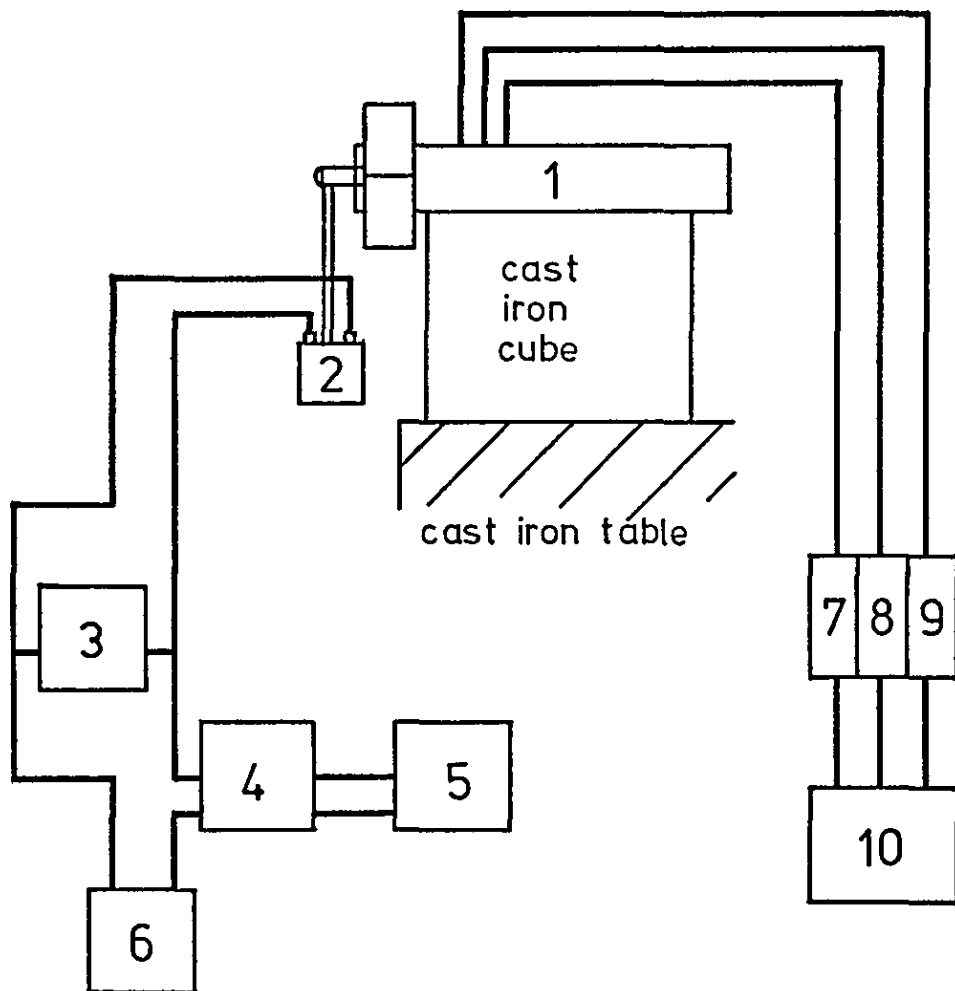
1	dynamometer
2	vibrator
3	oscilloscope
4	10 watt amplifier
5	beat frequency oscillator
6	avometer
7,8 & 9	d.c. strain bridge amplifiers
10	ultra-violet oscillograph

Fig.5.18   Electrical circuit diagram for the dynamic calibration of the three component dressing-force dynamometer.
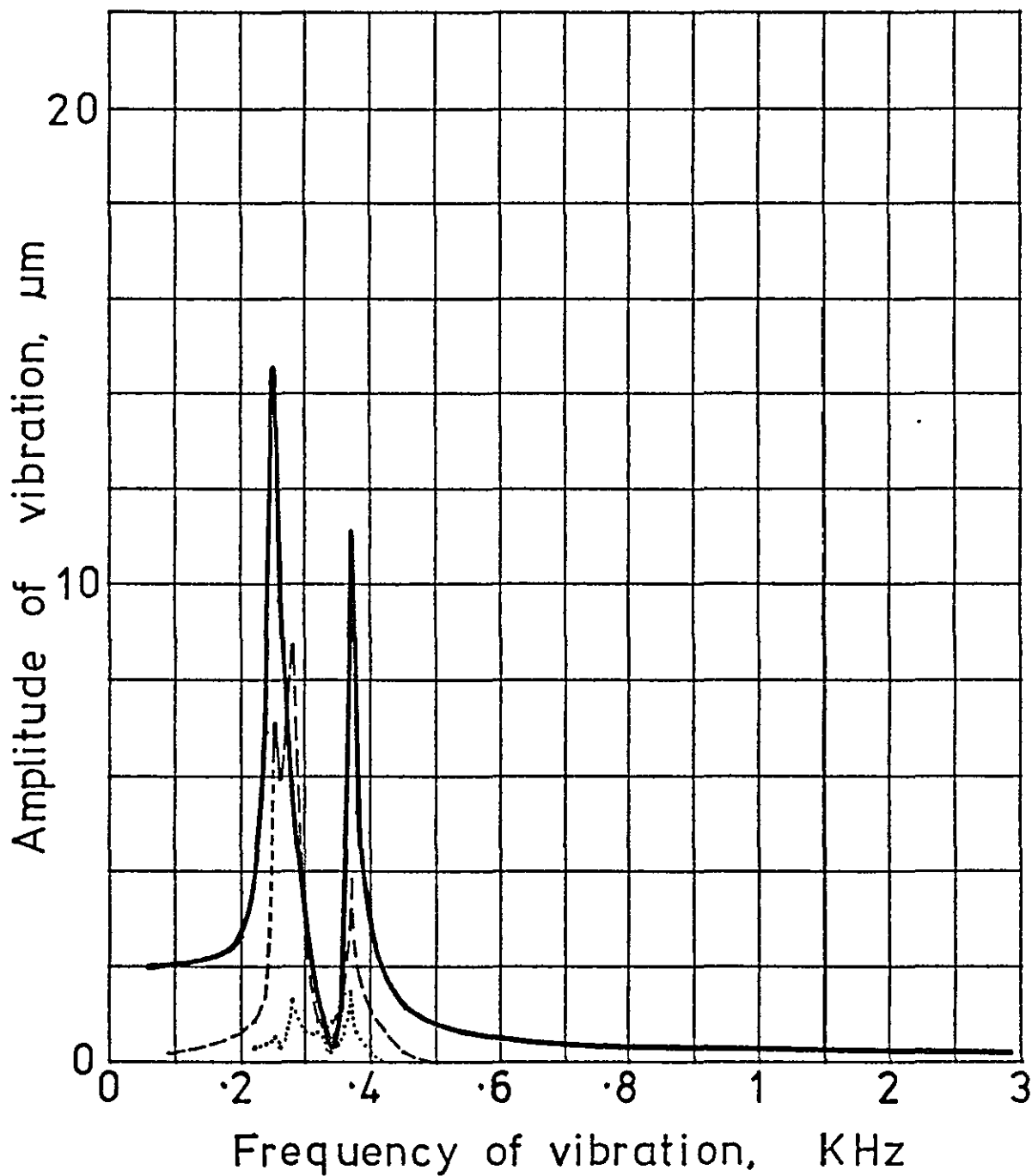
Fig. 5.19   Dynamic calibration of the
                Dressing Dynamometer.

Key :-

Dynamic load of ±4 N. applied to F_a axis

———— represents F_a axis

------   " F_t "

············   "   . F_r "
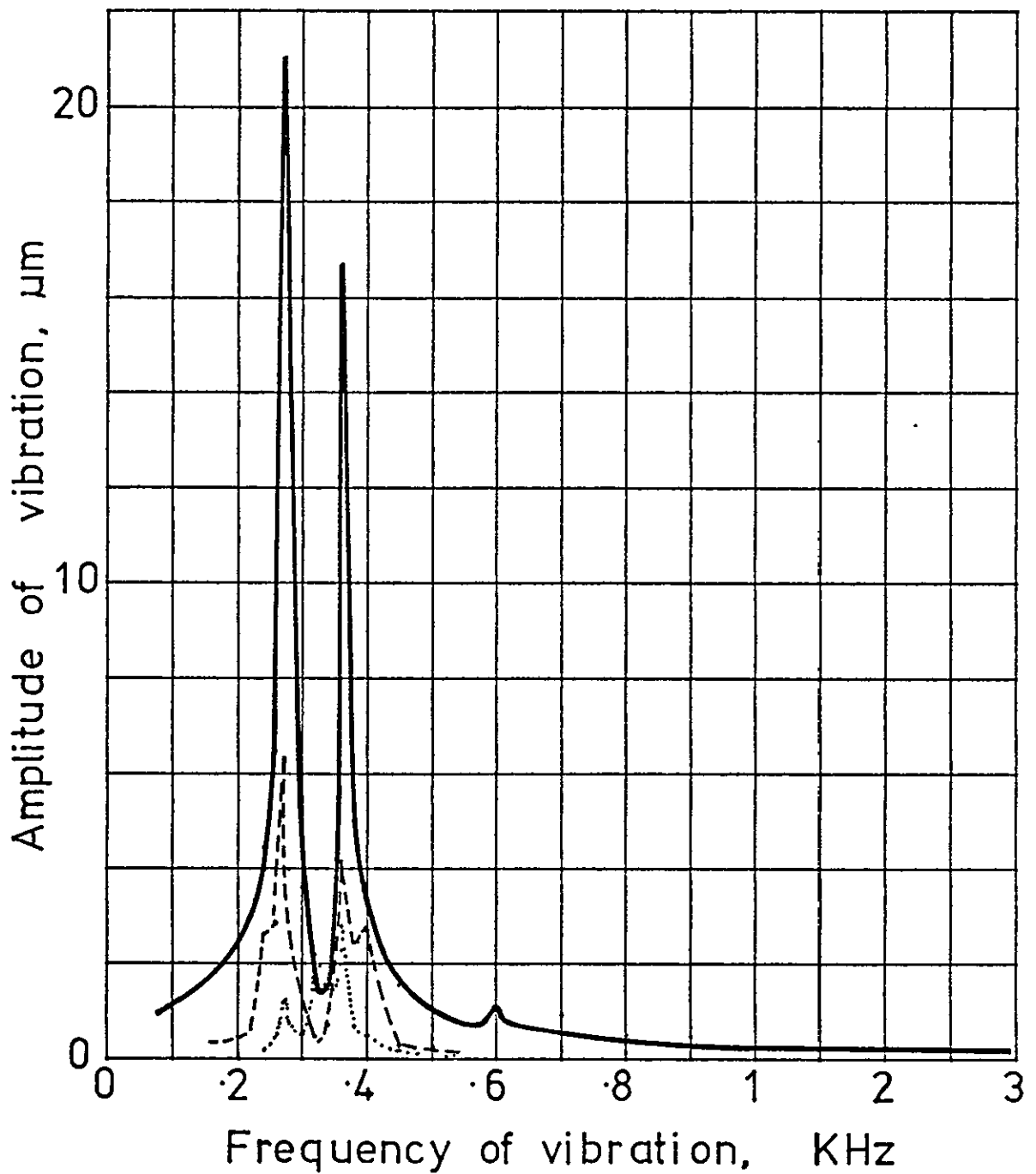
Fig. 5.20   Dynamic calibration of the
Dressing Dynamometer.

Key :-

Dynamic load of ±4 N applied to F_t axis

———————   represents F_t axis

– – – – – –   " F_a "

· · · · · · · · · · ·   "   . F_r "
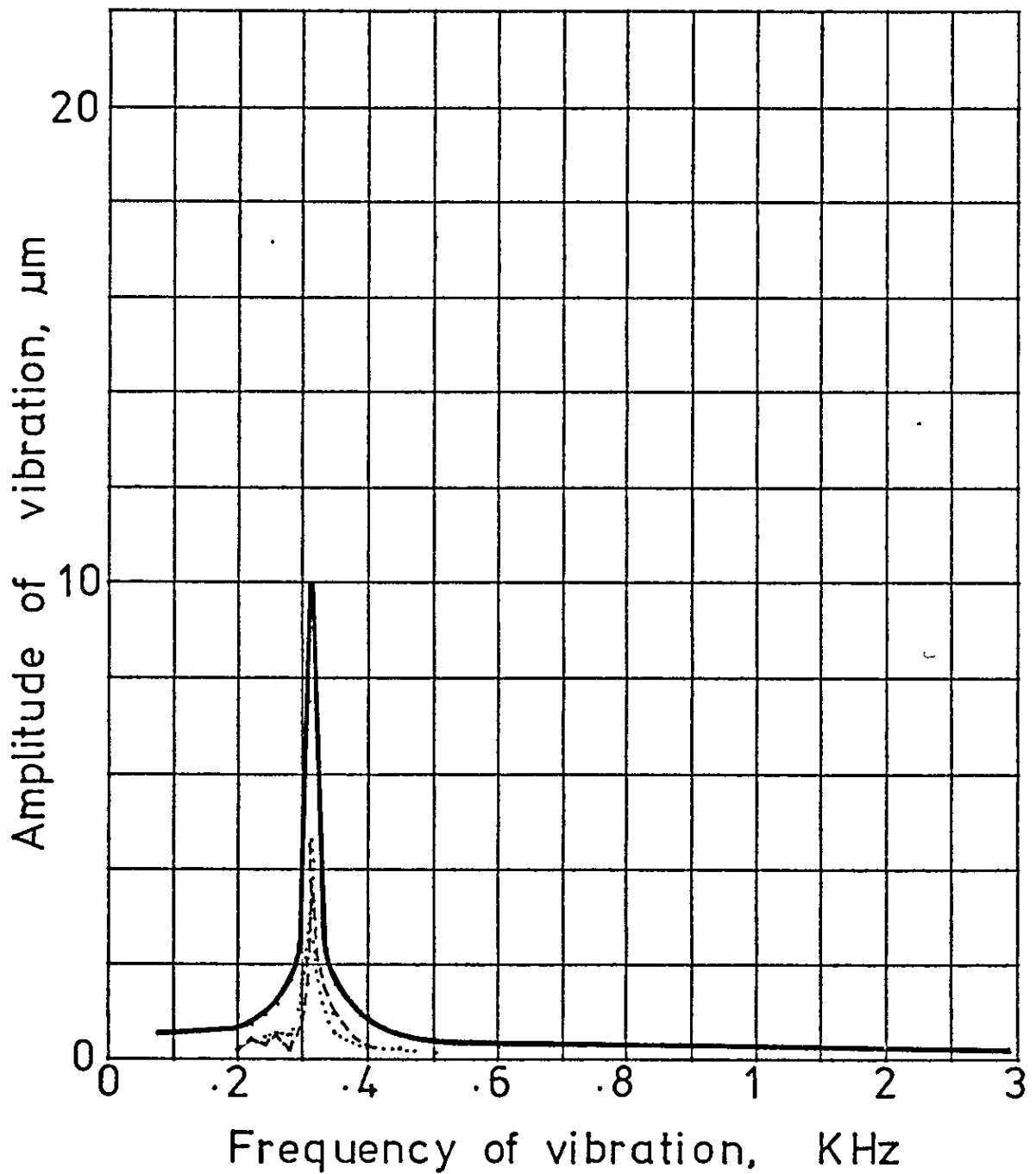
Fig. 5.21 Dynamic calibration of the
Dressing Dynamometer.

Key:-

Dynamic load of ±4 N. applied to F_r axis

———— represents F_r axis

– – – – – – " F_t "

.... " F_a "

Part No.	Part name.
1	Gear box cover plate.
2	Gear box.
3	Top slide.
4	Clamping arm (2 off).
5	Clamp screw (2 off).
6	Clamp nut (2 off).
7	In-feed dial.
8	Micrometer screw.
9	Micrometer screw clamp block.
10	Transducer clamp block.
11	Mitronic transducer.
12	Top slide locking screw.
13	Transducer housing block.
14	Bottom slide.
15	Pinion gear.
16	Worm gear.
17	Location pin (2 off).
18	Spacer.
19	Worm gear housing.
20	Rear bearing *.
21	Micrometer nut and screw.
22	Micrometer nut locating block.
23	Front bearing *.
24	Collar.
25	Extension spring.
26 } 27	Locking screw thrust pad.

* for locating the in-feed
micrometer screw

Parts list for the three component
dressing force dynamometer in-feed slide
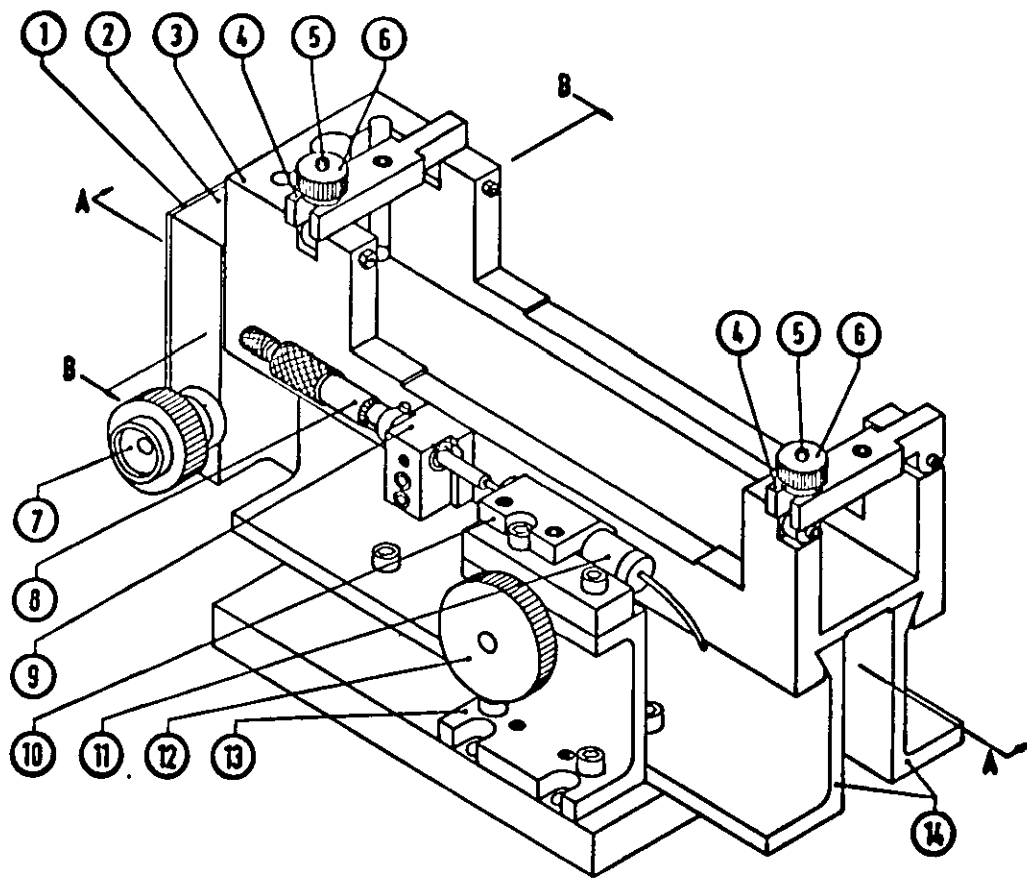
Isometric view of the infeed slide.
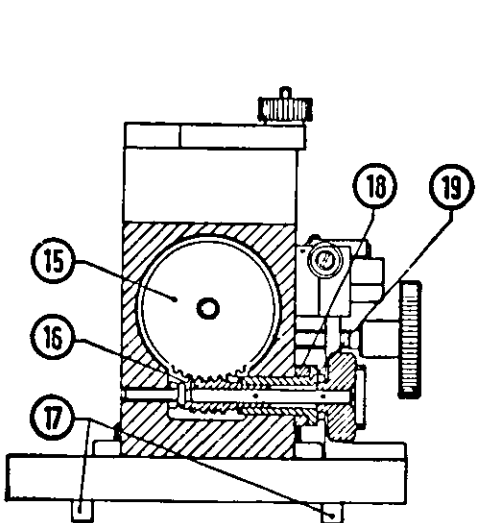
Sectional view of the reduction
gear housing looking in the direction
of the arrows "B - B."
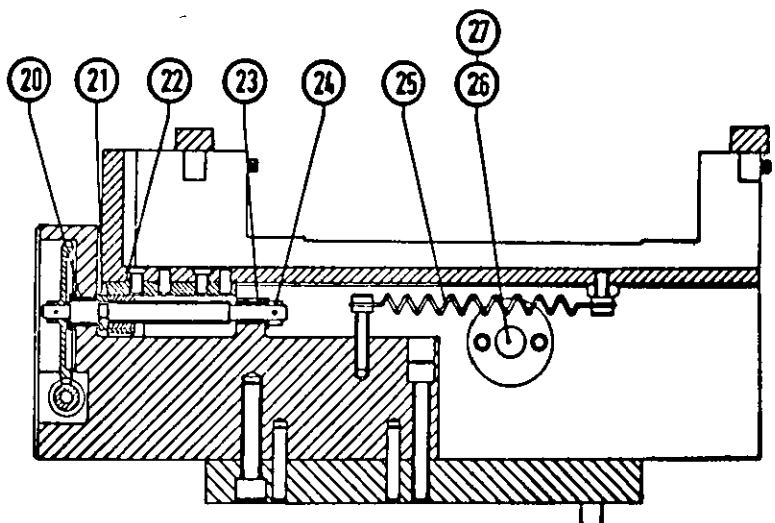
Sectional view of the slide looking in
the direction of the arrows "A - A."

Fig.5.22 Views of the three component dressing-force
dynamometer infeed slide.
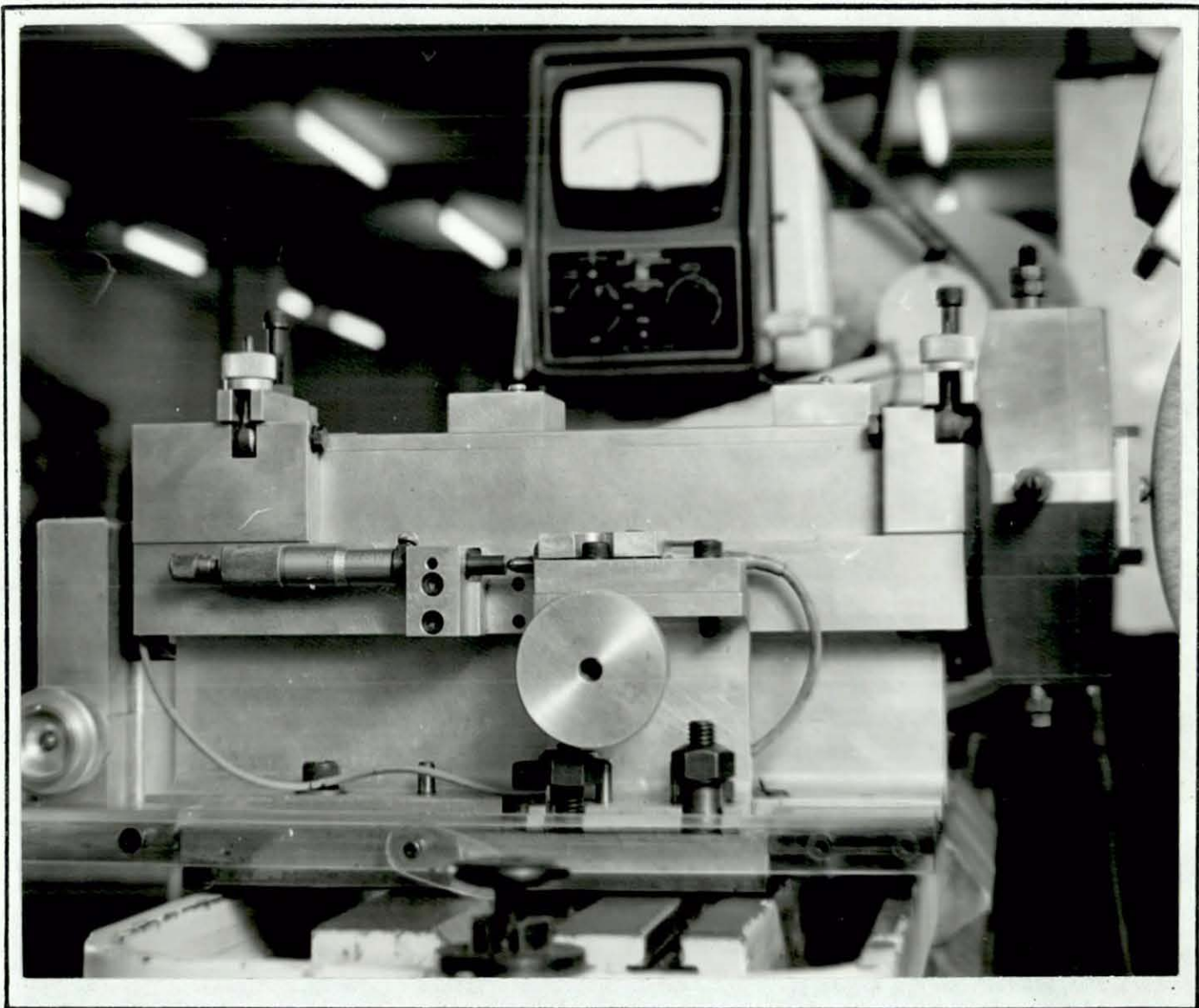
Fig. 5.23 The three component dressing -
force dynamometer and slide, mounted
on the cylindrical grinding machine table.
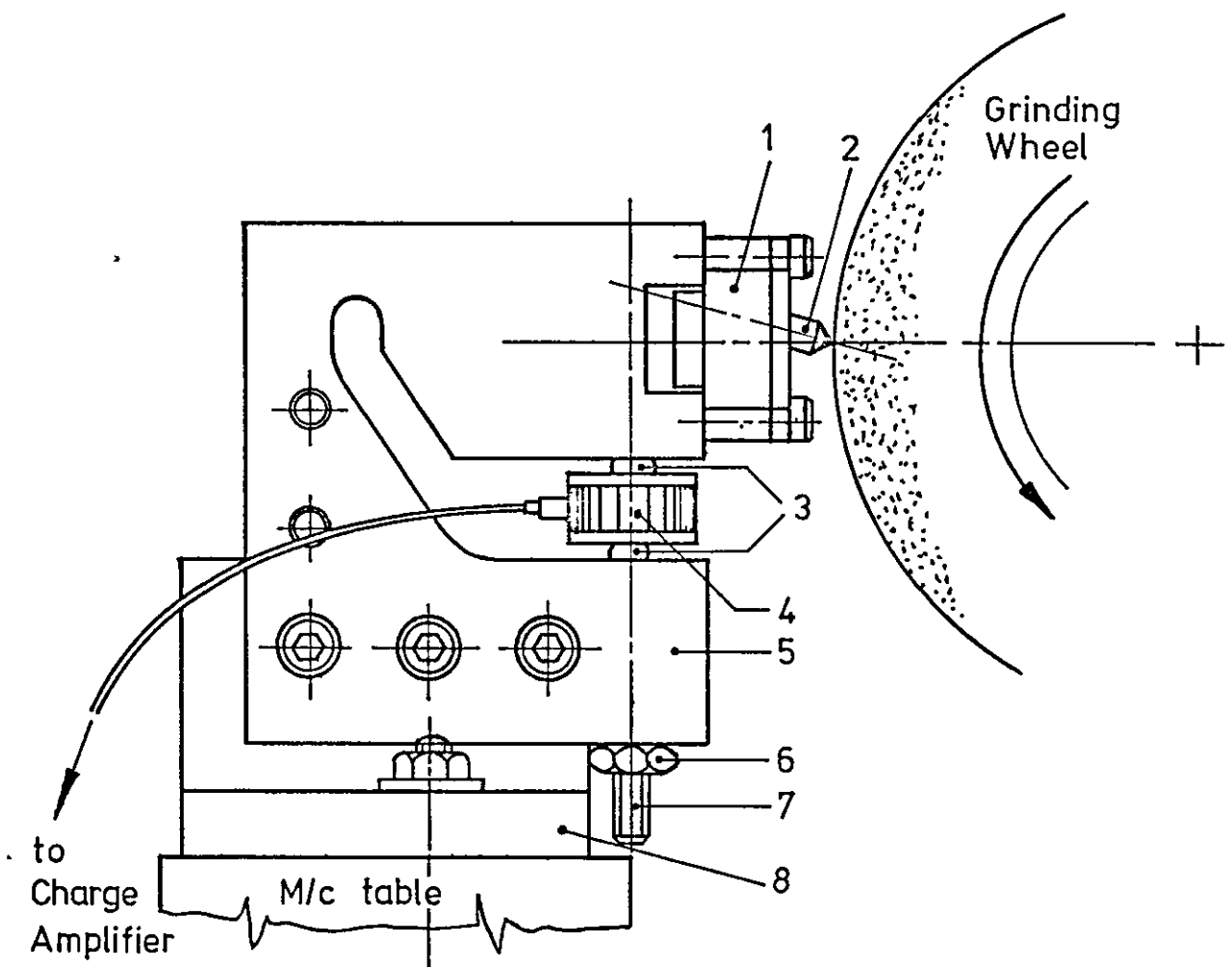
1	Tool holder
2	Diamond tool
3	Ball bearings
4	Quartz force transducer
5	Dynamometer body
6	Lock nut
7	Preload screw
8	Base plate

Fig.5.24 Schematic representation of the
Cantilever dressing-force dynamometer
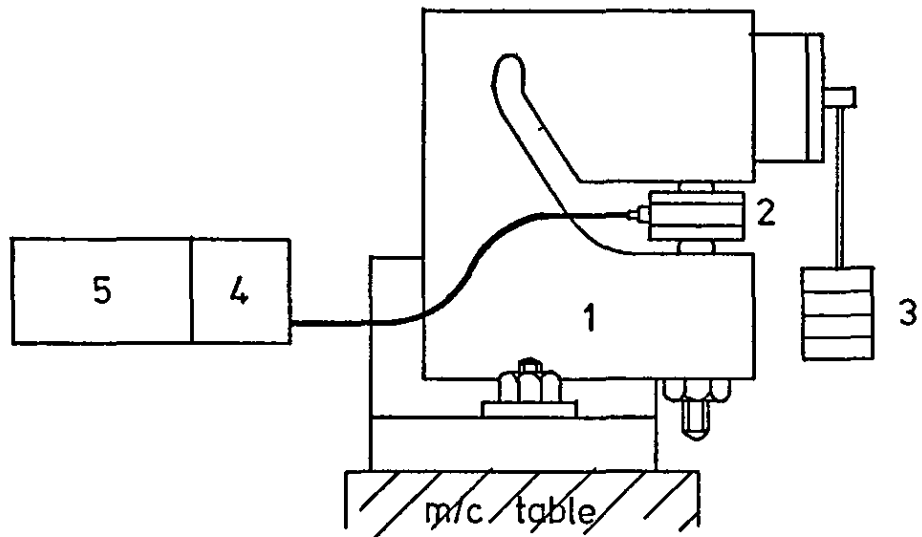
Set-up for the F_t axis

1   dynamometer
2   quartz force transducer
3   dead weights
4   charge amplifier
5   readout galvanometer
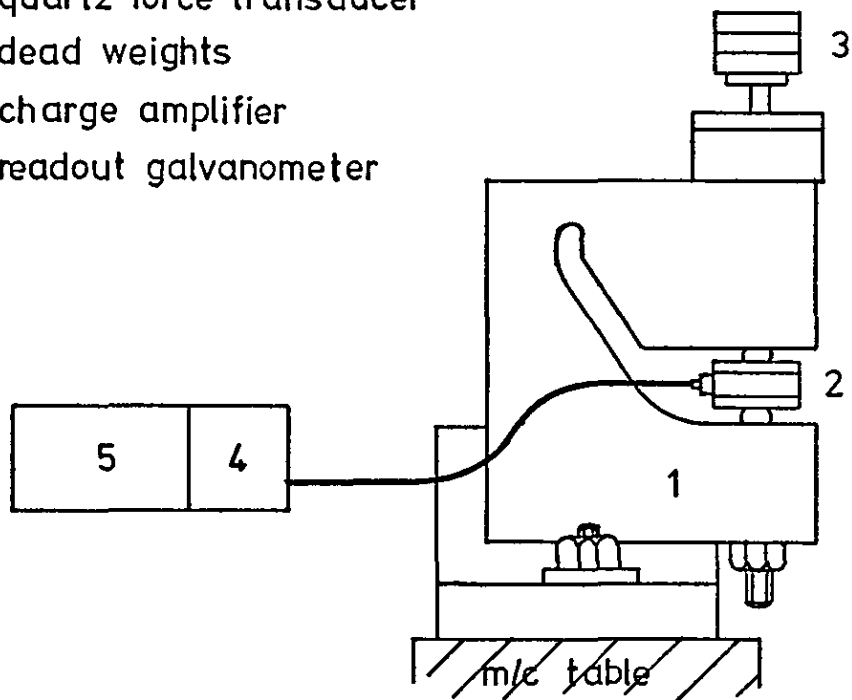
Set-up for the F_r axis

Fig.5.25   Schematic representation of the calibration set-up for the cantilever-type two component dressing-force dynamometer
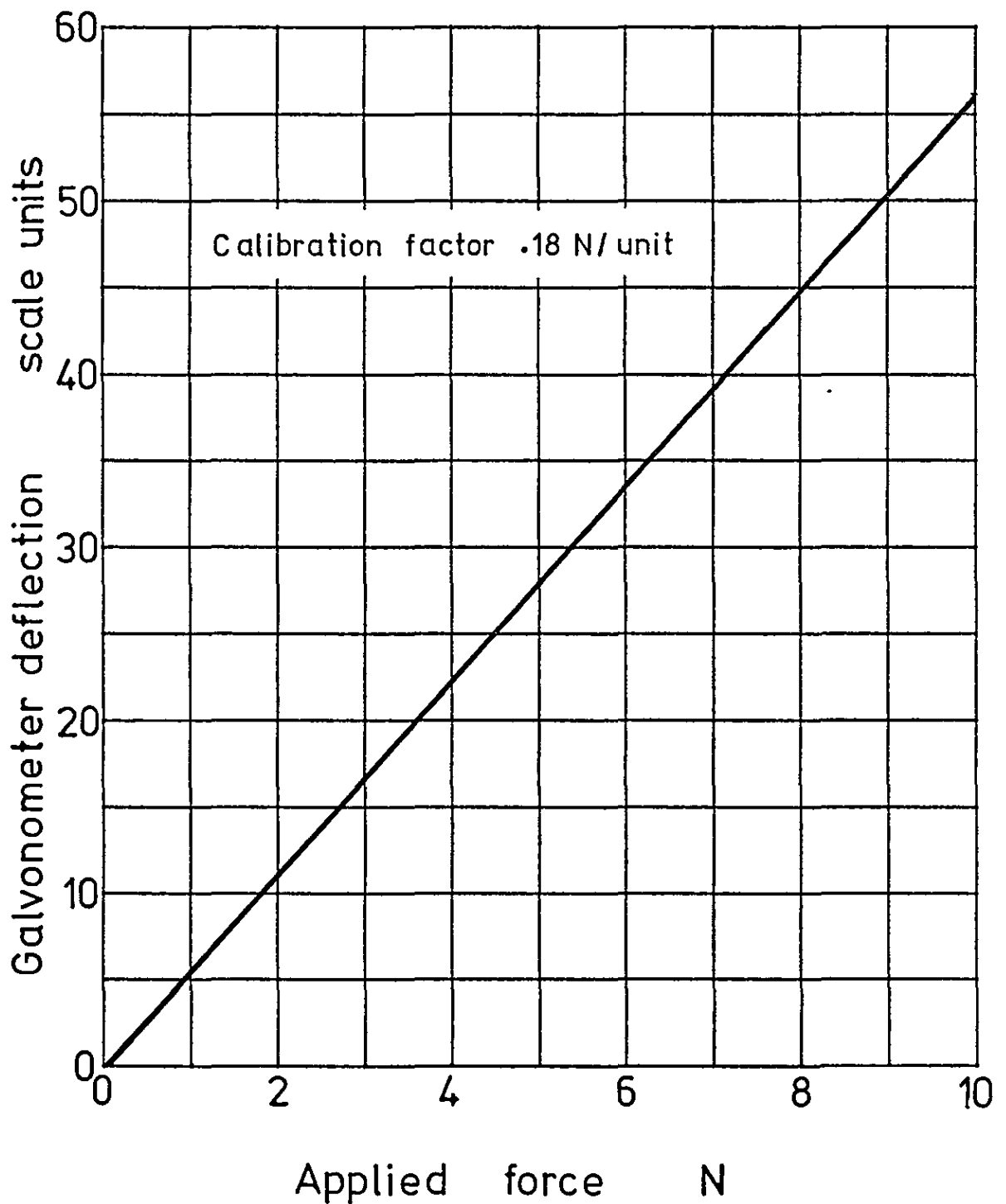
Fig. 5. 26   Calibration chart for the tangential component of force as measured by the two component dressing-force dynamometer
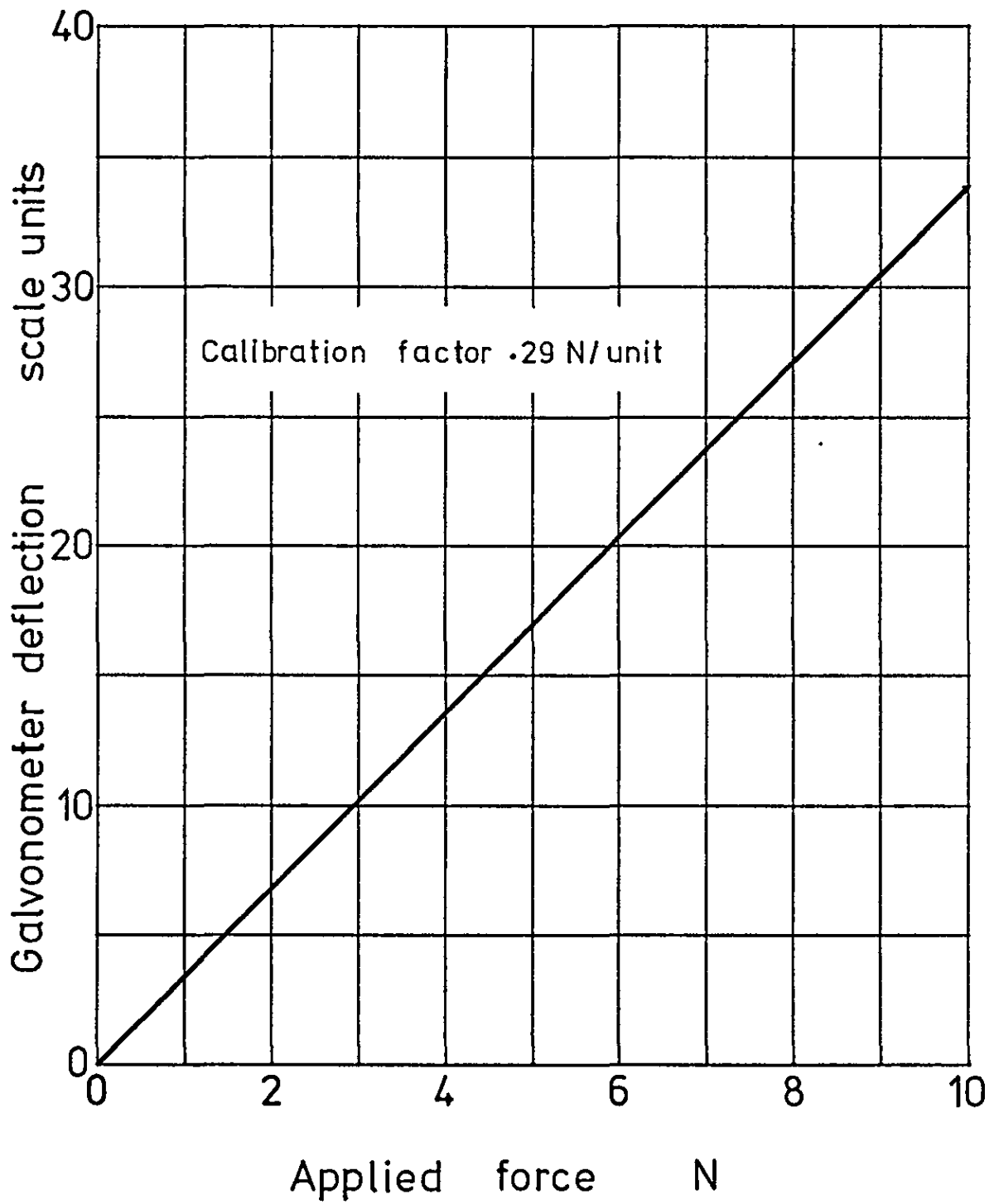
Fig. 5.27   Calibration chart for the radial component of force as measured by the two component dressing - force dynamometer
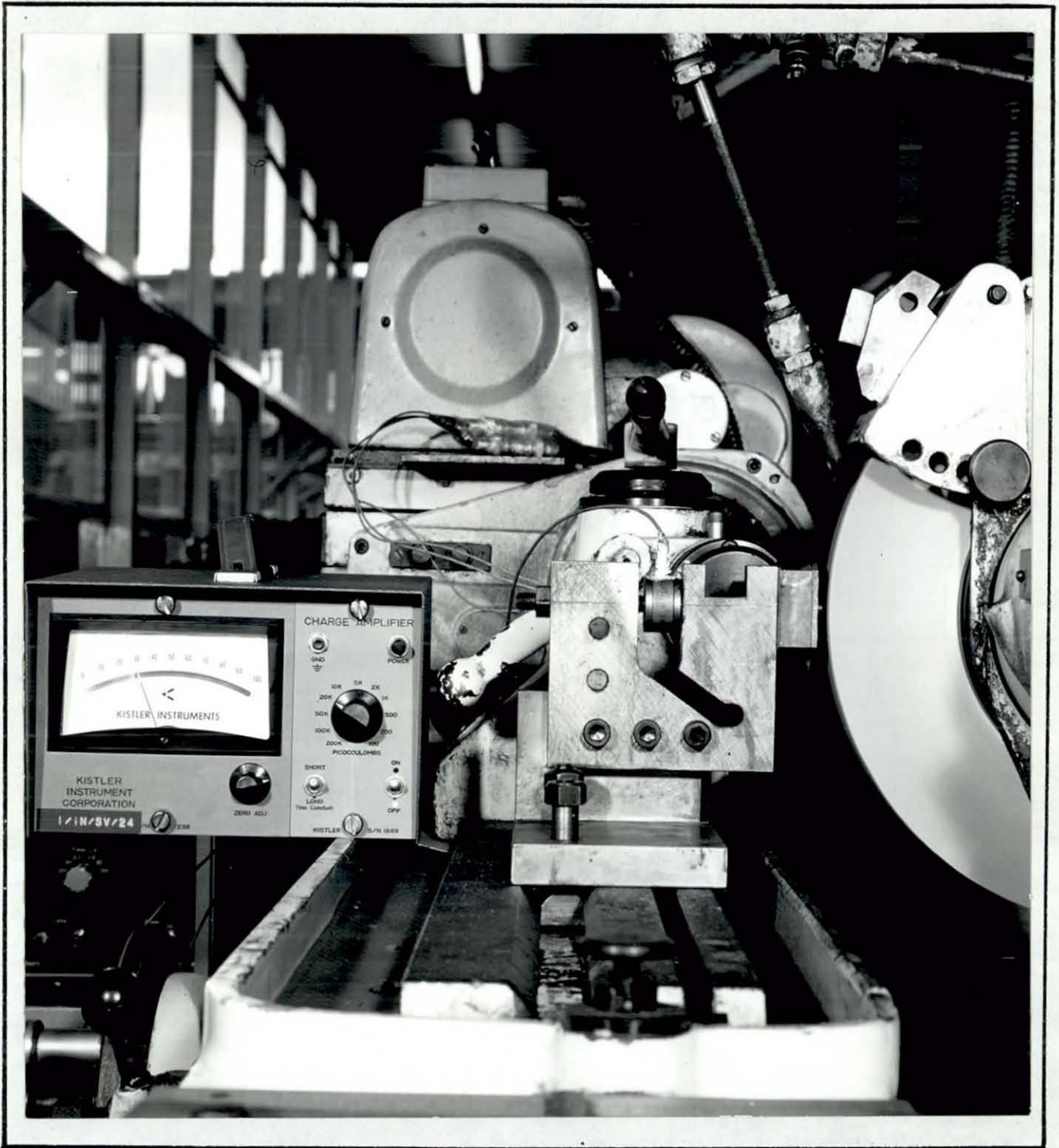
Fig. 5.28 The two component dressing-force dynamometer mounted on the grinding machine table.
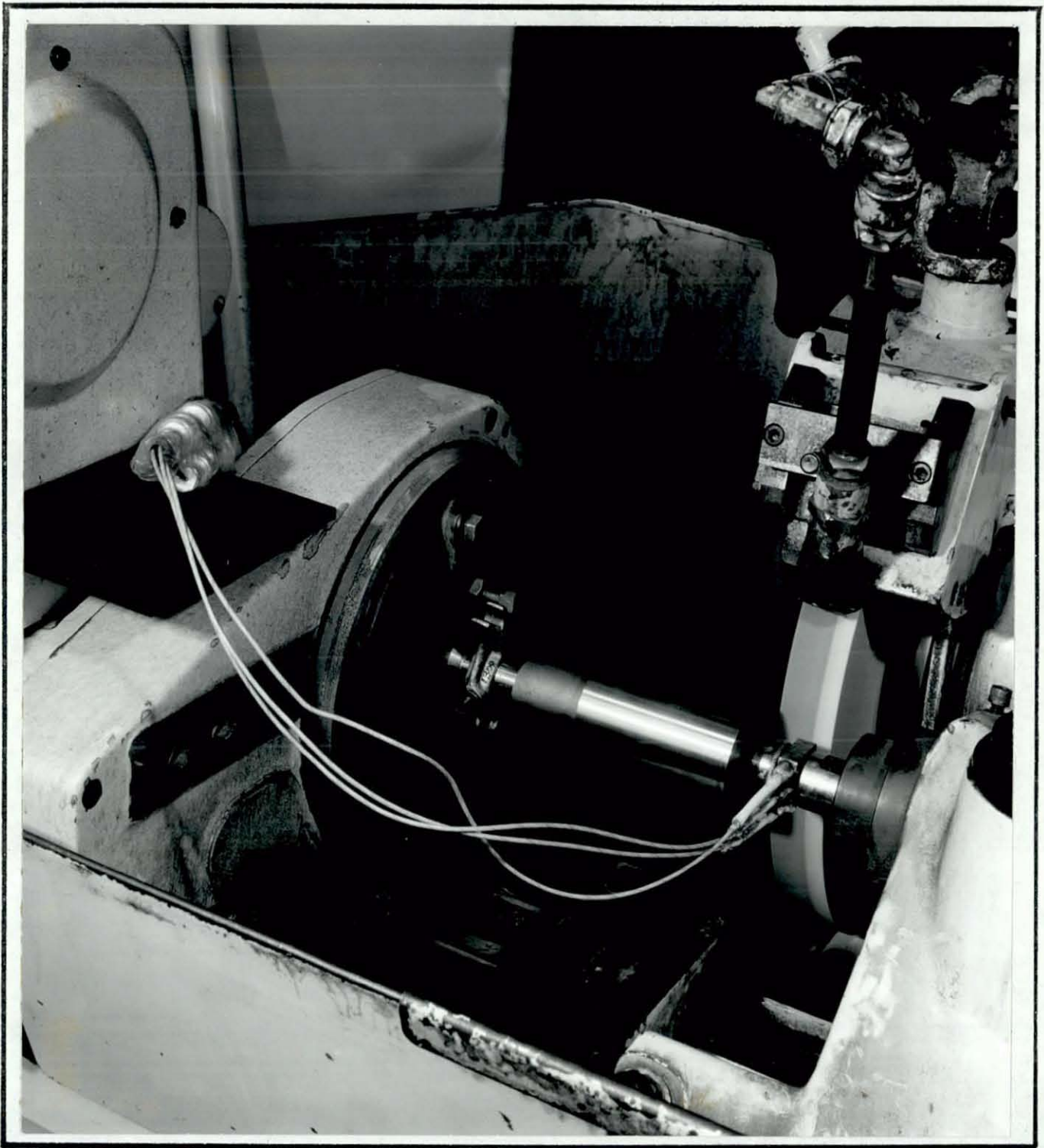
Fig. 5.29 The three component grinding-force
dynamometer mounted in the grinding
machine tailstock.

Front view

Sectional view on `X-X´
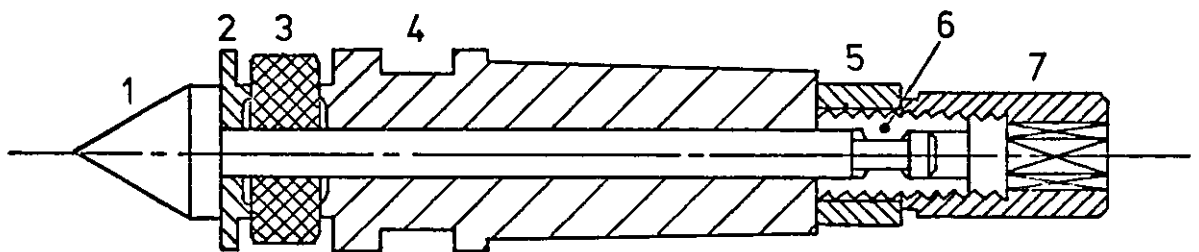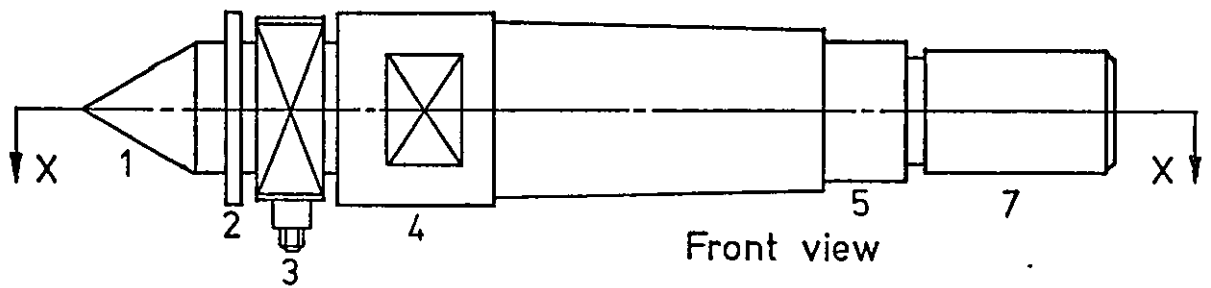
1	Cone centre
2	Shielding washer
3	Quartz force transducer
4	No. 3 Morse taper shank body
5	Retaining ring
6	Split collet
7	Preload nut

Fig. 5.30 Schematic representation of the three-component, grinding force dynamometer
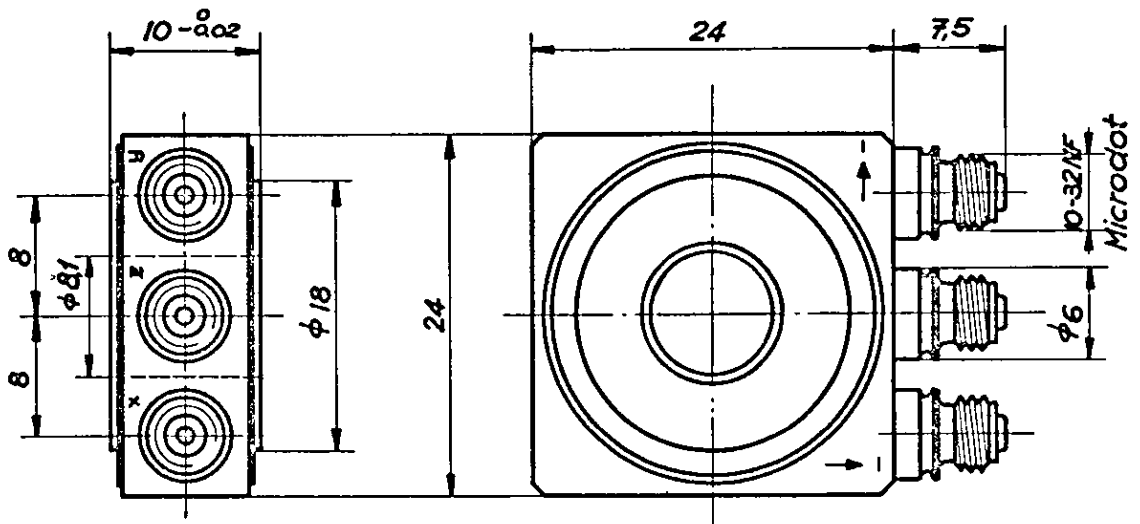
Quartz force transducer for decomposing a
dynamic or quasistatic force in 3 perpendicular
components. High resolution, high rigidity,
small dimensions.

TECHNICAL DATA		1kp = 9·81 N	
measuring ranges with an external			
preload of	kp	2500	
compression(+),traction(-)(z-axis)	kp	±500	
shear (x-, y-axis)	kp	±250	
resolution	kp	0.001	
overload	%	20	
sensitivity: compression + traction(z)	pC/kp	41	1)
shear (x,y)	pC/kp	75	1)
rigidity (z-direction)	kp/µm	85	
rigidity (x- and y-direction)	kp/µm	30	
resonant frequency in z-direction,			
loaded with 400 gr	kHz	8	1)
linearity (max. error)	%	±1	
cross influence of the			
components	%	<5	
insulation resistance	Ω	$5 \cdot 10^{13}$	
capacity (x,y,z each)	pF	30	
temperature coefficient	%/°C	0.02	
working temperature range	°C	-60 bis +150	
weight	gr	32	

Fig.5.31 Three component Quartz force
transducer
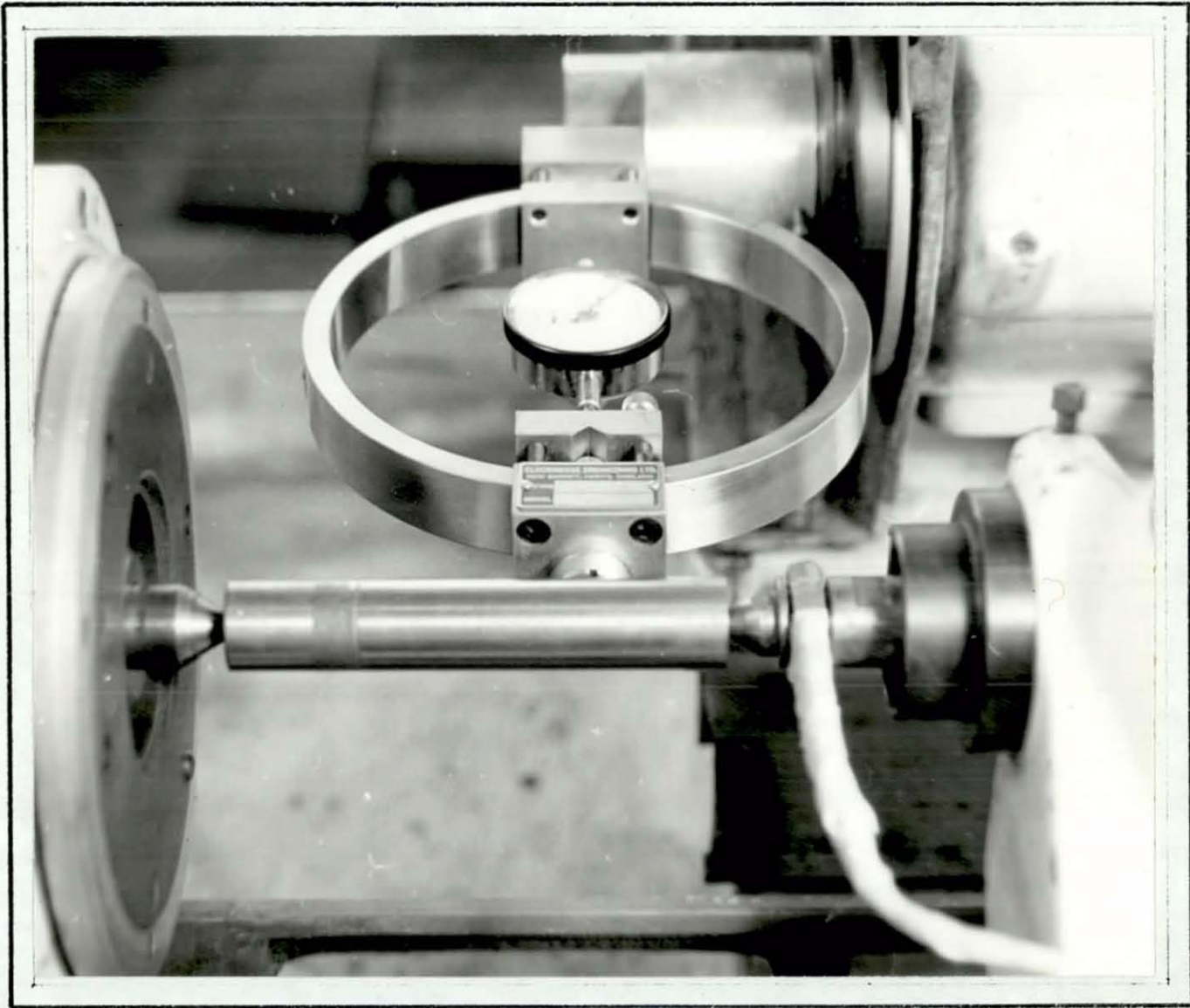
Fig. 5.32 Static calibration set up for the
three component grinding-force
dynamometer.
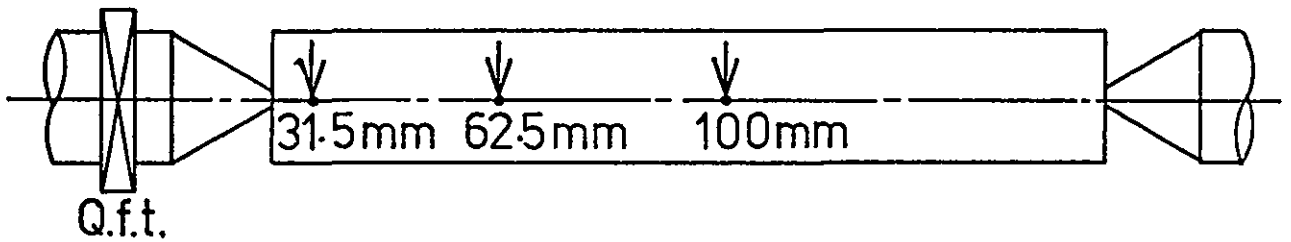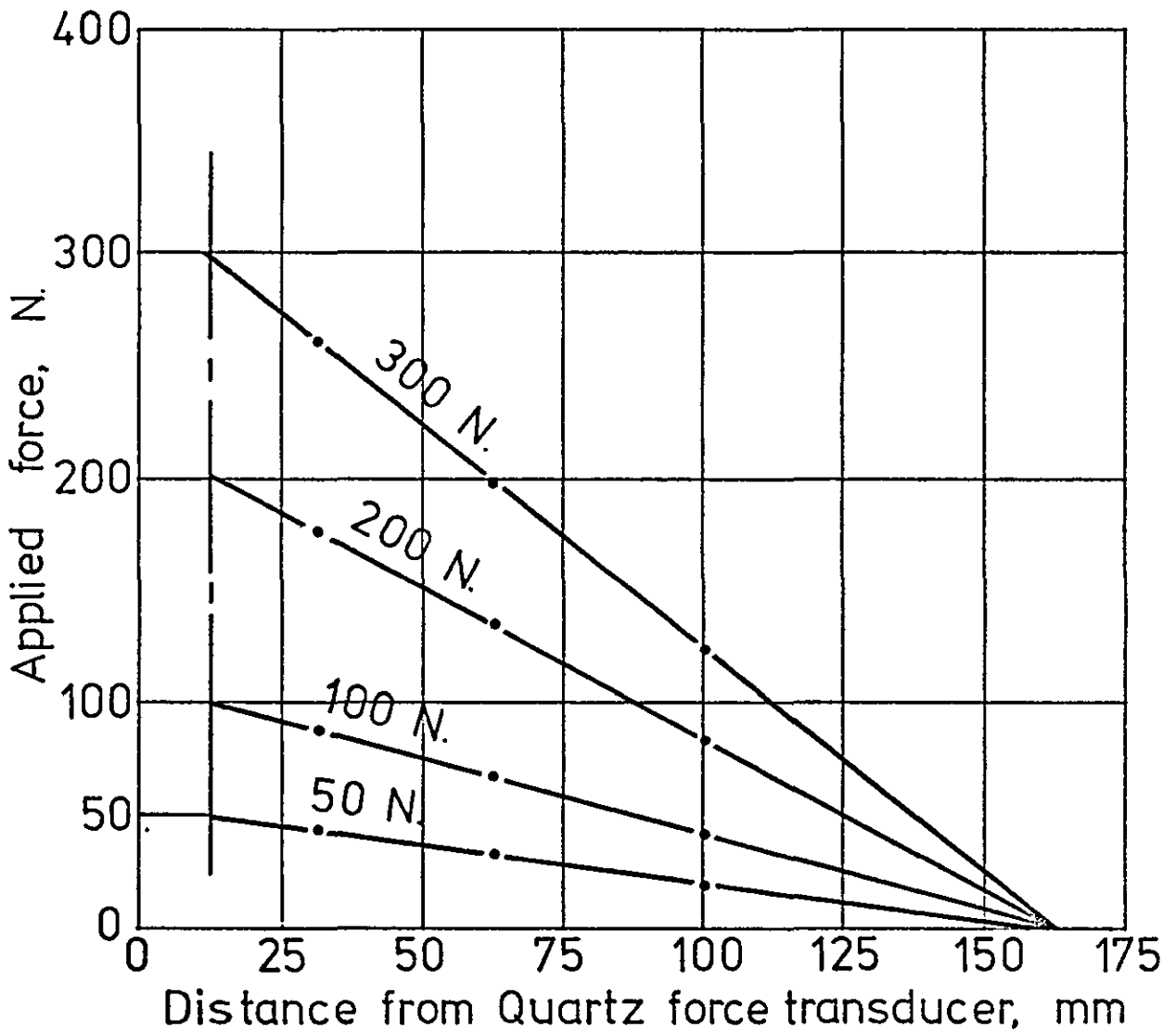
Fig. 5.33   Calibration of the radial
force component in cylindrical
traverse grinding for the
configuration shown.
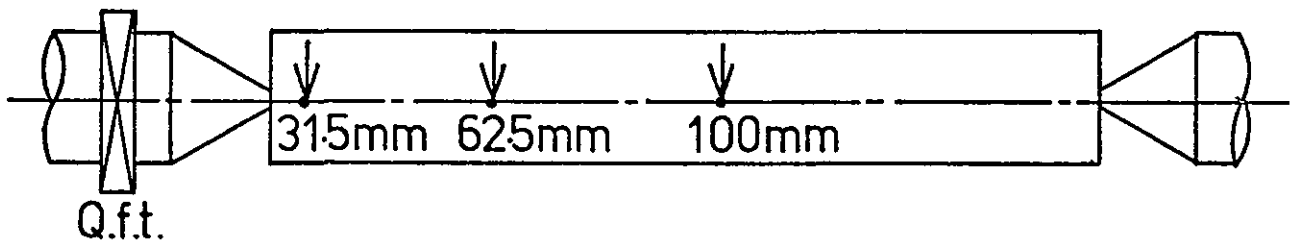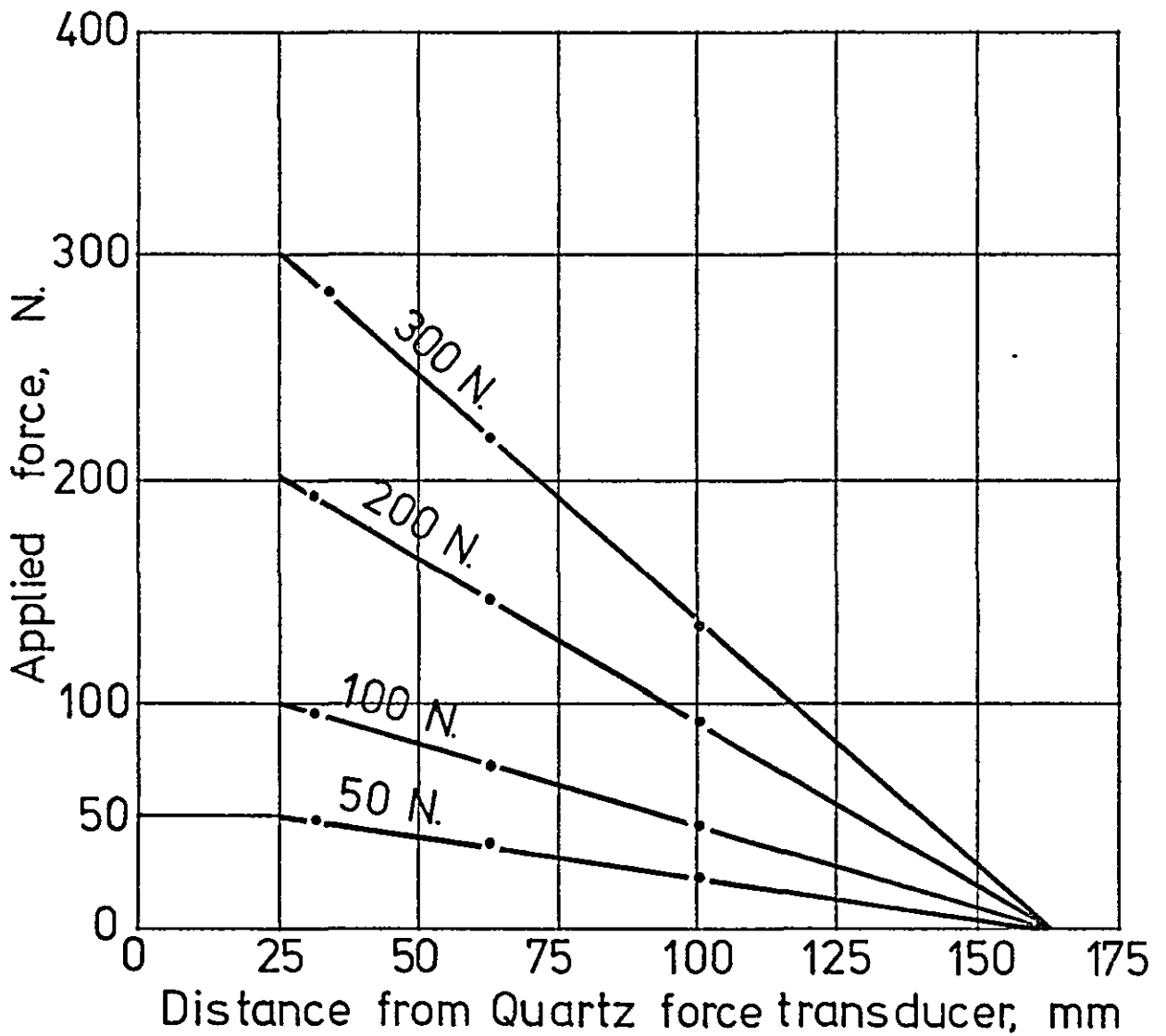
Fig. 5.34 Calibration of the tangential force component in cylindrical traverse grinding for the configuration shown.

CHAPTER 6

EXPERIMENTAL MATERIALS, TESTS AND PROCEDURES

6.1   INTRODUCTION

The experimental work for this research project has been conducted in two phases to satisfy the objectives put forward by the Science Research Council Co-ordinators. These were:-

1. To investigate the dressing of Aluminium Oxide grinding wheels when using single point diamond tools, with a view to establishing criteria for efficient wheel dressing.

2. To investigate the effects of wheel dressing and grinding conditions on the cylindrical grinding process, with a view to establishing criteria for efficient rough and finish grinding of a particular workpiece material.

The following conditions were advised:-

Wheel Dressing:-

Grinding   wheel: Aluminium Oxide grits,
                          Vitrified Bond.

Range of single point diamond tools.

Range of diamond angle settings.

Range of values of in-feed and cross-feed:-

| In-feed | 2.5 - 25 μm |
| Cross-feed | 12   - 500 μm/rev of wheel |

Grinding:-

Workpiece material : En 31 Ball bearing steel (hardened)

6.2   EXPERIMENTAL MATERIALS

6.2.1 Grinding Wheels

The following 305 mm $\emptyset$ x 25 mm wide grinding wheels were recommended by two manufacturers, as being representative of the types used in industry for the cylindrical grinding of hardened carbon-chromium steel.

NORTON ABRASIVES LTD.

32A60 – K8VBE

38A46 – K5VBE,

UNIVERSAL GRINDING WHEEL Co. LTD.

A60KV

A46KV

For the wheel dressing experiments all four grinding wheels were used. For the grinding experiments only one grinding wheel was used, to minimise the number of variables present. This was the 32A60 – K8VBE grinding wheel, manufactured by NORTON ABRASIVES LTD.

The grinding wheel compositions and symbols are explained as follows:-

Grinding wheels consist of two main essentials. The Abrasive which does the actual grinding or cutting, and the Bond which holds the abrasive particles together. In order to provide chip clearance, air spaces or voids must be left between adjacent grains.

Abrasive type:- A, 32A, 38A.

When grinding steels, the abrasive material used is Aluminium Oxide, designated A. This material is produced by fusing the soft clay-like mineral Bauxite in special electric furnaces. After cooling, the resultant mass is crushed to form grit particles, which are referred to as blocky polyhedra.

The Aluminium Oxide produced by this process has varying degrees of purity, e.g., the notation 38A means a high purity fused material of about 99.5% Al_2O_3 composition. The grits are often blended to give the required cutting characteristics for any particular grinding operation, e.g. cool, fast-cutting etc.

Grit size:- 46, 60.

When the fused Aluminium Oxide has been crushed, it is separated out by sieving through a series of screens . which have a specific number of holes per linear inch. The grit particles are graded according to the hole sizes

through which they pass, giving an indication of their mean diameter, e.g. 46 grits have a diameter of approximately 350 μm, and 60 grits have a diameter of approximately 250 μm. Grinding conditions are governed to a large extent by grit size, e.g. large grits are used for efficient stock removal, and smaller grits for improved surface finish.

Bond type: V, VBE.

About 75% of grinding wheels have a vitrified bond, which is basically China Clay. The porosity and strength of wheels made with this type of bond give high stock removal and high precision. It is not affected by water, acid, oils or ordinary temperature variations.

Bond grade: K

Bond grade is designated by letters of the alphabet, A - soft to Z - hard. For the majority of precision grinding operations, the grades required fall between F and N, whilst grades for rough grinding range from M to Z. K grade is medium - soft.

Structure number: 5,8.

The structure number, which is designated by the numbers 0 - dense to 12 - open, gives an indication of the grit density and pore size of the voids in the grinding wheel. It also gives an indication of the proportion of the bonding material in the grinding wheel, which varies from 10% to 30% of the total volume.

6.2.2 Diamond dressing tools.

The diamonds used in this research work were supplied by L.M. Van Moppes and Sons, and were selected for their uniformity and quality. Each diamond, which weighed approximately 1K, was set in a steel holder (see fig. 5.6), the diamond size being governed by the size of the grinding wheel to be dressed (see fig. 2.10). Figs. 6.1 and 6.2, show views of two of the several diamonds used, namely an octahedron diamond and a dodecahedron diamond respectively.

6.2.3 Workpiece material

The workpiece material used for the cylindrical

grinding experiments was En 31 ball-bearing steel supplied by
S.K.F. STEEL LTD., a subsidiary of the SKEFCO BALL BEARING
Co LTD. This material has been adopted by other investigators
involved in the Science Research Council Co-ordinated
Grinding Programme. The test pieces were made from 50 mm ⌀
bar, and were 150 mm long. The length to be ground was
75 mm, and the remaining portion was turned down to 25 mm ⌀
so that a grinding carrier could be fitted.

The material specification and condition was as
follows:-

Material composition %			Material type
C	.9	- 1.2	
Si	.10	- .35	
Mn	.30	- .75	
S	.05 max		En 31
P	.05 max		BS 970 - 1955
Ni	-		
Cr	1.0	- 1.6	
Mo	-		

Material condition

Austenised 860° C	Soaking time 2 hrs.
Oil quenched	Oil temperature 60° C
Tempered	1 hr. at 170° C
Ensuing hardness	63 - 64 Rockwell Scale C.
	(approx. 800 VPN)

6.2.4   Grinding coolant.

Cimcool S4, which is a semi-synthetic, semi-transparent
fluid made by CINCINNATI MILACRON LTD., was used in the
proportion of 30 : 1 water to oil mixture.

Typical physical properties:-

Colour	Light pink
Viscosity	38.5 seconds (Saybolt) at 100° F
Flash point	Nil
Fire point	Nil
Freezing point	Minus 1° C

Specific gravity   1.015 at 20° C
pH   10

6.3   WHEEL DRESSING PROCEDURES AND TESTS

6.3.1 Programme of dressing tests.

The dressing of grinding wheels was conducted in four parts as follows:-

1. A series of tests in which the effect of drag angle on diamond wear was observed by recording the wear on sharp diamonds pictorially, and the accompanying force when dressing grinding wheels at set values of in-feed and cross-feed.

2. A series of tests in which the effects of drag angle, diamond wear, in-feed and cross-feed on dressing force and grinding wheel surface roughness were observed, when dressing four grinding wheels with an initially sharp diamond.

3. A series of tests in which the effects of in-feed and cross-feed on dressing force and grinding wheel surface roughness were observed when dressing four grinding wheels at a fixed drag angle with a blunt diamond.

4. A single test in which the effect of continuous dressing on diamond wear, dressing force and grinding wheel surface roughness was observed,for constant conditions of in-feed, cross-feed and drag angle.

6.3.2 Pre-test procedures.

1. Dynamic wheel balancing.

All grinding wheels were balanced in situ with the aid of the ELTRODYN dynamic balancing equipment after mounting in the grinding machine. See statement 4.5.3 for the balancing procedure.

The grinding wheels were checked after each test for any out-of-balance which may have occured through wheel wear, and rebalanced when necessary.

2. Pre-test wheel dressing.

In order to keep the test conditions as uniform as possible, a pre-dressing procedure was adopted,[8] which involved the preparation of the grinding wheel surface with a worn diamond, using several values of in-feed with one value of cross-feed. The purpose of the pre-dressing was two-fold:-

(i) to maintain a uniform wheel surface condition prior to finish-dressing, and

(ii) to minimise wear on the diamond tools being used in the tests.

Each pre-dressed wheel surface was checked against that of its predecessor for consistency by a surface finish analysis of a plunge-ground piece of thin plastic strip, before the commencement of each new dressing cycle. The procedure adopted was as follows:-

N$\underline{o}$ of passes	In-feed μm	Cross-feed μm/rev of wheel
4	25	25
4	12	25
4	5	25

NB. The pre-dressing procedure was carried out using a table mounted dressing fixture. See fig. 4.10.

6.3.3 Setting and measurement of test parameters.

1. Orientation of the diamond dressing tools.

It has been demonstrated that the resistance of diamond to abrasion varies considerably with changes in the direction of abrasion and in the orientation of an abraded facet,[5,12] hence location marks were made on the diamond tools to ensure precise orientation in the holders, which were in turn accurately located in the dynamometers. The orientation was maintained constant for each test, so that the diamond tool had the same presentation to the grinding wheel for each value of "drag angle" used. (The term "drag angle" is taken as meaning the angle measured between the diamond tool axis, and a line passing through the wheel centre from the point of contact on the wheel face. This

line lies in the horizontal plane. The sign convention adopted is that drag angles measured above the datum line are positive, and those measured below are negative.)

2. Measurement of dressing force.

The force generated during wheel dressing was measured with either the three-component force dynamometer, having a strain gauge measuring system, or the two-component force dynamometer, having a piezo-electric measuring system. (The two-component force dynamometer was used with very blunt diamonds, because of its greater stiffness.) These dynamometers are shown in figs. 5.23 and 5.28 respectively.

Setting of the dynamometers was as follows:-

Three-component force dynamometer:- Initially the dynamometer was advanced to within a few micro-metres of the pre-dressed grinding wheel face by manipulation of the grinding machine controls. The dressing diamond was then brought into contact with the wheel face by using the micro-adjustment on the dynamometer slide, and the depth of cut (in-feed) was applied through the dynamometer slide after zeroing the dynamometer. The force readings (F_a, F_r, F_t) were recorded on light-sensitive paper.

Two-component force dynamometer:- The dressing diamond was brought into contact with the grinding wheel face using the grinding machine controls, and the depth of cut (in-feed) was applied by the same means after zeroing the dynamometer. The force readings (F_r, F_t) were read directly from a meter scale and tabulated. These readings were taken independently, since this dynamometer was capable of recording only one force component at a time.

When using the above mentioned dynamometers, the dressing traverse rate (cross-feed) was set with the thyristor controlled, d.c. motor module, which was fitted as an alternative to the grinding machine hydraulic table traverse. See fig. 4.5.

3. Measurement of grinding wheel surface finish (Ra).

A value of grinding wheel surface roughness was

obtained after the execution of a dressing cycle   by
analysing the surface of four rapidly plunge-ground pieces of thin
plastic strip with a RANK TAYLOR HOBSON "TALYSURF" INSTRUMENT,
MODEL 3, No 112/321-746.   (This has a full scale, Centre
Line Average Index Reading of 200 μ in. (5 μm). The metre
cut-off wave length used was .o3 in. (.76 mm). An average
value of C.L.A. Index (Ra), taken for each set of strips,
was recorded in each case. The measurement of Ra can be
seen in fig. 6.3.

4.   Assessment of diamond wear.

Two methods for obtaining diamond tool wear were
used, depending upon the conditions being observed for the
particular test. For the tests where the effects of drag
angle on diamond wear were being observed, the wear trend
was shown pictorially after viewing the worn diamond profile
on an ISOMA S.A. OPTICAL PROJECTOR, TYPE 119 GXB. (Max.
Mag. x100), and also observing the wear through a RANK
TAYLOR HOBSON "TALYDEN" BENT MICROSCOPE, MODEL B, which
had a x5 mag. standard objective, and a x10 mag. simple
eyepiece. For the test where diamond wear was required
volumetrically for comparison with the volume of grinding
wheel dressed away in the same time, the wear area on the
diamond tip was measured using the above mentioned micro-
scope, which had a vertical and a horizontal linear measuring
scale calibrated for 1 division = .001 in. (25 μm) when
using the x5 mag. objective. The depth of diamond wear,
measured along the tool holder axis, was obtained using a
micrometer screw held in a specially made fixture, see
fig. 6.4. The second method of measuring diamond wear
was adopted from work conducted by G. PAHLITZSCH[5], which
was of a similar nature

5.   Measurement of the volume of grinding wheel
     dressed away.

Loss of wheel due to dressing was obtained by
measuring the change in height of a step machined in the
wheel face. This measurement was taken from a plunge

ground piece of thin plastic strip, using a MERCER
STAND AND DIAL TEST INDICATOR, MODEL 120, calibrated to
measure a maximum deflection of .2 in. (5 mm) in steps of
.0001 in. (2.5 μm). The initial step height was .o2 in.
(.5 mm) deep. As the loss of wheel height approached this
value the step was remachined to form a new datum. From
these readings, and known width of grinding wheel and its
diameter, the volume of wheel dressed away was calculated.
Fig. 6.5 shows the strip measurement.

6.3.4 The wheel dressing tests.

N.B.   Values of dressing force and grinding wheel surface
finish obtained from the following tests are recorded in
Appendix VI. Values of diamond wear and wheel lost through
dressing, measured volumetrically, are also recorded in
Appendix VI.

Graphical representation of the above results, and
pictorial representation of diamond tool wear are presented
in chapter 7.

TEST No 1.

Objective:-

To record the dressing force and tool wear (pictorially),
when dressing with a diamond tool which is presented to
the grinding wheel at different values of drag angle, the
in-feed and cross-feed remaining constant.

Test conditions:-

Dressing conducted without coolant

In-feed   12.5 μm   (constant)

Cross-feed   .5 mm/rev (constant)

Drag angles   +15° to -15° in steps of 5°

Diamond tool   No 63794/1 (sharp) 1.00 K.wt.

(Fig. 6.2)   Included angle 120° 37'
                 (measured in the vertical
                 plane, perpendicular to the
                 wheel face.)

Grinding wheel   A46 KV

Order of events:-

The test was conducted using the following order of drag angles:-

0°, $+5^{\circ}$, $+10^{\circ}$, $+15^{\circ}$, -15°, -10°, and -5°, with the before-mentioned parameters being measured at each step. Each dressing cycle was repeated three times. (Fig. 6.6 shows a general view of the test set-up.)

TEST No 2.

A continuation of TEST No 1, with the value of cross-feed changed to .1 mm/rev, all other test conditions remaining the same as before. The objective and procedure were the same as for TEST No 1. Each dressing cycle was repeated fifteen times.

TEST No 3.

Objective:-

To take four grinding wheels and two diamond tools of different geometry, and record values of dressing force and diamond wear (pictorially), whilst dressing with different values of drag angle, the in-feed and cross-feed remaining constant.

Test conditions:-

Dressing conducted without coolant

In-feed   12.5 μm   (constant)

Cross-feed   .1 mm/rev   (constant)

Drag angles $+15^{\circ}$ to -15° in steps of 5°

Diamond tools   No 71784/2 (sharp) 1.05 K. wt.
                Included angle 95°
                No 70795/2 (sharp) 1.00 K. wt.
                Included angle 143° $35'$
                (measured in the vertical plane,
                perpendicular to the wheel face.)

Grinding wheels   A60 KV
                         A46 KV
                    32A60 – K8VBE
                    38A46 – K5VBE

Order of events:-

.The test sequence was as follows:-

Grinding wheel	Diamond tool
32A60–K8VBE	
38A46–K5VBE	No 71784/2
A46 KV	Inc. Angle 95°
A60 KV	
32A60–K8VBE	
38A46–K5VBE	No 70795/2
A60 KV	Inc. Angle 143° 35'
A46 KV	

For each grinding wheel and diamond combination, values of the before mentioned parameters were recorded for each value of drag angle used. Each dressing cycle was conducted using the following order of drag angles:-
$0°$, $+5°$, $+10°$, $+15°$, $-15°$, $-10°$ and $-5°$.

TEST No 4.

Objective:-

To record the dressing force, tool wear (pictorially) and the resulting grinding wheel surface roughness, when dressing with a sharp diamond tool presented to the grinding wheel at three different drag angles, and with the in-feed and cross-feed being varied over a range of values.

Test conditions:-

Dressing conducted without coolant.

In-feed	5 μm to 25 μm in steps of 5 μm
Cross-feed	.1 mm/rev to .5 mm/rev in steps of .1 mm
Drag angles	$+5°$, $+10°$ and $+15°$
Diamond tool	No 63794/2 (sharp) .90 K. wt.
(Fig. 6.1)	Included angle 115° 55' (measured in the vertical plane, perpendicular to the wheel face.)
Grinding wheel	32A60–K8VBE

Order of events:-

With the drag angle constant at $+5^\circ$, and the in-feed constant at 5 μm, the cross-feed was varied from .1 mm/rev of wheel to .5 mm/rev of wheel in steps of .1 mm, with the dressing force and grinding wheel surface roughness being recorded for each dressing cycle. The sequence of events was repeated for values of in-feed, increasing each time by 5 μm up to a maximum value of 25 μm. The whole test was then repeated for the other two values of drag angle, namely $+10^\circ$ and $+15^\circ$, with the same readings being taken as before. The diamond tool wear was recorded (pictorially) at the end of the test.

TEST No 5.

Repeat of TEST No 4 using an A60KV grinding wheel, all other test conditions remaining the same as before.

TEST No 6.

Repeat of TEST No 4 using an A46KV grinding wheel, all other test conditions remaining the same as before.

TEST No 7.

Repeat of TEST No 4 using a 38A46-KVBE grinding wheel, all other test conditions remaining the same as before.

TEST No 8.

Objective:-

To record the dressing force, tool wear (pictorially) and the resulting grinding wheel surface roughness when dressing with a blunt diamond tool presented to four grinding wheels in turn, using one value of drag angle, and a range of values of in-feed and cross-feed.

Test conditions:-

Dressing conducted with coolant.

In-feed   5 μm to 25 μm in steps of 5 μm.

Cross-feed   .1 mm/rev to .5 mm/rev in steps of .1 mm.

Drag angle   +5° (constant)

Diamond tool   (origin unknown)

wear area dimensions at

commencement of test:-

maximum width   1.3 mm

maximum depth   1.0 mm

Grinding wheels   A46KV

A60KV

32A60 -K8VBE

38A46 -K5VBE

Order of events:-

The test was conducted using the following order of grinding wheels:-

38A46-K5VBE, 32A60-K8VBE, A46KV and A60KV. With the drag angle constant at +5°, and the in-feed constant at 5 µm, the cross-feed was varied from .1 mm/rev of wheel to .5 mm/rev of wheel in steps of .1 mm, with the dressing force (F_r and F_t) and grinding wheel surface roughness being recorded for each dressing cycle. The sequence of events was repeated for values of in-feed, increasing each time by 5 µm up to a maximum value of 25 µm. The test was repeated for each grinding wheel in turn, with the diamond tool wear being recorded (pictorially) at the start and finish of each test.

TEST No 9.

Objective:-

To record the dressing force, diamond wear (volume-trically), volume of grinding wheel dressed away and wheel surface roughness, when dressing a grinding wheel over a long period of time with a diamond tool presented at fixed values of in-feed, cross-feed and drag angle.

Test conditions:-

Dressing conducted without coolant.

In-feed   12.5 µm (constant)

Cross-feed   .1 mm/rev (constant)

Drag angle	+15° (constant)
Diamond tool	No 71784/4 (sharp) .90 K.wt.
	Included angle 138°
	(measured in the vertical
	plane, perpendicular to the
	wheel face.)
Grinding wheel	38A46-K5VBE

Order of events:-

The three-component dressing force dynamometer and the table mounted dressing fixture were fitted side by side on the grinding machine table, so that the diamond tool could be transferred from one to the other at various stages in the test.

Initially, the diamond tool was mounted in the dynamometer, and the readings of the before-mentioned parameters were recorded every fifth pass up to the fiftieth one. Readings were taken again after seventy and one hundred passes, and then every fiftieth pass up to the end of the test. For the dressing cycles in between those at which readings were taken, the diamond tool was transferred to the table mounted fixture. This procedure commenced after the twenty-fifth pass.

6.4   CYLINDRICAL GRINDING PROCEDURES AND TESTS

6.4.1   Programme of grinding tests.

The cylindrical traverse grinding was conducted in three parts as follows:-

1. A short series of tests in which the effects of grinding cross-feed (traverse rate) on workpiece surface roughness and grinding ratio was observed for constant dressing and grinding conditions.

2. A longer series of test in which the effects of dressing conditions for "rough-grinding" on workpiece surface roughness, grinding ratio and grinding force (F_R and F_T components) were observed for constant grinding conditions.

3. A series of tests in which the effects of dressing conditions for "fine-grinding" on workpiece surface roughness and grinding force (F_R and F_T components) were observed for constant grinding conditions.

N.B. The term grinding ratio is the ratio of the volume of metal removed, to the volume of grinding wheel worn away at the same time.

6.4.2 Pre-test procedures.

1. Grinding machine warming-up period.

The grinding machine was allowed to warm-up for a period of ninety minutes each time it was started from cold. This was to allow stable operating conditions to be attained. During this period, the grinding head, workhead and hydraulic table traverse were operated.

2. Dynamic wheel balancing and pre-test wheel dressing.

Dynamic wheel balancing and pre-test wheel dressing were conducted in the manner described in statement 6.3.2. Dressing of the grinding wheel for each test condition was achieved using the table mounted dressing fixture, with the in-feed being applied through the grinding machine controls, and the cross-feed being applied through the thyristor controlled table traverse unit. Each dressing condition was applied in a single pass.

3. Measurement of grinding wheel surface finish (Ra).

Before the commencement of each grinding test a value of grinding wheel surface roughness in the "as-dressed" condition was obtained as described in statement 6.3.3.

4. Workpiece preparation.

After the workpiece had been machined to the required dimensions, they were heat-treated by the SKEFCO BALL BEARING Co LTD., to their specification. See statement 6.2.1. Each workpiece was then cylindrically ground to remove the surface scale which had formed during heat-treatment, and to form a datum surface from which to work. The workpieces were checked for hardness at three points along their length, and surface finish tests were carried out to check the consistency of each

ground surface.

5. Mounting of the workpiece between grinding centres.

A constant axial thrust was applied to each workpiece through the grinding centres to ensure similar starting conditions for each test. The thrust force was monitored by the piezo-elecric grinding-force dynamometer.

6. Setting of the in-feed and cross-feed rates, and traverse length when grinding.

In-feed and cross-feed rates were set for each test using the grinding machine hydraulic control valves.

The table traverse was set such that the machine table reversed direction after the grinding wheel had cleared the workpiece by about 5 mm at the end of each stroke.

6.4.3 Measurement of test parameters.

1. Measurement of grinding force.

The force generated during grinding was measured with the three-component grinding force dynamometer, which had a piezo-electric measuring system. See fig. 5.30. Values of F_R and F_T (radial and tangential force components respectively) were recorded on light-sensitive paper. The axial force component was not measured.

N.B. A preliminary grinding force test was conducted to observe the effect of change of workpiece diameter on F_R and F_T. The results are shown in Appendix VII.

2. Measurement of workpiece surface finish (Ra).

A value of workpiece surface roughness was obtained at points throughout the tests by analysing the workpiece surface with a RANK TAYLOR HOBSON "TALYSURF" INSTRUMENT, MODEL 3. The metre cut-off wave length used was .03 in. (.76 mm). Several readings were taken along the workpiece length, and an average value of C.L.A.Index (Ra) was recorded. The measurement of Ra can be seen in fig. 6.7.

3. Measurement of the volumes of workpiece ground away, and grinding wheel worn away, in the same time.

The volume of workpiece ground away was calculated from readings of change in workpiece diameter, measured at

points throughout the test with a micrometer, and known workpiece length. At the same time, readings of radial wheel wear were recorded using the method described in statement 6.3.3, and the corresponding volume of wheel worn away was calculated.

4. Check of workpiece roundness.

At points throughout certain of the grinding tests, traces of workpiece roundness were made using a RANK TAYLOR HOBSON "TALYROND INSTRUMENT, MODEL 50, with a $2\frac{1}{2}$ in. pick-up arm. These traces were used as a means of identifying the point in the tests at which chatter occured between the workpiece and grinding wheel, since this point marked the onset of rapid wheel wear.

6.4.4 The cylindrical traverse grinding tests.

N.B. All readings taken in the grinding tests are recorded in Appendix VII. Graphical representation of the above results, and traces of grinding wheel and workpiece surface roughness, and workpiece roundness, are presented in chapter 7.

TEST Nos. 1 to 4 included.

Objective:-

To record the grinding ratio and workpiece surface roughness when grinding EN 31 steel at several cross-feed rates, with in-feed remaining constant, and dressing conditions constant.

Test conditions:-

Dressing:- (constant conditions for all four tests)
     Dressing conducted without coolant.

In-feed	25 μm
Cross-feed	.3 mm/rev of wheel
Drag angle	+15°
Diamond tool	No 71784/2 (sharp) 1.05 K.wt.
	Vertical included angle 108°
	Horizontal included angle 95°

perpendicular to the wheel
                        face, and in the horizontal
                        plane respectively).
        Grinding wheel   32A60-K8VBE

Grinding:-
        Grinding conducted with coolant.
        Workpiece material   EN 31 (hardened).
        Wheel speed   1,800   rev/min
        Work speed   90   rev/min
        In-feed   12.5   μm/pass   (radial)
        Cross-feed   2.5,   6.5,   13.5 and 20.5 mm/sec

Order of events:-
The grinding wheel and workpiece were prepared
before each test as descibed in statement 6.4.2, and pre-
test readings of workpiece length and diameter were recorded.
Grinding commenced with a cross-feed of 20.5mm/sec, and
readings of loss of grinding wheel radius, change in
workpiece diameter and workpiece surface roughness were
recorded at various points throughout the test.   In all,
one hundred grinding passes were made with approximately
14 cm^3 of metal being ground away. The procedure was then
repeated for the other three values of cross-feed. See fig.
6.8 for a typical test set-up.

        TEST Nos 5 to 16 inclusive.
        Objective:-
        To record the grinding ratio, workpiece surface
roughness and grinding force (F_R and F_T components) when
"rough-grinding" EN 31 steel under constant grinding
conditions, using a wheel dressed under different conditions
with a sharp diamond.

        Test conditions:-
        Dressing:-
        Dressing conducted without coolant.
        In-feed   5, 12.5, 18 and 25 μm

```
          Cross-feed              .1,   .3 and .5 mm/rev of wheel
          Drag angle                      +15°
          Diamond tool            No 71784/2  (sharp) 1.05 K.wt.
          Grinding wheel               32A60-K8VBE
```

Grinding:- (Constant for all tests)
```
          Grinding conducted with coolant.
          Workpiece material EN 31 (hardened)
          Wheel speed             1,800 rev/min
          Work speed                 90 rev/min
          In-feed                 12.5  μm/pass (radial)
          Cross-feed              13.5  mm/sec
```

Order of events:-

The tests were conducted with the following order of
dressing in-feed and cross-feed values. (Twelve separate
tests.)
```
          In-feed                 25, 18, 12.5, 5 μm
          Cross-feed              .3, .1, .5      mm/rev of wheel
```

The grinding wheel and workpieces were prepared
before each test as described in statement 6.4.2, and pre-
test readings of workpiece length and diameter were recorded
as well as a talyrond-trace being made of each workpiece
used. From the start of each test readings of loss of
grinding wheel radius, change in workpiece diameter,
workpiece surface roughness and grinding force were taken
at intervals of twenty passes, up to about the two-
hundreth pass, after which readings were taken every forty
passes up to the end of each test. Talyrond traces were
also made of the workpiece at various points. In each
of the twelve tests undertaken, approximately 60 cm^3 of
metal was removed from the workpieces.

Test Nos 17 and 18.
These two tests were a repeat of TEST Nos 7 and 11
respectively, except that the in-feed in grinding was changed
to 5 μm/pass (radial). Readings of the before-mentioned

parameters were taken with the interval between readings being increased towards the end of the tests. (Grinding force was not measured.) Again approximately 60 cm^3 of metal was removed from the workpiece for each test.

TEST Nos 19 to 30 inclusive.
Objective:-

To record the workpiece surface roughness, workpiece roundness and grinding force (F_R and F_T components), when "fine-grinding" EN 31 steel at different cross-feed rates, using a grinding wheel dressed under different conditions with a blunt diamond.

Test conditions:-
Dressing:-

Dressing conducted without coolant.

In-feed	5, 12, 18 and 25 μm
Cross-feed	.1, .3, and .5 mm/rev of wheel
Drag angle	+10°
Diamond tool	No 63794/2 (blunt) .90 K.wt.
Grinding wheel	32A60-K8VBE

Grinding:-

Grinding conducted with coolant.

Workpiece material	EN 31 (hardened)
Wheel speed	1,800 rev/min
Work speed	90 rev/min
In-feed	5 μm/pass (radial)
Cross-feed	5, 7.5, 10, 12 and 14 mm/sec

Order of events:-

The grinding wheel and five workpieces were prepared before the start of each grinding test, as described in statement 6.4.2, with pre-test readings of the workpiece diameters being recorded, and talyrond-traces being made of all the workpieces used. Twelve grinding tests were conducted i.e., one for every dressing condition, with readings of grinding force (F_R and F_T components),

workpiece diameter and surface roughness being recorded
after four passes of the workpiece at each of the five
values of cross-feed used. A different workpiece was used
for each cross-feed rate. Talyrond-traces were also made
of each workpiece.

Diamond № 63794 / 2

Profile view

115° 55'
Inc. Angle

x25 Mag.
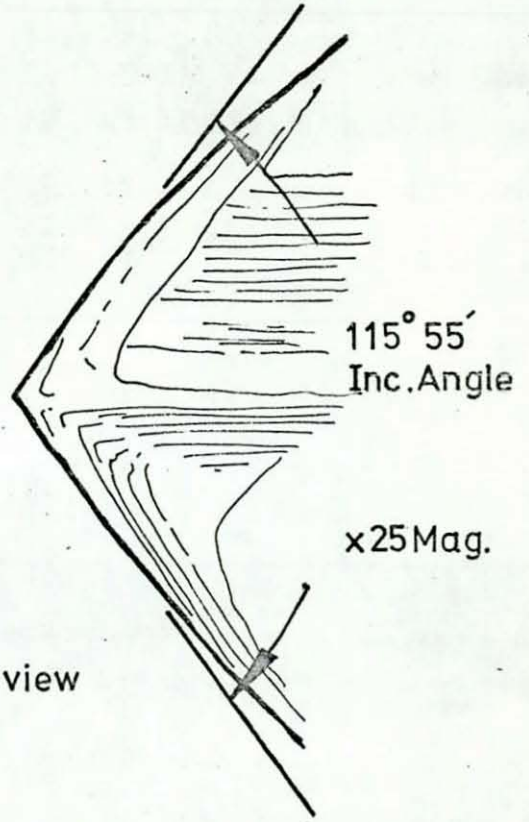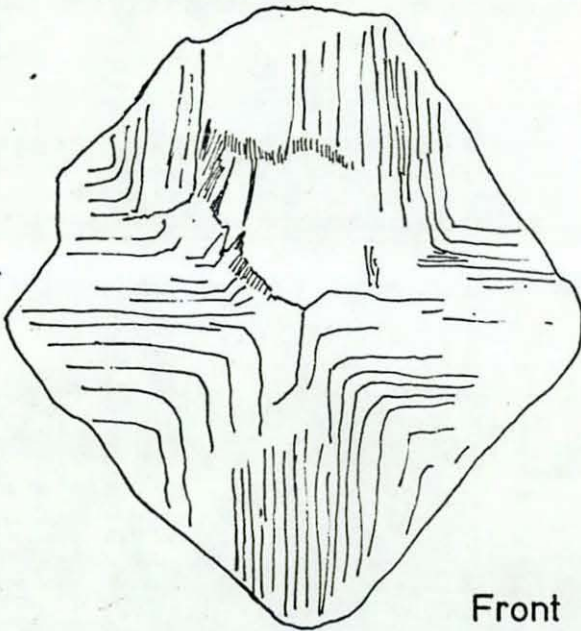
Front view

Fig. 6.1   Front and profile views of a
particular octahedron diamond
dressing tool before use.

Diamond № 63794/1

120° 37′
Inc. Angle

Profile view

×25 Mag.

natural flat

76 μm

254 μm
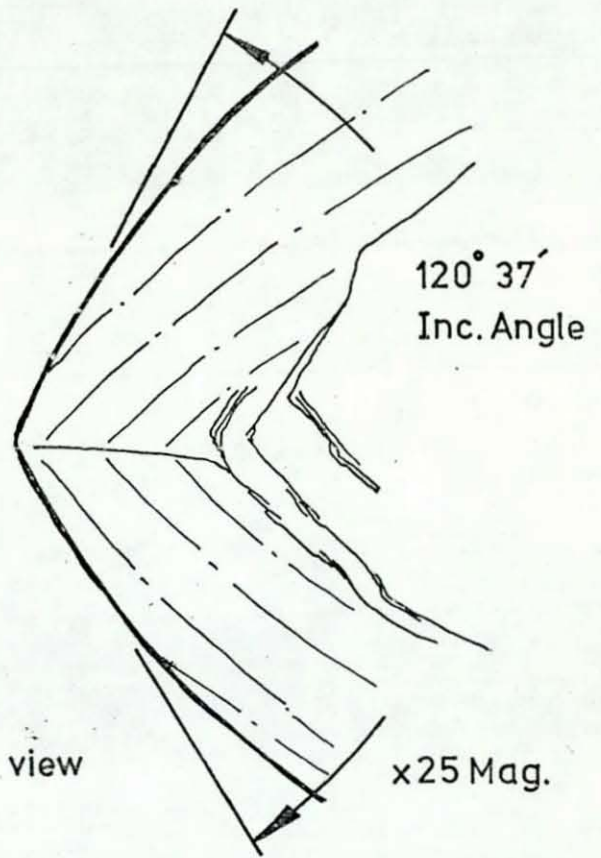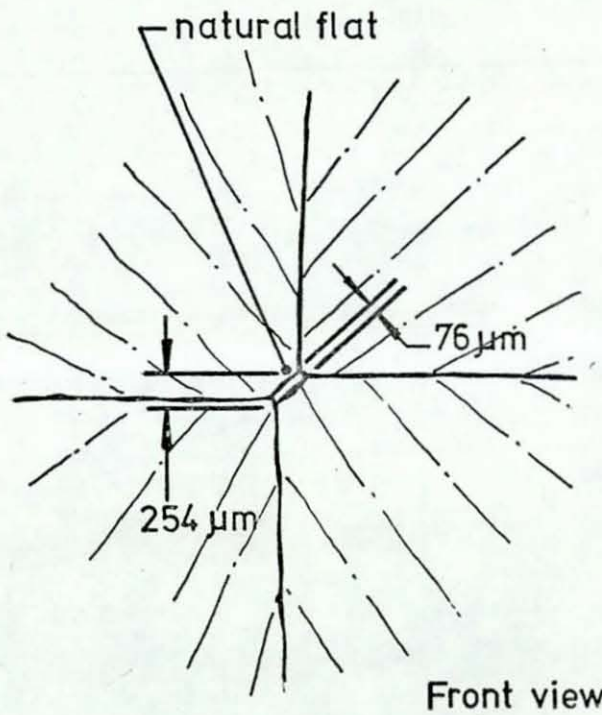
Front view
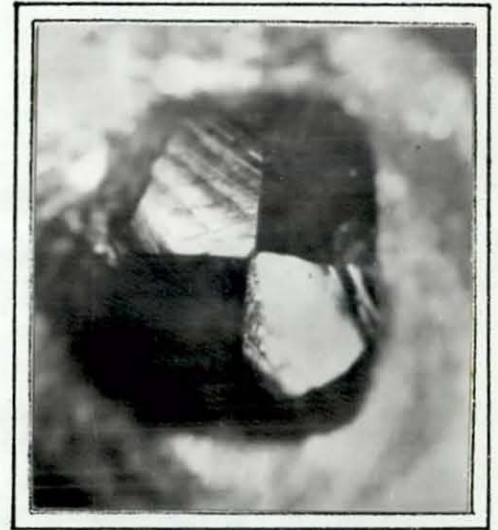
Fig. 6.2 Front and profile views of a
particular dodecahedron diamond
dressing tool before use.
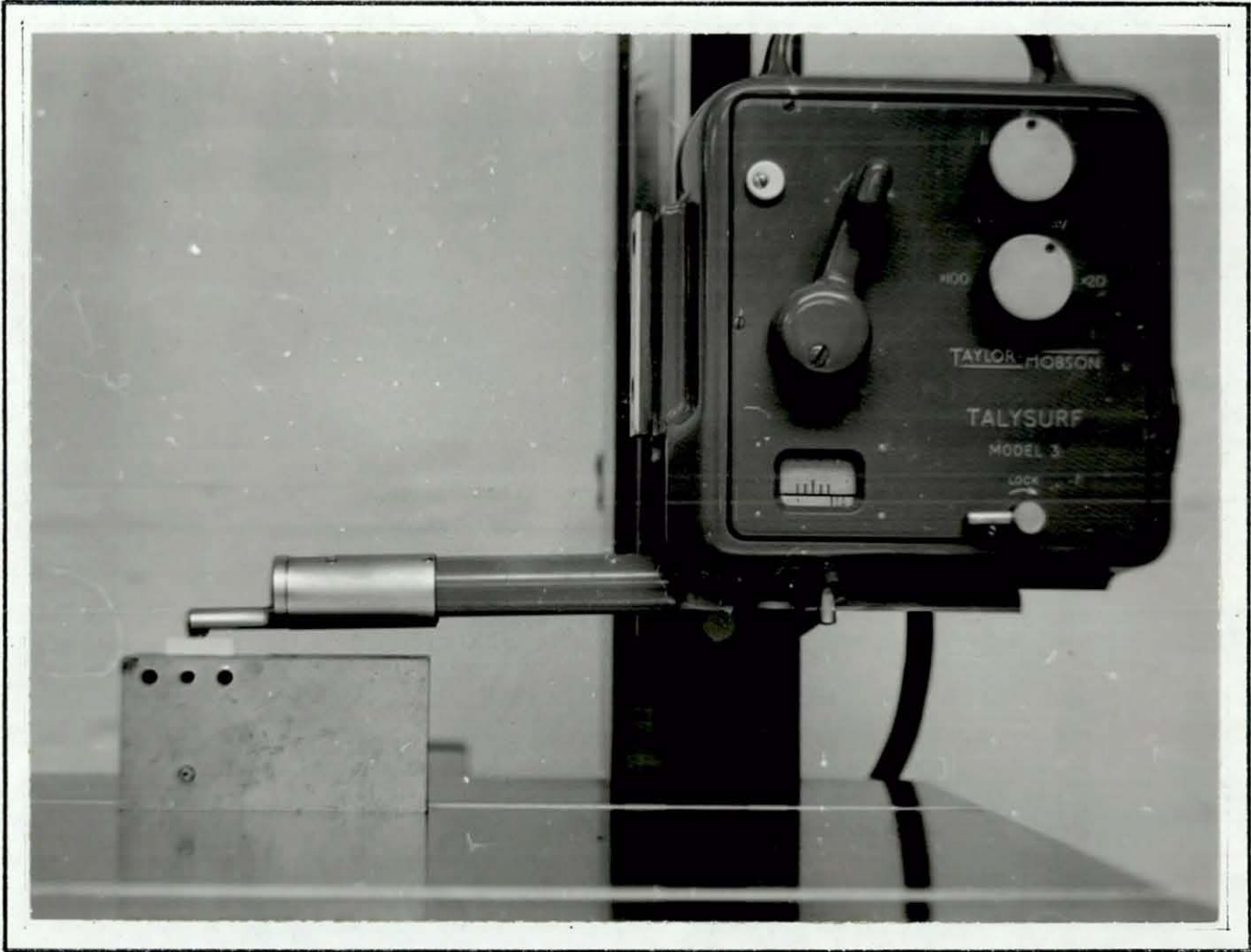
Fig. 6.3 The measurement of grinding wheel
surface roughness after dressing.
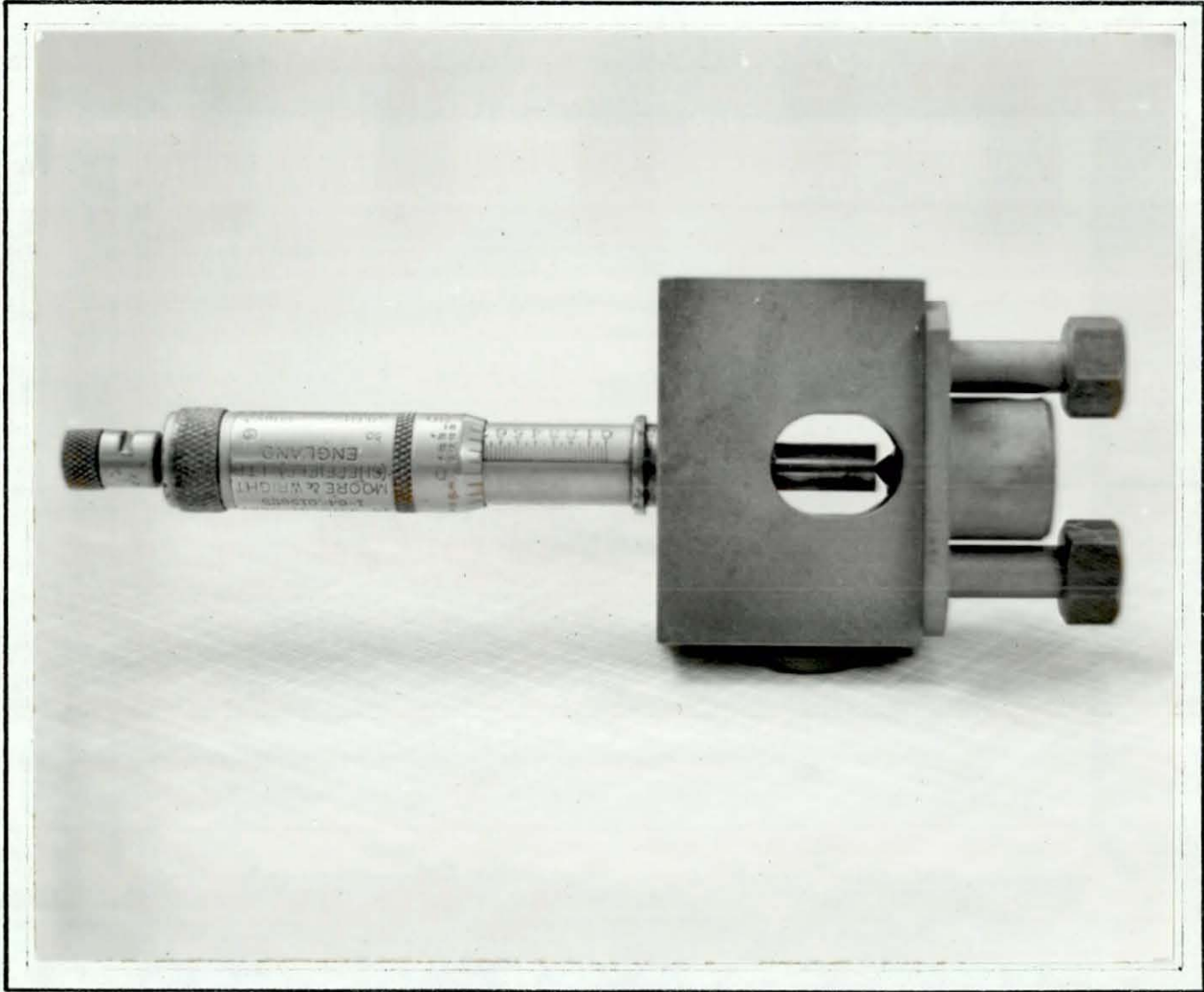
Fig. 6.4 The measurement of diamond wear
using a special fixture.
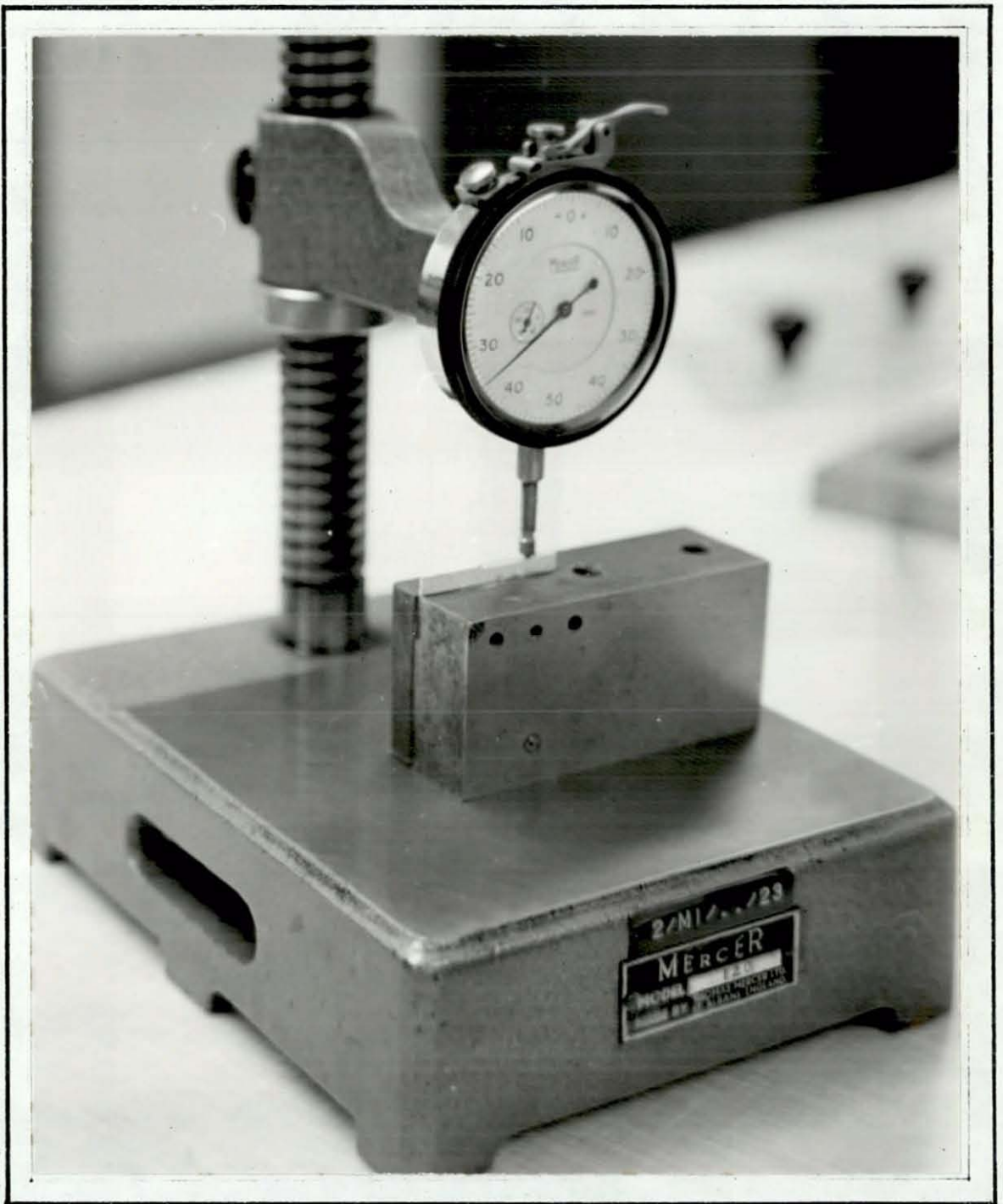
Fig. 6.5 Measurement of loss of wheel height
due to dressing.
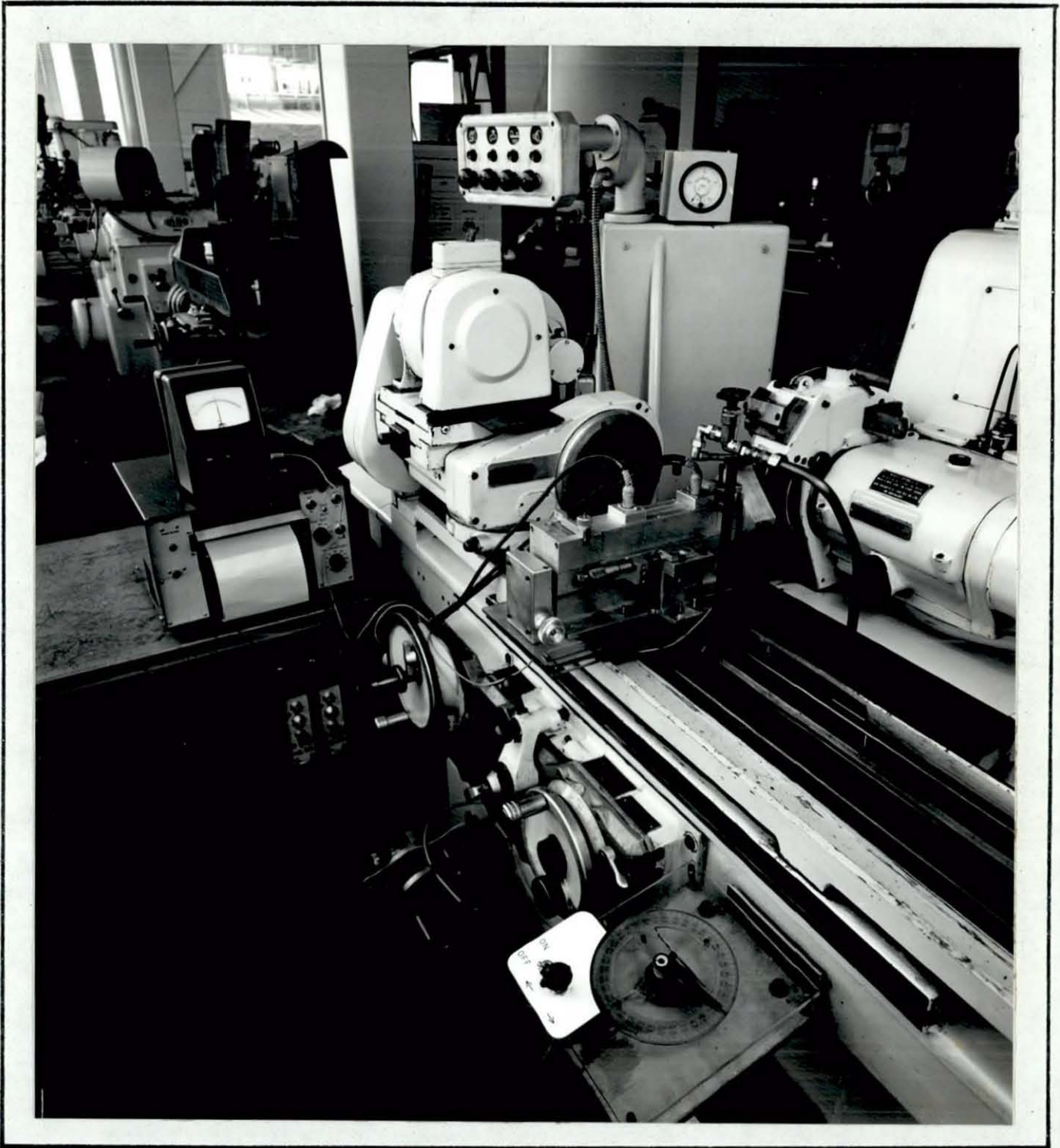
Fig. 6.6 <u>Test set up for the measurement of</u>
<u>dressing force for different values</u>
<u>of drag angle.</u>
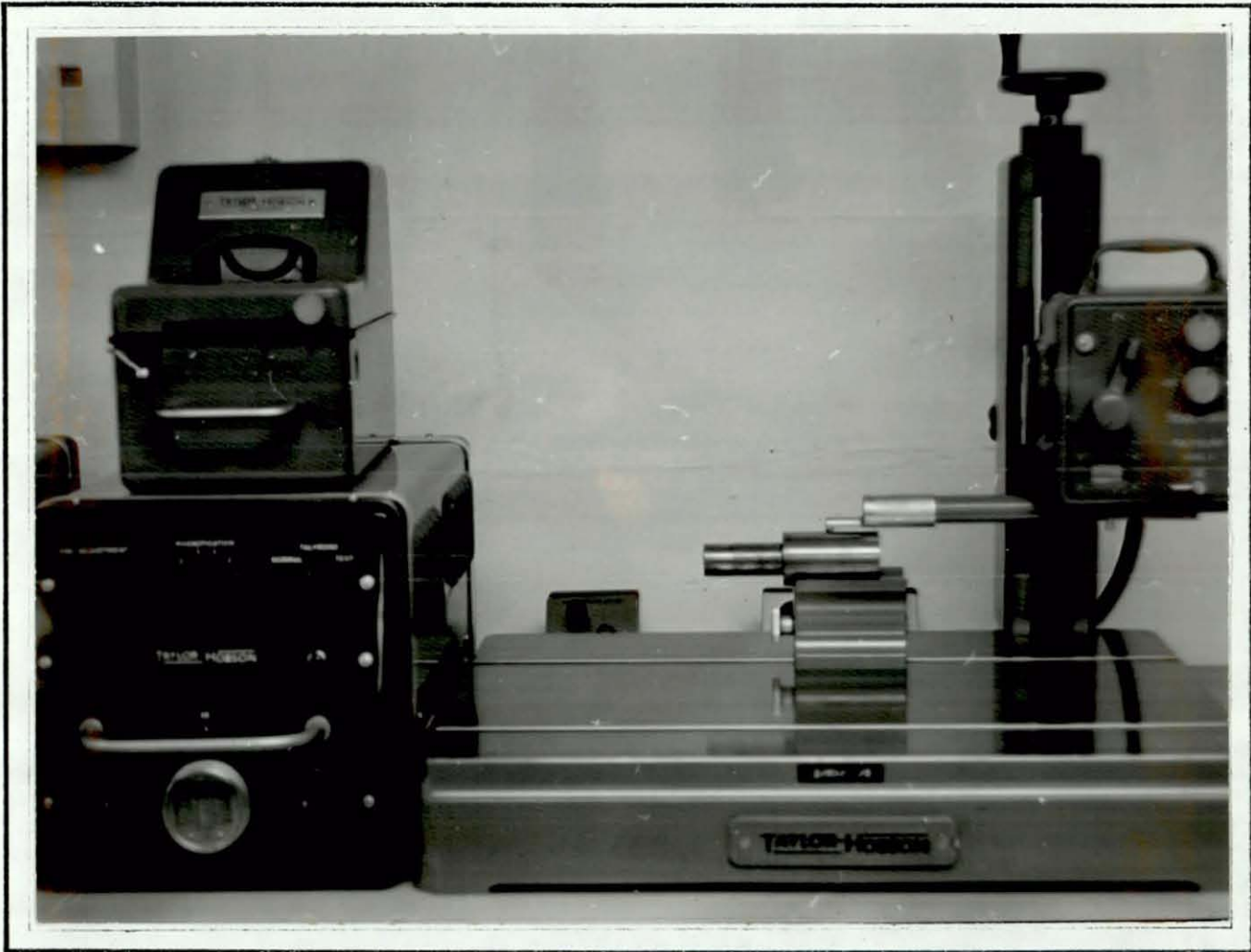
Fig. 6.7 The measurement of workpiece surface
roughness after grinding.
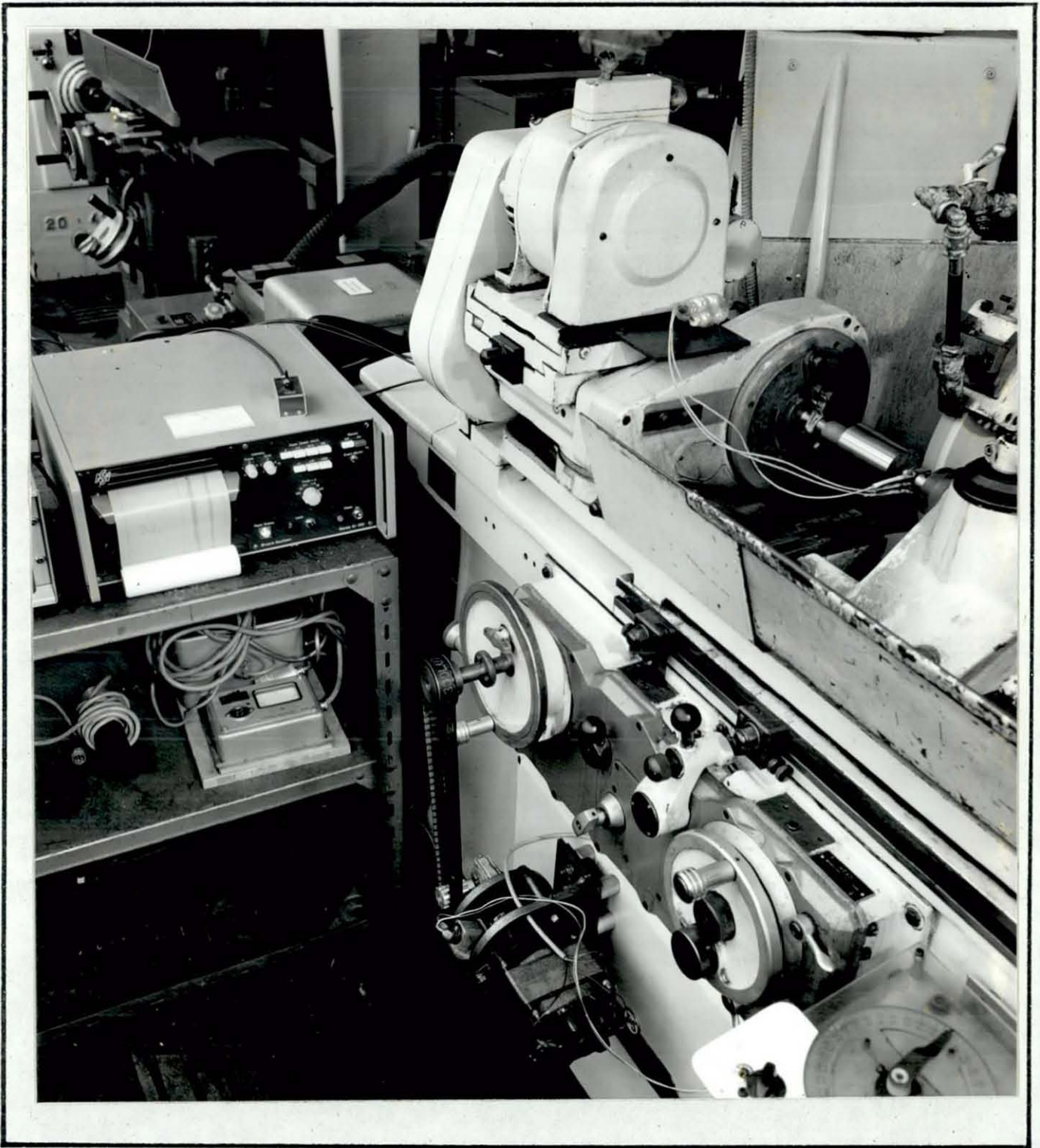
Fig. 6.8 A typical grinding test set up.